THESE DE DOCTORAT

PRESENTEE PAR

Raphaela Azevedo Rafael

POUR L'OBTENTION DU TITRE DE

DOCTEUR DE L'UNIVERSITE DE LILLE

Ecole doctorale: Sciences de la Matière, du Rayonnement et de l'Environnement

Spécialité: Chimie de Matériaux

Development of catalysts for the valorization of lignin: Hydrodeoxygenation of dimeric aryl ethers

Développement de catalyseurs pour la valorisation de la lignine, hydrodésoxygénation d'aryl éthers dimériques

Soutenue le 9 novembre 2022 devant le jury composé de :

Pr. Erwann Guenin	Université de Technologie de Compiègne	Rapporteur
Dr. Dorothée Laurenti	IRCELYON- CNRS	Rapporteur
Pr. Carole Lamonier	Université de Lille	Examinateur et Présidente
MCF Guillaume Clet	Université de Caen Normandie	Examinateur
MCF Frédéric Richard	Université de Poitiers	Examinateur

Dr. Eric Marceau	Université de Lille	Directeur de thèse
Pr. Fabio Bellot Noronha	Centrale Lille/CNRS	Directeur de thèse
Dr. Robert Wojcieszak	Centrale Lille/CNRS	Co-encadrant

THESE DE DOCTORAT

PRESENTEE PAR

Raphaela Azevedo Rafael

POUR L'OBTENTION DU TITRE DE

DOCTEUR DE L'UNIVERSITE DE LILLE

Ecole doctorale: Sciences de la Matière, du Rayonnement et de l'Environnement

Spécialité: Chimie de Matériaux

Development of catalysts for the valorization of lignin: Hydrodeoxygenation of dimeric aryl ethers

Développement de catalyseurs pour la valorisation de la lignine, hydrodésoxygénation d'aryl éthers dimériques

Soutenue le 9 novembre 2022 devant le jury composé de :

Pr. Erwann Guenin	Université de Technologie de Compiègne	Rapporteur
Dr. Dorothée Laurenti	IRCELYON- CNRS	Rapporteur
Pr. Carole Lamonier	Université de Lille	Examinateur et Présidente
MCF Guillaume Clet	Université de Caen Normandie	Examinateur
MCF Frédéric Richard	Université de Poitiers	Examinateur

Dr. Eric Marceau	Université de Lille	Directeur de thèse
Pr. Fabio Bellot Noronha	Centrale Lille/CNRS	Directeur de thèse
Dr. Robert Wojcieszak	Centrale Lille/CNRS	Co-encadrant

ACKNOWLEDGEMENTS

I would like to express my sincere gratitude to my supervisors Dr. Eric Marceau and Pr. Fabio Bellot Noronha, and my co-supervisor Robert Wojcieszak for their support and guidance in my PhD work. Thank you for all the valuable discussion, motivation, and encouragement throughout these 3 years.

I express my profound gratitude to Pr. Erwann Guenin and Dr. Dorothée Laurenti who accepted to judge my work and be the reviewers. I would also like to thank Pr. Carole Lamonier, Dr. Guillaume Clet, Dr. Frédéric Richard, and Pr. Harry Bitter who honored me by accepting to participate in the jury.

I would like to thank the French government through the Programme Investissement d'Avenir (I-SITE ULNE / ANR-16-IDEX-0004 ULNE) managed by the Agence Nationale de la Recherche, CNRS, the Métropole Européen de Lille (MEL) and the Region Hauts-de-France for "CatBioInnov" project, for the financial support.

I would like to thank all my colleagues and the technical staff in UCCS, especially Svetlana Heyte, Joelle Thuriot, Olivier Gardoll, Jean-Charles Morin, Johann Jezequel, and Ahmed addad from the UMET group for their assistance in my work.

I would like to thank all my friends, especially, Priscilla Magalhães, Leticia Forrer, Elise Albuquerque, Leandro Souza, Mateus Paiva, Marcelo Avelar, Deizi Peron, Jonathan Bassut, Camila Teles, and Camila Ferraz for all support, help and the great moments.

Finally, I would like to thank my dear family for supporting me and being by my side in every moment of my life.

SUMMARY

LIST OF FIGURES…….……..…7

LIST OF SCHEMES……...12

LIST OF TABLES……...13

ABSTRACT……16

RÉSUMÉ…...……..17

Chapter 1 Introduction 18

1.1. Introduction 19

1.2. Thesis structure 20

Chapter 2 Literature Review 23

2.1 Lignocellulosic biomass 24

2.2 Bio-oil from lignocellulosic biomass 26

2.3 Hydrodeoxygenation of bio-oil 27

2.4 HDO of model molecules representative of lignin 28

2.4.1 The effect of reaction conditions 29

2.4.1.1 Temperature 29

2.4.1.2 Pressure 34

2.4.2 Effect of solvent 39

2.4.2.1 In the absence of catalysts 39

2.4.2.2 In the presence of catalysts 41

2.4.3 Phenolic dimers representative of lignin 42

2.4.3.1 Catalysts used for the conversion of benzyl phenyl ether (BPE), model molecule representative of the α-O-4 linkage 42

2.4.3.1.1 Non-acidic support 42

2.4.3.1.2 Acidic supports 44

2.4.3.2 Catalysts used for the conversion of phenethoxybenzene (PEB), model molecule representative of β-O-4 linkage 57

2.4.3.2.1 Non-acidic supports 57

2.4.3.2.2 Acidic supports 61

2.4.3.3 Catalysts used for the conversion of diphenyl ether (DPE) model molecule representative of 4-O-5 linkage 76

2.4.3.3.1 Non-acidic supports 76

2.4.3.3.2 Acidic supports 85
2.5 Partial conclusion 101
Chapter 3 Experimental Procedure 103
3.1 Catalysts preparation 104
3.1.1 Preparation of palladium-based catalysts by incipient wetness impregnation (imp) 104
3.1.2 Preparation of ruthenium-based catalysts by incipient wetness impregnation 104
3.1.3 Preparation of Pd-based catalysts by colloidal (col) method 105
3.2 Catalysts characterization 105
3.2.1 Inductively coupled plasma optical emission spectrometry with (ICP-OES) 105
3.2.2 X-Ray fluorescence spectroscopy (XRF) 106
3.2.3 N_2 physisorption 106
3.2.4 X-Ray diffraction (XRD) 106
3.2.5 Temperature-programmed reduction (H_2-TPR) 107
3.2.6 Temperature-programmed desorption of ammonia (NH_3-TPD) 107
3.2.7 Infrared spectroscopy analysis (FTIR-Py) 108
3.2.8 Scanning transmission electron microscopy (STEM) 109
3.3 Catalytic test 110
3.3.1 Substrates 110
3.3.2 Catalytic system description 111
3.3.3 Catalytic reaction description 112
3.3.4 Analytical methods 112
Chapter 4 Catalysts Characterization 115
4.1 Palladium-based catalysts 116
4.2 Ruthenium-based catalysts 125
Chapter 5 Conversion of dimeric aryl ethers over supported Ru and Pd-based catalysts 130
5.1 Introduction 131
5.2 Hydrodeoxygenation of BPE over Ru and Pd-based catalysts 131
5.3 Hydrodeoxygenation of PEB over Ru and Pd-based catalysts 136
5.4 Hydrodeoxygenation of DPE over Ru and Pd-based catalysts 139
5.5 Conclusion 144
Chapter 6 Effect of support and metal particle size for hydrodeoxygenation of Benzyl phenyl ether over Pd-based catalysts 145

6.1 Introduction 146
6.2 Action of bare supports on BPE conversion..... 146
6.3 The competition between Pd and acidic sites for BPE conversion 149
6.5 Pressure and temperature effect for the conversion of BPE over $Pd/Nb_2O_{5\text{-col}}$..... 156
6.6 Conclusion 159
Chapter 7 Hydrodeoxygenation of phenethoxybenzene over Pd-based catalysts 161
7.1 Introduction 162
7.2 HDO of PEB over impregnated Pd catalysts..... 162
7.3 HDO of PEB over colloidal Pd catalysts..... 166
7.4 Conclusions 172
Chapter 8 Hydrodeoxygenation of diphenyl ether and typical model molecules of lignin over Pd-based catalysts 175
8.1 Introduction 176
8.2 DPE conversion over large Pd particles 176
8.3 Effect of support and metal particle size for DPE conversion 179
8.3 Conversion of typical monomers and dimers representative of lignin over $Pd/Nb_2O_{5\text{-col}}$.....182
8.4 Conclusions 190
Chapter 9 General conclusions and perspectives 191
9.1 Conclusions 192
9.2 Perspectives 196
References..... 197
Annexes..... 204
Annex 1 Typical chromatograms and mass spectra 205
Annex 2 Nitrogen adsorption-desorption isotherms..... 219
Annex 3 PDF data cards 224
Annex 4 Stem images and particle size distributions 232
Annex 5 Pore volume for the catalysts prepared by incipient wetness impregnation.. 235
Annex 6 Corresponding factor.....235

LIST OF FIGURES

Figure 2.1 Representation of a softwood and hardwood lignin structure……...25

Figure 2.2 Model molecules representative of lignin containing β-O-4, α-O-4, and 4-O-5 linkages…….……28

Figure 2.3 (a) Arrhenius plots [ln (TOF) vs 1/T] for three model molecules compounds. (b) Relationship between apparent activation energy and BDE for the three model compounds. Reaction conditions: H_2O, 6 bar of H_2, 57% Ni/SiO_2[24]…….29

Figure 2.4 Conversion and product distribution of PEB over Ru/C in water and 8 bar of H_2 as a function of temperature [25]…….30

Figure 2.5 Possible C-O-C cleavage of PEB over Ru/C…….30

Figure 2.6 Product distribution of PEB conversion over Ru/SZ in water as a function of temperature [27]…...……....32

Figure 2.7 Conversion of PEB over 20 % Ni/Hβ, under 40 bar H_2 in n-hexane[28]….33

Figure 2.8 Effect of temperature on DPE conversion over Pd-Ni/HZSM5. Reaction conditions: substrate (1mmol), 1Pd-10Ni/HZSM5, 20 bar of H_2, n-hexane. Adapted [29]…….……34

Figure 2.9 TOFs measured at 120°C for the conversion of model molecule representative of α-O-4, β-O-4, and 4-O-5 over Ni/SiO_2…….35

Figure 2.10 Conversion of PEB over Ni/Hβ at 220 °C, in n-hexane as solvent[28]…...36

Figure.2.11 Influence of hydrogen pressure for the conversion of PEB at 240 °C, over Ru/SZ [23] using water as solvent……37

Figure 2.12 Conversion of DPE and yield of products curves as a function of reaction time. Reaction conditions: substrate (1.70 g), 57 wt% Ni/SiO_2 (300 mg), 120°C, 6 and 40 bar of H_2, water…….37

Figure 2.13 Ionic and radical mechanism pathways for the conversion of BPE. V. Roberts et al [32]…….…….……..….40

Figure 2.14 Reaction pathway proposed by He et al.[31] for the conversion of BPE over Ni/SiO_2 at 250 °C and 40 bar of H_2 in water and undecane…….....43

Figure 2.15 Reaction pathway for BPE conversion over SAA catalysts……45

Figure 2.16 Conversion of BPE and yield of products curves as a function of reaction time. Reaction conditions: substrate (1mmol), CoMo/SZ (20mg), 300°C, 20 bar of H_2, decalin[14]……46

Figure 2.17 Conversion of BPE and yield of products curves as a function of reaction time[31]. Reaction conditions: substrate (9.20g, 0.010 mol), 10% Ni/HZSM5 (50mg), 250 °C, 40 bar of H_2, water……..……..49

Figure 2.18 (a) TEM images of Ni/SiO_2 catalysts prepared by the DP method, at different calcination temperatures. (b) TOF as a function of Ni particle size for C-O bond cleavage of PEB, at 120 °C under 6 bar H_2 in water.....58

Figure 2.19 Conversion of PEB and yield of products curves as a function of reaction time over Ru/C catalyst. Reaction conditions: substrate (1g), Ru/C (100mg), 240°C, 8 bar of H_2, water [25]….……59

Figure 2.20 Product distribution PEB conversion over Ni/C, Ru/C, and Pd/C catalysts. Reaction conditions: substrate (0.167 mmol), catalyst (25mg), 150°C, 20 bar of H_2, methanol……..60

Figure 2.21 (a) Product distribution of PEB over different Nb_2O_5 supported catalysts; (b) Conversion of PEB and selectivity of aromatics[26]…….62

Figure 2.22 (a) Conversion of PEB as a function of reaction time. Reaction Conditions: substrate (1mmol), CoMo/SZ (20 mg), 300 °C, 20 bar of H_2. (b) Reaction pathway for PEB conversion over CoMo/SZ[14]……..……..63

Figure 2.23 Conversion of PEB as a function of reaction time over (a) Ru/SZ and (b) Pd/SZ. Reaction conditions: substrate (1g), catalyst (20mg), 240°C, 8 bar of H_2, water……...64

Figure 2.24 Conversion of PEB over Ni/Hβ at 220 °C, 40 bar H_2 in n-hexane[28]…...66

Figure 2.25 Reaction mechanism proposed by Zhou et al[28] for the conversion of PEB over Ni/Hβ……67

Figure 2.26 Effect of silica/alumina ratio for PEB conversion over NiMoS-USY [44]. Products: Cycloalkanes: methyl cyclopentane, methylcyclohexane, and ethylcyclohexane; BTE: benzene, toluene, and ethylbenzene; mono/alkyl phenol: phenol, 3 and 4-ethylphenol, and m-cresol; phenolic dimers: 3 and 4-phenethylphenol; deoxygenated dimers were not specified…….....69

Figure 2.27 Reaction pathway of PEB over NiMoS-USY[44]……...69

Figure 2.28 (a) Product distributions and (b) reaction pathway for DPE conversion over Ni/SiO_2, at 120 °C, 6 bar H_2 in water……77

Figure 2.29 Reaction pathway for DPE conversion over Ru/C, at 120 °C, in isopropanol……...78

Figure 2.30 (a) Conversion of DPE and selectivity of products curves as a function of reaction time. Reaction conditions: substrate (0.8 mmol), Pt/C (5mg), 200 °C, 20 bar of H_2, water. (b) Reaction pathway proposed by Guvenatam et al [47]…….……..…81

Figure 2.31 Product distribution for DPE conversion over Pd/C in water[48]……82

Figure 2.32 Mechanistic pathway for the reductive hydrolysis of aryl ethers on Pd surface, proposed by Wang et al.[48] R=phenyl, cyclohexyl, phenylethyl, and n-butyl……..83

Figure 2.33 Product distribution as a function of DPE conversion over $5Co/CeO_2$ (A) and $0.01Ru1.99Co/CeO_2$ (B) at 200 °C and 20 bar H_2…….84

Figure 2.34 Conversion of DPE, the yield of products curves as a function of reaction time and the reaction pathways. Conditions reactions: substrate (1 mmol), CoMo/SZ (20mg), 300 °C, 20 bar of H_2, decalin[14]……86

Figure 2.35 Reaction pathway for the conversion of DPE over Ni/Nb_2O_5 at 220°C, 10 bar H_2 in isopropanol[53]……88

Figure 2.36 Product distribution for DPE conversion over Rh/Nb_2O_5 at 260 °C, 10 bar H_2 in *n*-decane[26]…….……..89

Figure 2.37 Product distribution for the conversion of DPE over $Ni/NbPO_4$ (a), $Ni/ZrNbPO_4$ (b), $Ni/ZrPO_4$ (c)[54]……...90

Figure 2.38 Product distribution as a function of time for DPE conversion of Ru/H-Beta[40]……....92

Figure 2.39 Reaction pathway for DPE conversion over Ru/H-Beta proposed by Yao et al [40]……...……92

Figure 2.40 Product distribution as a function of DPE conversion. Reaction conditions: substrate (1mmol), 1Pd-10Ni/HZSM5 (100 mg), *n*-hexane, 220°C, 20 bar H_2[29]…….……95

Figure 3.1 Autoclave Parr Reactor……...110

Figure 3.2 Example of GC-FID chromatogram for the products obtained after reaction……...112

Figure 4.1 XRD patterns of support (a) and Pd-based catalysts: impregnated catalysts (b) and colloidal catalysts (c). (▼) HZSM5, (◊) ZrO_2 tetragonal, (♠) ZrO_2 monoclinic (▽) γ-Al_2O_3, (O) Anatase, (•) Rutile (❖) Pd……117

Figure 4.2 NH_3-TPD profiles for supported Pd catalysts: (a) impregnated catalysts, (b) colloidal catalysts…….121

Figure 4.3 Infrared spectrum of adsorbed pyridine on Pd-based catalysts at 150 °C. (a) impregnated catalysts, (b) colloidal catalysts……122

Figure 4.4 TEM image and particle size distribution for (a-b) Pd/$Nb_2O_{5\text{-imp}}$ and (c-d) Pd/$Nb_2O_{5\text{-col}}$……125

Figure 4.5 XRD patterns of supports and Ru-based catalysts. (▼) HZSM5, (♣) Ru……...125

Figure 4.6 TPR profiles of ruthenium-supported catalysts……..126

Figure 4.7 Acidic properties of Ru/HZSM5 (a) NH_3-TPD profiles (b) Infrared spectrum of adsorbed pyridine……127

Figure 4.8 TEM images and particle size distribution for (a-b) Ru/$SiO_{2\text{-imp}}$ and (c-d) Ru/$HZSM5_{\text{-imp}}$……128

Figure 6.1 Yield to different products as a function of BPE conversion. Reaction condition: 62 mmol BPE, 15 mL decalin, Pd/HZSM5 (15 – 75 mg), 230 °C, 18 bar of H_2 in decalin, 3h…….150

Figure 6.2 Conversion of BPE and product distribution at different H_2 pressures over Pd/$Nb_2O_{5\text{-col}}$ catalyst. Reaction conditions: Reactant (62 mmol), decalin (15 ml), Pd/$Nb_2O_{5\text{-col}}$ (30 mg), 230 °C, 3h…….157

Figure 6.3 Conversion of BPE and product distribution at different reaction temperatures over $Pd/Nb_2O_{5\text{-col}}$ catalyst. Reaction conditions: Reactant (62 mmol), decalin (15 ml), $Pd/Nb_2O_{5\text{-col}}$ (30 mg), 18 bar H_2, 3h.)……158

Figure 7.1 Product distribution as a function of time for the conversion of PEB over $Pd/Nb_2O_{5\text{-imp}}$……...165

Figure 7.2 Product distribution as a function of PEB conversion over $Pd/TiO_{2\text{-col}}$……168

Figure 7.3 Product distribution as a function of PEB conversion over $Pd/Nb_2O_{5\text{-col}}$……169

Figure 8.1 Comparison between the assistance of Lewis and Bronsted acid sites of support in the reaction pathway……..181

LIST OF SCHEMES

Scheme 2.1 Reaction pathways for the conversion of BPE over different catalysts presented in the literature…….53

Scheme 2.2 Reaction pathways for the conversion of PEB over different catalysts….72

Scheme 2.3 Reaction pathways for DPE conversion proposed by the literature…….100

Scheme 5.1 Reaction route for BPE conversion over Pd and Ru-based catalysts….135

Scheme 5.2 Reaction route for PEB conversion over Pd and Ru-based catalysts.....138

Scheme 5.3 Reaction route for DPE conversion over Pd and Ru-based catalysts….142

Scheme 6.1 Reaction pathways for the conversion of BPE over supported Pd catalysts……..155

Scheme 7.1 Reaction pathways for the conversion of PEB over supported Pd catalysts……..173

Scheme 8.1 Reaction pathways for the conversion of DPE over impregnated catalysts……..177

Scheme 8.2 Reaction pathways for the conversion of DPE over colloidal catalysts……..179

Scheme 8.3 Hydrodeoxygenation of phenol over $Pd/Nb_2O_{5\text{-col}}$…….……183

Scheme 8.4 Hydrodeoxygenation of anisole proposed by the literature[83-85]……..185

Scheme 8.5 Hydrodeoxygenation of guaiacol over $Pd/Nb_2O_{5\text{-col}}$……...186

Scheme 8.6 Hydrodeoxygenation of 4-propylphenol over $Pd/Nb_2O_{5\text{-col}}$……187

Scheme 8.7 Hydrodeoxygenation of 2,3-dihydrobenzofuran over $Pd/Nb_2O_{5\text{-col}}$…...189

LIST OF TABLES

Table 2.1 Common linkages and their approximate abundance in softwood and hardwood…….25

Table 2.2 Physical properties and elemental composition of bio-oil and crude oil. Adapted from [17]……...27

Table 2.3 Effect of temperature in the conversion of PEB under 10 bar H_2 in *n*-decane……...……31

Table 2.4 Effect of pressure on DPE conversion over Pd-Ni/HZSM5. Reaction conditions: substrate (1 mmol), 1Pd-10Ni/HZSM5 (200 mg), 220°C, *n*-hexane……..38

Table 2.5 Products of the hydrogenolysis of DPE conducted in different solvents on Raney Ni. Reaction conditions: substrate (2.9 mmol), Raney Ni (100mg), 90 °C, 50 bar of H_2……41

Table 2.6 Catalytic performance of SA, AA, and SAA catalysts for the conversion of BPE at 100°C under 5 bar H_2 in *n*-decane……...……45

Table 2.7 Product distribution for the conversion of BPE over CoZn/Off Al H-beta under 40 bar of H_2 in methanol…….51

Table 2.8 Catalysts and reaction conditions reported in the literature for the conversion of BPE……54

Table 2.9 Initial rate of reaction, TOF, and total acidity for PEB……70

Table 2.10 Catalysts and reaction conditions reported in the literature for the conversion of PEB……73

Table 2.11 Product distribution for the conversion of DPE over Ru, Pt, and Pd-supported on activated carbon……..78

Table 2.12 Product distribution for DPE conversion over Ru, Pt, and Pd-supported on activated carbon, methanol, and 5 bar H_2…….80

Table 2.13 Products selectivity for the conversion of DPE over Pd/C, Pt/C, and Ni/SiO_2…….81

Table 2.14 Product distribution for DPE conversion over Ni-base catalysts…….86

Table 2.15 Conversion of DPE over Cu/Nb_2O_5, Co/Nb_2O_5, and Ni/Nb_2O_5 at 220°C, 10 bar H_2 in isopropanol……...……88

Table 2.16 Product distribution for DPE conversion over different catalysts[35]…….91

Table 2.17 Conversion of DPE over different catalysts at 220°C, 20 bar of H_2, and n-hexane as a solvent……...94

Table 2.18 Reaction conditions and catalysts used for the conversion of DPE presented in the literature…….97

Table 3.1 List of commercial products used…….....109

Table 3.2 GC analytical methods parameters…….111

Table 4.1 Pd content, specific surface area, pore volume, particle size, and disperse on of palladium-supported catalysts……...115

Table 4.2 Total amount of ammonia desorbed, acidic sites strength distribution, and concentration of Lewis and Brønsted acidic sites for palladium-based catalysts……..120

Table 4.3 Pd content, specific surface area, pore volume, particle size, and dispersion of palladium-supported catalysts……...……..…125

Table 4.4 Total amount of ammonia desorbed, acidic sites strength distribution, and concentration of Lewis and Brønsted acid sites for ruthenium-based catalysts…….……127

Table 5.1 Conversion of BPE, mass balance, and product distribution for Ru and Pd-based catalysts…….……..…131

Table 5.2 Conversion of PEB, mass balance, and product distribution for Ru and Pd-based catalysts……..136

Table 5.3 Conversion of DPE, mass balance, and product distribution for Ru and Pd-based catalysts……..139

Table 6.1 Conversion of BPE, mass balance, and product distribution for supports and impregnated Pd catalysts…….146

Table 6.2 Conversion of BPE, mass balance, and product distribution using catalysts prepared by the colloidal method……152

Table 7.1 Conversion of PEB, mass balance, and product distribution for supports and impregnated catalysts……...162

Table.7.2 Conversion of PEB, mass balance, and product distribution for colloidal catalysts……..166

Table 8.1 Conversion of DPE, mass balance, and product distribution for impregnated catalysts…….176

Table 8.2 Conversion of DPE, mass balance, and product distribution for colloidal catalysts……..178

Table 8.3 HDO of model molecules compounds representative of lignin over Pd/Nb_2O_5-$_{col}$……...182

Abstract

The present thesis aims at studying the role of the support and metal particle size on the hydrodeoxygenation reactions (HDO) of benzyl phenyl ether (BPE), phenethoxybenzene (PEB), and diphenyl ether (DPE) chosen as model molecules representative of the main ether linkages present in the lignocellulosic biomass. The reactions were carried out in the liquid phase at 230 °C and 18 bar of H_2. Pd-supported on different oxides (SiO_2, TiO_2, Nb_2O_5, Al_2O_3, ZrO_2, and HZSM5) were synthesized by incipient wetness impregnation and deposition of metal particles prepared by the colloidal method. The acidic sites of the support promote the cracking of the C-O ether bond of BPE, but for PEB and DPE, this effect is less pronounced due to the higher energy required to break these linkages. The hydrogenolysis of the C-O ether bond takes place on the metallic Pd particles, producing the respective arenes. However, the Pd particle size can directly affect the product distribution after C-O cleavage. Due to the larger Pd particle size, impregnated catalysts favor the hydrogenolysis and exhibit a higher selectivity to alkylated products, whereas a smaller Pd particle size, obtained for catalysts prepared by the colloidal route, increases the selectivity to deoxygenated products. Over these catalysts, the formation of alkylated products is suppressed, but the hydrogenation of BPE, PEB, and DPE aromatic rings occurs in parallel to hydrogenolysis also promoted by Pd particles. The performance of Ru-based catalysts was also evaluated in the same reaction conditions. In the presence of Ru, alkylated products are produced even in the absence of acidic sites.

Keywords: Hydrodeoxygenation; Hydrogenolysis; Alkylation; Ether linkage

Résumé

Cette thèse a pour but d'étudier le rôle du support et de la taille des particules métalliques sur les réactions d'hydrodésoxygénation (HDO) du benzyl phényl éther (BPE), du phenethoxybenzène (PEB) et du diphényl éther (DPE) choisis comme molécules modèles représentatives des principales liaisons éther présentes dans la biomasse lignocellulosique. Les réactions ont été réalisées en phase liquide à 230 °C et sous 18 bar de H_2. Les catalyseurs au Pd supporté sur différents oxydes (SiO_2, TiO_2, Nb_2O_5, Al_2O_3, ZrO_2 et HZSM5) ont été synthétisés par imprégnation par voie humide et par dépôt de particules métalliques préparées par voie colloïdale. Les sites acides du support favorisent le craquage de la liaison éther C-O du BPE mais pour le PEB et le DPE, cet effet est moins prononcé en raison de l'énergie plus élevée requise pour rompre ces liaisons. L'hydrogénolyse de la liaison éther C-O a lieu sur les particules de Pd métallique, produisant les arènes respectifs. Cependant, la taille des particules de Pd peut directement affecter la distribution des produits après le clivage de la liaison C-O. En raison de la taille plus importante des particules de Pd, les catalyseurs imprégnés favorisent l'hydrogénolyse et présentent une sélectivité plus élevée pour les produits alkylés, tandis que la taille plus petite des particules de Pd, obtenue pour les catalyseurs préparés par voie colloïdale, augmente la sélectivité pour les produits désoxygénés. Sur ces catalyseurs, la formation de produits alkylés est supprimée, mais l'hydrogénation du cycle aromatique des BPE, PEB et DPE se produit parallèlement à l'hydrogénolyse, également favorisée par les particules de Pd. La performance des catalyseurs à base de Ru a également été évaluée dans les mêmes conditions de réaction. En présence de Ru, des produits alkylés ont été produits même en l'absence de sites acides.

Mots clés : Hydrodésoxygénation ; Hydrogénolyse ; Alkylation ; Liaison éther

Chapter 1
Introduction

1.1. INTRODUCTION

As a result of the decline of fuel reserves and the rise of environmental concerns about the use of fossil-based energy, several government targets have been established to increase the internal production of energy and chemicals from renewable sources like biomass [1,2].

The lignocellulosic biomass is an abundant, non-edible, and renewable resource for the production of high-value-added chemicals and fuels in future biorefineries[1,3,4]. Lignin, one of the most abundant components of lignocellulosic biomass, has limited application due to its complex structure [5]. According to the International Lignin Institute (ILI), more than 40 million tons of lignin are annually produced. Approximately 2% of industrial lignin is commercially used, while the rest is burnt for heat generation through combustion. However, there is an enormous potential market for value-added chemicals and fuels from lignin [6].

The bio-oil produced from the fast pyrolysis of lignocellulosic biomass has been considered a potential alternative source for petroleum-based fuel and the chemical industry [7]. However, due to its low calorific power, high acidity, and high oxygen content, the bio-oil is chemically and thermally unstable. Then, to be used as a fuel, bio-oil must be upgraded [8–10].

The hydrodeoxygenation (HDO) process is a promising technology for improving the quality of bio-oil [11,12]. Meanwhile, due to the complexity and the variety of molecules in the bio-oil, model molecules representative of the different C-C and C-O bonds are commonly used to enable the understanding of the mechanism of HDO. The main C-O and C-C bonds present in lignin are the β-O-4, 4-O-5, α-O-4, 5-5, and β-5 linkages.

The conversion of benzyl phenyl ether (BPE), phenethoxybenzene (PEB), and diphenyl ether (DPE), typical model molecules representative of the α-O-4, β-O-4, and

4-O-5 ether linkages, respectively, has been studied in the literature under different reaction conditions. In summary, metals such as Ni, Ru, Pt, and Pd-supported on non-acidic or acidic supports are considered promising for the HDO reactions of aryl dimeric ethers. However, the mechanism of cleavage of the α-O-4, β-O-4, and 4-O-5 ether bonds, and the extent of competition of this hydrogenolysis reaction with parallel reactions of hydrogenation and alkylation, are still under debate. How do the metal properties affect the HDO reactions? How can the properties of the support affect the conversion of model molecules representative of lignin? Which support properties are required to increase the HDO activity with respect to the parallel routes?

Therefore, this thesis aims at investigating the role of the support as well as the type of metal in the mechanism of cleavage of dimeric aryl ethers representing α-O-4, β-O-4, and 4-O-5 ether linkages, in the liquid phase. The influence of the type of metal and acidic sites will initially be studied using Pd and Ru-supported on SiO_2 and HZSM5. Then, in order to evaluate the influence of metal properties and type of support, a systematic study will be performed by preparing Pd catalysts through two different methodologies (incipient wetness impregnation and deposition of particles prepared by a colloidal method). Different oxides (SiO_2, TiO_2, Nb_2O_5, Al_2O_3, ZrO_2, and HZSM5) will be used as supports with various acidity and acidic sites (Lewis and Brønsted). Among these catalysts, the performance of an active catalyst, $Pd/Nb_2O_{5\text{-col}}$, will be especially evaluated in the HDO of phenolic monomers and dimers representative of lignin.

1.2. THESIS STRUCTURE

This doctoral thesis is divided into 8 chapters, as described below:

Chapter 2 – Literature Review

An overview of the reaction conditions and catalysts used in the hydrodeoxygenation of model molecules representative of the main ether linkages present in lignin structure (α-O-4, β-O-4, and 4-O-5).

Chapter 3 – Experimental Procedure

The description of catalyst preparation, characterization procedures, and catalytic reactions performed in this thesis.

Chapter 4 – Catalysts characterization

The results and discussion of the characterization of the catalysts used in this thesis.

Chapter 5 – Conversion of phenolic dimers over supported Ru and Pd-based catalysts

The effectiveness of Pd and Ru-supported over SiO_2 and HZSM5 is compared for the HDO of benzyl phenyl ether, phenethoxybenzene, and diphenyl ether at 230 °C, under 18 bar of H_2 in decalin.

Chapter 6 - Effect of support and metal particle size for the hydrodeoxygenation of benzyl phenyl ether over Pd-based catalysts

A series of Pd-based catalysts supported on different oxides (SiO_2, TiO_2, Nb_2O_5, Al_2O_3, and HZSM5) and with different Pd particle size is used for the HDO of benzyl phenyl ether at 230 °C, under 18 bar of H_2, in decalin as a solvent. In addition, the effect of temperature and pressure on the HDO reaction is also evaluated.

Chapter 7 – Hydrodeoxygenation of phenethoxybenzene over Pd-based catalysts

The HDO of phenethoxybenzene is studied over Pd-supported catalysts at 230 °C, under 18 bar of H_2, in decalin as a solvent.

Chapter 8 – Hydrodeoxygenation of diphenyl ether and typical model molecules of lignin over Pd-based catalysts.

The HDO of diphenyl ether is studied over Pd-supported catalysts in the same reaction conditions used for the former molecules (230 °C, 18 bar of H_2 in decalin). In addition, the HDO of other phenolic monomers and dimers representative of lignin was studied.

Chapter 9 – General conclusion and perspectives

The main conclusions from all chapters are presented, as well as suggestions for future work.

Chapter 2
Literature review

2.1 LIGNOCELLULOSIC BIOMASS

Biomass is considered to be the fourth largest energy resource and the only renewable carbon source available worldwide [2]. According to its use, biomass can be classified into two categories: edible and non-edible. The edible biomass consists of starch sugar crops and oil seed vegetable plants, while non-edible biomass, also known as lignocellulosic or second-generation biomass, involves agricultural, forest, and municipal waste material [8].

The production of first-generation bio-fuel as bio-ethanol and bio-diesel, is currently obtained from starch and sugar feedstock (edible biomass). However, their production is limited and competes with food supplies. In this context, the production of biofuels from non-edible biomass has been considered a potential feedstock for the renewable production of fuels, chemicals, and energy [1,13].

The lignocellulosic biomass is composed mainly of three biopolymers: cellulose (40-50%), hemicellulose (25-35%), and lignin (15-20%) [1,5]. Cellulose is constituted by units of glucose linked by β-glycosidic bonds. Hemicellulose is composed of sugars with 5 and 6 carbons such as D-xylose, D-galactose, D-arabinose, and D-glucose. Lignin is the most complex fraction composed by propyl-phenyl units substituted with hydroxyl and methoxy radicals[1,8]. Currently, cellulose and hemicellulose are widely used for the production of bioethanol and other chemical products, whereas lignin has limited application due to its complex structure, which makes its depolymerization difficult [13]. Approximately 2% of industrial lignin is commercially used while the rest is burnt for heat generation through combustion [14]

Lignin is an amorphous polymer consisting of three monolignols: p-coumaryl, coniferyl, and sinapyl alcohol, Fig 2.1. The composition and amount of lignin vary according to the type of biomass, but generally, softwoods have more lignin than

hardwoods and grasses [13]. Table 2.1 lists the main C-O and C-C linkages present in the softwood and hardwood. As it can be observed, the β-O-4 ether bond is the most predominant linkage in the lignin structure of both kinds of wood, and consequently the most abundant among the three ether linkages [2,13,15].

Table 2.1: Common linkages and their approximate abundance in softwood and hardwood

Linkage	β-O-4	5-5	β-5	4-O-5	β-1	β-β	α-O-4	Ref.
Softwood (Spruce)	43-60%	19-22%	9-12%	4-7%	7-9%	2-4%	-	13
Softwood (Spruce)	43-50%	10-25%	9-12%	4%	3-7%	2-4%	6-8%	2
Hardwood (Birch)	60%	9%	6%	6.5%	7%	-	-	13
Hardwood (*Eucalyptus globulus*)	50-65%	4-10%	4-6%	4%	5-7%	3-7%	4-8%	2

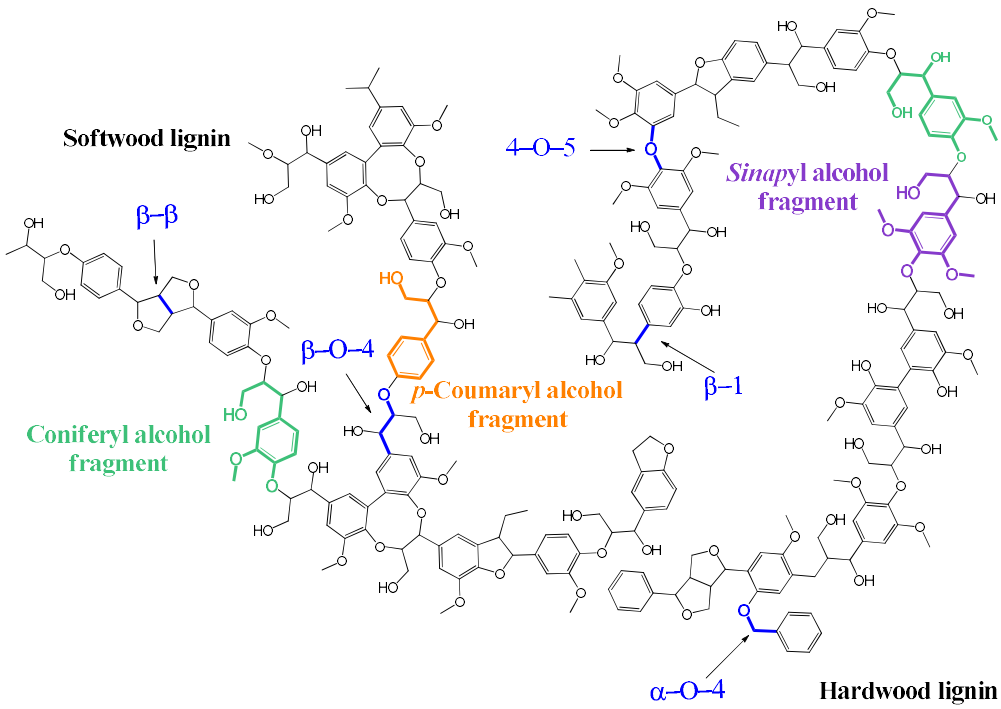

Figure 2.1: Representation of a softwood and hardwood lignin structure.

2.2 BIO-OIL OIL FROM LIGNOCELLULOSIC BIOMASS

Lignocellulosic biomass can be depolymerized by different technologies for the production of fuels and chemicals such as fast pyrolysis [10,16]. In this thermal process, biomass is heated at moderate temperatures (400-600°C) at atmospheric pressure, which, in the absence of oxygen, produces volatile species and a solid material collected as biochar. A portion of the volatiles present in the gas phase condenses into a viscous, polar, and dark-brown liquid, termed bio-oil. Process conditions and feedstock can vary, directly affecting the composition of the bio-oil obtained from fast pyrolysis, but in general, the bio-oil is a complex mixture of acids, aldehydes, alcohols, esters, sugars, phenol, and phenol derivatives [8,12].

Table 2.2 shows a comparison of the bio-oil from fast pyrolysis and the crude oil from a petroleum refinery, in terms of physical properties and elemental composition. Compared to crude oil, bio-oil contains a high amount of water (> 15 %), which makes it immiscible with petro-fuels. The presence of organic compounds whose density is higher than water leads to phase separation and confers a high viscosity to bio-oil. The presence of organic acids also confers a high acidity (pH 2-4), which can increase the risk of corrosion. Due to the high oxygen content, bio-oil is thermally and chemically unstable. Condensation and polymerization reactions between the oxygenated compounds can occur, further increasing the bio-oil viscosity. In addition, the oxygenated compounds are also responsible for the low calorific power (16-20 MJ/kg) compared to crude oil (44 MJ/kg). Then, bio-oil must be upgraded to be used directly as a fuel or mixed with crude oil [8,17].

Table 2.2: Physical properties and elemental composition of bio-oil and crude oil. Adapted from [17].

	Bio-oil	**Crude oil**
Water (%)	15-30	0.1
pH	2.8 – 3.8	-
Density (kg/ L)	1.05 – 1.25	0.86
μ50ºC (cP)	40 – 100	180
HHV (MJ/ kg)	16 – 19	44
C (%)	55 – 65	83 – 86
H (%)	5 – 7	11 – 14
O (%)	28 – 40	< 1
S (%)	< 0.05	< 4
N (%)	< 0.4	< 1

2.3 HYDRODEOXYGENATION OF BIO-OIL

Several studies have highlighted that the most effective process for improving the quality of bio-oil is the hydrodeoxygenation (HDO) reaction, which aims at removing the oxygen to produce hydrocarbons, Eq. 2.1. In this process, high hydrogen pressure (1-200 bar) and temperatures (200-450°C) are often used, in the presence of heterogeneous catalysts [1,12,16,18–23].

$$R - OH + H_2 \rightarrow R - H + H_2O \qquad \text{(Eq. 2.1)}$$

The quality of the final product is commonly evaluated by its O/C and H/C ratio; a high H/C ratio indicates a high quality of liquid products. Thus, the key to HDO reactions is to select and design a catalyst with which to achieve high oxygen removal with minimum hydrogen consumption.

2.4 HDO OF MODEL MOLECULES REPRESENTATIVE OF LIGNIN

Due to the complexity and the variety of molecules present in bio-oil, the HDO of model molecules, phenolic and/or benzylic dimeric ethers considered to represent linkages in lignin, is commonly used.

The metal choice as well as the support selection strongly affects the product distribution in the conversion of these model molecules. Two main successive steps for the HDO reaction take place in the metal sites: (i) hydrogenolysis of the C-O ether bond and (ii) hydrogenation of functional groups and/or of intermediates formed after cleavage. On the other hand, dehydration, isomerization, and hydrolysis, an alternative route to hydrogenolysis, involve acidic sites [23].

In the next sections, it is carried out an overview of the catalysts (metals and supports) and of the reaction conditions used for the conversion of aryl dimeric ethers, principally: benzyl phenyl ether (BPE) (α-O-4), phenethoxybenzene (PEB) (β-O-4), and diphenyl ether (DPE) (4-O-5), Fig 2.2.

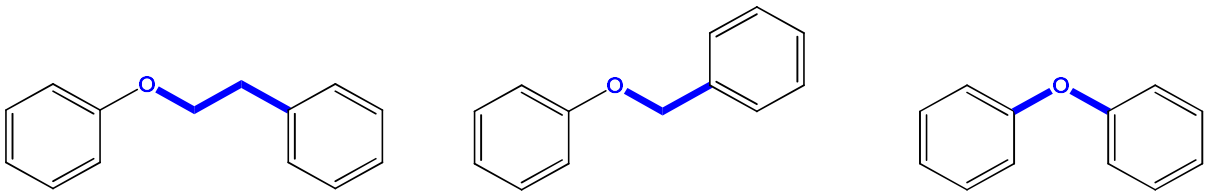

Phenethoxybenzene **(PEB)** (β–O–4) | Benzyl phenyl ether **(BPE)** (α–O–4) | Dyphenyl ether **(DPE)** (4–O–5)

Figure 2.2: Model molecules representative of lignin-containing β-O-4, α-O-4, and 4-O-5 linkages.

2.4.1 The effect of reaction conditions

2.4.1.1 Temperature

The 4-O-5 aryl ether bond (bond dissociation energy (BDE)= 314 kJ.mol^{-1}) is stronger than the β-O-4 (BDE = 289 kJ.mol^{-1}), and α-O-4 (BDE = 218 kJ.mol^{-1}) aliphatic bonds. The apparent activation energy follows the order: 97 kJ/mol (4-O-5) > 86 kJ/mol (β-O-4) > 72 kJ/mol (α-O-4) (Fig 2.3) [24]. Therefore, it is expected that the cleavage of the weaker aliphatic ether bonds (α-O-4 and β-O-4) is favored. However, the TOF calculated at 120 °C for the hydrogenolysis of DPE (4-O-5; TOF = 26 mol.mol $_{ni(suf)}^{-1}$.h^{-1}) was found to be higher than the TOF for the hydrogenolysis of PEB (β-O-4; TOF = 13 mol.mol $_{ni(suf)}^{-1}$.h^{-1}). He et al.[24] attributed this result to the different C-O bond cleavage mechanisms for 4-O-5, β-O-4, and α-O-4 bonds. The C-O bond cleavage for PEB (β-O-4) and BPE (α-O-4) proceeded by hydrogenolysis on the metal particles, whereas the C-O bond cleavage of DPE (4-O-5) occurred by hydrogenolysis and hydrolysis, which increased the conversion.

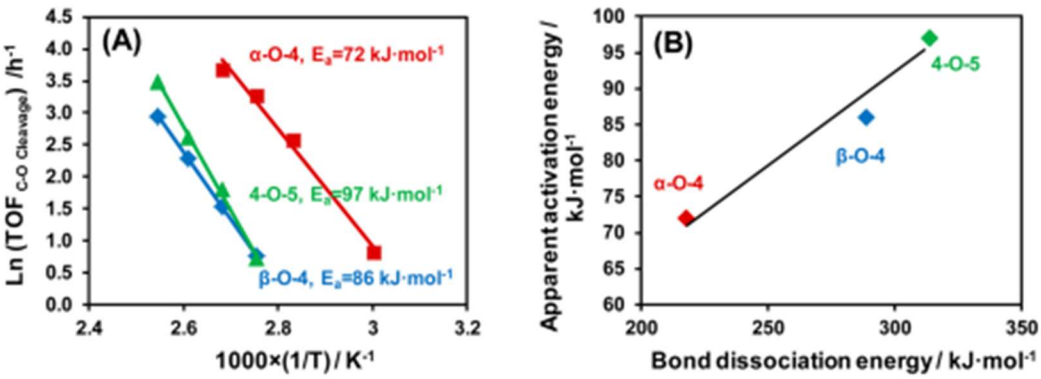

Figure 2.3: (a) Arrhenius plots [ln (TOF) vs 1/T] for three model molecules compounds. (b) Relationship between apparent activation energy and BDE for the three model compounds. Reaction conditions: H_2O, 6 bar of H_2, 57% Ni/SiO_2.

Luo and Zhao [25] evaluated the influence of reaction temperature for the conversion of PEB (molecule representative of the β-O-4 linkage) over Ru/C under 8 bar of H_2 and

water as a solvent. At low temperature (180 °C), the main products were ethylbenzene, phenol, and phenylethanol, with minor amounts of benzene, cyclohexane, and cyclohexanone (Fig. 2.4). This result suggests that PEB can be both converted into ethylbenzene and phenol by the cleavage of the C_{aliph}-O bond, or into phenylethanol and benzene by hydrogenolysis of the C_{arom}-O bond of PEB (Fig. 2.5). In addition, the partial and full hydrogenation of the PEB aromatic rings was also observed at low temperature (20 %). When increasing the temperature to 240 °C, the cleavage of the C_{aliph}-O bond was favored, whereas the formation of partial and full hydrogenation products was suppressed. Therefore, at low temperature, the hydrogenolysis and hydrogenation reactions of PEB co-existed, but upon increasing the temperature, the hydrogenolysis of the C_{aliph}-O bond became the main pathway.

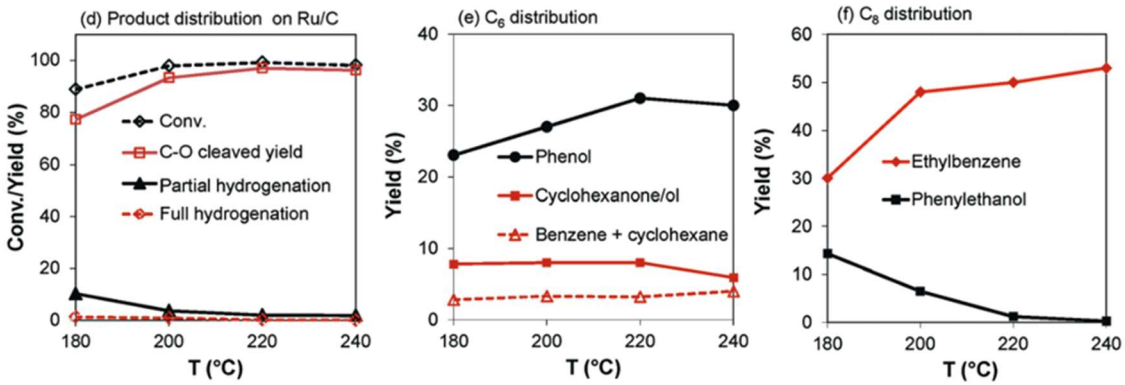

Figure 2.4: Conversion and product distribution of PEB over Ru/C in water and 8 bar of H_2 as a function of temperature [25].

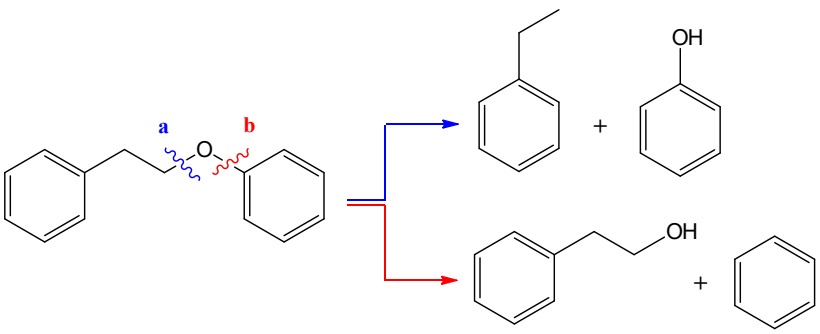

Figure 2.5: Possible C-O-C cleavage of PEB over Ru/C.

Guan et al.[26] studied the conversion of PEB over Rh/Nb_2O_5 as a function of temperature under 10 bar H_2 in dodecane as solvent. The results are presented in Table 2.3. The authors observed that the increase of temperature from 220 to 300 °C gradually decreased the formation of hydrogenated products (cyclohexane and ethylcyclohexane), while the selectivity to aromatics (benzene and ethylbenzene) increased. Furthermore, since the authors reported that there was no formation of cyclohexanone/cyclohexanol in the reaction, it can be assumed that the temperature increase also favored the direct hydrogenolysis of phenol to produce benzene.

Table 2.3: Effect of temperature in the conversion of PEB under 10 bar H_2 in *n*-decane.

		Selectivity (%)					
Temp. (°C)	**Conv. (%)**	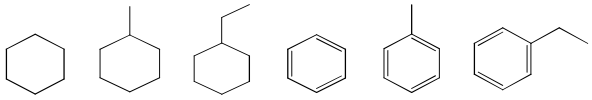					
220	100	33.1	1.4	22.4	5.7	7.1	30.3
260	99	12.1	0.5	3.9	27.9	4.1	50.6
300	100	8.9	0.4	5.2	58.7	4	22.3

Luo et al. [27] evaluated the conversion of PEB over Ru/SZ (sulfated zirconia) under 8 bar of H_2 in water, in a range of temperature from 120 to 260 °C. At low temperatures (120-180 °C), the main products were cyclohexanol/cyclohexanone, phenol, and ethylbenzene, indicating that the hydrogenolysis of the C_{aliph}-O bond of PEB and the hydrogenation of the resulting products both occurred (Fig 2.6). When increasing the temperature (up to 260 °C), the main products were benzene and ethylbenzene, which indicates that the mere hydrogenolysis of PEB occurred as the main pathway. Therefore, the hydrogenolysis and hydrogenation reactions co-existed at low temperatures (120-200 °C), but when increasing the temperature from 200 to 260 °C, the hydrogenolysis was the

main reaction pathway. The competition between the hydrogenolysis and hydrogenation reactions as a function of temperature was explained by the concentration and the strength of adsorbed H species. According to the authors, at low temperatures, the concentration of adsorbed H species is high and then, hydrogenolysis and hydrogenation take place. When increasing the temperature, the H species adsorbed near benzene desorb faster than the H adsorbed close to the oxygen atom of the PEB molecule, which favors the hydrogenolysis reaction.

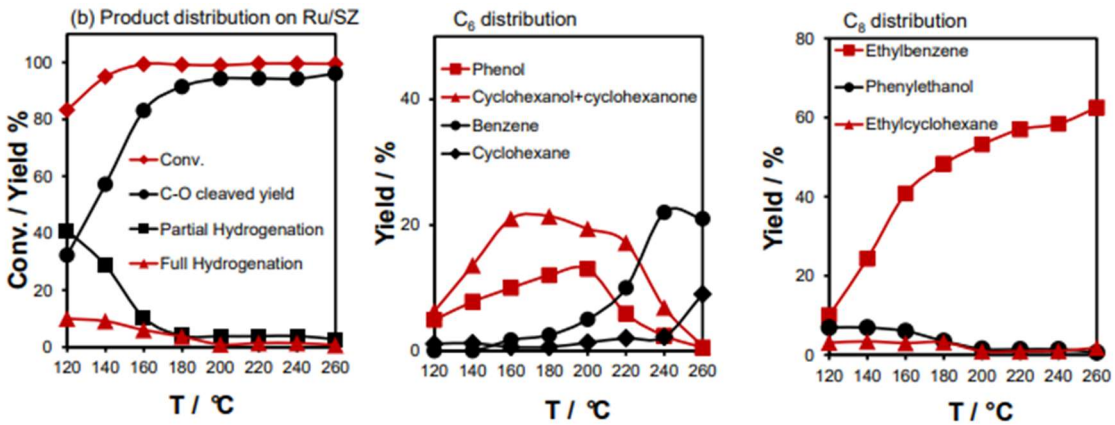

Figure 2.6: Product distribution of PEB conversion over Ru/SZ in water as a function of temperature [27].

The influence of reaction temperature for the PEB conversion was also studied over 20 wt.% Ni/Hβ [28] under 40 bar H_2, in n-hexane as solvent (Fig 2.7). At low temperatures (< 140 °C), the hydrogenation of the PEB aromatic rings was predominant concerning the production of cyclohexane and ethylcyclohexane, indicating that the hydrogenolysis of PEB hydrogenated products was difficult at a temperature lower than 140 °C. As the temperature increased from 140 °C to 220 °C, cyclohexane and ethylcyclohexane became the main products, while the yield of PEB hydrogenated products decreased to zero. However, the increase in temperature from 220 °C to 280 °C decreased the PEB conversion and the total selectivity to cyclohexane and

ethylcyclohexane. This was attributed to the agglomeration of nickel particles which can inhibit the partial and full hydrogenation of PEB, and consequently decrease PEB conversion. Therefore, the partial and full hydrogenation of PEB aromatic rings was considered by the authors as key to understanding the conversion of PEB into cyclohexane and ethylcyclohexane. Finally, the temperature rises also increased the yield of 1,2-dicyclohexylethane, indicating that the rearrangement of PEB was promoted at high temperature.

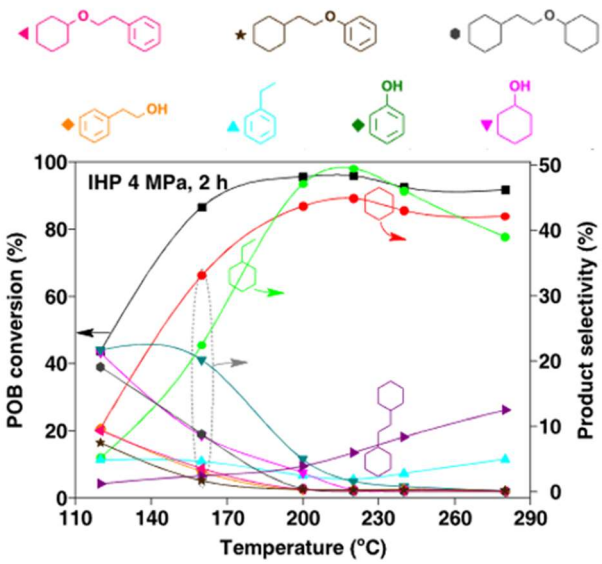

Figure 2.7: Conversion of PEB over 20 % Ni/Hβ, under 40 bar H_2 in n-hexane [28].

Zhao et al.[29] investigated the effect of reaction temperature on the conversion of DPE (a typical model molecule of 4-O-5 linkage) over palladium and nickel supported over HZSM5 in n-hexane at 20 bar of H_2 (Fig. 2.8). At 120 °C, the conversion of DPE was 11.1% and the products formed were cyclohexane, cyclohexanol, cyclohexyl phenyl ether, and dicyclohexyl ether. When increasing the temperature from 120 to 220 °C, the conversion of DPE increased to 100% and the only product formed was cyclohexane. The authors proposed that the selectivity for deoxygenated products was favored at high

temperatures. Additionally, increasing the temperature inhibited the partial and complete hydrogenation of DPE.

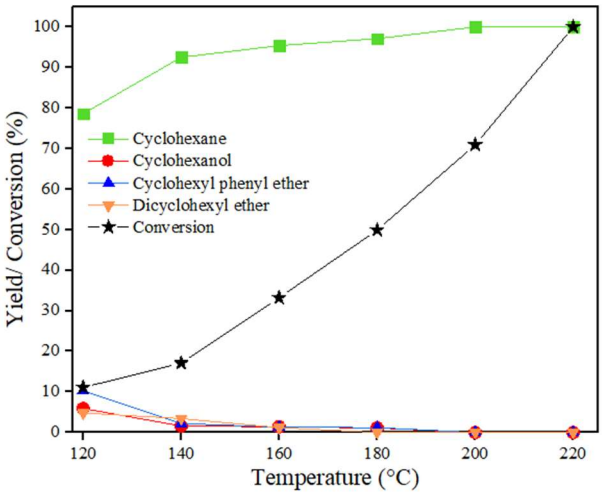

Figure 2.8: Effect of temperature on DPE conversion over Pd-Ni/HZSM5. Reaction conditions: substrate (1mmol), 1Pd-10Ni/HZSM5, 20 bar of H_2, *n*-hexane. Adapted [29].

Globally speaking, these studies reveal that at low reaction temperature, the hydrogenolysis of the C-O bond and full/partial hydrogenation reactions can coexist. However, when increasing the temperature, the hydrogenolysis of the C-O bond of the dimer molecule appears as the main reaction pathway, and parallel or subsequent hydrogenation reactions seem to be more difficult.

2.4.1.2 Pressure

He et al.[24] investigated the impact of the hydrogen pressure on the conversion of model molecules representative of α-O-4, β-O-4, and 4-O-5 linkages (BPE, 2-phenylethyl phenyl ether, and DPE) in H_2O, at 120 °C, over Ni/SiO_2 (Fig. 2.9). There is no reaction in the absence of H_2, regardless of the molecule. When increasing the hydrogen pressure up to 6 and 10 bar, the rate of cleavage of the β-O-4 and 4-O-5 bonds increased. A further

increase in the pressure decreased the reaction rate. This indicates that hydrogen and the substrate compete for the active sites at high pressure. In contrast, the rate of the C-O cleavage of the molecule representative of the α-O-4 linkage continuously increased with the pressure of H_2 up to 80 bar. This is due to the higher rate of cleavage of the C-O bond in α-O-4. In this case, the product desorption is reported to be the rate-determining step. A higher H_2 pressure promotes the product removal and, consequently, the reaction rate. In contrast, at 100 bar, the TOF of C−O bond cleavage of α-O-4 decreased, which was attributed to the now-existing adsorption competition between the reactant and hydrogen on metallic sites.

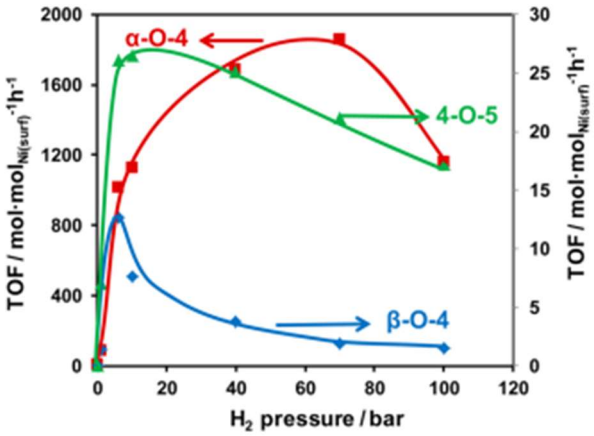

Figure 2.9: TOFs measured at 120°C for the conversion of model molecule representative of α-O-4, β-O-4, and 4-O-5 over Ni/SiO_2.

The effect of hydrogen pressure on the conversion of PEB was studied by Zhou et al.[28] over 20 wt.% Ni/Hβ, at 220 °C in *n*-hexane (Fig. 2.10). Under 10 bar of H_2 16 % of PEB was mainly converted into 2-phenethylphenol (42.8 %), ethylbenzene (26.2 %), phenol (14.4 %), and cyclohexane (10.3 %). It can be noted that phenol was partially converted to cyclohexane, but ethylbenzene was not transformed into ethylcyclohexane. When increasing the pressure up to 40 bar, the PEB conversion strongly increased, the yield of ethylbenzene and phenol decreased, while the cyclohexane and ethylcyclohexane

yield greatly increased. In addition, as the pressure increased, the yield of 2-phenethylphenol decreased progressively to zero, while the (2-cyclohexylethyl) benzene, intermediate for the conversion of 2-phenylethanol to 1,2-dicyclohexylethane, increased.

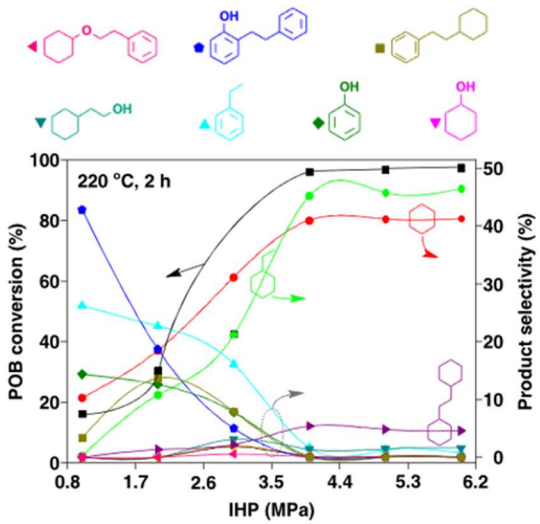

Figure 2.10: Conversion of PEB over Ni/Hβ at 220 °C, in *n*-hexane as solvent [28].

Luo et al.[27] used PEB as a model molecule to study the effect of the hydrogen pressure on the performance of a Ru/SZ catalyst at 240 °C in water. The hydrogenolysis of PEB was the major reaction pathway at low pressure of hydrogen (<10 bar), producing phenol and ethylbenzene. However, when increasing the pressure of hydrogen to 30 bar, the major reaction pathway was changed, and the full and partial hydrogenation of PEB aromatic rings was favored (Fig. 2.11).

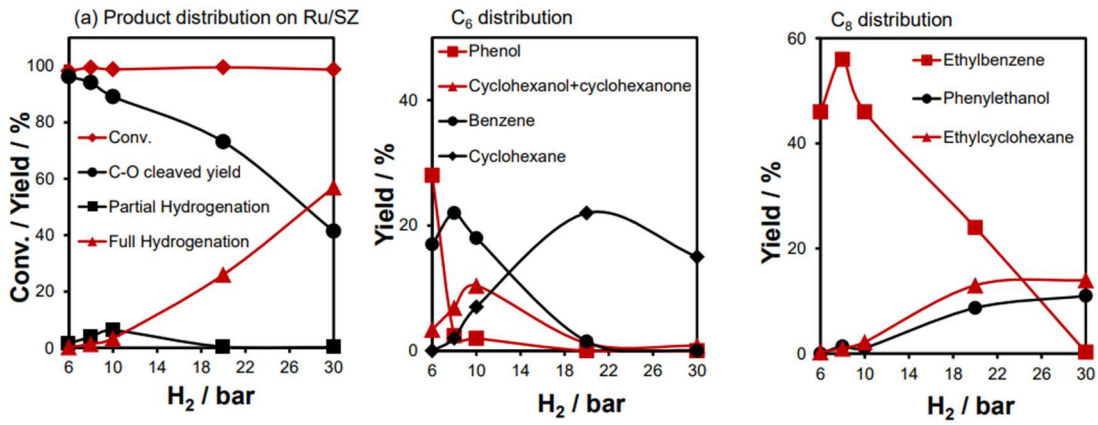

Figure.2.11: Influence of hydrogen pressure for the conversion of PEB at 240 °C, over Ru/SZ [23] using water as solvent.

The effect of the variation of pressure (0.6 to 10 MPa) on the conversion of DPE, and product distribution, over nickel supported on silica at 120 °C, in water as a solvent, is shown in Fig. 2.12 [30]. The TOF of DPE C–O bond cleavage increased up to 10 bar and then decreased. The hydrogenolysis rate increased as the pressure increased to 10 bar, due to the increase of surface coverage by H species. At high pressure, the reaction rate decreased as a result of the lower concentration of DPE that competes with hydrogen. The hydrogenolysis products (cyclohexanol and benzene) were mainly formed in the 0–10 bar pressure range. A further increase in pressure favored the hydrogenation of one of the aromatic rings of DPE to cyclohexyl phenyl ether.

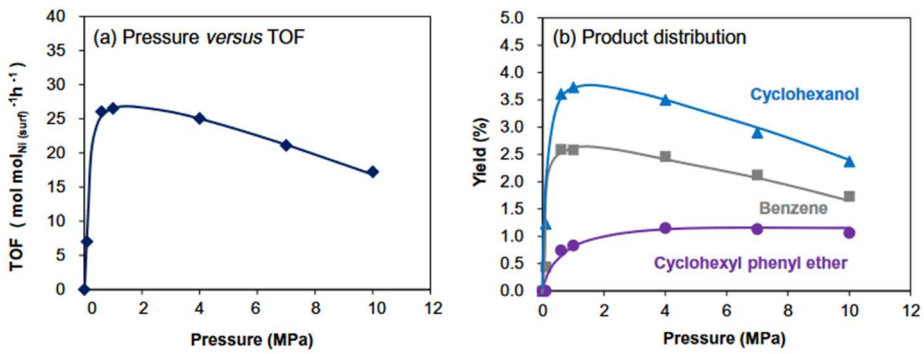

Figure 2.12: Conversion of DPE and yield of products curves as a function of reaction time. Reaction conditions: substrate (1.70 g), 57 wt% Ni/SiO_2 (300 mg), 120°C, 6 and 40 bar of H_2, water.

Zhao et al.[29] evaluated the effect of hydrogen pressure (5, 10, and 20 bar of H_2) on the conversion of DPE over Pd-Ni/HZSM5 at high temperature (220 °C), using *n*-hexane as a solvent (Table 2.4). When the reaction was conducted at low hydrogen pressure, the conversion of DPE was 11.1% and the main products were cyclohexane, benzene, and phenol. When increasing the pressure of hydrogen to 20 bar, the conversion of diphenyl ether and the selectivity to cyclohexane increased to 100%.

Table 2.4: Effect of pressure on DPE conversion over Pd-Ni/HZSM5. Reaction conditions: substrate (1 mmol), 1Pd-10Ni/HZSM5 (200 mg), 220°C, *n*-hexane.

		Selectivity (%)		
H_2 pressure (bar)	Conv. (%)	Benzene	Phenol	Cyclohexane
5	54.4	35.1	10.1	56.3
10	67.2	5.1	0.0	94.7
20	100	0.0	0.0	100.0

Therefore, the effect of pressure depended on the type of C-O bond and the choice of catalyst. For model molecules containing β-O-4 and 4-O-5 linkages, the effect of pressure on the reaction rate is felt at a lower pressure than for the α-O-4 linkage. This is likely due to the higher reaction rate for the cleavage of α-O-4 linkage. At high hydrogen pressure, the literature proposes a competition between the ether and H_2 in some instances, but it is difficult to draw a general conclusion. In addition, hydrogenolysis and hydrogenation are competitive reactions, and a higher H_2 pressure favors the hydrogenation of the aromatic ring of the model molecules containing 4-O-5 and β-O-4 linkages.

2.4.2 Effect of solvent

2.4.2.1 In the absence of catalysts

The conversion of BPE has been reported using non-polar and polar solvents even in the absence of a catalyst, which is due to the high reactivity of the α-O-4 linkage.

He et al. [31] studied the conversion of BPE using a non-polar solvent (undecane) at 250 °C and 40 bar of H_2. For the reaction carried out without a catalyst, a low conversion of BPE was obtained (9.7% under H_2), with high selectivity to what will be called "alkylated" products (above 90%), such as 2-benzylphenol (2-BPH) and 4-benzylphenol (4-BPH) (coupling of aromatic cycles via a $-CH_2-$ moiety). According to the authors, the cleavage of the C-O bond took place via pyrolysis, and the alkylated products were formed through free-radical reactions.

The authors also evaluated the effect of a polar solvent (water) on the conversion of BPE without a catalyst. BPE was mainly converted into phenol and benzyl alcohol in the aqueous phase. In this case, the hydrolysis reaction was catalyzed by the hydronium ions from water dissociated at high temperature (250 °C). Furthermore, alkylated products were formed by the recombination of radical intermediates.

According to the literature [32], the conversion of BPE in superheated water indeed occurs through hydrolysis and pyrolysis pathways, as described in Fig. 2.13. Benzyl alcohol and phenol are formed via a heterolytic pathway (Reaction 1.1). The heterolytic cleavage of BPE may also produce a benzyl cation that reacts with phenol to form 2 and 4-benzyl phenol (Reaction 1.2). In the pyrolysis reaction, the C_{aliph}-O bond of BPE is broken homolytically, producing highly reactive phenoxy and benzyl radicals. These radicals may react with hydrogen and produce phenol and toluene (Reaction 2.1); or they

can react with themselves, producing dimers (Equations 2.2 and 2.3); or with the initial substrate, leading to the formation of trimers (Equation 3).

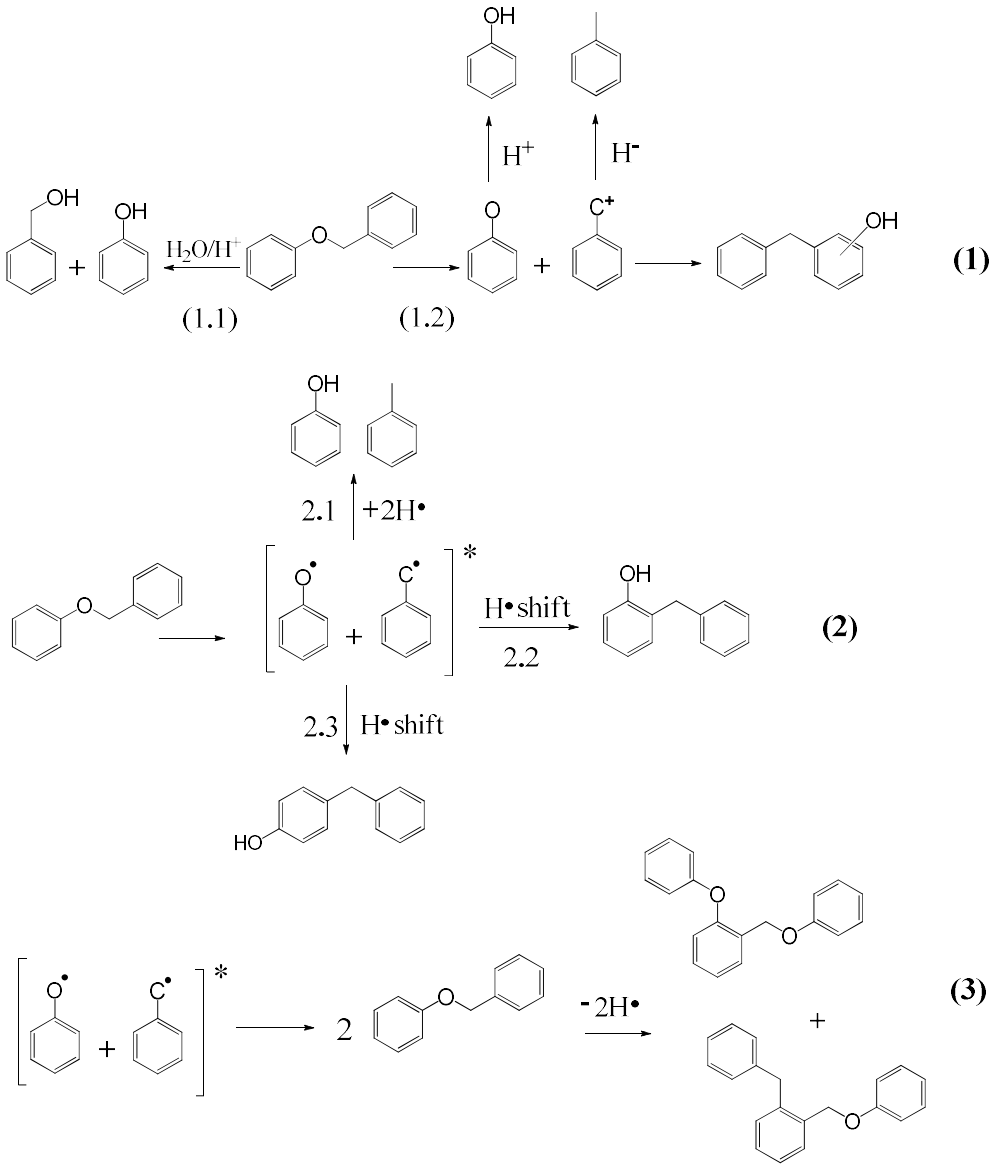

Figure 2.13: Ionic and radical mechanism pathways for the conversion of BPE. V. Roberts et al.[32]

In summary, for the conversion of BPE, alkylated products could be observed even in the absence of a catalyst (furthermore, from a catalyst presenting acidic sites). In the aqueous phase, the formation of benzyl phenols could be catalyzed by hydronium ions, while in a non-polar solvent, these products were formed via free radical reactions.

2.4.2.2 In the presence of catalysts

Wang and Rinaldi [33] investigated the effect of different solvents on the conversion of DPE over the Raney Ni catalyst at 90°C and 50 bar of H_2. The conversion and selectivity to different products after 2.5 h are reported in Table 2.5.

Table 2.5: Products of the hydrogenolysis of DPE conducted in different solvents on Raney Ni. Reaction conditions: substrate (2.9 mmol), Raney Ni (100mg), 90 °C, 50 bar of H_2.

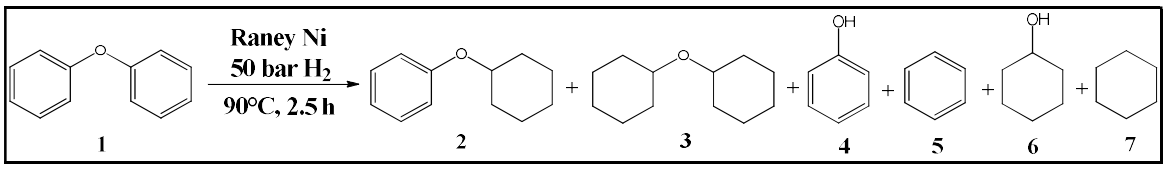

Solvent	Conv (%)	Selectivity [%]								
		2	3	4	5	6	7	4.6	5.7	Σ(4.6)/ Σ(5.7)
Methanol	12.4	13.7	0	25.7	32.3	16.8	11.5	1.53	2.81	0.97
Ethanol	33.0	11.8	0.3	10.7	26.7	33.6	16.9	0.32	1.58	1.02
2-propanol	72.7	15.0	1.9	1.6	15.4	40.5	25.6	0.04	0.60	1.03
Hex-F-2-PrOH	100	0.0	67.3	0.0	0.0	16.6	16.1	0.0	0.0	1.03
1-butanol	32.0	9.3	0.7	9.2	22.5	36.8	21.5	0.25	1.05	1.05
2-butanol	55.1	15.4	0.8	10.3	18.0	32.1	23.4	0.32	0.77	1.02
t-butanol	21.7	20.4	1.4	18.4	17.2	21.4	21.2	0.86	0.81	1.04
Ethyl acetate	47.0	21.0	1.8	8.1	15.7	30.1	23.3	0.27	0.67	0.98
Tetrahydrofuran	29.6	15.5	0.0	14.2	25.3	27.6	17.4	0.51	1.45	0.98
2-Me-THF	61.1	24.1	1.7	2.9	12.8	34.4	24.1	0.08	0.53	1.01
1,4-dioxane	17.8	24.5	0	24.1	22.0	13.3	16.1	1.81	1.37	0.98
n-heptane	99.0	9.6	36.5	0.0	1.5	27.5	24.9	0.0	0.06	1.04
Decalin	99.6	6.3	41.4	0.0	0	26.6	25.7	0.0	0	1.04
MCH	100	0	55.4	0.0	0	22.8	21.8	0.0	0	1.05

The comparison among the solvents is difficult because of the large range of conversions. For all the solvents listed, the main products were dicyclohexyl ether, benzene, cyclohexanol, and cyclohexane. However, for *n*-heptane and decalin, a small amount of cyclohexyl phenyl ether was also observed. Dicyclohexyl ether and cyclohexyl

phenyl ether are formed by the complete and partial hydrogenation of the aromatic rings of DPE, respectively. Cyclohexanol is formed by the hydrogenation of phenol, whereas cyclohexane is produced by the hydrogenation of benzene because there is presumably no acidic group to catalyze the dehydration reaction of cyclohexanol on Raney Ni.

2.4.3 Phenolic dimers representative of lignin

2.4.3.1 Catalysts used for the conversion of benzyl phenyl ether (BPE), model molecule representative of the α-O-4 linkage

A summary of the reaction conditions and catalysts used for BPE conversion, as well as a summary of the main reaction pathways observed for each catalyst, will be found at the end of the section (Table 2.8 and Scheme 2.1).

2.4.3.1.1 Non-acidic support

He et al.[31] investigated the role of the metal phase on the conversion of BPE using undecane and water (250 °C and 40 bar of H_2) in the presence of 70% wt.% Ni/SiO_2. Using undecane, the main products formed were toluene (45.5 %), phenol (19.1 %), cyclohexanone/cyclohexanol (15.6 %), and alkylated products (13.7 %). In comparison to the experiment without a catalyst, the conversion of BPE increased (15%) and the selectivity to alkylated products significantly decreased from 85.4 to 13.7%. The same products were obtained when water was used as a solvent. These results suggest that the Ni particles catalyze the hydrogenolysis of the C_{aliph}-O bond of BPE, regardless of the polarity of the solvent (Fig. 2.14). The lower formation of alkylated products in the presence of the catalyst indicates that the rate of hydrogenolysis has become higher than the rate of pyrolysis and hydrolysis. Concerning the alkylated products, the authors

proposed that they are formed via hydrolysis and alkylation (in water) or through pyrolysis and free radical reactions (in undecane) (Fig.2.14).

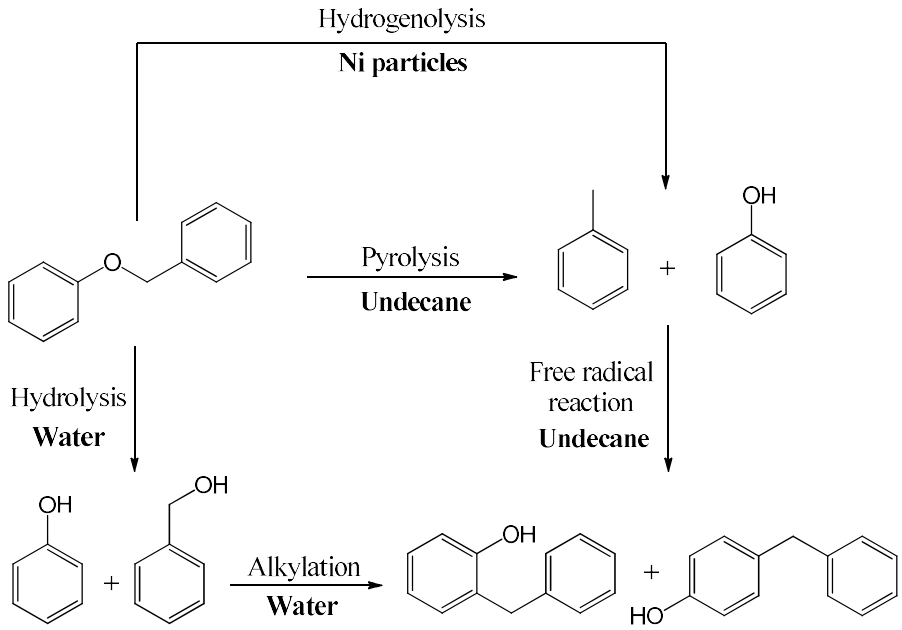

Figure 2.14: Reaction pathway proposed by He et al.[31] for the conversion of BPE over Ni/SiO_2 at 250 °C and 40 bar of H_2 in water and undecane.

The conversion of BPE over 57 wt. % Ni/SiO_2 catalyst was performed at lower temperature and pressure (120 °C, 6 bar of H_2) in water [24]. The main products formed were also toluene and phenol, with the minor formation of cyclohexanone and cyclohexanol in the whole range of conversion. The authors suggested that the metal promotes both: (i) the hydrogenolysis of the C_{aliph}-O bond of BPE, producing toluene and phenol; and (ii) the hydrogenation of phenol to cyclohexanone and cyclohexanol. In comparison to their previous work [31], the decrease in reaction temperature and hydrogen pressure suppressed the formation of alkylated products.

In conclusion, when the support of the catalyst is non-acidic, the conversion of BPE starts with the cleavage of the C_{aliph}-O ether bond by hydrogenolysis on metal particles, to produce toluene and phenol. Phenol can be partly hydrogenated, but deoxygenation does not take place.

2.4.3.1.2 Acidic supports

Yoon et al.[34] studied the performance of silica-alumina aerogel (SAA) containing different Al/(Si + Al) ratios (0.38, 0.57, and 0.73 mol/mol), as well as silica aerogel (SA) and alumina aerogel (AA), for the conversion of BPE in *n*-decane as solvent (100 °C and 5 bar H_2). Only SAA-38 and SAA-57 were active for the conversion of BPE. Although the density of acidic sites was low, SAA-38 and SAA-57 showed the highest amount of Brønsted acidic sites among the materials evaluated. Both catalysts were highly selective to the formation of alkylated products (Table 2.6). For SAA-38, 93 % of BPE was converted into phenol, 2-BPH, 4-BPH, and other alkylated products (benzyl-toluene, diphenylethane, and dibenzylphenols).

The authors proposed that Brønsted acidic sites were responsible for the production of 2 and 4-BPH, probably through Claisen rearrangement. Initially, phenol and toluene were formed by the cleavage of BPE, but only trace amounts of toluene were detected. According to the authors, the adsorbed toluene might rapidly react with some of the intermediates formed to produce dibenzylphenols (through the combination of one phenol and two toluenes), and benzyl-toluene and diphenylethane (by the combination of two toluenes) (Fig. 2.15). These reactions were catalyzed by the Brønsted acidic sites. This mechanism is in line with the one described above in heated water.

To evaluate the influence of Brønsted acidic sites in the conversion of BPE, a control experiment using SAA-38 and 2,6-di-tert-butylpyridine (an organic base that blocks Brønsted sites) was performed. The addition of 0.18 μmol of 2,6-di-tert-butylpydine decreased the conversion of BPE from 93.0 to 6.4 % with 2-BPH formed as a main product. Based on this result, the authors suggested that the BPE alkylation was improved in the presence of Brønsted acidic sites and possibly inhibited by Lewis acidic sites.

Table 2.6: Catalytic performance of SA, AA, and SAA catalysts for the conversion of BPE at 100°C under 5 bar H_2 in *n*-decane.

		Selectivity (mol %)			
Catalyst	**X_{BPE} (%)**	**Phenol**	**2BP**	**4BP**	**Others alkylated products**
SA	0	0	0	0	0
SAA-38	93.0	11.6	62.3	5.2	73.5
SAA-57	49.6	8.1	37.6	2.3	23.8
SAA-73	0	0	0	0	0
AA	0	0	0	0	0

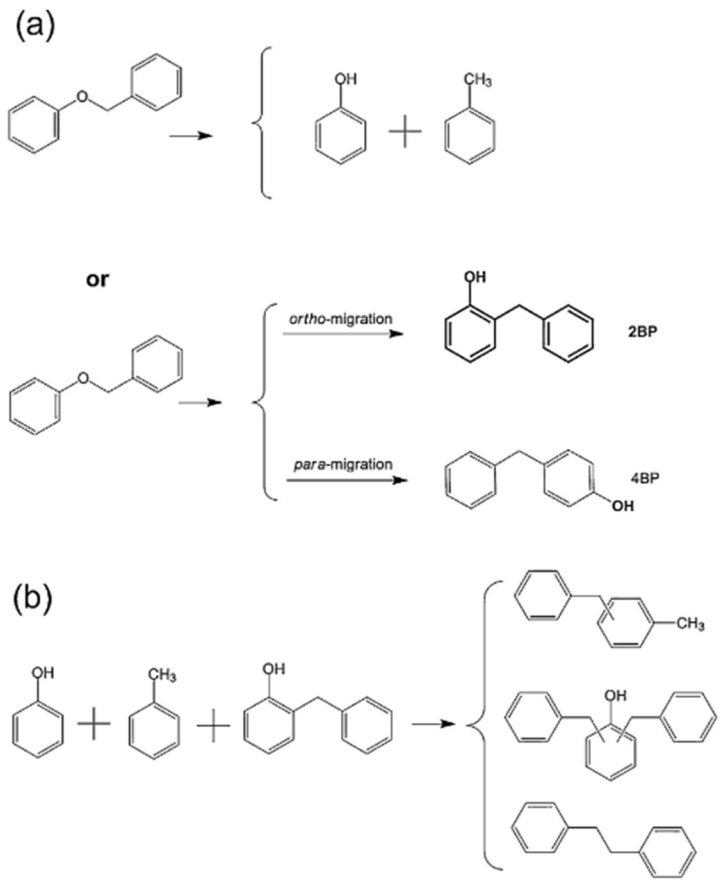

Figure 2.15: Reaction pathway for BPE conversion over SAA catalysts.

Cobalt molybdenum sulfide supported over sulfated zirconia (CoMo/SZ) was used by Song et al. [14] to study the conversion of BPE at 300 °C, 20 bar of H_2, in decalin as a solvent. Fig. 2.16 shows the product distribution as a function of time. It is noticed

that toluene and phenol are the main products formed at the beginning of the reaction. However, after 1 h, the yield of phenol decreased while the yield of benzene increased. The authors proposed that, initially, BPE was absorbed on both CoMo sulfide and Lewis acidic sites of sulfated ZrO_2. The hydrogenolysis of the C_{aliph}-O bond of BPE, producing phenol and toluene, was facilitated by the generated S-H bond on the CoMo sulfide phase. Then, the hydrogenolysis of the C_{arom}-O bond (HDO) of phenol, producing benzene, occurred over the CoMo sulfide surface. The authors highlighted that the Lewis acidic sites of ZrO_2 (Zr^{4+} cations) facilitated the adsorption of oxy compounds like BPE and increased the dispersion of CoMoS, which enhanced the hydrogenolysis activity. Although Brønsted acidic sites are present at the surface of CoMo/SZ, the role of these sites on the conversion of BPE was not established by the authors.

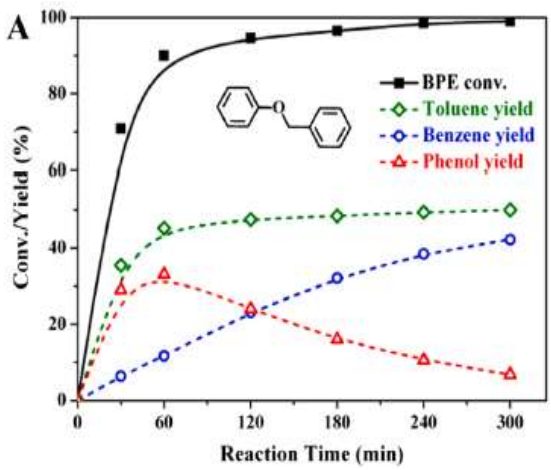

Figure 2.16: Conversion of BPE and yield of products curves as a function of reaction time. Reaction conditions: substrate (1mmol), CoMo/SZ (20mg), 300°C, 20 bar of H_2, decalin [14].

Guo et al. [35] studied the performance of 5 wt. % Ru/Nb_2O_5-SiO_2 for the conversion of BPE. The reaction was carried out at 230 °C in a mixture of water/isopropanol without external hydrogen gas. After 20 h, BPE was selectively converted to benzene (92%) and toluene (82%). The authors proposed that the deoxygenation of BPE proceeds through

the direct cleavage of the C-O ether bond to produce arenes, rather than via sequential hydrogenation and dehydration steps. So, phenol and toluene were formed by hydrogenolysis of the C_{aliph}-O bond of benzyl phenyl ether, and benzene was produced by the direct cleavage of the C_{arom}-O bond of phenol. The authors suggested that the HDO of BPE was promoted by a synergistic effect between Ru and the NbO_x species of the support.

Jiang et al. [36] studied the conversion of BPE over Ni/Al_2O_3 reduced at different temperatures (500, 550, 600, 650, and 700 °C). The reaction was performed at 150 °C in isopropanol, used as a solvent as well as a hydrogen source. In the absence of catalysts or in the presence of bare Al_2O_3, no conversion was observed. In the presence of Ni/Al_2O_3, the increase of reduction temperature increased the BPE conversion from 15.4 % ($Ni/Al_2O_{3\text{-}500}$) to 58.9 % ($Ni/Al_2O_{3\text{-}650}$). However, over $Ni/Al_2O_{3\text{-}700}$, the decrease of BPE conversion (33.1 %) was attributed to the increase in the Ni particle size (10.2 nm). For all catalysts, BPE was cleaved into phenol and toluene. Cyclohexanone and cyclohexanol were observed at a low extent (< 5 %).

Zhao and Lercher [37] studied the role of metal and acidic sites in the conversion of BPE at 200 °C, 50 bar of H_2, and water as a solvent. Initially, the reaction was performed over HZSM5 alone, which mainly produced 2-BPH (63% yield) and phenol (37% yield). When the reaction was carried out in the presence of HZSM5 and Pd/C simultaneously, only deoxygenated products were formed, cyclohexane (48 %) and methylcyclohexane (52 %). The alkylation pathway was suppressed. They proposed that the C_{aliph}-O bond of BPE was first cleaved over palladium particles, producing phenol and toluene, which were rapidly hydrogenated to methylcyclohexane and cyclohexanol, respectively, over the metal sites. Then, the acidic sites of HZSM5 catalyzed the dehydration of cyclohexanol to cyclohexene, which was hydrogenated by the metal, producing

cyclohexane. These results revealed that the rate of *hydrogenolysis* of the C_{aliph}-O bond of BPE to phenol and toluene over Pd particles was much higher than the rate of *hydrolysis* of the C_{aliph}-O bond into phenol and benzyl phenol catalyzed by the hydronium ions, which inhibited the alkylation side-reaction over the acidic sites of HZSM5.

He et al. [31] investigated the influence of acidic sites on the conversion of BPE in aqueous phase (250 °C, 40 bar of H_2) using two different amounts of HZSM5 zeolite. Phenol, benzyl alcohol, and dimers were produced regardless of the amount of catalyst. However, the product distribution varied significantly. Increasing the amount of catalyst increased the selectivity of alkylated products and decreased the formation of phenol and benzyl alcohol. These results confirm that in the absence of a metal, hydrolysis and alkylation are the major reaction pathways for BPE conversion in aqueous phase in the presence of acidic sites.

They subsequently studied the effect of both metal and acidic sites in the same catalyst for the conversion of BPE. The bifunctional catalyst was 10 wt.% Ni/HZSM5. The main products formed were phenol and toluene, with small amounts of benzyl alcohol and alkylated products (Fig. 2.17). Phenol and toluene were produced by the metal-catalyzed hydrogenolysis, whereas phenol and benzyl alcohol as well as alkylation products were obtained via the hydrolysis reaction. This reaction was catalyzed by the acidic sites of the zeolite and by protons from water dissociation at high temperatures. Over 10 wt.% Ni/HZSM5, the hydrogenolysis reaction catalyzed by metallic Ni particles was the main pathway for the cleavage of the C-O bond from BPE, while the hydrolysis was a minor route. The role of the acidic sites is also evidenced when the product distribution obtained with Ni/SiO_2 and Ni/HZSM5 catalysts are compared. Hydrolysis products were only formed over Ni/HZSM5 and the selectivity to alkylated products was higher for this bifunctional catalyst.

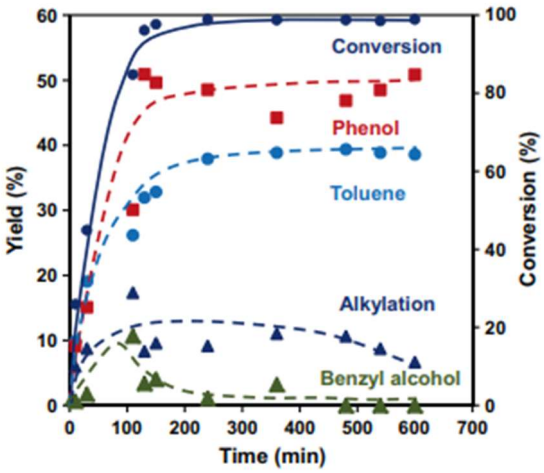

Figure 2.17: Conversion of BPE and yield of products curves as a function of reaction time [31]. Reaction conditions: substrate (9.20g, 0.010 mol), 10% Ni/HZSM5(50mg), 250 °C, 40 bar of H_2, water.

The performance of 10 wt.% Ni/HZSM5 was also evaluated in the same reaction conditions using undecane as solvent. BPE was mainly converted into phenol (19.4 %), toluene (32.4 %), and alkylated products (32.4 %). Therefore, He et al.[31] concluded that metallic Ni particles are the active sites for the hydrogenolysis of the C-O bond of BPE in both the aqueous and non-polar solvents. Here, the alkylated products are formed through pyrolysis and free radical reactions.

Zhao and Lercher[38] evaluated the activity of 20 wt.% Ni/HZSM5 for the conversion of BPE at 250 °C, 50 bar of H_2, and water as solvent. The main products were cyclohexane (42 %), methylcyclohexane (36 %), and toluene (18 %). Compared to the tests with BPE over 10%Ni/HZSM5 performed by He et al. [31] in the same solvent and temperature conditions, the higher loading of Ni used by Zhao and Lercher[38] enhanced the hydrogenation of phenol and toluene produced by the C-O cleavage of BPE. After hydrogenolysis, phenol was hydrogenated to cyclohexanol, and toluene to methylcyclohexane. Then, cyclohexanol was dehydrated to cyclohexene, due to the presence of the acidic sites of HZSM5. Finally, cyclohexene was hydrogenated to

cyclohexane over the metal sites. In this case, alkylation products and benzyl alcohol, formed by hydrolysis of BPE, were not observed.

Zhao et al.[29] evaluated the performance of both palladium and nickel supported over HZSM5 for the conversion of BPE, at 220 °C, 20 bar of H_2, and *n*-hexane as a solvent. The main products were methylcyclohexane (44.7 %), cyclohexane (29.4 %), and cyclohexanol (17.1 %). However, the HDO of BPE over the monometallic catalysts was not carried out, which makes the comprehension of the role of each metal difficult.

Zhang et al.[39] studied the BPE conversion over 1 wt. % Ru/HZSM5 at 200 °C, 50 bar of H_2 and water. The complete conversion was achieved and BPE was transformed into cyclohexane (34.5 %), methylcyclohexane (48.8 %), and *t*-butylcyclohexane (13 %). In comparison to the 10%Ni/HZSM5 catalyst tested under the same pressure conditions [31], Ru promoted the complete hydrogenation of phenol and toluene formed via the hydrogenolysis step, while phenol and toluene remained unreacted over the Ni-based catalyst. The unexpected formation of *t*-butylcyclohexane was not explained by the authors.

Ruthenium-supported over H-beta zeolite (0.5 wt. % of Ru) was tested for the conversion of BPE at 140 °C, under 40 bar H_2, in water [40]. Cyclohexane (35.7 %), methylcyclohexane (19.9 %), cyclohexyl methanol (16.4 %), and 1-cyclohexyl-2-methylcyclohexane (27.6 %) were formed as products. The authors did not present a reaction pathway for the conversion of BPE.

Dou et al.[41] studied the conversion of BPE over cobalt and zinc supported on dealuminized H-Beta zeolite (CoZn/Off-Al H-beta, "Off" means dealuminated material) under 40 bar of H_2 and in methanol as solvent. For this catalyst, the reactions were carried out in a range of temperature from 140 to 260 °C and the results are reported in Table 2.7.

Table 2.7 Product distribution for the conversion of BPE over CoZn/Off Al H-beta under 40 bar of H_2 in methanol.

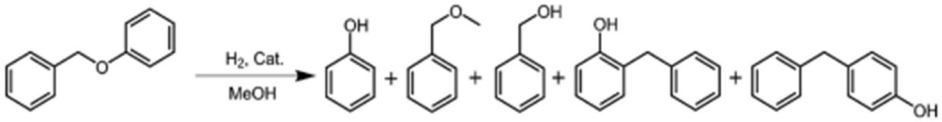

			Yield (%)				
Entry	T (°C)	Conv. (%)	4	5	6	7	8
1	140	6.3	-	0.8	0.2	3.6	0.5
2	160	16.0	2.0	5.4	1.0	5.7	0.7
3	180	29.5	13.2	10.7	2.5	14.0	1.1
4	200	50.2	15.8	13.0	2.8	32.4	2.0
5	220	66.3	28.2	25.5	2.7	35.1	3.0
6	240	100	55.4	51.0	3.4	40.8	3.8
7	260	100	57.5	53.7	3.7	39.7	2.5

The conversion of BPE and product distribution strongly depended on the temperature. At 140 °C, 6.3 % of BPE was converted, and only at high temperatures (240 and 260 °C), the complete conversion was achieved. Phenol, methyl benzyl ether, and 2-BPH were the main products formed at all temperatures. The authors suggested that the conversion of BPE involves two main competitive reaction pathways: (i) the methanolysis of BPE to form phenol and methyl benzyl ether, products 4 and 5; and (ii) the rearrangement of BPE into 2-BPH, product 7. The hydrolysis of BPE into phenol and benzyl alcohol was also observed to a minor extent. 4-BPH can be formed by condensation of phenol and methyl benzyl ether, or by rearrangement of 2-BPH. Finally, the authors proposed that the alkylated products can also be obtained by the homolytic cleavage of BPE into phenol and toluene, followed by recombination.

Increasing the reaction temperature increased the methanolysis reaction as well as the formation of alkylated products. The authors reported an essential role of Lewis acidic sites in the formation of 2 and 4-BPH since the alkylation reaction did not take place

without a catalyst. On the other hand, phenol and methyl benzyl ether were formed, indicating that the methanolysis of BPE can occur at 240 °C even in the absence of catalysts.

Table 2.8 summarizes all catalysts and reaction conditions described in this section, while scheme 2.1 shows the main reaction pathways for BPE conversion reported in the literature. As previously mentioned, BPE can be cleaved without a catalyst into benzyl and phenoxy radicals (non-polar solvent) or into phenol and benzyl alcohol (aqueous phase). After cleavage, the intermediates formed can recombine to themselves or to BPE to form dimers and trimers, respectively. In the presence of bare acidic support (SAA and HZSM5), the same products can be observed. In the presence of metal, the BPE conversion mainly proceeds via hydrogenolysis, to produce toluene and phenol. Then, depending on the reaction conditions, toluene can be hydrogenated into methylcyclohexane, whereas phenol can be hydrogenated to cyclohexanone/ cyclohexanol or, in some cases, converted into benzene by hydrogenolysis. It was observed that the hydrogenation of phenol occurred faster than the hydrogenation of toluene. In general, the hydrogenation step was more favored over Ru and Pd-based catalysts than over Ni-based ones. The presence of acidic sites is fundamental for the dehydration of cyclohexanol and the production of the deoxygenated product, cyclohexane. From the literature discussed, over CoMo/SZ, the presence of Lewis acidic sites can favor the hydrogenolysis step due to the generation of the S-H bond on the CoMo sulfide phase, whereas the Brønsted acidic sites promote the formation of alkylated products, 2 and 4-BPH.

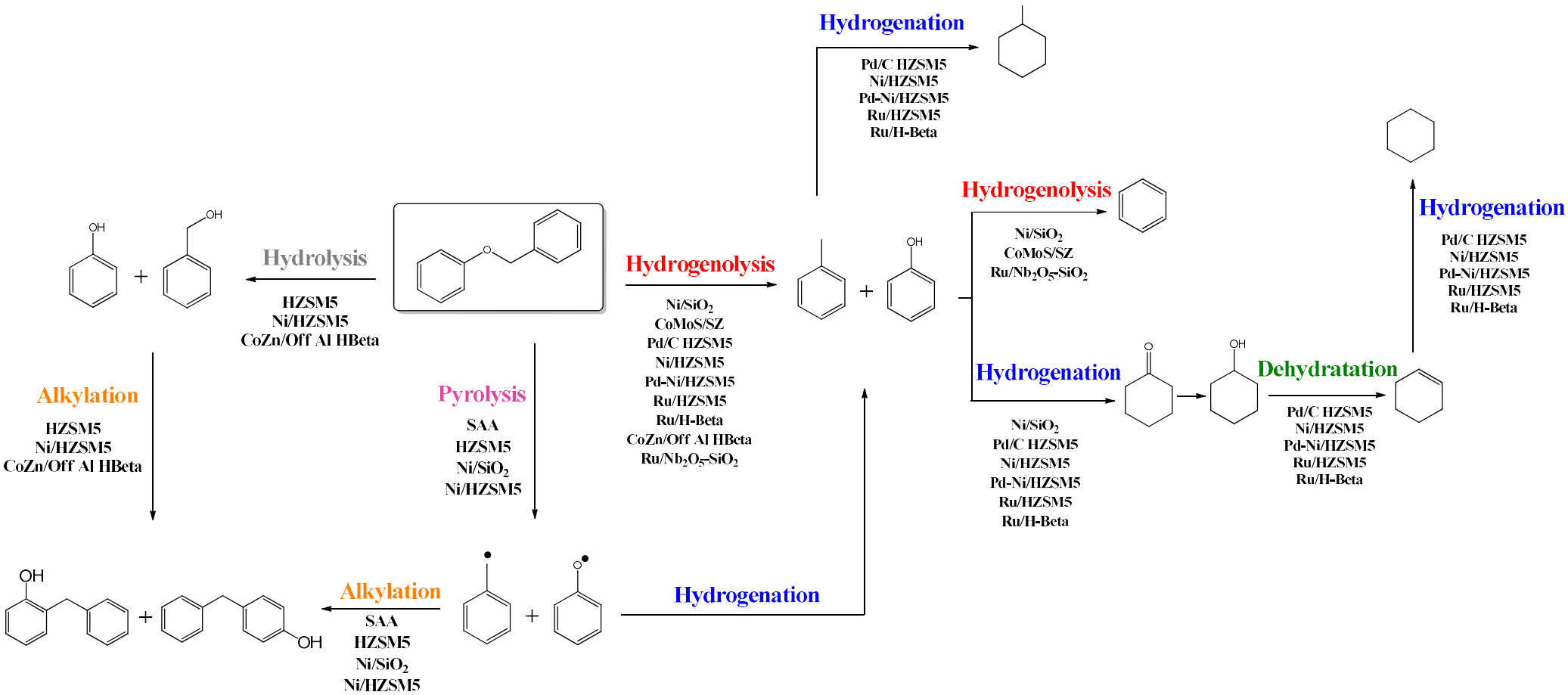

Scheme 2.1 Reaction pathways for the conversion of BPE over different catalysts presented in the literature.

Table 2.8: Catalysts and reaction conditions reported in the literature for the conversion of BPE.

Catalysts	Reaction conditions	Solvent	Main products	Conclusion	Ref.
70% Ni/SiO_2	T: 250°C P: 40 bar H_2	Water/ Undecane	Phenol, toluene, cyclohexanol, cyclohexanone, 2 and 4-BPH	Without a catalyst, BPE was cleaved by pyrolysis (undecane) or hydrolysis (water). When Ni was used, the hydrogenolysis takes place and the effect of solvent is less felt.	31
57% Ni/SiO_2	T: 120°C P: 6 bar H_2	Water	Phenol, toluene.	The conversion of BPE proceeds by hydrogenolysis catalyzed by the metal sites.	24
CoMoS/SZ	T: 300°C P: 20 bar H_2	Decalin	Benzene, toluene	The hydrogenolysis of BPE was facilitated by generated S-H bond formed on CoMo sulfide.	14
Ni/Al_2O_3	T: 150°C P: Without H_2	Isopropanol	Phenol, toluene	The conversion of BPE proceeds by hydrogenolysis of the C_{aliph}-O bond of BPE. The increase in the Ni reduction degree increased the BPE conversion.	36
Ru/Nb_2O_5-SiO_2	T: 230°C P: Without H_2	Water / Isopropanol	Benzene, toluene	The synergistic effect between Ru and NbOx species of the support promoted the direct cleavage and deoxygenation of BPE.	35
Silica-Alumina aerogel (SAA)	T: 150-250°C P: 5-40 bar H_2	*n*-decane	2 and 4-BPH	The Brønsted acidic sites directly affect the conversion of BPE and the formation of alkylated products.	34

Table 2.8: Catalysts and reaction conditions reported in the literature for the conversion of BPE. (continuation)

Catalysts	Reaction conditions	Solvent	Main products	Conclusion	Ref.
Pd/C and HZSM5	T: 200°C P: 50 bar H_2	Water	Cyclohexane, methylcyclohexane	The metal sites catalyzed the hydrogenolysis of BPE into phenol and toluene. Then, toluene was hydrogenated and the deoxygenation of phenol was performed via hydrogenation/dehydration catalyzed over metal and acidic sites, respectively.	37
HZSM5 **10% Ni/HZSM5**	T: 250°C P: 40 bar H_2	Water/ Undecane	Phenol, toluene, alkylated products	Over the bare support, hydrolysis of BPE and alkylation reaction occur as main reaction pathways. When Ni was used, BPE was mainly converted by hydrogenolysis.	31
20% Ni/HZSM5	T: 150°C P: 20 bar H_2	Water	Toluene, methylcyclohexane, cyclohexane	Metal sites promoted the cleavage of BPE to produce phenol and toluene. Then, cyclohexane was formed from phenol by a sequential hydrogenation-dehydration reaction promoted by the metal and acidic sites, respectively.	38
Pd-Ni/HZSM5	T: 220°C P: 20 bar H_2	n-hexane	Cyclohexane, methylcyclohexane, cyclohexanol.	The reaction pathway for BPE conversion was not proposed.	29
Ru/HZSM5	T: 200°C P: 50 bar H_2	Water	Cyclohexane, methylcyclohexane, t-butyl cyclohexane	The reaction pathway for BPE conversion was not proposed. However, the authors highlighted that the Brønsted acidic sites catalyzed the alkylation reaction via transalkylation and isomerization.	39

Table 2.8: Catalysts and reaction conditions reported in the literature for the conversion of BPE. (continuation)

Catalysts	Reaction conditions	Solvent	Main products	Conclusion	Ref.
Ru/H-Beta	T: 170°C P: 40 bar H_2	Water	Cyclohexane, methylcyclohexane, cyclohexyl methanol, 1-cyclohexyl-2-methylcyclohexane	The reaction pathway for BPE conversion was not proposed.	40
CoZn/Off Al H-beta	T: 140-260°C P: 40 bar H_2	Methanol	Phenol, benzyl methyl ether and 2-BPH	At temperatures below 220 °C, the rearrangement is the predominant reaction pathway. When the temperature increases; the methanolysis reaction becomes competitive.	41

2.4.3.2 Catalysts used for the conversion of phenethoxybenzene (PEB), model molecule representative of β-O-4 linkage

A summary of the reaction conditions and catalysts used for PEB conversion, as well as a summary of the main reaction pathways observed for each catalyst, will be found at the end of the section (Table 2.10 and Scheme 2.2).

2.4.3.2.1 Non-acidic supports

The conversion of PEB has been extensively studied in the literature because the β-O-4 bond is the main ether linkage present in the lignin structure. The hydrogenolysis of the C_{aliph}-O bond of PEB produces phenol and ethyl benzene. For this ether, the solvent does not contribute to the C-O cleavage due to the high activation energy required. In the absence of catalysts, PEB remained unchanged even using high-temperature water [27].

He et al.[24] studied the relationship between the rate of hydrogenolysis of the C_{aliph}-O bond of PEB and the Ni particle size for Ni/SiO_2 (120 °C, 6 bar of H_2, in water as a solvent). Ni/SiO_2 catalysts calcined at various temperatures were prepared to obtain different Ni particle sizes (Fig. 2.18 a). The TOF for the hydrogenolysis of PEB, measured in the same reaction conditions, is plotted as a function of the Ni particle size in Fig. 2.18 b. The TOF increased and achieved a maximum at around 5.9 nm and then slightly decreased, indicating that the hydrogenolysis of the C_{aliph}-O bond of PEB is a structure sensitive reaction.

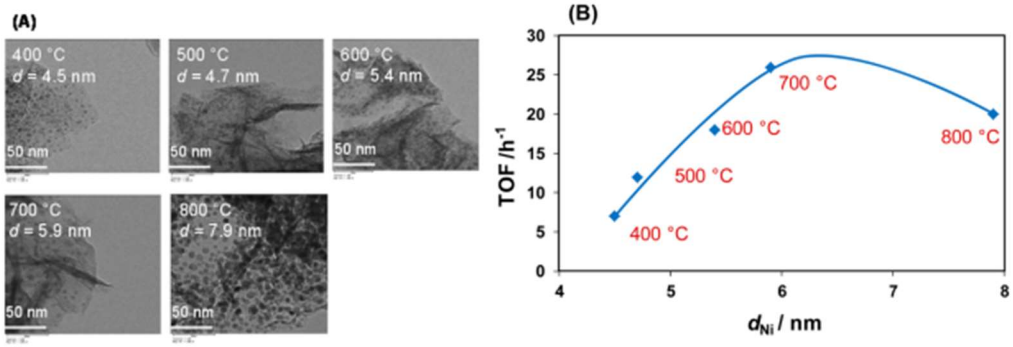

Figure 2.18: (a) TEM images of Ni/SiO_2 catalysts prepared by the DP method, at different calcination temperatures. (b) TOF as a function of Ni particle size for the C-O bond cleavage of PEB, at 120 °C under 6 bar H_2 in water.

The conversion of PEB over 57 wt.% of Ni/SiO_2 (120 °C, 6 bar of H_2 in water) produced mainly cyclohexanol (~49%) and ethylbenzene (~47%) with a small amount of ethylcyclohexane (~2%), and a product of partial hydrogenation of PEB (~2%) [24]. Considering the products observed, the authors proposed that the metal catalyzes the hydrogenolysis of the C_{aliph}-O bond of PEB, producing phenol and ethylbenzene. Phenol was not detected, which suggests that it is rapidly hydrogenated to cyclohexanol on Ni particles. Deoxygenation does not occur due to the absence of catalyst acidity. Ethylcyclohexane can be formed by the hydrogenation of ethylbenzene.

Luo and Zhao[25] compared the performance of Ru, Pd, and Pt supported on activated carbon for the conversion of PEB (240 °C, 8 bar of H_2, in water). For Ru/C, the main products formed are ethylbenzene and phenol at the beginning of the reaction (Fig. 2.19). After 30 min, the yield of phenol decreased and the yield of cyclohexanol/cyclohexanone and benzene increased. While phenol was rapidly converted to cyclohexanol, ethylbenzene remained unreacted, and the authors proposed that the high conversion of phenol can be attributed to the stronger adsorption of oxygen from the hydroxyl group onto the metal sites, as well as by the larger solubility of phenol in water. The same products were observed for Pd/C, whereas cyclohexanol was not formed over Pt/C. Ru/C and Pd/C exhibited higher activity for the C-O bond cleavage, but Pd/C led to

a more pronounced phenol hydrogenation to cyclohexanol. On the other hand, Pt/C presented low conversion and hydrogenation activity.

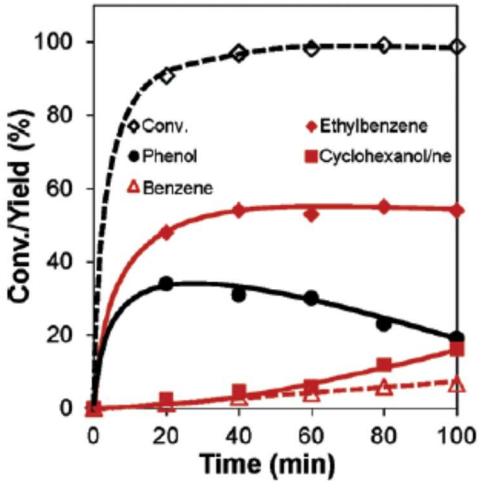

Figure 2.19: Conversion of PEB and yield of products curves as a function of reaction time over Ru/C catalyst. Reaction conditions: substrate (1g), Ru/C (100mg), 240°C, 8 bar of H_2, water [25].

Song et al.[42] investigated the effect of the type of metal on the conversion of PEB over Ni, Pd, and Ru-supported over activated carbon. The reaction was carried out at 150 °C, 20 bar of H_2, in methanol as a solvent. The product distributions are presented in Fig 2.20. Cyclohexanol, ethylcyclohexane, and the fully hydrogenated product of PEB (2-(cyclohexylethoxy) cyclohexane) were formed for all catalysts. In addition to these products, methoxycyclohexane and cyclohexyl methanol were also produced for Pd/C. However, the formation of cyclohexanol, methylcyclohexane, and methoxycyclohexane has not been well elucidated by the authors.

The selectivity to the C-O-C bond cleavage products followed the order: Ni (85%) > Pd (69%) > Ru (40%). Ni exhibited the highest ability to break the C-O ether bond of PEB, while Ru promoted mainly the PEB hydrogenation.

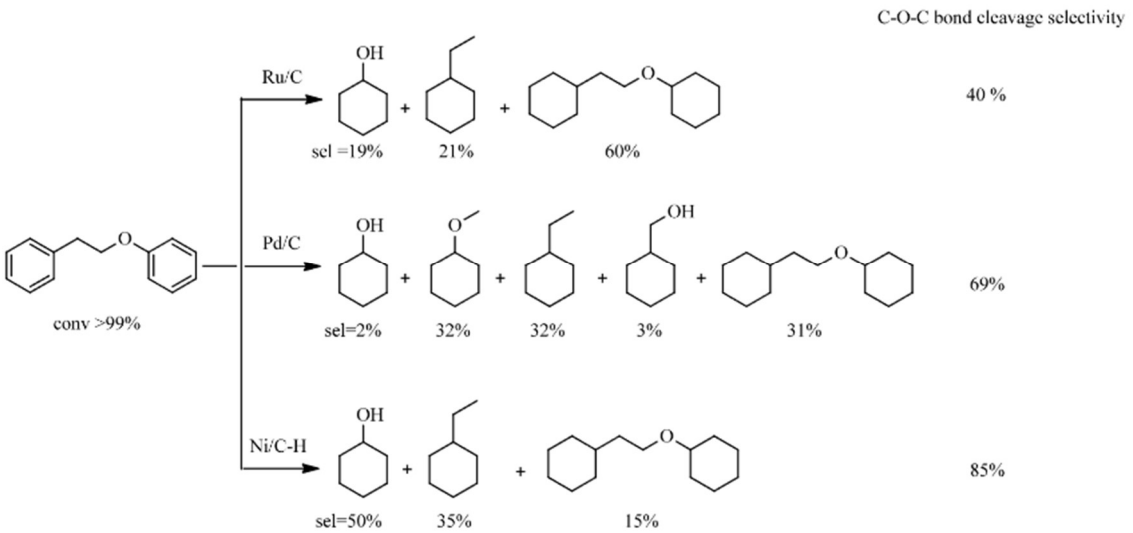

Figure 2.20: Product distribution PEB conversion over Ni/C, Ru/C, and Pd/C catalysts. Reaction conditions: substrate (0.167 mmol), catalyst (25mg), 150°C, 20 bar of H_2, methanol.

Unlike Song et al.[42], who also used Ru/C and Pd/C for PEB conversion, products from the complete hydrogenation of the aromatic rings were not observed by Luo and Zhao[25]. Considering the hydrogen pressure used in both works, these results suggest that a high hydrogen pressure (20 bar) favored the complete hydrogenation of PEB, whereas the hydrogenolysis reaction was promoted at low hydrogen pressure (8 bar).

Regarding the results discussed so far, over catalysts with no acidity, the conversion of PEB may follow two reaction pathways depending on the H_2 pressure and the type of metal: (i) the hydrogenolysis of the C_{aliph}-O bond to produce ethylbenzene and phenol; (ii) the full hydrogenation of PEB into (2-(cyclohexylethoxy) cyclohexane). Under low hydrogen pressure, PEB was mainly converted into ethylbenzene and phenol by hydrogenolysis, while under high hydrogen pressure, the hydrogenation of the intermediates formed after hydrogenolysis, as well as the hydrogenation of PEB aromatic rings are favored. Deoxygenation does not take place due to the absence of acidic sites.

2.4.3.2.2 Acidic supports

Guan et al.[26] evaluated the effect of Pd, Pt, Rh, and Ru-supported over niobium oxide in the conversion of PEB at 260 °C, 10 bar of H_2 in *n*-decane. The product selectivity and the conversion are presented in Fig 2.21. Over bare Nb_2O_5, PEB was selectively converted (~50 %) into phenol and ethylbenzene. Among the supported catalysts, Rh/Nb_2O_5 exhibited the highest conversion of PEB (99 %) while Ru/Nb_2O_5 presented the lowest one (83 %). Pd/Nb_2O_5 and Rh/Nb_2O_5 produced only deoxygenated products. Ethylbenzene, benzene, and cyclohexane were mainly formed in both cases, however, Rh/Nb_2O_5 exhibited the highest selectivity to aromatic products (ethylbenzene and benzene).

The authors proposed that the cleavage of PEB can occur by two reaction pathways: (i) the metal can promote the hydrogenolysis of its C_{aliph}-O bond to form ethylbenzene and phenol – major route; and (ii) the metal can promote the hydrogenolysis of its C_{arom}-O bond to produce phenyl ethanol and benzene – minor route. Following the major reaction route, ethylbenzene was hydrogenated to ethylcyclohexane by the metal sites, while phenol was directly deoxygenated into benzene by hydrogenolysis. Finally, cyclohexane can be formed from benzene hydrogenation.

The formation of cyclohexane by a sequential hydrogenation/dehydration of phenol was dismissed by the authors. In an isolated experiment, under the same reaction conditions, phenol was used as a substrate, and as a function of time only benzene and cyclohexane were observed during the whole conversion. The authors also proposed that toluene can be produced from phenyl ethanol, and methylcyclohexane can be formed by toluene hydrogenation. Considering the results described above, the authors assumed that Rh and Pd were the best metals to remove oxygen. While Rh was more selective to

produce aromatic compounds, Pd was the metal that gave the higher hydrogenation activity.

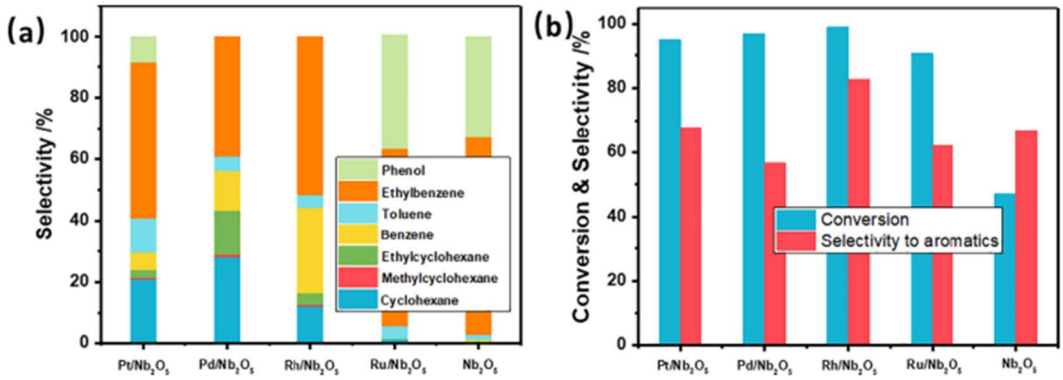

Figure 2.21: (a) Product distribution of PEB over different Nb_2O_5 supported catalysts; (b) Conversion of PEB and selectivity of aromatics [26].

Song et al.[14] studied the performance of cobalt molybdenum sulfide catalysts supported over sulfated zirconia for the conversion of PEB at 300 °C, 20 bar of H_2 in decalin as a solvent. During the reaction, the main products were ethylbenzene and benzene, but a small yield of phenol was also observed (Fig. 2.22 a). As mentioned above for BPE, the authors proposed that PEB initially adsorbs on both CoMo sulfide and Lewis acidic sites of sulfated ZrO_2. The hydrogenolysis of the C_{aliph}-O bond of PEB, producing phenol and ethylbenzene, was facilitated by the generated S-H bond on CoMo sulfide sites, which can react with the adsorbed oxygenated compounds. Then, the hydrogenolysis of the C_{arom}-O bond (HDO) of phenol, producing benzene, was subsequently performed over the CoMo sulfide surface, Fig. 2.22 b. In addition, the authors highlighted that the catalyst acidity, especially Lewis acidic sites, can improve HDO because they can facilitate the adsorption and reaction of oxygenated compounds. However, the role of the Brønsted acidic sites of sulfated zirconia was not mentioned by the authors.

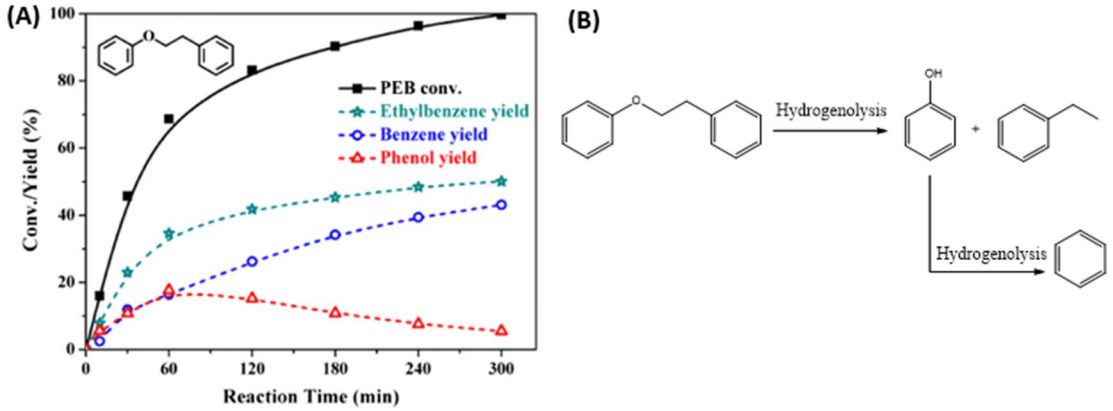

Figure 2.22: (a) Conversion of PEB as a function of reaction time. Reaction Conditions: substrate (1mmol), CoMo/SZ (20 mg), 300 °C, 20 bar of H_2. (b) Reaction pathway for PEB conversion over CoMo/SZ.

The conversion of PEB was performed over different acidic supports (Nafion, Amberlyst, sulfate zirconium, and zeolite: HZSM5, Hβ, and HY) as well as over ruthenium[25,27], and palladium[25] supported over sulfated zirconia at 240 °C, 8 bar of H_2 and in water as solvent. In the absence of metal, no material was active for the PEB conversion. When the reaction was carried out over Ru/SZ, the main products formed at the beginning of the reaction were ethylbenzene and phenol, by hydrogenolysis of the C_{aliph}-O ether bond of PEB, catalyzed by the metal sites (Fig. 2.23 a). After 30 min of reaction, the yield of phenol decreased whereas the yield of benzene increased, indicating that phenol was converted into benzene. Ethylbenzene remained stable during the whole reaction time. The authors proposed that, after hydrogenolysis, cyclohexanol, formed via phenol hydrogenation, was dehydrated to cyclohexene on the Brønsted acidic sites of the zirconia. Then, benzene was formed by the dehydrogenation of cyclohexene.

Comparing the product distribution obtained with Ru/SZ (Fig. 2.23 a) and Ru/C (Fig. 2.19) previously described in the same reaction conditions (240 °C and 8 bar H_2), the most important difference is the yield of benzene formed. The higher yield of benzene formed in the presence of sulfated-zirconia is likely due to the presence of Brønsted acidic

sites, which promotes the dehydration of cyclohexanol into cyclohexene, later dehydrogenated to benzene.

For Pd/SZ, initially, the main products were ethylbenzene and cyclohexanone. After 40 min of reaction, the yield of cyclohexanone decreased while the yield of cyclohexanol increased (Fig. 2.23 b). These results indicate that the metal promoted the hydrogenolysis of the C_{aliph}-O bond of PEB producing ethylbenzene and phenol. Then, phenol was converted into cyclohexanone/cyclohexanol by the hydrogenation of the aromatic ring of phenol, promoted by the metal.

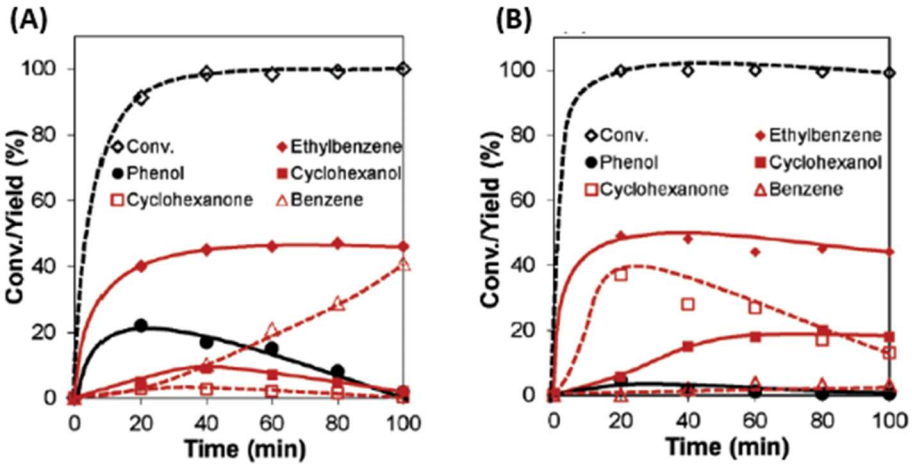

Figure 2.23: Conversion of PEB as a function of reaction time over (a) Ru/SZ and (b) Pd/SZ. Reaction conditions: substrate (1g), catalyst (20mg), 240°C, 8 bar of H_2, water.

Comparing the products formed over Ru/SZ (Fig. 2.23 a) with those obtained over Pd/SZ (Fig. 2.23 b), there is no formation of benzene on Pd/SZ. In a separate experiment using phenol as a substrate, the authors observed that over Pd/SZ the conversion of cyclohexanone into cyclohexanol was relatively slow, which led to a very small formation of cyclohexanol, which therefore blocks the pathway to benzene. In contrast, over Ru/SZ, phenol was rapidly converted into cyclohexanol which was favorable to benzene formation.

Ni supported on silica-alumina (30 wt. % of Ni) was used for PEB conversion at high temperature and H_2 pressure (300 °C, 60 bar of H_2) in dodecane as a solvent, by Kong et al.[43]. After 2 h, a mixture of ethylcyclohexane (30 %), cyclohexane (40 %), and benzene/ toluene (20 %) was formed as main products. The authors proposed that at high temperatures, PEB can be converted via: (i) the cleavage of the C_{aliph}-O bond to form ethylbenzene and phenol; or (ii) the cleavage of the C_{arom}-O bond to produce benzene and 2-phenyl ethanol. Ethylcyclohexane and cyclohexane were formed through the hydrogenation of ethylbenzene and benzene, respectively, probably due to the high H_2 pressure used. In addition, the authors also suggested that cyclohexane can be formed via a phenol hydrogenation/dehydration sequence, and ethylcyclohexane by dehydration/hydrogenation of 2-phenyl ethanol.

Zhao and Lercher[38] studied the conversion of PEB over 20 wt.% Ni/HZSM5 at 250 °C, 50 bar of H_2 in water. The main products formed were cyclohexane (45 %), ethylbenzene (37%), and ethylcyclohexane (15 %). To a minor extent, alkylated products (1,2-dicyclohexylethane and 1-ethyl-3-methylcyclopentane) were also observed (3 %). The authors suggested that Ni promoted the cleavage of PEB to produce phenol and ethylbenzene. Then, ethylbenzene was hydrogenated to ethylcyclohexane and the hydrodeoxygenation of phenol took place by a sequential hydrogenation and dehydration reaction, to produce cyclohexane promoted by the metal and the acidic sites, respectively. The formation of alkylated products was not elucidated.

Compared to the previous work which used Ni supported over silica-alumina for PEB conversion (300 °C and 60 bar H_2), the high amount of Ni used by Kong et al.[43] may be responsible to the complete hydrogenation of ethylbenzene, since a similar hydrogen pressure was used in both works (50 and 60 bar of H_2). In addition, the low temperature

used by Zao and Lercher[38] did not favor the cleavage of the C_{arom}-O bond of PEB to form 2-phenyl ethanol and benzene.

Nickel supported on zeolite β (20 wt. % Ni) was used to study the conversion of PEB at 220 °C, 40 bar H_2 in *n*-hexane as a solvent[28]. Over bare Hβ, 11 % of PEB was converted into phenol (36 %), 2-phenethylphenol (2-PEP; 38 %), and 4-phenethylphenol (4-PEP; 20 %). First, PEB was cleaved by H^+ addition to produce the intermediates 2-phenyleth-1-ylium and phenol. Then, 2 and 4-PEP were formed by the attack of 2-phenyleth-1-ylium onto the 2 or 4 position in phenol. When the reaction was performed over Ni/Hβ, a PEB conversion of 96 % was achieved, producing ethylcyclohexane (45 %), cyclohexane (40 %), and 1,2-dicyclohexylethane (6 %) as main products, Fig. 2.24.

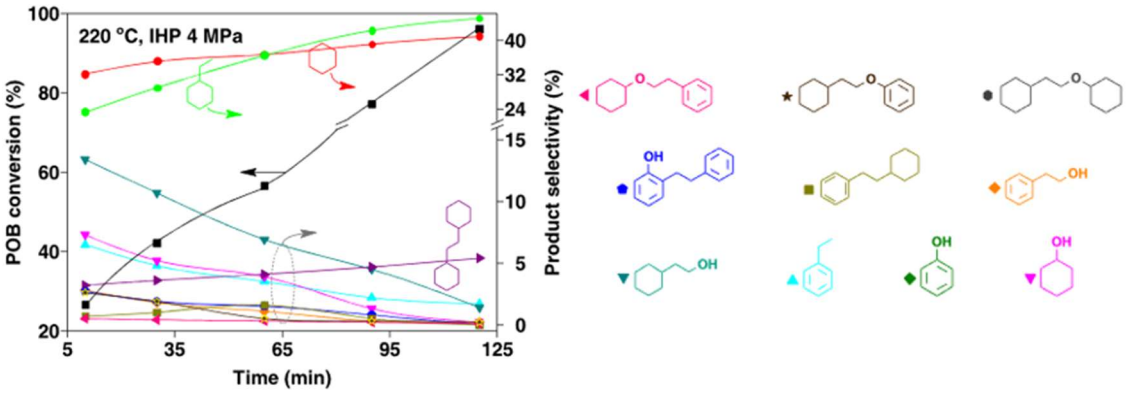

Figure 2.24: Conversion of PEB over Ni/Hβ at 220 °C, 40 bar H_2 in *n*-hexane [28].

In the presence of the metal, the intermediate 2-phenyleth-1-ylium formed after PEB cleavage can be successively hydrogenated to ethylbenzene and ethylcyclohexane, while phenol can be hydrogenated to cyclohexanone and cyclohexanol. Then, due to the presence of acidic sites, cyclohexanol can be dehydrated and then hydrogenated to cyclohexane. In addition, the authors proposed that the PEB conversion can also proceed by partial and full hydrogenation of its aromatic rings, due to the detection of (2-(cyclohexyloxy) ethyl) benzene, (2-(cyclohexylethoxy) benzene, and (2-

cyclohexylethoxy) cyclohexane, Fig. 2.25. Finally, 1,2-dicyclohexylethane can be produced by the dehydration of 2 and 4-PEP formed over acidic sites.

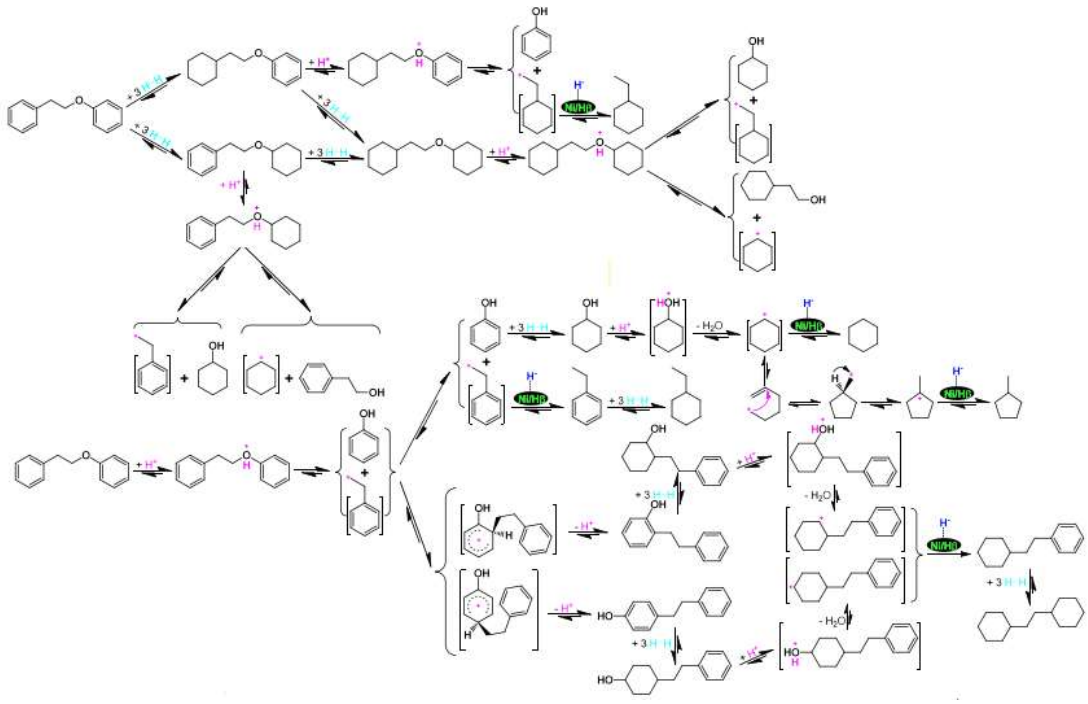

Figure 2.25 Reaction mechanism proposed by Zhou et al [28]. for the conversion of PEB over Ni/Hβ.

Compared to Zhao and Lercher[38] which used 20 wt.% Ni/HZSM5 for PEB conversion (250 °C and 50 bar H_2), ethylbenzene was fully hydrogenated to ethylcyclohexane over 20 wt.% Ni/Hβ (at 220 °C and 40 bar H_2), even with a larger particle size (32 nm and 24 nm, respectively) and lower H_2 pressure. In addition, over Ni/Hβ, 1,2-dicyclohexylethane was produced to a high extent, probably due to the higher acidity of Ni/Hβ (0.35 and 0.22 mmol g^{-1}, respectively).

Ruthenium-supported over zeolite β was used for the conversion of PEB by Yao et al.[40]. The reaction was carried out at 170°C, 40 bar of H_2 in water as a solvent. After 8 h, PEB was almost completely converted (99 %) into cyclohexane (37.4 %), ethylcyclohexane (24 %), cyclohexyl ethanol (23.6 %), and bicycloalkanes (14.5 %). The

authors did not propose a reaction pathway for the PEB conversion but suggested that the high amount of cyclohexyl ethanol observed should be due to its slow dehydroxylation reaction rate (8.8 h^{-1}) compared to the phenol (1020.3 h^{-1}).

The performance of Pd/C in the presence of HZSM5 was evaluated by Zhao and Lercher [37] for the PEB conversion (200 °C, 50 bar of H_2) in water as a solvent. Cyclohexane (46 %) and ethylcyclohexane (54 %) were formed because of the very high pressure of H_2. The authors proposed that palladium promoted the hydrogenolysis of PEB into phenol and ethylbenzene. The subsequent hydrogenation of ethylbenzene and phenol to ethylcyclohexane and cyclohexanol, respectively, also occurred on Pd. The acidic sites from HZSM5 catalyzed the dehydration of cyclohexanol, producing cyclohexene which can be hydrogenated by the metal into cyclohexane.

Ethylcyclohexane (51.6 %) and cyclohexane (48.2 %) were also the only products observed for the conversion of PEB over palladium and nickel supported over HZSM5 at 200 °C, 20 bar of H_2 in *n*-hexane [29]. However, the authors did not present a reaction pathway for PEB conversion.

Salam et al.[44] studied the effect of the silica/alumina ratio (SAR = 12, 30, and 80) on the performance of NiMoS catalysts supported on USY zeolite for the conversion of PEB at 345 °C, 50 bar H_2 in dodecane as a solvent. In the presence of bare Y30, 85 % of PEB was converted after 6 h, with a high selectivity to phenolic dimers, 3 and 4-phenethyl phenol (3 and 4-PEP) (51 %). The other bare supports (Y12 and Y80) were not evaluated. In the presence of metal, PEB was completely converted after 2 h over NiMoY30, and after 3 h over NiMoY12 and NiMoY80, Fig. 2.26. The authors suggested that for all the catalysts, the hydrogenolysis of PEB into phenol and ethylbenzene catalyzed by the metal sites occurred simultaneously with the transalkylation reaction to form 4 and 3-PEP on the acidic sites. Mono and alkyl phenols (m-cresol, 2, and 4-ethylphenol) were produced

by hydrocracking of the phenolic dimers (Fig. 2.27). In addition, a small amount of toluene, methylcyclopentane, methylcyclohexane, and 1,1-bicyclohexyl were also observed.

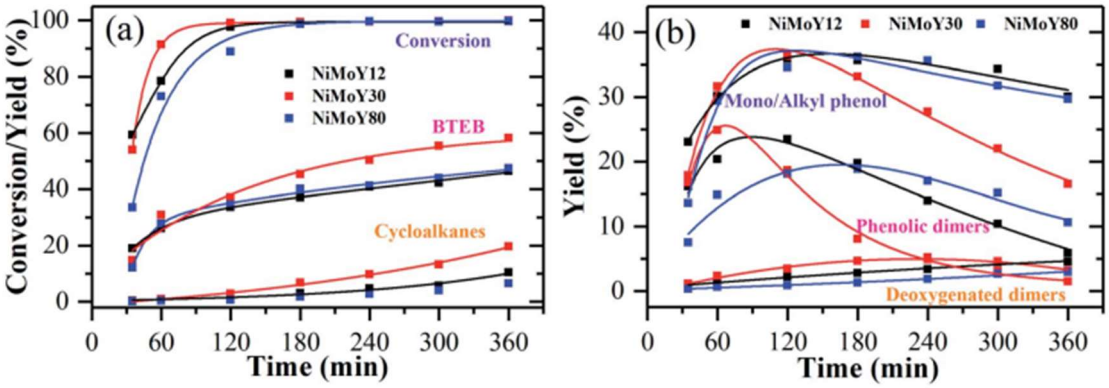

Figure 2.26: Effect of silica/alumina ratio for PEB conversion over NiMoS-USY [44].
Products: Cycloalkanes: methyl cyclopentane, methylcyclohexane, and ethylcyclohexane; BTE: benzene, toluene, and ethylbenzene; mono/alkyl phenol: phenol, 3 and 4-ethylphenol, and m-cresol; phenolic dimers: 3 and 4-phenethylphenol; deoxygenated dimers were not specified.

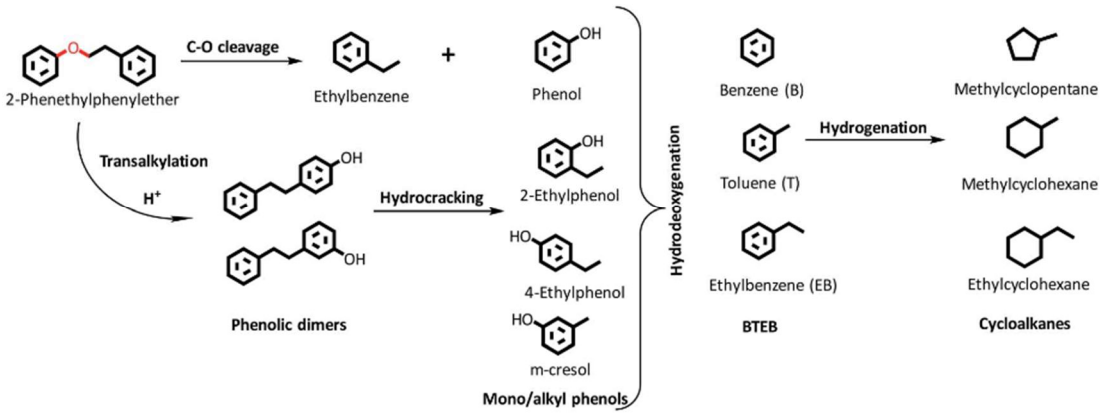

Figure 2.27: Reaction pathway of PEB over NiMoS-USY [44].

The initial rates for the formation of alkylated products (4 and 3-PEP) were calculated and the values are reported in Table 2.9. Combining these results with the total acidity, the authors concluded that the high density of acidic sites favored the formation of alkylated products. The authors also correlated the activity of the catalysts to the presence of Brønsted acidic sites. They suggested that due to the higher amount of

Brønsted acidic sites (368 μmol g^{-1}), NiMoY12 promoted mainly the transalkylation reaction instead of HDO. On the other hand, over NiMoY80, the conversion of PEB was slower and only few alkylated products were formed due to its low amount of Brønsted acidic sites (202 μmol g^{-1}). To conclude, they attributed the superior activity of NiMoY30 in the formation of hydrogenolysis and deoxygenated products to its moderate total acidity, better pore accessibility, and higher dispersion of Ni over NiMoY30.

Table 2.9: Initial rate of reaction, TOF, and total acidity for PEB.

Catalyst	Initial rate of hydrogenolysis (mmol g^{-1} h^{-1})	Initial rate of alkylation reactions (mmol g^{-1} h^{-1})	Total acidity (μmol g^{-1})
NiMoY12	78	24	686
NiMoY30	61	26	571
NiMOY80	50	14	477

Table 2.10 summarizes the catalysts and the different reaction conditions used for the conversion of PEB, while scheme 2.2 shows the different reaction pathways for the PEB conversion presented in this section. Unlike BPE, the conversion of PEB is not affected by the solvent. Over catalysts without acidic sites, the conversion of PEB occurs by hydrogenolysis of its C_{aliph}-O bond catalyzed by the metal sites, to produce ethylbenzene and phenol. After cleavage, phenol is easily hydrogenated to cyclohexanol/cyclohexanone, while ethylbenzene is only hydrogenated to ethylcyclohexane under high hydrogen pressure (20 bar). Due to the absence of acidic sites, the deoxygenation of the intermediates formed after hydrogenolysis does not occur.

Regarding the catalysts with acidic sites, the hydrogenolysis of the C_{aliph}-O bond of PEB into phenol and ethylbenzene was reported to be catalyzed over bare Nb_2O_5 and zeolite supports (Hβ and USY) in organic solvents. However, after cleavage, the zeolite promotes the alkylation reaction of phenol and toluene to form 2, 3, and 4-PEP. In the

presence of metal, phenol appears as an intermediate that is transformed differently depending on the conditions and the catalyst. Metals supported over Nb_2O_5 and sulfated zirconia favor the deoxygenation of phenol through cleavage of the C_{arom}-OH bond to form benzene, while metals supported over zeolites (HZSM5, Hβ, and USY) promote the formation of cyclohexane via a hydrogenation-dehydration route of phenol.

The external source of hydrogen is required in the HDO reaction since the reaction catalyzed by hydrogen transfer in isopropanol is not enough to pursue the reaction after hydrogenolysis. From the literature discussed, it is possible to assume that obtaining deoxygenated products requires high temperature and pressure, but a balance must be found in terms of pressure, as too high H_2 pressure can favor the competitive hydrogenation of the substrate. Globally speaking, a comparison between the different works is difficult because of the very different experimental conditions and characteristics of the catalyst (metal, acidity).

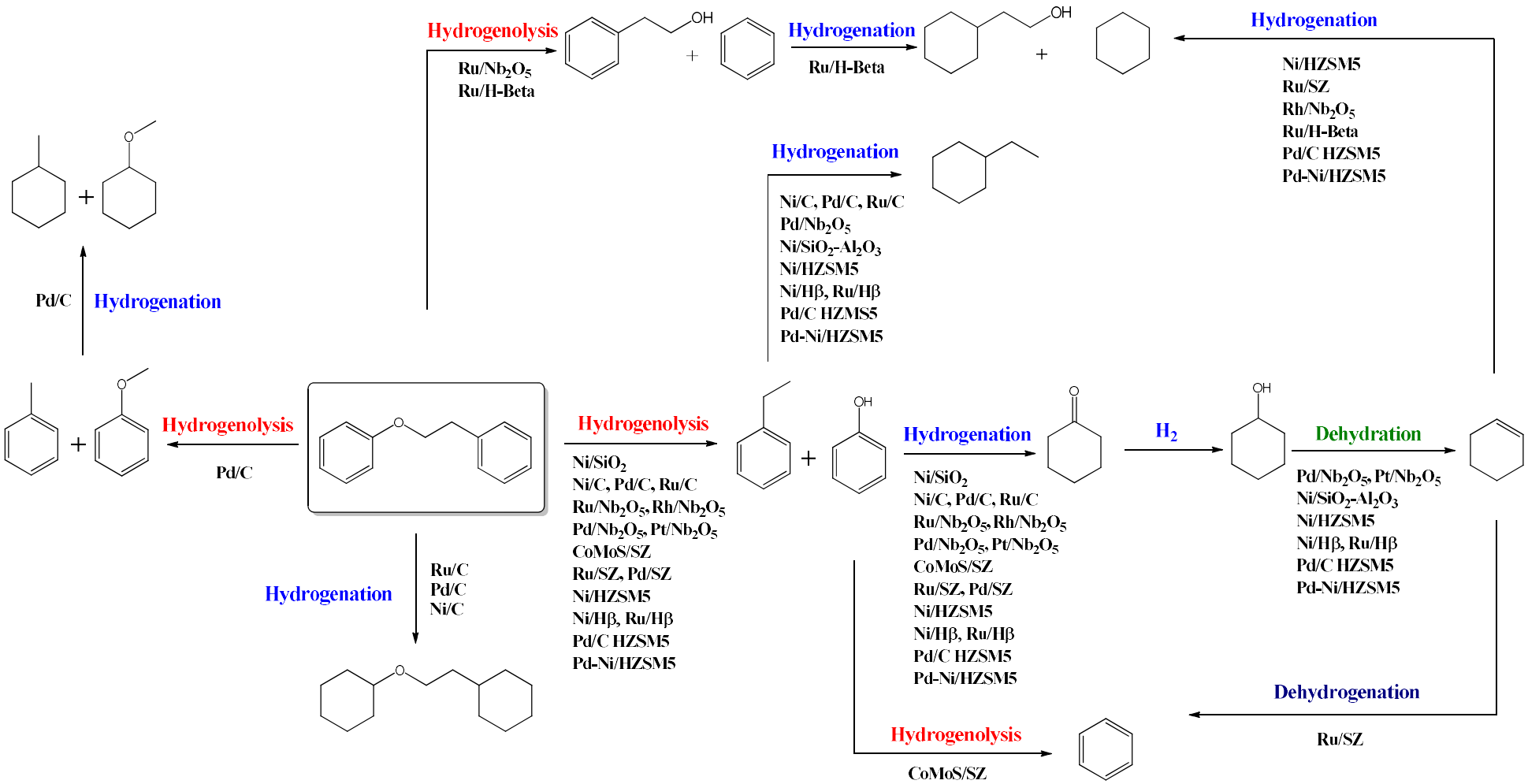

Scheme 2.2: Reaction pathways for the conversion of PEB over different catalysts.

Table 2.10: Catalysts and reaction conditions reported in the literature for the conversion of PEB.

Catalysts	Reaction conditions	Solvent	Main Products	Main conclusions	Ref.
40% Ni/SiO_2 **57% Ni/SiO_2**	T: 120°C P: 6 bar H_2	Water	Ethylbenzene, phenol	larger Ni particle size showed higher selectivity to C-O cleavage by hydrogenolysis.	24
Ru/C **Pd/C** **Pt/C**	T: 240°C P: 8 bar H_2	Water	Ethylbenzene, phenol, cyclohexanol	The conversion of PEB proceeds by hydrogenolysis of the C_{aliph}-O bond of PEB.	25
Ni/C **Ru/C** **Pd/C**	T: 150°C P: 20 bar H_2	Methanol	Ethylcyclohexane, cyclohexanol, hydrogenated products	The main reaction pathway depends on the metal: Ni catalyzes more the hydrogenolysis of PEB leading to ethylbenzene and phenol, while Ru favors the complete hydrogenation of PEB. Over Pd, the hydrogenolysis of the C_{aliph}-C_{aliph} bond of PEB competes with its complete hydrogenation.	42
Pd/Nb_2O_5 **Pt/Nb_2O_5** **Rh/Nb_2O_5** **Ru/Nb_2O_5**	T: 260 °C P: 10 bar H_2	*n*-decane	Ethylbenzene, phenol benzene, cyclohexane	Rh/Nb_2O_5 and Pd/Nb_2O_5 promoted the complete hydrodeoxygenation of phenethoxybenzene.	26
CoMoS/SZ	T: 300°C P: 20 bar H_2	Decalin	Ethylbenzene, benzene, phenol	CoMoS was responsible for: (i) hydrogenolysis of PEB leading to ethylbenzene and phenol; (ii) hydrogenolysis of phenol producing benzene.	14

Table 2.10: Catalysts and reaction conditions reported in the literature for the conversion of PEB. (continuation)

Catalysts	Reaction conditions	Solvent	Main Products	Main conclusions	Ref.
Ru/C **Ru/SZ** **Pd/SZ**	T: 240°C P: 8 bar H_2	Water	Ethylbenzene, cyclohexanol, benzene	Besides the hydrogenolysis of PEB to form ethylbenzene and phenol, Ru promotes the hydrogenolysis of phenol to benzene. On Ru/SZ, the acidic sites promote the dehydration of cyclohexanol to cyclohexene.	25,27
Ni/SiO_2-Al_2O_3	T: 300°C P: 60 bar H_2	Dodecane	Cyclohexane and ethylcyclohexane	Ni/ASA promoted two competitive reactions pathways for the conversion of phenethoxybenzene: (i) the C_{arom}-O cleavage of phenethoxybenzene into benzene and 2-phenyl ethanol and (ii) the C_{aliph}-O cleavage to produce phenol and ethylbenzene.	43
20% Ni/HZSM5	T: 250°C P: 20 bar H_2	Water	Ethylbenzene, ethylcyclohexane, cyclohexane.	Metal sites promoted the cleavage of PEB to produce phenol and ethylbenzene. Then, phenol produces cyclohexane by a sequential hydrogenation-dehydration reaction promoted by the metal and acidic sites.	38
Hβ **Ni/Hβ**	T: 220°C P: 40 bar H_2	*n*-hexane	Phenol, 2-phenethylphenol ethylcyclohexane, cyclohexane	In the presence of Ni and under these reaction conditions, the conversion of phenethoxybenzene could start by direct C_{aliph}-O cleavage or by its partial and/or complete hydrogenation.	28
Ru/H-Beta	T: 170°C P: 50 bar H_2	Water	Cyclohexane, ethylcyclohexane, and cyclohexyl ethanol	The metal sites promoted the C_{aliph}-O cleavage of phenethoxybenzene to form ethylbenzene and phenol, and the C_{arom}-O cleavage to form 2-phenyl ethanol and benzene.	40

Table 2.10: Catalysts and reaction conditions reported in the literature for the conversion of PEB. (continuation)

Catalysts	Reaction conditions	Solvent	Main Products	Main conclusions	Ref.
Pd/C and HZSM5	T: 200°C P: 50 bar H_2	Water	Ethylcyclohexane, cyclohexane	Metal promotes: (i) hydrogenolysis of PEB to form ethylbenzene and phenol; (ii) Hydrogenation of ethylbenzene. The acidic sites promote the dehydration of cyclohexanol to form cyclohexane	37
Pd-Ni/HZSM5	T: 220°C P: 20 bar H_2	n-hexane	Ethylcyclohexane, cyclohexane	Metal promotes: (i) hydrogenolysis of PEB to form ethylbenzene and phenol; (ii) hydrogenation of ethylbenzene. The acidic sites promote the dehydration of cyclohexanol on the way to cyclohexane	29
NiMoS/Y (Si/Al = 12,30 and 80)	T: 345°C P: 50 bar H_2	Dodecane	Ethylbenzene, benzene and mono/alkyl phenol	NiMoY30 showed the highest C-O hydrogenolysis and HDO activity due to the better dispersion of Ni over the support, moderate acidity, and higher accessibility to the products.	44

2.4.3.3 Catalysts used for the conversion of diphenyl ether (DPE) model molecule representative of 4-O-5 linkage

A summary of the reaction conditions and catalysts used for DPE conversion, as well as a summary of the main reaction pathways observed for each catalyst, can be found at the end of the section (Table 2.18 and Scheme. 2.3).

2.4.3.3.1 Non-acidic supports

Among the ether linkages studied in our work, 4-O-5 is the strongest and most stable ether bond, which makes DPE an attractive model molecule for studying HDO reactions. For DPE, as well as for PEB, the solvent does not contribute to its hydrogenolysis in the absence of catalyst [24,30,45]. The literature reports that in the presence of non-acidic supports (SiO_2) [30] or even over an acidic support (HZSM5)[29,38] DPE remains unreacted.

He et al.[24,30] used Ni/SiO_2 to study the conversion of DPE at 120 °C, 6 bar of H_2 in water. At the beginning of the reaction, cyclohexanol (selectivity = 65 %), benzene (selectivity = 25 %), and cyclohexyl phenyl ether (selectivity = 10 %) were observed (Fig. 2.28 a). As the reaction progressed, the yield of cyclohexanol and benzene increased while the yield of cyclohexyl phenyl ether initially increased, then decreased to zero. After 11 h, cyclohexanol, benzene, and cyclohexane were the only products observed. Considering that the selectivity to cyclohexanol was much higher than that for benzene, the authors suggested that the conversion of DPE occurred mainly by two parallel reactions: (i) DPE hydrogenolysis to form phenol and benzene and (ii) DPE hydrolysis to produce two molecules of phenol. Then, cyclohexanol and cyclohexane were formed via phenol and benzene hydrogenation, respectively (Fig. 2.28 b). In addition, DPE can be

also partially hydrogenated to produce cyclohexyl phenyl ether. In a separate test using cyclohexyl phenyl ether as feed, the rate of its hydrogenolysis was relatively low (0.8 $mol.mol_{Ni}^{-1}\ h^{-1}$), and the authors dismissed the possibility that cyclohexanol and benzene were formed from the hydrogenolysis of cyclohexyl phenyl ether.

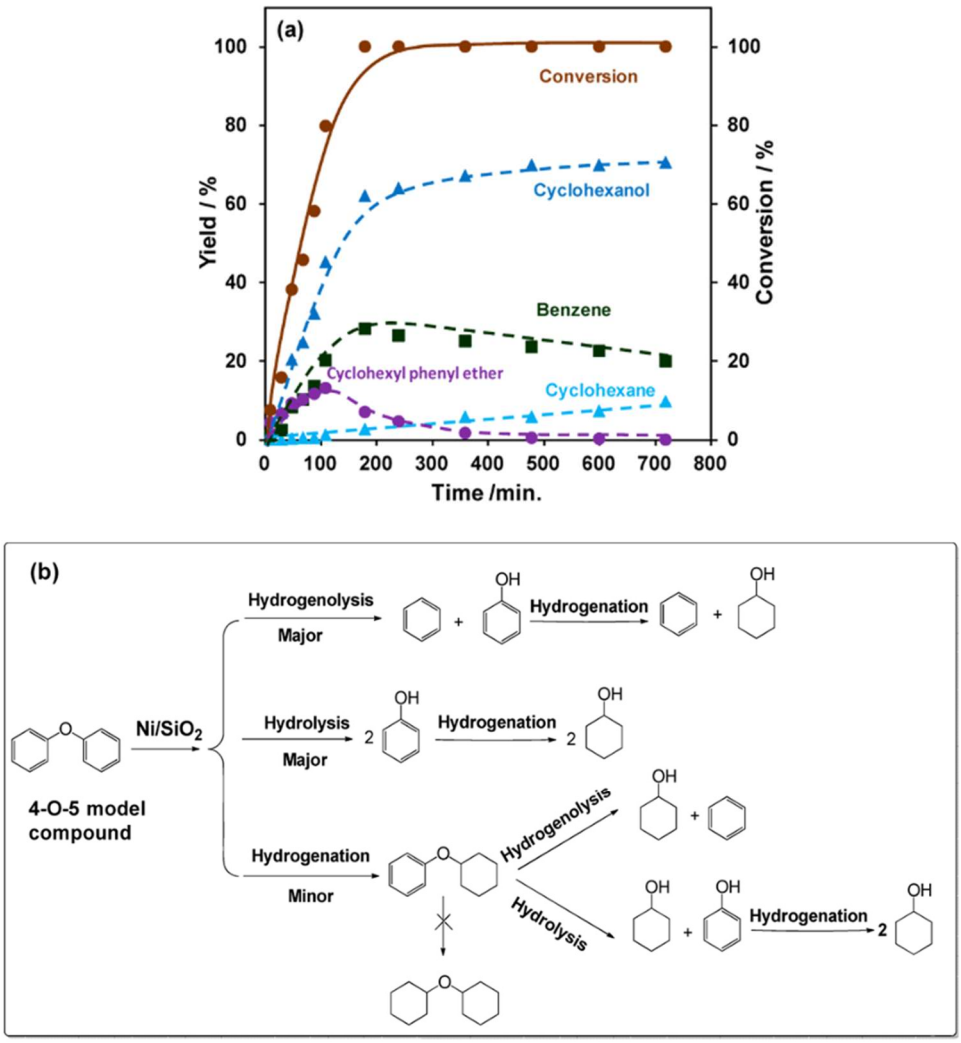

Figure 2.28: (a) Product distributions and (b) reaction pathway for DPE conversion over Ni/SiO_2, at 120 °C, 6 bar H_2 in water.

Ruthenium, platinum, and palladium-supported over carbon were used to study the conversion of DPE at 120 °C, without an external source of H_2, in isopropanol [45]. Over Ru/C, DPE was completely converted into cyclohexanol, benzene, and cyclohexane,

Table 2.11. 77.6 % of DPE was converted over Pt/C and the same products were observed; however, phenol was not completely hydrogenated to cyclohexane. Pd/C showed the lowest conversion (4.2 %) and the only products formed were phenol and benzene.

Table 2.11: Product distribution for the conversion of DPE over Ru, Pt, and Pd-supported on activated carbon.

		Yield (%)			
Catalyst	Conversion (%)	Cyclohexane	Cyclohexanol	Phenol	Benzene
Ru/C	>99	16.3	49.5	0	33.2
Pt/C	77.6	21.6	32.7	4.3	14.9
Pd/C	4.2	0	0	2.1	2.0

Reaction conditions: DPE (1 mmol), isopropanol (66 mmol), 120°C, 10 h. Catalysts: 10 wt % Pt/C (0.05 g), 10 wt % Pd/C (0.1 g), and 10 wt % Ru/C (0.1 g).

Regarding the catalytic test over Ru/C, the authors suggested that Ru can coordinatively bind to the free electron pairs of the oxygen atom of DPE, promoting its cleavage into phenoxide and phenyl radicals, which can be subsequently hydrogenated to form benzene and phenol by the active hydrogen from isopropanol on the surface of Ru (Fig. 2.29). Then, cyclohexane and cyclohexanol are formed from benzene and phenol hydrogenation, respectively. Considering the reaction conditions, Pd promoted only the hydrogenolysis of DPE, while Ru and Pt were able to hydrogenate the intermediates formed after DPE cleavage.

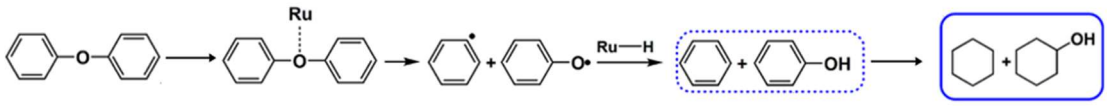

Figure 2.29: Reaction pathway for DPE conversion over Ru/C, at 120 °C, in isopropanol.

Wu et al.[46] also evaluated the activity of Pd/C, Pt/C, Ru/C as well as Ru/C modified by Cl, Br, and I atoms, and Ru/SiO_2 for the conversion of DPE at 120 °C and 5 bar of H_2, in methanol. Among the unmodified supported catalysts over carbon, Ru showed the highest activity in the cleavage of the C_{arom}-O bond of DPE, and the highest selectivity to cyclohexane and cyclohexanol (79.2 %), Table 2.12. Over Pd/C, 58.4 % of DPE was converted, and the main product was cyclohexyl phenyl ether obtained by partial hydrogenation of the DPE aromatic rings. Finally, Pt/C showed the lowest conversion of diphenyl ether (3.3 %). Compared to Ru/C, Ru/SiO_2 exhibited lower activity in DPE conversion (47 %) and the main products were cyclohexyl phenyl ether, cyclohexane, and cyclohexanol. The higher activity of Ru/C was related to the smaller Ru particle size on carbon (metal dispersion of 45 and 6.7 %, respectively) and the higher hydrogenolysis rate (0.87 and 0.06 min^{-1}, respectively).

Compared to the previous work [45] which used the same catalysts (Pd/C, Pt/C, and Ru/C) to study the conversion of DPE at 120 °C, the external source of hydrogen promoted the partial and complete hydrogenation of diphenyl ether over metal sites.

After this metal screening, the authors evaluated the conversion of DPE over Ru/C modified with Cl, Br, and I. Over Cl-Ru/C, phenol and benzene were not completely hydrogenated after DPE hydrogenolysis, but cyclohexane and cyclohexanol were still the main products formed. Over Br-Ru/C, phenol and benzene were the main products and the simple hydrogenolysis occurred as the main pathway. Finally, I-Ru/C was not active to convert DPE in these reaction conditions. The authors concluded that the presence of Br almost fully inhibited the hydrogenation of aromatic rings due to the strong interaction between Br and Ru, and the bromine selective adsorption on the catalyst surface. Over Cl-Ru/C, the hydrogenolysis and hydrogenation of DPE both proceeded.

Table 2.12: Product distribution for DPE conversion over Ru, Pt, and Pd-supported on activated carbon, methanol, and 5 bar H_2.

Cat.	X_{DPE} (%)	Selectivity (%)					
			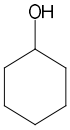	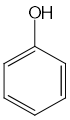		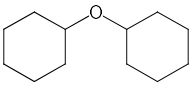	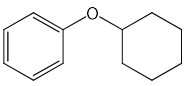
Pd/C	58.4	1.8	1.7	0.4	1.9	5.0	84.8
Pt/C	3.3	0.0	0.0	0.0	0.0	0.00	98.8
Ru/C	100	40.3	38.9	0.0	0.0	19.1	0.2
Ru/SiO_2	47.4	23.5	20.8	4.6	5.1	4.2	39.5
Cl-Ru/C	100	35.6	31.9	9.7	8.9	12.5	0.4
Br-Ru/C	99.8	5.1	2.6	45.6	44.7	0.0	0.0
I-Ru/C	0.8	0.0	0.0	0.0	0.0	0.0	0.0

Reaction conditions: DPE (100 mg), methanol (5 g), catalyst (50 mg), 120 °C, 5 bar H_2, 6h.

Ruthenium-supported over silica was also used by Yao et al.[40] to study the DPE conversion in aqueous phase (120 °C, 40 bar H_2). After 3 h, DPE was converted (X_{DPE} = 72 %) into cyclohexanol (51.2 %), cyclohexane (23.4 %), cyclohexyl phenyl ether (12.9 %), and dicyclohexyl ether (12.6 %). The authors did not propose a reaction pathway for the DPE conversion over Ru/SiO_2. The higher H_2 pressure used compared to Wu et al.[46] (6 bar H_2) increased the DPE conversion and favored the complete hydrogenation of phenol and benzene after DPE cleavage.

Guvenatam et al.[47] studied the performance of Pt/C for the conversion of DPE at 200°C, 20 bar of H_2 in water as a solvent. Fig. 2.30 a presents the product distribution as a function of reaction time. Cyclohexane and cyclohexanol were the main products formed, but dicyclohexyl ether and cyclohexanone were also observed in minor amounts. The authors proposed that the hydrogenation of the DPE aromatic rings toward dicyclohexyl ether occurred in competition with DPE hydrogenolysis into cyclohexanone and cyclohexane catalyzed by Pt sites, Figure 2.30 b.

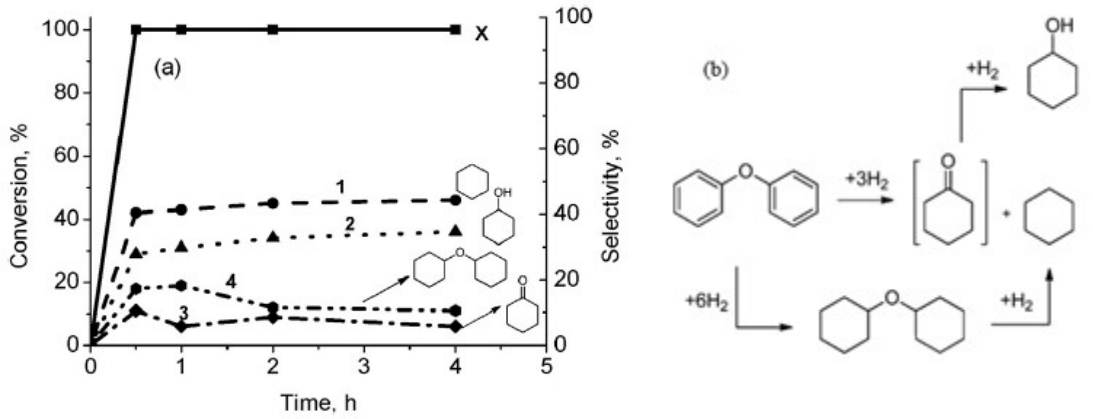

Figure 2.30 (a) Conversion of DPE and selectivity of products curves as a function of reaction time. Reaction conditions: substrate (0.8 mmol), Pt/C (5mg), 200 °C, 20 bar of H_2, water. (b) Reaction pathway proposed by Guvenatam et al.[47]

Wang et al.[48] evaluated the performance of Pd/C, Pt/C, and Ni/SiO_2 in the conversion of DPE at 200 °C, 40 bar of H_2 in water as a solvent. All catalysts were compared in the conversion range higher than 92 % and the products formed were divided into 3 groups: (i) hydrogenolysis products (2 x [Cyclohexene and benzene]), (ii) hydrolysis products ([phenol + cyclohexanone + cyclohexanol] – the hydrogenolysis products), and (iii) hydrogenation products of DPE represented by phenyl cyclohexyl ether and dicyclohexyl ether. The authors observed that over Pd/C, DPE was preferentially cleaved by reductive hydrolysis to produce phenol and cyclohexanone, while over Pt/C and Ni/SiO_2, the direct hydrogenolysis of DPE occurred as the main reaction pathway, Table 2.13.

Table 2.13: Products selectivity for the conversion of DPE over Pd/C, Pt/C, and Ni/SiO_2.

	Carbon selectivity (%)		
Catalyst	Hydrogenolysis	Hydrolysis	Hydrogenation
5 % Pd/C	2	88	10
5 % Pt/C	40	30	30
64 % Ni/SiO_2	60	38	2

The products yield versus DPE conversion over Pd/C at 190 °C in water is shown in Fig.2.31. Cyclohexyl phenyl ether (50 %), phenol (25 %), and cyclohexanone (25 %) were the primary products with constant selectivities up to a conversion of 40%. It is possible to observe that phenol and cyclohexanone were initially formed in the same proportions instead of two molecules of phenol via conventional hydrolysis. As the reaction progressed, the yield of cyclohexanone, cyclohexanol, and dicyclohexyl ether increased while the yield of cyclohexyl phenyl ether decreased to zero. When the complete conversion was achieved, cyclohexanone (47 %), cyclohexanol (25 %), and phenol (17 %) were the main products observed.

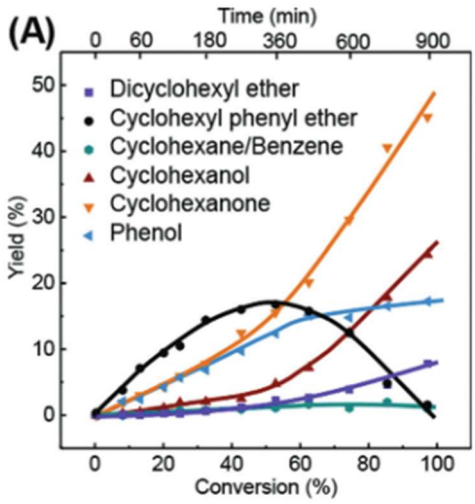

Figure 2.31: Product distribution for DPE conversion over Pd/C in water.

The authors proposed that in the presence of Pd/C and water, the conversion of DPE starts with the hydrogen addition onto one of the aromatic rings of DPE, to form two types of intermediates in which the oxygen atom is connected to a vinylic or alkyl carbon atom (e.g., cyclohex-1-enyl phenyl ether and cyclohex-3-enyl phenyl ether), Fig. 2.32. The intermediates formed can be further hydrogenated to form cyclohexyl phenyl ether or dicyclohexyl ether. However, an isolated experiment showed that cyclohex-1-enyl phenyl ether mainly reacts by reductive hydrolysis to produce phenol and cyclohexanone.

In addition, they also evaluated the conversion of DPE over Pd/C in decalin as a solvent in the same reaction conditions (200 °C, 40 bar). In this case, the authors reported that the hydrogenation of the aromatic rings accounts for more than 95 % of selectivity and that C_6 oxygenated compounds (phenol, cyclohexanol, and cyclohexanone) were produced in exactly the same quantity as the sum of benzene and cyclohexane.

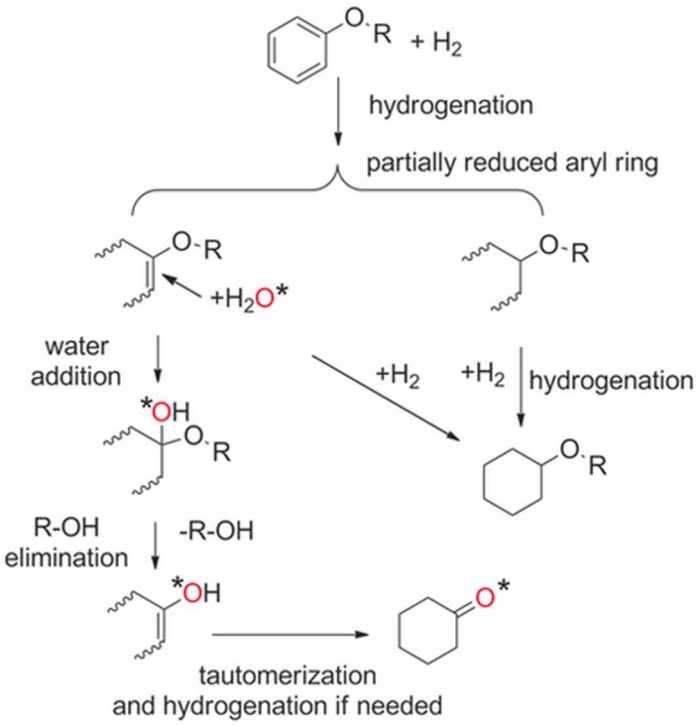

Figure 2.32: Mechanistic pathway for the reductive hydrolysis of aryl ethers on Pd surface, proposed by Wang et al.[48] R=phenyl, cyclohexyl, phenylethyl, and n-butyl.

Zhang et al.[49] evaluated the performance of Co/CeO_2 and the bimetallic $RuCo/CeO_2$ for the conversion of DPE at 200 °C, 20 bar of H_2 in decalin. Over 2 % Co/CeO_2, after 160 min, only 14.5 % of DPE was converted into benzene (43.1 %) and cyclohexanol (43.9 %) as main products. After increasing the Co content to 5 wt. %, DPE was fully converted at the same reaction time. At low conversion, benzene and cyclohexanol were the main products over $5Co/CeO_2$ (Fig. 2.33 a). As the conversion increased, the yield of benzene increased to a maximum of 27.4 % (around 80 % of

conversion), then gradually decreased while the yield of cyclohexane increased. In contrast, the yield of cyclohexanol linearly increased when the DPE conversion increased. The authors proposed that, first, the hydrogenolysis of DPE takes place to produce phenol and benzene. Phenol can be easily hydrogenated to cyclohexanol, while cyclohexane is formed by benzene hydrogenation. Considering the low amount of cyclohexyl phenyl ether and dicyclohexyl ether formed, the hydrogenation of DPE aromatic rings occurred only to a minor extent.

When the Co-based catalyst was promoted with a very low quantity of Ru (0.01Ru1.99Co/CeO_2), the same products were observed. However, a high amount of cyclohexane was formed (Fig. 2.33 b). Considering the calculated TOF, the catalyst promoted with ruthenium was 4 times more active than Co/CeO_2 catalysts. The authors proposed that the presence of a small amount of Ru could enhance the reduction of cobalt oxide during the catalyst preparation, resulting in more metallic Co active sites. In addition, the presence of Ru could increase the effect of H_2 spillover, which improved the hydrogenolysis of the C_{arom}-O bond of DPE and the hydrogenation steps.

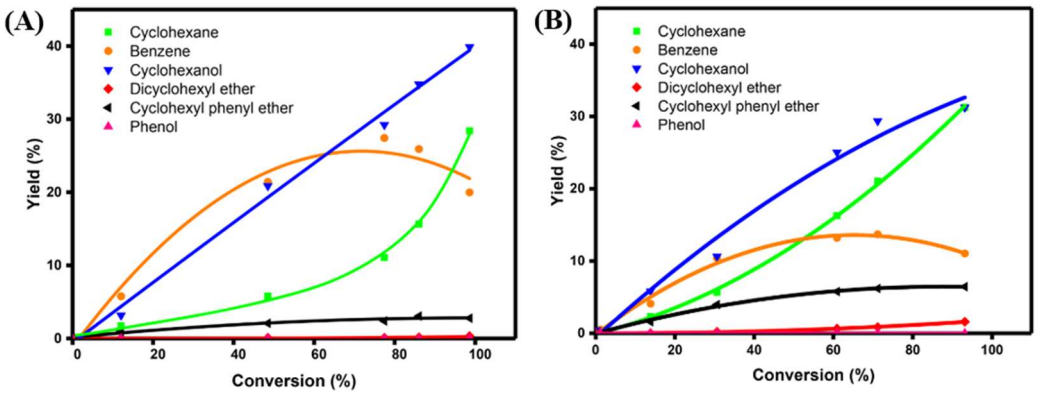

Figure 2.33: Product distribution as a function of DPE conversion over 5Co/CeO_2 (A) and 0.01Ru1.99Co/CeO_2 (B) at 200 °C and 20 bar H_2

Concerning the results presented above, DPE can be cleaved by three different reaction pathways over non-acidic catalysts: (i) through direct hydrogenolysis into benzene and phenol, (ii) via conventional hydrolysis to produce 2 molecules of phenol, or (iii) via reductive hydrolysis to form cyclohexanone and phenol. In general, the intermediates formed can be hydrogenated to produce cyclohexanol and cyclohexane. In addition, depending on the reaction conditions, the hydrogenation of the DPE aromatic rings may also occur.

2.4.3.3.2 Acidic supports

Shu et al.[50] evaluated the activity of Ru/TiO_2 in the conversion of DPE. The reaction was carried out at 260 °C, 10 bar of H_2, in octane as a solvent, and the only products formed were cyclohexane (86%) and 1,1-bicyclohexyl (14%). However, the authors did not propose a reaction pathway for the formation of these products.

DPE conversion was studied by Wang and Rinaldi [51] over Raney Ni and Ni-based catalysts supported on different oxides (Al-SBA-15, Al_2O_3, and ZrO_2), in methylcyclohexane as solvent (200 °C, 50 bar of H_2). The complete conversion was achieved with almost all the catalysts evaluated, Table 2.14. Over Raney Ni, Ni/Al_2O_3, and Ni/ZrO_2, DPE was mainly converted into dicyclohexyl ether, cyclohexanol, and cyclohexane. Over Ni/Al-SBA-15, complete deoxygenation was achieved in which cyclohexane and 1,1-bicyclohexyl (2%) were the only products formed. The reaction pathway was not proposed. However, the authors highlighted that by combining the Ni hydrogenation ability with Al-SBA-15 which exhibited a high surface area (607 $m^2\ g^{-1}$) and high acidity, DPE could be quantitatively converted into cyclohexane.

Table 2.14: Product distribution for DPE conversion over Ni-based catalysts.

Catalyst	X (%)	Selectivity (%)				
Raney Ni	100	-	38	-	29	32
Ni/ZrO_2	96	14	19	8	24	32
Ni/Al_2O_3	99	3	44	-	24	29
Ni/Al-SBA-15*	100	-	-	-	-	98

*1,1-bicyclohexyl was formed (2%).

Song et al.[14] evaluated the performance of cobalt molybdenum sulfide supported over sulfated zirconia for the conversion of DPE at 300 °C, 20 bar of H_2 in decalin as a solvent. As can be seen in Fig. 2.34, the products formed were benzene and phenol. As was the case for the previous molecules, the authors proposed that DPE initially adsorbs on both CoMo sulfide and Lewis acidic sites of sulfated ZrO_2. The hydrogenolysis of the C_{arom}-O bond of DPE, producing phenol and benzene, was facilitated by the generated S-H on the CoMo sulfide phase. Then the hydrogenolysis of the C_{arom}-O bond (HDO) of phenol was subsequently performed over the CoMo sulfide surface, producing more benzene.

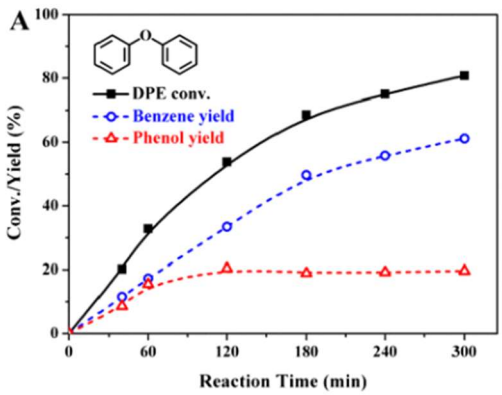

Figure 2.34: Conversion of DPE, the yield of products curves as a function of reaction time and the reaction pathways. Conditions reactions: substrate (1 mmol), CoMo/SZ (20mg), 300 °C, 20 bar of H_2, decalin [14]

Shao et al.[52] used palladium-supported on niobium oxide and silica (4 wt.% of Pd and 10 wt.% Nb_2O_5) for the conversion of DPE at 170 °C, 25 bar of H_2, in dodecane as solvent. After 24 h, DPE was completely converted to cyclohexane. The authors did not discuss the reaction pathway but proposed that NbO_x species could efficiently promote the C_{arom}-O cleavage of DPE and assist the hydrodeoxygenation process.

Jiang et al.[53] evaluated the activity of Ni, Co, and Cu supported on niobium oxide for the conversion of DPE at 220 °C, 10 bar of H_2, in isopropanol as a solvent. The DPE conversion increased as follows: Cu/Nb_2O_5 (60.7 %) < Co/Nb_2O_5 (67.8 %) < Ni/Nb_2O_5 (99.7 %), Table 2.15. Globally speaking, the main products observed were benzene, phenol, cyclohexanol, and cyclohexane. The authors proposed that first, DPE was mainly cleaved into phenol and benzene by hydrogenolysis, followed by their hydrogenation into cyclohexanol and cyclohexane, respectively, Fig. 2.35. To a minor extent, DPE can be partially hydrogenated to form cyclohexyl phenyl ether, which can follow two steps: (i) its hydrogenolysis to form cyclohexane and phenol, or benzene and cyclohexanol; and/or (ii) its hydrogenation into dicyclohexyl ether, and further hydrogenolysis into cyclohexane and cyclohexanol.

The higher conversion over Ni/Nb_2O_5 was attributed to the easier H_2 adsorption onto the Ni surface and to activated hydrogen radicals, which led to a higher hydrogenolysis activity. Additionally, the authors highlighted that Ni/Nb_2O_5 showed fewer acidic sites compared to the literature values. Due to this, Ni/Nb_2O_5 promoted the phenol hydrogenation but not dehydration to produce cyclohexane.

Table 2.15: Conversion of DPE over Cu/Nb_2O_5, Co/Nb_2O_5, and Ni/Nb_2O_5 at 220°C, 10 bar H_2 in isopropanol.

Catalyst	X_{DPE} (%)	Yield (%)					
			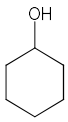	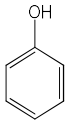		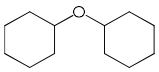	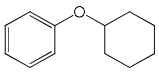
Cu/Nb_2O_5	60.7	38.9	31.2	18.7	16.3	0.8	4.6
Co/Nb_2O_5	67.8	42.6	41.5	12.0	12.6	3.5	8.9
Ni/Nb_2O_5	99.7	80.0	91.8	4.5	16.5	0.9	2.3

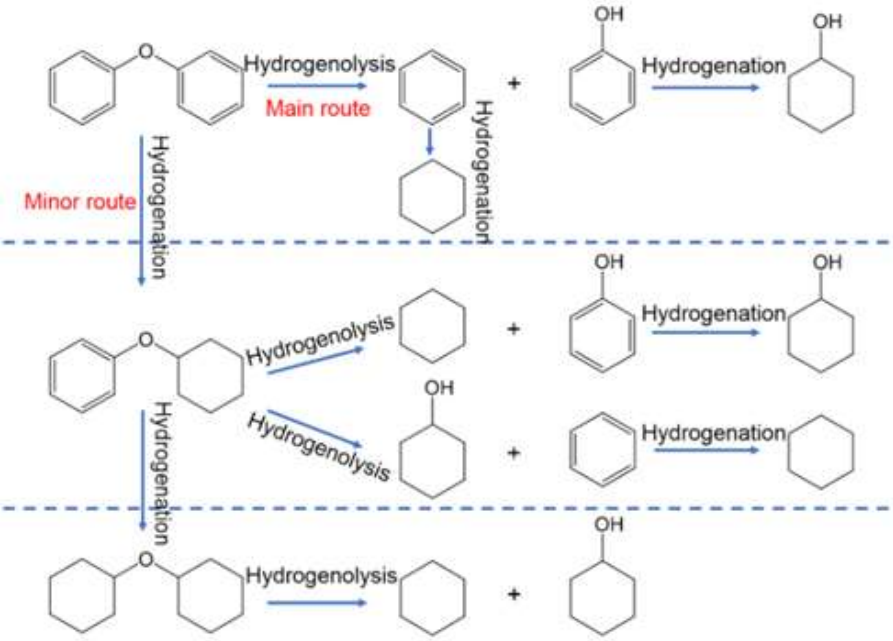

Figure 2.35: Reaction pathway for the conversion of DPE over Ni/Nb_2O_5 at 220°C, 10 bar H_2 in isopropanol.

Rhodium supported over niobium oxide was employed by Guan et al.[26] to study the conversion of DPE at 260 °C, 10 bar of H_2, in *n*-decane. At the beginning of the reaction, the main products were benzene and phenol formed by hydrogenolysis of DPE, Fig. 2.36. As the reaction progressed, it was possible to observe that the selectivity of

phenol progressively decreased while the selectivity of benzene increased, indicating that benzene was also formed by hydrogenolysis of the C_{arom}-O bond of phenol.

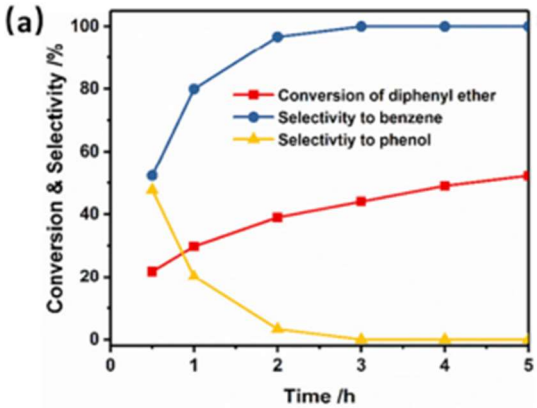

Figure 2.36: Product distribution for DPE conversion over Rh/Nb_2O_5 at 260 °C, 10 bar H_2 in *n*-decane [26].

Jin et al.[54], studied the conversion of DPE over Ni-based catalysts supported on niobium phosphate, zirconium phosphate, and Zr-doped with niobium phosphate at 180 °C, 5 bar of H_2 in *n*-decane. Over $Ni/NbPO_4$, DPE was converted (14.7 %) producing phenol (PHE; selectivity = 38.2 %), benzene (BEN; selectivity = 47.0 %), and cyclohexane (CHN; selectivity = 14.8 %) after 5.5 h (Fig 2.37 a). The authors suggested that due to its low acidity and large Ni particle size (24 nm), $Ni/NbPO_4$ favored the hydrogenolysis of DPE into phenol and benzene, followed by the hydrogenation of benzene to cyclohexane.

Over $Ni/ZrNbPO_4$ the conversion of DPE increased up to 59 %. Initially, benzene, phenol, and cyclohexanol (CHL) were formed (Fig. 2.37 b). As the reaction progressed, the yield of phenol decreased while the yield of cyclohexanol increased, indicating that after DPE cleavage phenol was hydrogenated to cyclohexanol. A small yield of cyclohexyl phenyl ether (CPE) was also observed, indicating that the partial hydrogenation of DPE occurred. After 4 h, the yield of cyclohexanol produced from

phenol or via hydrogenolysis of CPE started to decrease, while the yield of cyclohexane increased, suggesting that the dehydration of cyclohexanol was taking place. Compared to Ni/$NbPO_4$, after 5.5 h, benzene (selectivity = 53.2 %), cyclohexane (selectivity = 25.1 %), and cyclohexanol (selectivity = 15.6 %) were formed as main products. The higher activity of Ni/$ZrNbPO_4$ was attributed to its smaller Ni particle size (17 nm) and moderate acidity. Finally, due to its higher acidity and even smaller Ni particle size (12 nm), Ni/$ZrPO_4$ exhibited the highest DPE conversion (70 %). At the end of the reaction, cyclohexane (selectivity = 57.3 %) and benzene (selectivity = 35.7 %) were the major products formed (Fig. 2.37 c).

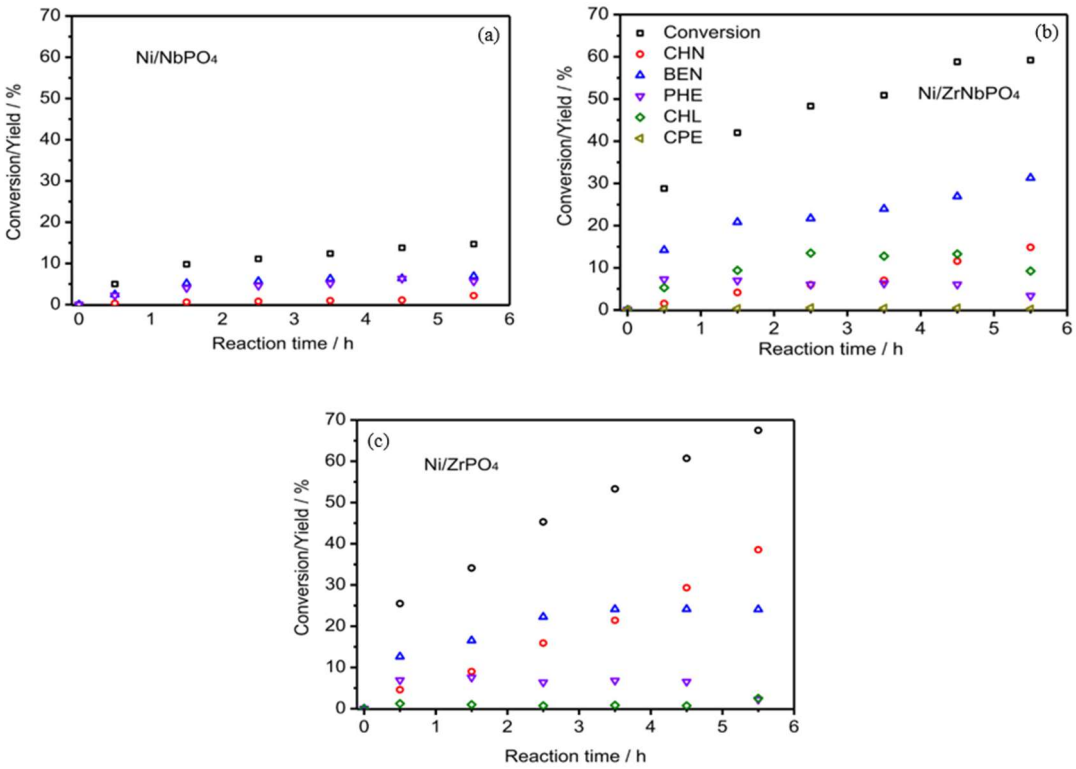

Figure 2.37: Product distribution for the conversion of DPE over Ni/$NbPO_4$ (a), Ni/$ZrNbPO_4$ (b), Ni/$ZrPO_4$ (c) [54].

Yao et al.[40] used Ru-based catalysts supported over Al_2O_3 and different zeolites for the conversion of DPE at 120°C, 40 bar of H_2 in water as a solvent, Table 2.16. All catalysts were compared at similar conversion. It is possible to observe that the selectivity

to cyclohexane follows the trend: Ru/HZSM5 (73.2 %) > Ru/H-beta (66 %) > Ru/H-USY (51 %) > Ru/Al_2O_3 (33.5 %). Among the catalysts supported on zeolites, the selectivity to cyclohexane can be related to the total acidity, as the highest selectivity was achieved with the most acidic catalyst (acidity order: Ru/HZSM5 > Ru/H-Beta > Ru/USY > Ru/MOR). However, the products selectivity can be also affected by the pore structure of the zeolite. Due to the small pore diameter of Ru/HZSM5 (0.49 nm), the DPE diffusion was slower than in the other zeolites with larger pore diameters (0.70 nm), and a considerable amount of cyclohexyl phenyl ether and dicyclohexyl ether was also observed.

Table 2.16: Product distribution for DEP conversion over different catalysts [40].

Catalysts	X_{DPE} (%)	Selectivity (%)			
			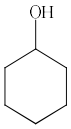	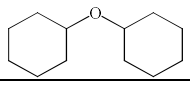	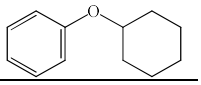
Ru/Al_2O_3	72.6	33.5	52.9	10.6	3.1
Ru/H-MOR	73.2	34.5	45.1	10.6	9.8
Ru-USY	65.8	51.1	45.1	0.7	2.9
Ru/H-Beta	70.4	66.0	30.5	0.8	2.7
Ru/HZSM5	74.5	73.2	2.5	11.1	13.2

The effect of the Ru content on Ru/H-Beta catalysts was also evaluated. The increase of Ru loading from 0.5 to 1 % increased the DPE conversion from 55.4 to 80.5 %. However, when 2 % of Ru was used, the DPE conversion decreased to 64.3 %. Although the increase of Ru content did not significantly change the Ru particle size, the density of acidic sites was affected. The authors observed that the increase of Ru content drastically decreased the total density of Lewis acidic sites in Ru/H-Beta (from 107 to 9 $\mu mol\ g^{-1}$), while the density of Brønsted acidic sites was almost the same, indicating that Lewis acidic sites are fundamental in the HDO of DPE over Ru/H-Beta.

The product distribution as a function of time for DPE conversion over 0.5 w.t% Ru/H-Beta is shown in Fig. 2.38. At the beginning of the reaction, benzene, cyclohexanol, and cyclohexane were formed as main products. The benzene selectivity was approximately the sum of cyclohexane and cyclohexanol selectivities. Throughout the reaction, as benzene and cyclohexanol selectivities decreased, the selectivity to cyclohexane increased until 3 h, when a conversion of 95 % was achieved. The authors proposed that, first, DPE was cleaved into phenol and benzene, Fig. 2.39. The absence of phenol indicated that its hydrogenation into cyclohexanol was faster than benzene conversion. Cyclohexane could be formed by two different pathways: (i) benzene hydrogenation or (ii) cyclohexanol dehydration into cyclohexene, followed by its hydrogenation. In addition, to a low extent, DPE could also be hydrogenated to form cyclohexyl phenyl ether and dicyclohexyl ether, which could also be cleaved to phenol, cyclohexanol, and cyclohexane.

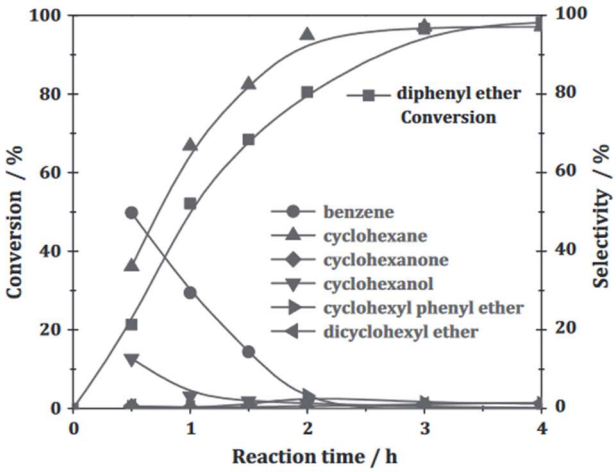

Figure 2.38: Product distribution as a function of time for DPE conversion of Ru/H-Beta [40].

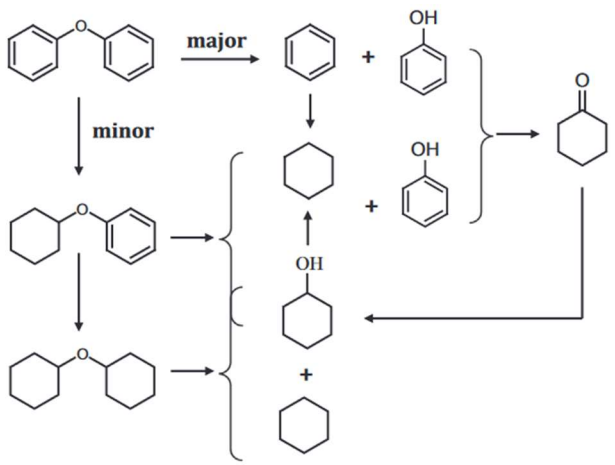

Figure 2.39: Reaction pathway for DPE conversion over Ru/H-Beta proposed by Yao et al.[40].

Zhang et al.[39] evaluated the conversion of DPE over Ruthenium-supported on zeolite HZSM5 (1 wt. %) at 200 °C, 50 bar of H_2 in water. After 4 h, DPE was selectively converted into cyclohexane (96.8 %). Similar results were observed by Zhao and Lercher [37] over Pd/C and HZSM5 in the same reaction conditions. After 2 h, cyclohexane was the only product obtained. The reaction pathway for DPE conversion was proposed in neither work. Compared to Yao et al.[40] who used 0.5 wt. % Ru/HZSM5 for DPE conversion (120 °C, 40 bar H_2), the high temperature favored the formation of cyclohexane, and products from full and partial hydrogenation of DPE were not detected.

Zhao and Lercher [38] used Ni supported on HZSM5 for DPE conversion in aqueous phase at 250 °C and 50 bar H_2. Under these reaction conditions, 64 % of DPE was selectively converted into cyclohexane (95 %) and benzene (5 %). The reaction pathway for DPE conversion was not proposed.

Palladium and nickel supported on HZSM5 as well as Ni/HZSM5 (10 wt.% Ni), and Pd/HZSM5 (1 wt.% Pd) were used by Zhao, et al.[29] to evaluate the conversion of DPE at 220 °C, 20 bar of H_2, in *n*-hexane. No conversion was observed over Ni/HZSM5, Table 2.17. Over Pd/HZSM5, 70.4 % of DPE was converted to form cyclohexane,

cyclohexyl phenyl ether, and dicyclohexyl ether. When bimetallic Pd-Ni/HZSM5 (1 wt.% Pd and 10 wt.% Ni) was used, DPE was completely converted to cyclohexane. The authors also evaluated the effect of the support for the conversion of DPE. Over Pd-Ni/Al_2O_3, only 34 % of DPE was converted and a high amount of cyclohexanol and hydrogenated products from DPE was observed. The high activity of Pd-Ni/HZSM5 for DPE HDO was related to its high amount of medium strength acidic sites.

Table 2.17: Conversion of DPE over different catalysts at 220°C, 20 bar of H_2, and *n*-hexane as a solvent.

Ent.	Catalyst	Conv (%)	Selectivity (%)				
				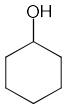	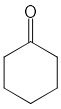	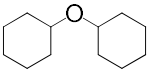	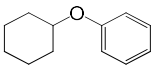
1	10Ni/HZSM5	0.0	0.0	0.0	0.0	0.0	0.0
2	1Pd/HZSM5	70.4	61.3	0.0	2.7	24.2	11.8
3	1Pd-10Ni/HZSM5	100	100	0.0	0.0	0.0	0.0
4	1Pd-10Ni/Al_2O_3	34.2	32.7	23.4	0.0	28.0	15.9

The product distribution as a function of DPE conversion over Pd-Ni/HZSM5 is presented in Fig.2.40. At low conversion, cyclohexane, benzene, cyclohexyl phenyl ether, and cyclohexanol were formed as main products. As DPE conversion increased, the selectivity to cyclohexane also increased, while the selectivity to the other products decreased. When complete conversion was achieved, cyclohexane was the only product detected. The authors proposed that cyclohexyl phenyl ether is an important intermediate in DPE conversion, which can follow three reaction pathways: (i) hydrogenation to form dicyclohexyl ether, (ii) hydrogenolysis of its C_{arom}-O bond into benzene and cyclohexanol or (iii) hydrogenolysis of its C_{aliph}-O bond into phenol and cyclohexane. The cyclohexanol formed by phenol hydrogenation or via cyclohexyl phenyl ether cleavage can be dehydrated to cyclohexene, thanks to the acidic sites. Then, cyclohexane was formed by

cyclohexene hydrogenation. Due to the low bond dissociation enthalpy of the C_{aliph}-O bond (277.76 kJ mol^{-1}) in cyclohexyl phenyl ether, compared to its C_{arom}-O bond (435.52 kJ mol^{-1}), the authors proposed that the hydrogenolysis of cyclohexyl phenyl ether into phenol and cyclohexane occurred as the main reaction pathway.

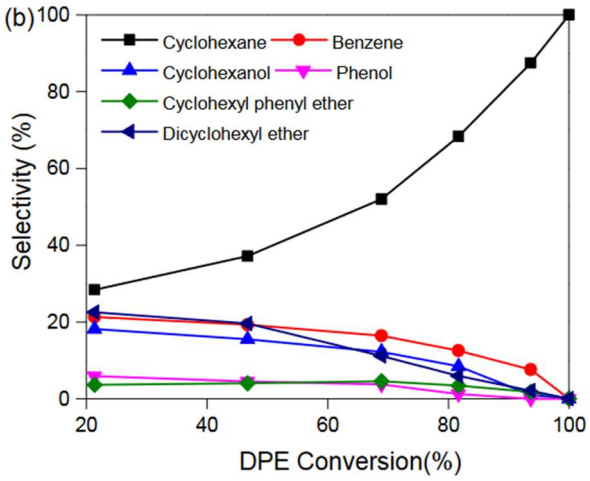

Figure 2.40: Product distribution as a function of DPE conversion. Reaction conditions: substrate (1mmol), 1Pd-10Ni/HZSM5 (100 mg), *n*-hexane, 220°C, 20 bar H_2.

Table 2.18 shows the different catalysts and reaction conditions used for DPE conversion reported in this section and the scheme 2.3 summarizes all the reaction pathways proposed in the literature. As reported for PEB, the conversion of DPE is not affected by the solvent, and over bare supports (SiO_2 and HZSM5), DPE remains unreacted independently of the type of solvent used, polar or non-polar.

Depending on the reaction conditions, DPE can be cleaved by two different reaction pathways: (i) hydrogenolysis to produce phenol and benzene; or (i) hydrolysis into two molecules of phenol. Over catalysts without acidic sites, phenol and cyclohexanone can be hydrogenated to cyclohexanol, while benzene can be hydrogenated to cyclohexane. Over acidic supports, cyclohexanol can be transformed into cyclohexane via dehydration/hydrogenation steps.

In parallel to the hydrogenolysis and/or hydrolysis of DPE, the partial and full hydrogenation of its aromatic rings can also occur, to form cyclohexyl phenyl ether (CPE) or dicyclohexyl ether (DCE), respectively. After DPE hydrogenation, the cleavage of CPE and DCE can also occur. Wang et al.[48] proposed that over Pd/C, CPE can be cleaved via reductive hydrolysis to form phenol and cyclohexanone, while Zhao et al.[29] reported that over Pd-Ni/HZSM5 in *n*-hexane, the hydrogenolysis of the C_{aliph}-O bond of CPE into phenol and cyclohexane occurs as the main reaction pathway, due to its lower bond dissociation enthalpy. Regarding DCE, its hydrogenolysis into cyclohexanol and cyclohexane seems to be more difficult and takes place depending on the reaction conditions.

Table 2.18 Reaction conditions and catalysts used for the conversion of DPE presented in the literature.

Catalysts	Reaction conditions	Solvent	Main products	Conclusion	Ref.
Raney Ni	T: 90°C P: 50 bar H_2	Hex-F-2-PrOH n-heptane decalin Methylcyclohexane	Completely hydrogenated products, cyclohexanol, cyclohexane	Metal promotes: (i) hydrogenolysis of DPE leading to phenol and benzene; (ii) hydrogenation of phenol to cyclohexanol, and (iii) benzene hydrogenation producing cyclohexane.	33
Ni/SiO$_2$	T: 200°C P: 6-40 bar H_2	Water	Benzene, cyclohexanol, cyclohexane	Hydrogenolysis and hydrolysis of DPE occur in parallel. In addition, when increasing the hydrogen pressure causes the hydrogenation of the DPE aromatic rings.	24,30
Ni/SBA-15	T: 200°C P: 50 bar H_2	Methylcyclohexane	Dicyclohexyl ether, cyclohexane, cyclohexanol	The absence of acidic sites favored the hydrogenation of DPE aromatic rings.	51
Pd/C **Pt/C** **Ru/C**	T: 120°C P: Without H_2	Isopropanol	Benzene, cyclohexanol, cyclohexane	The authors proposed that DPE can be cleaved into phenoxide and phenyl radicals over Ru/C. Among the catalysts the activity followed the trend: Ru/C > Pt/C > Pd/C.	45
Ru/C, Pt/C, Pd/C **Cl-Ru/C, Br-Ru/C, I-Ru/C** **Ru/SiO$_2$**	T: 120°C P: 5 bar H_2	Methanol	Cyclohexane, Cyclohexanol, dicyclohexyl ether, cyclohexyl phenyl ether	Ru/C presented the highest activity to cleavage DPE via hydrogenolysis while Pd/C favored the hydrogenation of the DPE aromatic rings. The addition of Br inhibited the DPE hydrogenation	46
Ru/SiO$_2$	T: 120°C P: 40 bar H_2	Water	Cyclohexanol, cyclohexane cyclohexyl phenyl ether, dicyclohexyl ether,	The reaction pathway for DPE conversion was not proposed.	40

Table 2.18 Reaction conditions and catalysts used for the conversion of DPE presented in the literature. (continuation)

Catalysts	Reaction conditions	Solvent	Main products	Conclusion	Ref.
Pt/C	T: 200°C P: 20 bar H_2	Water	Cyclohexane, cyclohexanol, dicyclohexyl ether	The hydrogenation of DPE aromatic rings occurs in competition with its hydrogenolysis/hydrogenation into cyclohexanone and cyclohexanol.	47
Pd/C **Pt/C** **Ni/SiO_2**	T: 200°C P: 40 bar H_2	Water/ decalin	Cyclohexanone, cyclohexanol, phenol	In water, DPE was mainly converted by reductive hydrolysis to form cyclohexanone and phenol, while decalin was selective to the aromatic rings hydrogenation of DPE.	48
Co/CeO_2 **RuCo/CeO_2**	T: 200°C P: 20 bar H_2	Decalin	Cyclohexanol, benzene, cyclohexane	DPE was converted by hydrogenolysis of its C_{arom}-O bond. The addition of Ru promoted the increase of the H_2 spillover effect, which enhances the hydrogenolysis of the C_{arom}-O bond of DPE and the hydrogenation steps.	49
Ru/TiO_2	T: 260°C P: 10 bar H_2	Octane	Cyclohexane, 1,1-bicyclohexyl	The reaction pathway for DPE conversion was not proposed by the authors	50
Ni/ZrO_2 **Ni/Al_2O_3** **Ni/Al-SBA-15**	T: 200°C P: 50 bar H_2	Methylcyclohexane	Cyclohexane, dicyclohexyl ether, cyclohexanol, 1,1-bicyclohexyl	The reaction pathway for DPE conversion was not proposed by the authors	51
CoMoS/SZ	T: 300°C P: 20 bar H_2	Decalin	Phenol, benzene	CoMoS are responsible for: (i) hydrogenolysis of DPE leading to phenol and benzene; (ii) hydrogenolysis of phenol producing benzene.	14
Pd/Nb_2O_5/SiO_2	T: 170°C P: 25 bar H_2	Dodecane	Cyclohexane	The reaction pathway for DPE conversion was not proposed by the authors, but the authors suggested that the NbOx species promoted the hydrogenolysis of DPE	52

Table 2.18 Reaction conditions and catalysts used for the conversion of DPE presented in the literature. (continuation)

Catalysts	Reaction conditions	Solvent	Main products	Conclusion	Ref.
Ni/Nb_2O_5 **Co/Nb_2O_5** **Cu/Nb_2O_5**	T: 220°C P: 10 bar H_2	Isopropanol	Benzene, phenol, cyclohexane, Cyclohexanol	The DPE conversion proceeded through its hydrogenolysis followed by the hydrogenation of the intermediates formed.	53
Rh/Nb_2O_5	T: 260°C P: 10 bar H_2	*n*-decane	Phenol, benzene	The metal promoted the hydrogenolysis of the C_{arom}-O bond of DPE to form phenol and benzene. Subsequent hydrogenolysis of phenol to benzene.	26
$Ni/NbPO_4$ **$Ni/ZrNbPO_4$** **$Ni/ZrPO_4$**	T: 180°C P: 5 bar H_2	*n*-decane	Benzene, cyclohexanol, cyclohexane	The formation of benzene and cyclohexane can be favored over $Ni/ZrNbPO_4$ which presented small particle size and moderate acidic strength.	54
Ru/Al_2O_3, Ru/H-MOR Ru-USY, Ru/H-Beta, and Ru/HZSM5	T: 120°C P: 40 bart H_2	Water	Cyclohexanol, cyclohexane	The increase in catalyst acidity increased the formation of cyclohexane. In addition, high Ru content decreased the Lewis acidic sites and consequently the HDO of DPE.	40
Ru/HZSM5	T: 200°C P: 50 bar H_2	Water	Cyclohexane	The reaction pathway was not proposed	39
Pd/C and HZSM5	T: 200°C P: 50 bar H_2	Water	Cyclohexane	The reaction pathway was not proposed	37
Ni/HZSM5	T: 250°C P: 50 bar H_2	Water	Cyclohexane, benzene	The reaction pathway was not proposed	38
Pd/HZSM5, Ni/HZSM5, Pd-Ni/HZSM5, Pd-Ni/Al_2O_3	T: 220°C P: 20 bar H_2	*n*-hexane	Cyclohexane	Cyclohexyl phenyl ether is an important intermediate that can be hydrogenated or cleaved by hydrogenolysis.	29

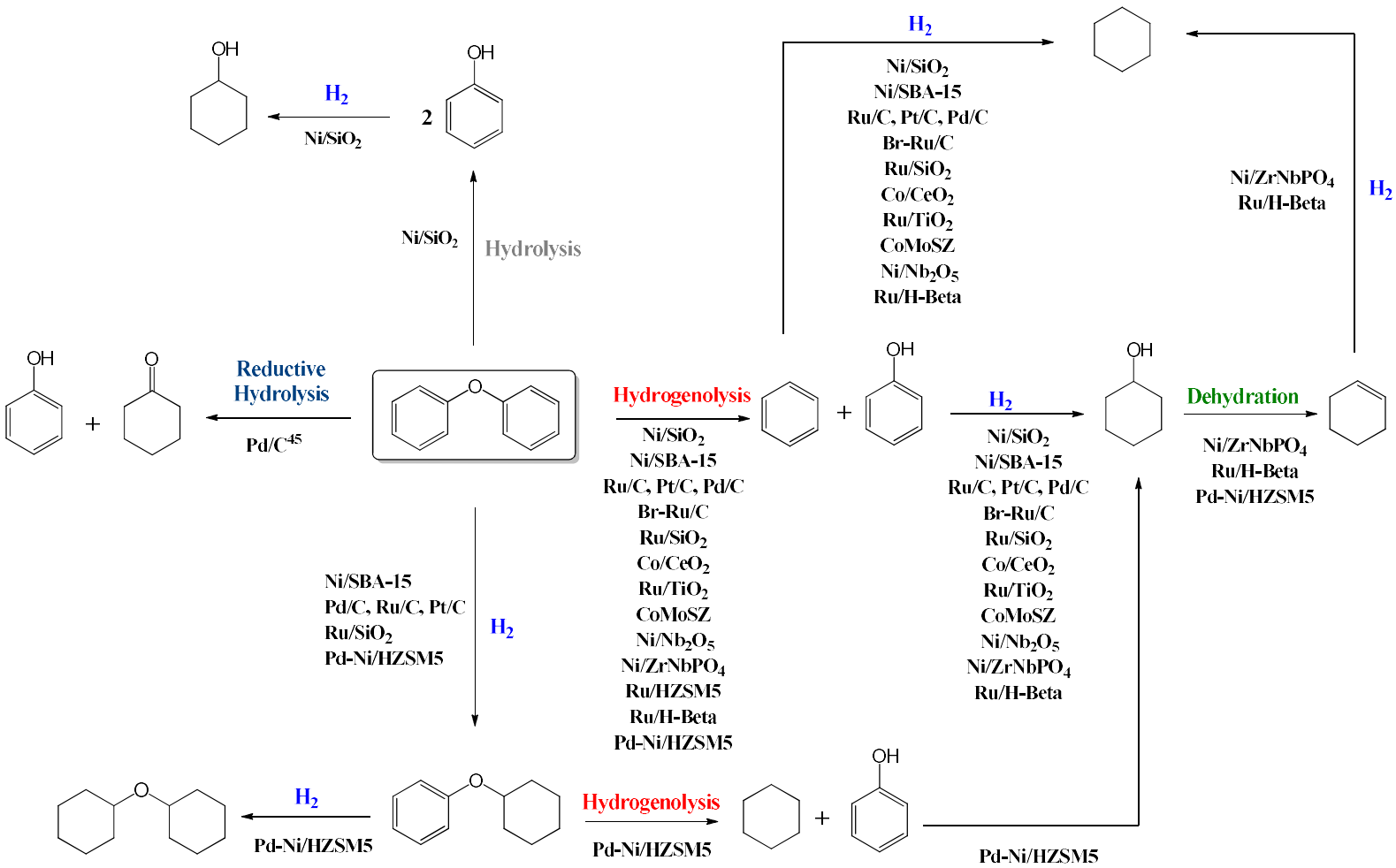

Scheme 2.3: Reaction pathways for DPE conversion proposed by the literature.

2.5 PARTIAL CONCLUSION

According to the various and very different works found in the literature, different metals (mainly Ni, Pd, Pt, and Ru) supported on SiO_2, C and acidic materials (a large range of zeolites was tested) have been widely used for the hydrodeoxygenation of dimeric aryl ethers (BPE, PEB, and DPE) representative of the main ether linkages present in the lignin fraction (α-O-4, β-O-4, and 4-O-5, respectively). It can be summarized that a better performance of the catalysts is based on a bifunctional mechanism, in which metal sites are responsible for the ether hydrogenolysis and hydrogenation of the intermediates formed after cleavage, while the acidic sites promote the dehydration step necessary to produce deoxygenated compounds. Side-reactions include alkylation reactions and partial hydrogenation of the initial substrate.

However, these studies used different reaction conditions (temperature, hydrogen pressure, and solvent) which makes a reliable comparison of the results and an assessment of the balance between the competing pathways difficult. In fact, there are only a few works in which different metals and supports are compared under the same conditions, and the effects of the nature of the metal and acidity of the support on the parallel and successive steps of the HDO reaction cannot be clearly delineated.

Therefore, in our work, the effect of the nature of metal as well as the effect of the type of support will be studied for the conversion of BPE, PEB, and DPE as feedstock. Pd and Ru are selected as active phases, and supports with different characteristics are evaluated (SiO_2, Al_2O_3, TiO_2, Nb_2O_5, ZrO_2, and HZSM5). The performance of all catalysts will be carried out in the liquid phase using a non-polar solvent (decalin). The choice of a non-polar solvent was done in order to avoid possible parallel reactions which

occur when a polar solvent is used and thus, to facilitate the understanding of the mechanism.

Chapter 3

Experimental Procedure

3.1 CATALYSTS PREPARATION

3.1.1 Preparation of palladium-based catalysts by incipient wetness impregnation (imp)

SiO_2 (fumed silica, average particle size 0.2 - 0.3 μm, Sigma Aldrich, S5505), TiO_2 (P25, Sigma Aldrich), Nb_2O_5, Al_2O_3 (Puralox NWa155), ZrO_2 (Saint Gobain), and HZSM5 (Zeolyst CBV 2314) were used to prepare the supported Pd catalysts by impregnation. Due to its low density, SiO_2 was moistened with deionized water and then, calcined in a muffle oven at 400 °C (2°C min^{-1}) for 3 h. Nb_2O_5 was obtained by calcination of niobic acid (CBMM) in a muffle oven at 400°C (2 °C min^{-1}) for 3 h. The Pd catalysts were prepared by incipient wetness impregnation using an aqueous solution of palladium (II) nitrate hydrate ($Pd(NO_3)_2.xH_2O$, Alfa Aesar) with the appropriate volume to ensure that all catalysts are loaded with 2 % of Pd. The pore volume is in annex 5. After impregnation, the samples were dried at 100 °C for 12 h and calcined in a muffle oven at 400 °C (2°C min^{-1}) for 3 h. The following catalysts were prepared: $Pd/SiO_{2\text{-imp}}$, $Pd/TiO_{2\text{-imp}}$, $Pd/Nb_2O_{5\text{-imp}}$, $Pd/Al_2O_{3\text{-imp}}$, $Pd/ZrO_{2\text{-imp}}$, and $Pd/HZSM5_{\text{-imp}}$.

3.1.2 Preparation of ruthenium-based catalysts by incipient wetness impregnation

SiO_2 (silica gel, Sigma Aldrich) and HZSM5 (Zeolyst CBV 2314) were used to prepare the supported Ru catalysts. Before impregnation, SiO_2 was calcined using the same procedure as previously described. 1 Ru wt% catalysts (Ru/SiO_2 and Ru/HZSM5) were prepared by incipient wetness impregnation of the supports using hydrated ruthenium (III) chloride ($RuCl_3.xH_2O$, Sigma-Aldrich). After impregnation, the powder

was dried at 100 °C for 12 h and calcined in a muffle oven using the same conditions described above.

3.1.3 Preparation of Pd-based catalysts by colloidal (col) method

Al_2O_3 (Puralox NWa155), TiO_2 (Sigma-Aldrich, P25 nanopowder), Nb_2O_5, and ZrO_2 (Saint Gobain) were used to prepare 1 wt.% $Pd/Al_2O_{3\text{-col}}$, $Pd/TiO_{2\text{-col}}$, $Pd/Nb_2O_{5\text{-col}}$, and $Pd/ZrO_{2\text{-col}}$ catalysts by a colloidal sol-immobilization method. Nb_2O_5 was obtained as described above (Section 3.1.1.). 0.094 mmol of potassium tetrachloropalladate (II) (98 % of Pd, Sigma-Aldrich) and 0.7 mL of a 2% solution of poly (vinyl alcohol) (Sigma Aldrich, Mw:9.000-10.000, 80% hydrolyzed) were added to 800 mL of deionized water, and the suspension was magnetically stirred for 10 min. Then, 4.7 mL of a 0.1M $NaBH_4$ solution (Sigma Aldrich) was added into the flask dropwise. After 30 min, 990 mg of support was added and the solution pH was corrected to 2 by the addition of H_2SO_4. The mixture was stirred for 2 h. Finally, the catalyst was filtered, washed with 400 mL of deionized water and dried in a muffle oven at 100°C for 3 h. For the sake of brevity, these catalysts will be called below "colloidal catalysts" (for: supported catalysts containing Pd particles prepared via a sol immobilization route).

3.2 CATALYSTS CHARACTERIZATION

3.2.1 Inductively Coupled Plasma Optical Emission Spectrometry with (ICP-OES)

The Pd content of each sample was determined by inductively coupled plasma optic emission spectrometry (720-ES ICP-OES, Agilent) with axial viewing and

simultaneous CCD detection. The samples (10 mg) were digested in a solution containing 250 µL of HF, 500 µl of H_2SO_4, and 4 ml of aqua regia (1 HNO_3 + 3HCl), and heated to 110°C for 2 h in an autodigestor Vulcan 42 (Questron). Then, the solutions were neutralized by a commercial base solution of triethylenetetramine (UNS1) and diluted up to 20 mL with ultrapure water.

3.2.2 X-Ray Fluorescence Spectroscopy (XRF)

The Ru content in each catalyst was determined by X-ray fluorescence (XRF) using an energy dispersive micro-X-Ray Fluorescence Bruker spectrometer (M4 TORNADO) with a rhodium X-ray tube, 50 kV/6000 mA (30 W).

3.2.3 N_2 physisorption

The specific surface area of the samples was measured using a Micromeritics ASAP 2020 analyzer by N_2 adsorption at the boiling temperature of liquid nitrogen. The samples were submitted to a treatment at 350 °C until a 9 mm Hg vacuum was reached for degassing and removing the adsorbed species. The specific surface areas were calculated from the Brunauer-Emmett-Teller (BET) method.

3.2.4 X-Ray Diffraction (XRD)

The crystalline phases of the materials were studied using X-ray powder diffraction (XRD). The analyses were carried out on a BRUKER D8 Advance diffractometer with Cu Kα radiation (λ = 0.1542 nm) over a 2θ range of 10 - 70º at a scan rate of 0.02 º/step and a scan time of 0.1 s/step. The crystalline phases were identified by

comparing the experimental diffractograms and the diffraction standards available from the Joint Committee on Powder Diffraction Standards – International Center for Diffraction Data (JCPDS – ICDD). The crystallite sizes of the samples were estimated using the Scherrer equation, described in Eq. 3.1:

$$d = \frac{K\lambda}{\beta \cos} \qquad \text{(Eq. 3.1)}$$

where K is a dimensionless shape factor, with a typical value of 0.9 (spherical particles), λ is the X-ray wavelength (0.1542 nm), β is the full width at half maximum of the diffraction peak, and θ is the Bragg angle corresponding to this diffraction.

3.2.5 Temperature-programmed reduction (H_2-TPR)

Temperature-programmed reduction under hydrogen (H_2-TPR) was performed to determine the reduction temperature as well as the degree of reduction of Ru catalysts. The TPR analyses were performed in an AutoChem II 2920 set-up. Before the analysis, the samples (50 mg) were submitted to a treatment with N_2 at 200 °C for 1 h to remove the adsorbed species. Then, the samples were cooled to room temperature and reduced with a mixture containing 5% H_2 in Ar (50 mL min^{-1}) up to 500 °C (5 °C min^{-1}).

3.2.6 Temperature Programmed Desorption of ammonia (NH_3-TPD)

The total density of acidic sites was measured by temperature-programmed desorption of ammonia (NH_3-TPD) in the AutoChem II equipment from Micromeritics, equipped with a thermal conductivity detector and a mass spectrometer. The catalysts prepared by incipient wetness impregnation (100 mg) were previously reduced under a flow of 40 mL/min in pure H_2 at a heating rate of 10 °C min^{-1} up to 400 °C, for 1 h, and then purged in a He flow (30 mL min^{-1}) for 30 min. After reduction, the samples were

cooled to 100 °C and the gas was switched to a mixture containing 10% NH_3 in He (30 mL min^{-1}) for 30 min. The physisorbed ammonia was flushed out with He (50 mL min^{-1}) for 2 h. Then, the catalysts were heated under He at 10 K min^{-1} up to 500 °C. The catalysts synthesized by the colloidal method underwent the same procedure described above but without the reduction step.

3.2.7 Infrared spectroscopy analysis (FTIR-Py)

The nature, strength, and number of acidic sites were measured by pyridine (Py) adsorption experiments followed by Fourier-Transform Infrared Spectroscopy (FTIR). The analyses were performed using a Thermo Nicolet Protege 460 instrument equipped with a CSi beam splitter and a MCT detector with a 2 cm^{-1} resolution. Before analysis, the calcined samples were pressed (1 ton cm^{-2}) into a self-supported wafer (2.01 cm^2), placed in a quartz sample holder and then in a quartz cell equipped with KBr windows.

The cell was connected to a vacuum line for different treatments. Catalyst samples were activated under high vacuum ($P < 10^{-7}$ mbar) at 450 °C overnight. Pyridine was then adsorbed at equilibrium (100 °C) and the samples were evacuated at 150, 250, 350, and 400 °C under high vacuum ($P < 10^{-7}$ mbar) for 30 min between spectra acquisition. The bands located at 1452 and 1543 cm^{-1} were used for the quantification of the coordinated pyridine to Lewis (εL = 2.22 cm μmol^{-1}) and Brønsted (εB = 1.67 cm μmol^{-1}) sites respectively, according to the Beer-Lambert law, described in Eq.3.2.

$$n = \frac{AS}{\varepsilon m} \qquad \text{(Eq. 3.2)}$$

where n is the number of acidic sites (μmol), A is the band area (absorbance units -AU), S is the wafer surface area (2.01 cm^2), ε is the molar extinction coefficient (cm μmol^{-1}), and m is the wafer mass (g).

3.2.8 Scanning transmission electron microscopy (STEM)

The Pd and Ru particle size distribution was measured by scanning transmission electron microscopy (STEM). Before STEM analyses, the impregnated catalysts were reduced as previously described (Section 3.1.1), and then passivated at room temperature under 5% O_2/N_2 (30 mL/min) for 2 h. The metal catalysts were dispersed in isopropanol by ultrasonication and the suspensions were dropped on holey carbon-coated copper grids. At least 200 particles were taken into account for the establishment of the size distribution. The images were obtained using a MET FEI Titan X-FEG with a voltage of 300 kV, equipped with a high-angle annular bright-field and dark-field detector (HAADF) which can provide images with Z contrast and with a resolution of 0.7 Å.

In addition, these data enabled the calculation of metal dispersion (D) by considering the mean diameter of the metal particles (d_p) based on equations 3.3 and 3.4:

$$dp = \frac{\Sigma nidi}{\Sigma ni} \qquad \text{(Eq. 3.3)}$$

$$D = 6\,\frac{Vm/am}{dp} \qquad \text{(Eq. 3.4)}$$

where n_i is the number of spherical particles of diameter d_i, Vm is the volume of the metal atom and am the surface area occupied by an atom. The volume of metal is described on equation 3.5:

$$Vm = \frac{M}{\rho\, N_A} \qquad \text{(Eq. 3.5)}$$

where M is the atomic mass, ρ the mass density and N_A is the Avogadro number (6.022×10^{23} mol^{-1}). In the case of palladium (M = 106.4 g mol^{-1}; ρ = 12.02 g cm^{-3}) ϑ_m =14.70 Å^3 and a_m= 7.93 Å^2. For ruthenium (M = 101.07 g mol^{-1}; ρ = 12.30 g cm^{-3}) ϑ_m =13.65 Å^3 and a_m= 6.35 Å^2. Replacing Vm and am values on the equation 3.4, we find the relationship between metal dispersion and the mean diameter particle (nm) for palladium and ruthenium-based catalysts, equations 3.6 and 3.7, respectively:

$$D\ (\%) = \frac{1{,}1093}{dp} x\ 100 \qquad \text{(Eq. 3.6)}$$

$$D\ (\%) = \frac{1{,}3521}{dp} x\ 100 \qquad \text{(Eq. 3.7)}$$

3.3 CATALYTIC TEST

3.3.1 Substrates

Benzyl phenyl ether (Sigma-Aldrich 99 %), phenethoxybenzene (Ambeed, 97 %), and diphenyl ether (Sigma-Aldrich, 99%) were used as feeds in the catalytic tests. The solvent used was anhydrous cis + trans decahydronaphthalene (decalin, Sigma Aldrich, 99 %). All products used as standards for chromatography calibration are summarized in table 3.1.

Table 3.1: List of commercial products used.

Product	Chemical formula	Phase	Supplier	Purity (%)
Anisole	C_7H_8O	Liquid	Sigma-Aldrich	99.0
Benzene	C_6H_6	Liquid	Sigma Aldrich	100.0
Bicyclohexyl	$C_{12}H_{22}$	Liquid	Sigma Aldrich	99.0
Cyclohexane	C_6H_{12}	Liquid	Sigma Aldrich	99.7
Cyclohexene	C_6H_{10}	Liquid	Sigma Aldrich	100.0
Cyclohexanol	$C_6H_{12}O$	Liquid	Sigma Aldrich	99.0
Cyclohexanone	$C_6H_{10}O$	Liquid	Sigma Aldrich	99.0
Ethylbenzene	C_8H_{10}	Liquid	Sigma Aldrich	99.0
Ethylcyclohexane	C_8H_{16}	Liquid	Sigma Aldrich	99.0
Guaiacol	$C_7H_8O_2$	Liquid	Sigma Aldrich	99.0
Methylcyclohexane	C_7H_{14}	Liquid	Sigma Aldrich	99.0

Table 3.1: List of commercial products used (continuation).

Product	Chemical formula	Phase	Supplier	Purity (%)
Phenol	C_6H_6O	Solid	Sigma Aldrich	99.0
Toluene	C_7H_8	Liquid	Alfa Aesar	99.0
2-BPH	$C_{13}H_{12}O$	Solid	Sigma Aldrich	98.0
2-Cyclohexyl ethanol	$C_8H_{16}O$	Liquid	Sigma Aldrich	99.0
2,3-Dihydrobenzofuran	$C_8H_8O_2$	Liquid	Sigma-Aldrich	99.0
4-BPH	$C_{13}H_{12}O$	Solid	Sigma Aldrich	99.0
4-Propylphenol	$C_9H_{12}O$	Liquid	Sigma-Aldrich	99.0

3.3.2 Catalytic system description

The catalytic experiments were conducted in a 50 mL batch Hastelloy Parr 4590 autoclave reactor equipped with a 0-200 bar pressure manometer, mechanical stirring, and a thermocouple (Figure 3.1).

Figure 3.1: Autoclave Parr Reactor.

3.3.3 Catalytic reaction description

Before the catalytic reaction, the impregnated catalysts were previously reduced under 30 bar H_2 (50 ml min^{-1}) at 400°C for 1 h in a Screening Pressure Reactor (SPR). After reduction, all catalysts were stored inside of a glove box. In a typical test, the reactor vessel was charged inside the glove box with a desired amount of catalyst (10 – 250 mg) and 15 mL of reaction mixture containing 62 or 31 mmol of substrate in decalin. After loading, the vessel was connected to the unit, purged 3 times with hydrogen, and pressurized with 18 bar of H_2. The reaction mixture was heated up to 230 °C (5 °C min^{-1}) and then stirred (600 rpm) for 3 h. In the end, the vessel was cooled in an ice bath below 40 °C.

3.3.4 Analytical methods

After reaction, the liquid samples were filtered and analyzed using a gas chromatograph GC-FID-MS (Agilent technologies 5977B MSD) equipped with a CP-Wax 52 CB column (polyethylene glycol phase, 30 m x 250 µm, 0.250 µm). The chromatographic method used is summarized in Table 3.2.

Table 3.2: GC analytical methods parameters.

Injection	Injection mode	Split-Splitless Inlet
	Temperature	250 °C
	Carrier gas	He
	Pressure	13.6 psi
	Total flow	24.69 mL min^{-1}
	Column flow	1.69 mL min^{-1}

Table 3.2: GC analytical methods parameters. (continuation)

Oven	Initial Temperature, T_0	40 °C (3.5 min)
	T_1 (rate)	150 °C (15 °C min^{-1}) / 1 min
	T_2 (rate)	195 °C (25 °C min^{-1}) / 2 min
	T_3 (rate)	205 °C (2 °C min^{-1}) / 1 min
	T_4 (rate)	250 °C (20 °C min^{-1}) / 10 min
	Equilibration time	0.25 min
	Total program time	33.88 min
	Final temperature, T_F	250 °C
Detector (FID)	Temperature	270 °C
	H_2 flow	40 mL min^{-1}
	Air flow	400 mL min^{-1}

The products were identified by their retention time in comparison with available standards and based on the mass spectrum. Fig. 3.2 shows a typical chromatogram. The chromatograms and the mass spectrum of each product obtained from the NIST database are available in Annex 1 (Fig. A1.1 – A1.40).

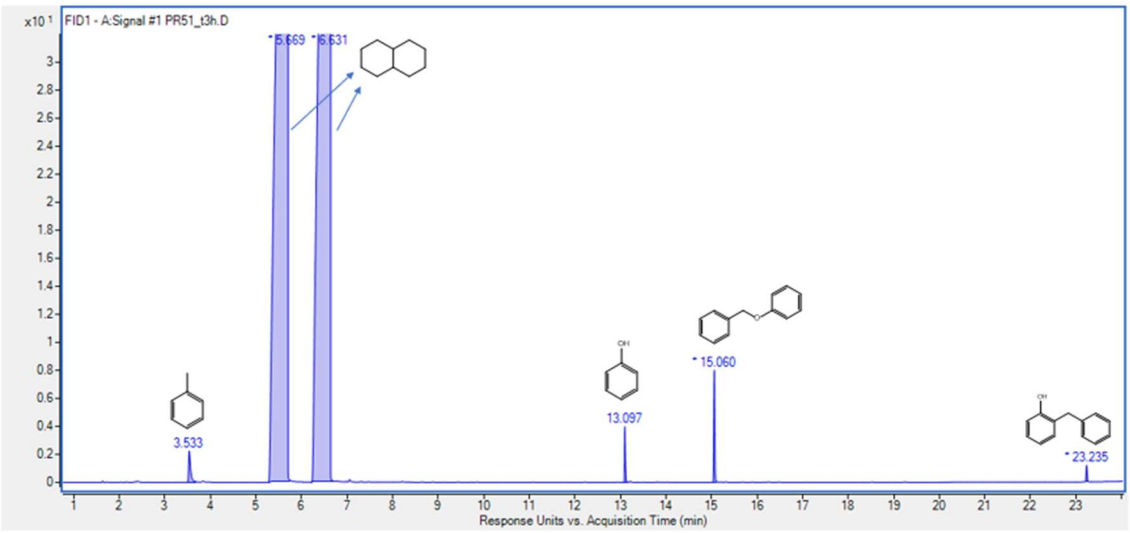

Figure 3.2: Example of GC-FID chromatogram for the products obtained after reaction.

The concentration of each product was calculated by external calibration according to eq.3.8, where y is the molar concentration of the compound (mol L^{-1}), a is the corresponding factor of the compound, and x is the area determined by peak integration. The corresponding factor obtained for each compound is in annex 6. When no standard was available, the corresponding factor of products with a similar chemical structure was used.

$$y = ax \qquad \text{(Eq. 3.8)}$$

The conversion of each substrate ($X_{subst.}$), product yield (Y), and mass balance (MB) were calculated as follows (Eq.3.9 – 3.11):

$$\text{Conversion (\%)} = \frac{\text{(Mass of subst.)0} - \text{(Mass of subst.)t}}{\text{(Mass of subst.)0}} \text{ x } 100 \qquad \text{(Eq. 3.9)}$$

$$\text{Yield (\%)} = \frac{Mass\ of\ product}{\text{(Mass of subst.)0}} \text{ x } 100 \qquad \text{(Eq. 3.10)}$$

$$\text{MB (\%)} = \Sigma \text{ yield} + \frac{\text{(Mass of subst.)t}}{\text{(Mass of subst.)0}} \qquad \text{(Eq. 3.11)}$$

where 0 corresponds to the reaction beginning and t corresponds to 3 h of reaction.

Chapter 4

Catalyst characterization

4.1 PALLADIUM-BASED CATALYSTS

Table 4.1 summarizes the chemical composition and the specific surface area of the Pd-supported catalysts. The Pd contents for all the samples were close to the nominal values, 2 wt.% for the catalysts prepared by incipient wetness impregnation and 1 wt.% for the ones prepared by the colloidal method, except $Pd/Al_2O_{3\text{-col}}$ and $Pd/ZrO_{2\text{-col}}$ for which the Pd content was 0.4 and 0.3 wt%, respectively. This result indicates that the deposition of Pd particles using the colloidal method is affected by the nature of the support.

Table 4.1: Pd content, specific surface area, pore volume, particle size, and dispersion of palladium-supported catalysts.

Catalysts	Pd wt% [a]	BET (m^2g^{-1})	Pore volume ($cm^3 . g^{-1}$)	d_p (nm) [c]	D (%) [e]
$Pd/SiO_{2\text{-imp}}$	1.8	182 (189) [b]	0.90	7.2 (17)[d]	15
$Pd/Al_2O_{3\text{-imp}}$	1.7	148 (151)	0.40	24.5	5
$Pd/TiO_{2\text{-imp}}$	2.0	45 (45)	0.23	9.0	12
$Pd/Nb_2O_{5\text{-imp}}$	1.9	66 (105)	0.11	6.8 (9) [d]	16
$Pd/ZrO_{2\text{-imp}}$	1.8	136 (141)	0.22	13.1	9
$Pd/HZSM5_{\text{-imp}}$	1.8	393 (485)	0.39	24.6 (22) [d]	5
$Pd/Al_2O_{3\text{-col}}$	0.4	158 (151)	0.40	3.8	27
$Pd/TiO_{2\text{-col}}$	0.9	56 (45)	0.22	3.4	30
$Pd/Nb_2O_{5\text{-col}}$	0.9	99 (105)	0.11	2.0	51
$Pd/ZrO_{2\text{-col}}$	0.3	154 (141)	0.18	2.7	38

[a] Measured by ICP.
[b] Specific surface area of support.
[c] Measured by TEM.
[d] Crystallite diameter estimated from XRD data by Scherrer equation.
[e] Calculated based on the particle size measured by TEM.

The surface areas of all the catalysts were quite similar to the ones of the respective supports, except for $Pd/Nb_2O_{5\text{-imp}}$ and $Pd/HZSM5_{\text{-imp}}$ which presented a decrease. $Pd/SiO_{2\text{-imp}}$ and $Pd/HZSM5_{\text{-imp}}$ exhibited the largest specific surface area (182 and 393 $m^2\ g^{-1}$, respectively), while the smallest ones were measured for $Pd/TiO_{2\text{-imp}}$, $Pd/TiO_{2\text{-col}}$,

and $Pd/Nb_2O_{5\text{-imp}}$ (45, 56 and 66 m^2 g^{-1}, respectively). The N_2 adsorption-desorption isotherms for all the supported catalysts, as well as those from all the supports, are presented in Annex 2 (Figs. A2.1 - A2.6). All samples display a type IV isotherm, except for HZSM5 and Pd/HZSM5 which exhibit a type I isotherm characteristic of microporous materials. For those who present a type IV isotherm, typical for mesoporous solids, a hysteresis loop of type H1 is observed for $Pd/SiO_{2\text{-imp}}$, $Pd/TiO_{2\text{-imp}}$, $Pd/TiO_{2\text{-col}}$, and $Pd/ZrO_{2\text{-imp}}$, while for the other materials, a hysteresis loop of type H3 is observed. In addition, for $Pd/ZrO_{2\text{-col}}$, a second step in the isotherm at P/Po = 0.8 indicates the presence of multi pore distribution.[55]

X-ray diffraction patterns for the supports and catalysts reduced at 400 °C and 30 bar of H_2 are shown in Fig.4.1. The diffractogram of SiO_2 exhibited a broad peak at 2θ = 20° corresponding to non-crystalline SiO_2. The diffractogram of Al_2O_3 exhibited the lines from γ-Al_2O_3 (PDF: 00-001-1310, Annex 3). For TiO_2, the characteristic lines corresponding to anatase (PDF: 01-073-1764, Annex 3) and rutile (PDF: 01-089-8303, Annex 3) were observed. Nb_2O_5 also appeared as poorly crystalline; the absence of a diffraction pattern is consistent with the calcination temperature, as reported in the literature [26,56]. The typical lines from tetragonal ZrO_2 (PDF: 00-050-1089, Annex 3) were observed for ZrO_2_I and ZrO_2_C, used for the preparation of $Pd/ZrO_{2\text{-imp}}$ and $Pd/ZrO_{2\text{-col}}$, respectively. However, a typical line from the monoclinic ZrO_2 phase (PDF: 04-002-8305, Annex 3) at 2θ = 28.4° was also observed for ZrO_2_C. Finally, HZSM5 exhibited the characteristic diffraction lines from the MFI zeolitic structure (PDF: 00-057-0145, Annex 3).

Concerning the Pd-based catalysts, the diffractograms exhibited the same phases as observed for the supports. The characteristic lines of metallic Pd at 2θ = 40.02° and 46.49° (PDF: 01-087-0638, Annex 3) could be observed only for the impregnated

catalysts $Pd/SiO_{2\text{-imp}}$, $Pd/Nb_2O_{5\text{-imp}}$, and $Pd/HZSM5_{\text{-imp}}$. The average crystallite size of palladium for $Pd/SiO_{2\text{-imp}}$, $Pd/Nb_2O_{5\text{-imp}}$, and $Pd/HZSM5_{\text{-imp}}$ was calculated using the Scherrer equation using the Pd° (111) line at 2θ = 40.02 °, and the results are reported in Table 4.1. The largest crystallite size (22.0 nm) was observed for $Pd/HZSM5_{\text{-imp}}$ and the smallest one for $Pd/Nb_2O_{5\text{-imp}}$ (9.0 nm). For the colloidal catalysts, the diffraction lines from metallic Pd were not detected, which is likely due to the small metal particle size obtained in these catalysts.

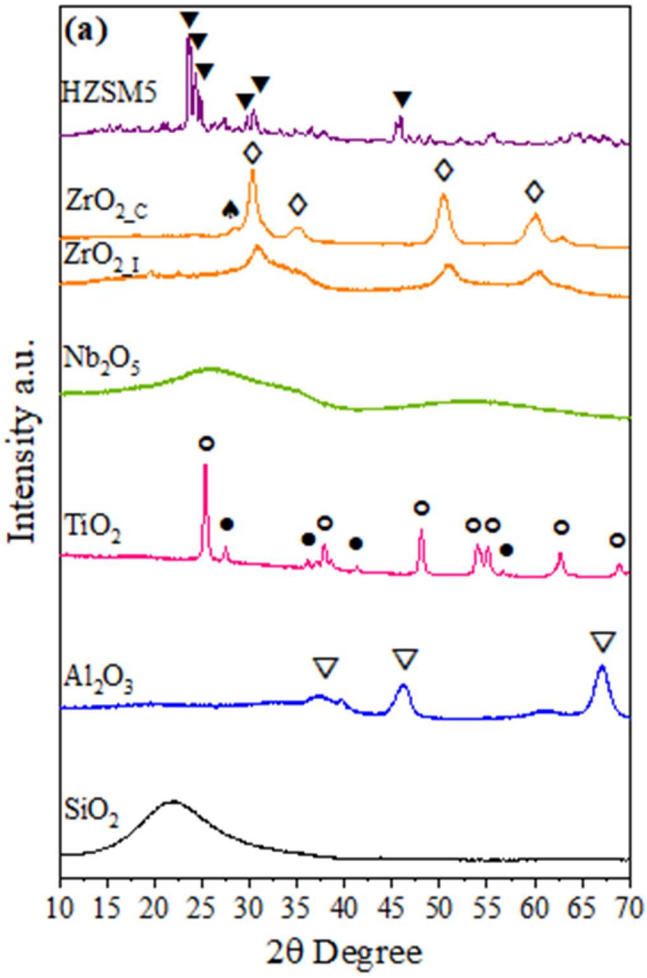

Figure 4.1: XRD patterns of support (a) and Pd-based catalysts: impregnated catalysts (b) and colloidal catalysts (c). (▼) HZSM5, (◊) ZrO_2 tetragonal, (♠) ZrO_2 monoclinic (▽) γ-Al_2O_3, (O) Anatase, (•) Rutile (❖) Pd.

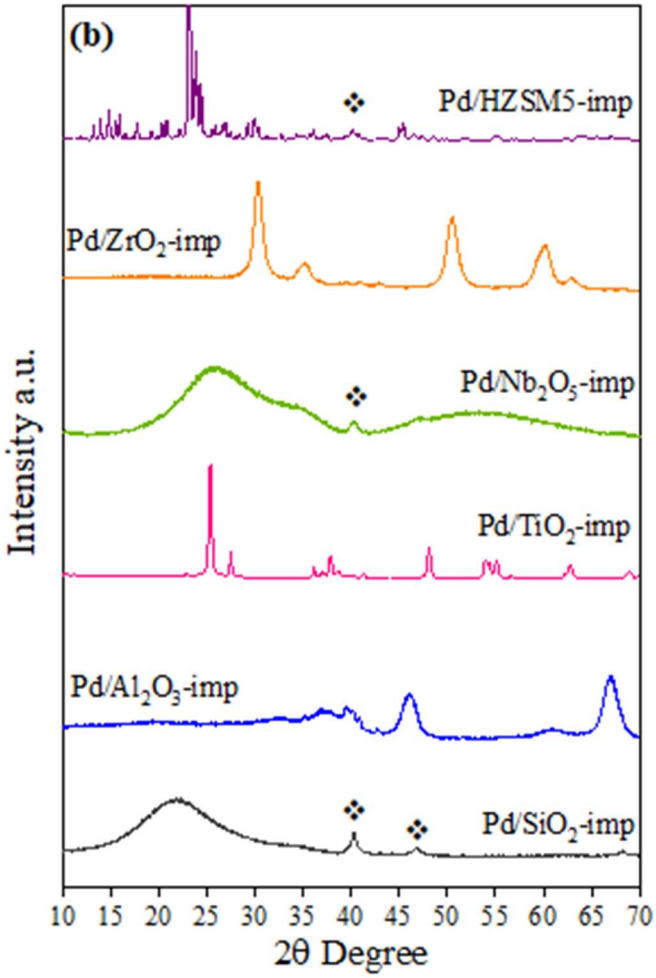

Figure 4.1: XRD patterns of support (a) and Pd-based catalysts: impregnated catalysts (b) and colloidal catalysts (c). (▼) HZSM5, (◊) ZrO_2 tetragonal, (▽) γ-Al_2O_3, (O) Anatase, (•) Rutile (❖) Pd. (Continuation)

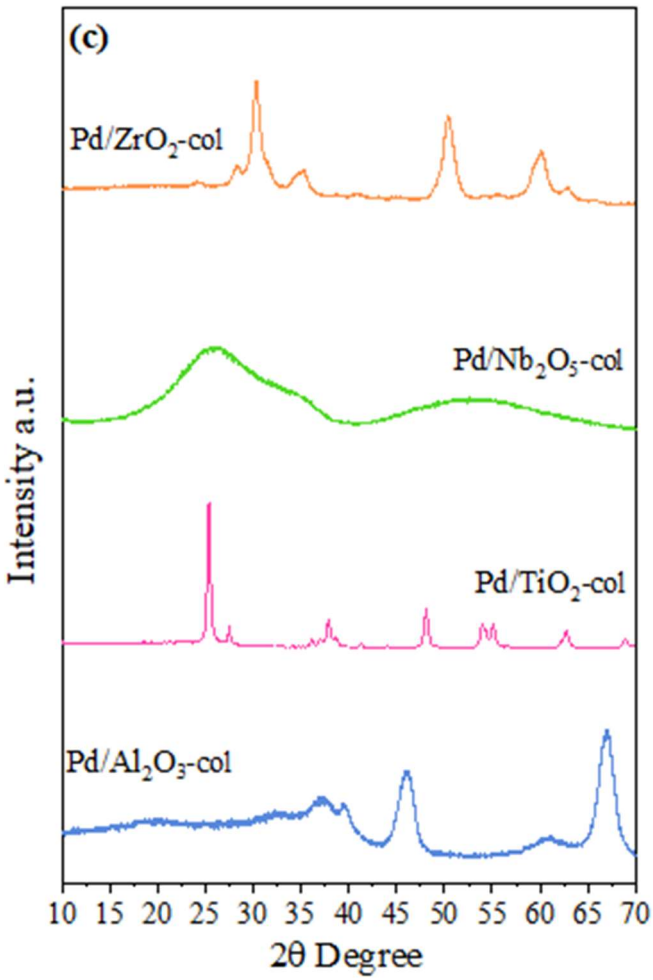

Figure 4.1: XRD patterns of support (a) and Pd-based catalysts: impregnated catalysts (b) and colloidal catalysts (c). (▼) HZSM5, (◊) ZrO_2 tetragonal, (▽) γ-Al_2O_3, (**O**) Anatase, (•) Rutile (❖) Pd. (Continuation)

The NH_3-TPD profiles are shown in Fig. 4.2. All catalysts exhibited multiple and poorly resolved peaks between 100 and 500 °C, indicating the presence of acidic sites with different strengths. The relative contribution of each desorption peak was obtained by decomposition of the TPD profiles, considering the adsorption of three acidic sites of different strengths (weak: T < 250 °C; medium: 250 < T < 320 °C; strong: T > 320 °C). The experimental data were fitted using a multiple-Gaussian function. Table 4.2 reports the total density of acidic sites as well as their distribution. Concerning the impregnated catalysts, $Pd/SiO_{2\text{-imp}}$ did not retain NH_3. Pd-supported over $HZSM5_{\text{-imp}}$ exhibited the highest concentration of sites (699 μmol/g of NH_3), and the order is:

$Pd/HZSM5_{-imp}$ >> Pd/ZrO_{2-imp} > Pd/Nb_2O_{5-imp} ≈ Pd/TiO_{2-imp} ≈ Pd/Al_2O_{3-imp}.

The colloidal catalysts exhibited a higher density of acidic sites compared to the respective impregnated catalysts, probably because these catalysts do not undergo any heat treatment after preparation (calcination and reduction at high temperature). Moreover, chloride and sulfate ions could remain on the surface of the catalysts, enhancing the acidity. In contrast, the impregnated catalysts were calcined at 400 °C in a muffle oven after metal impregnation and reduced before NH_3 adsorption, which may decrease their total density of acidic sites. Among the colloidal catalysts, Pd/ZrO_{2-col} exhibited the highest density of acidic sites (479 µmol/g of NH_3), while Pd/TiO_{2-col} exhibited the lowest one (231 µmol/g of NH_3). Concerning the distribution of the acidic sites, Pd/ZrO_{2-imp} and Pd/ZrO_{2-col} showed the highest fraction of strong acidic sites.

Table 4.2: Total amount of ammonia desorbed, acidic sites strength distribution, and concentration of Lewis and Brønsted acidic sites for palladium-based catalysts.

Catalysts	Ammonia desorbed (µmol g^{-1}) [a]	Acidic sites strength distribution (%) [a]			Lewis[b] (µmol g^{-1})	Brønsted[b] (µmol g^{-1})
		Weak	Medium	Strong		
Pd/SiO_{2-imp}	0	0	0	0	0	0
Pd/Al_2O_{3-imp}	160	26	35	35	142	0
Pd/TiO_{2-imp}	169	35	40	27	71	0
Pd/Nb_2O_{5-imp}	167	31	27	42	60	13
Pd/ZrO_{2-imp}	251	19	35	46	81	34
$Pd/HZSM5_{-imp}$	699	34	42	24	93	141
Pd/Al_2O_{3-col}	301	24	36	39	60	0
Pd/TiO_{2-col}	231	31	32	29	76	0
Pd/Nb_2O_{5-col}	259	39	31	28	82	22
Pd/ZrO_{2-col}	479	12	29	59	170	12

[a] Determined by NH_3-TPD

[b] Determined by pyridine adsorption-FTIR at 150 °C.

The concentration of Lewis and Brønsted acidic sites was measured by FTIR after the adsorption of pyridine. Fig.4.3 shows the spectra of pyridine adsorbed on Pd-based catalysts at 150 °C. The band at 1545 cm^{-1} represents the pyridine chemisorbed on the Brønsted acidic sites (BAS), while the band at 1445 cm^{-1} is attributed to the pyridine coordinated to Lewis acidic sites (LAS). Impregnated $Pd/Al_2O_{3\text{-imp}}$ and $Pd/TiO_{2\text{-imp}}$ exhibited only LAS, while $Pd/Nb_2O_{5\text{-imp}}$, $Pd/ZrO_{2\text{-imp}}$, and $Pd/HZSM5_{\text{-imp}}$ exhibited BAS and LAS. The same was observed for the colloidal catalysts. The concentration of BAS and LAS measured through the 1545 and 1450 cm^{-1} peak areas, respectively, are presented in Table 4.2. For the impregnated catalysts, the higher concentration of LAS was observed for $Pd/Al_2O_{3\text{-imp}}$, while Pd/HZSM5 exhibited the highest concentration of BAS, following the order: $Pd/HZSM5_{\text{-imp}}$ > $Pd/ZrO_{2\text{-imp}}$ > $Pd/Nb_2O_{5\text{-imp}}$. Regarding the colloidal catalysts, the highest concentration of LAS and BAS was observed for $Pd/ZrO_{2\text{-col}}$ and $Pd/Nb_2O_{5\text{-col}}$, respectively.

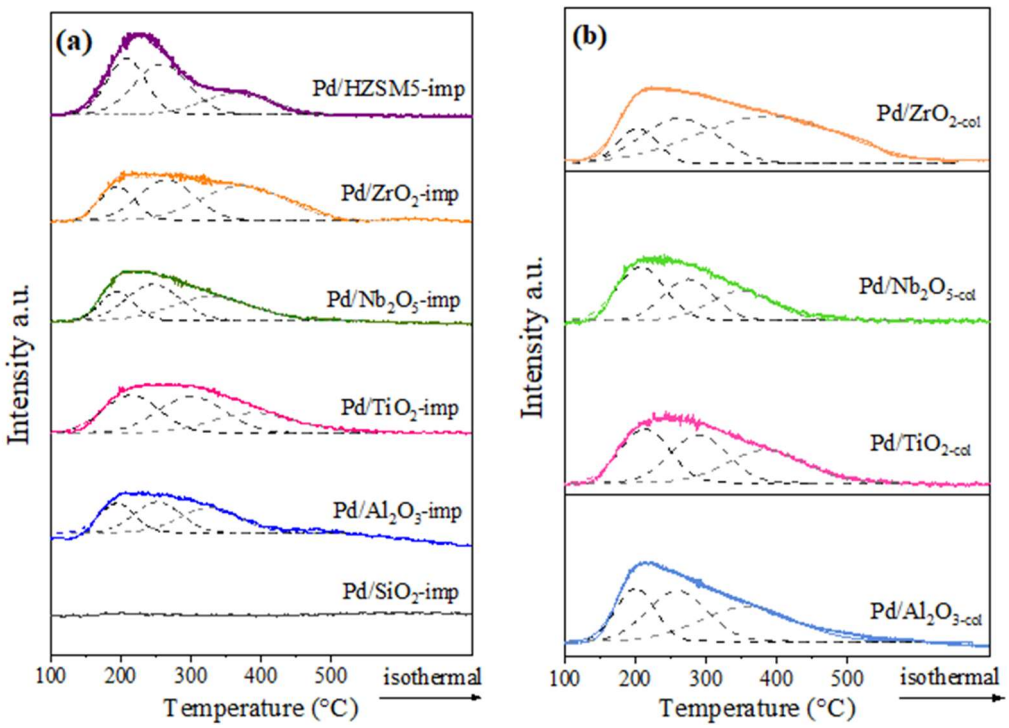

Figure 4.2: NH_3-TPD profiles for supported Pd catalysts: (a) impregnated catalysts, (b) colloidal catalysts.

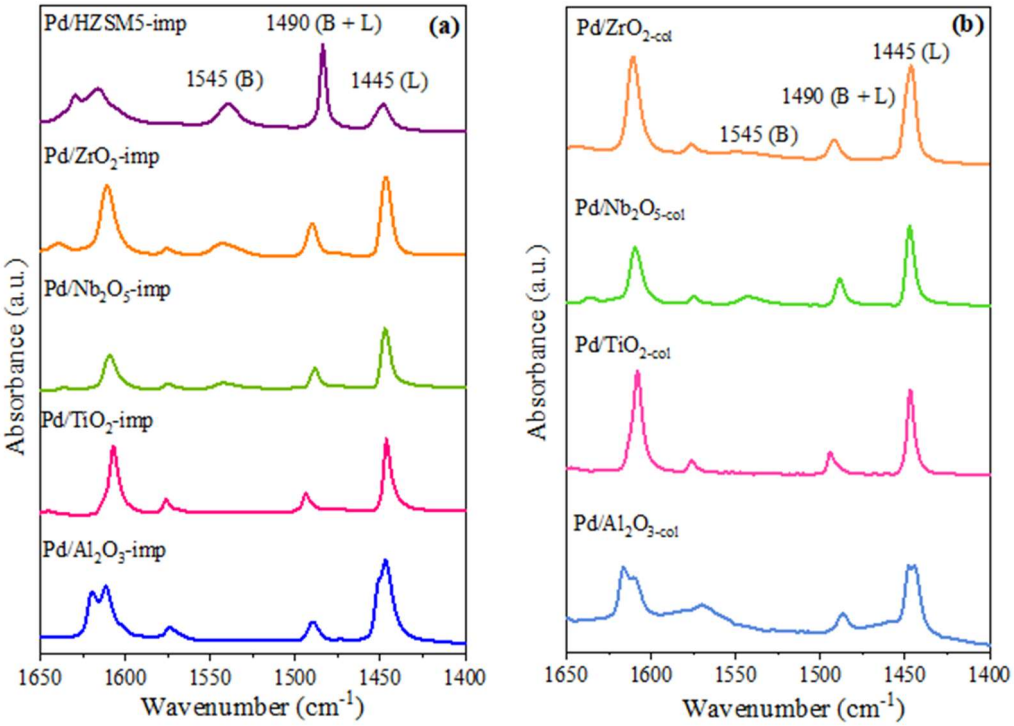

Figure 4.3: Infrared spectrum of adsorbed pyridine on Pd-based catalysts at 150 °C. (a) impregnated catalysts and (b) colloidal catalysts.

STEM images of $Pd/Nb_2O_{5\text{-imp}}$ and $Pd/Nb_2O_{5\text{-col}}$ and their respective particle size distribution are shown in Fig.4.4. The STEM images and the particle size distribution for the other impregnated and colloidal catalysts are presented in Annex 4 (Figs. A4.1 – A4.8). For all the catalysts, the palladium particles had a spherical, or close to spherical, shape. In general, all materials showed a good contrast and the palladium particles were easily distinguished from the support. However, for the zirconia-supported catalysts, due to the similar atomic number (Z) between Pd and Zr, the Z-contrast was poor and it was difficult to distinguish the Pd particles on the images. Therefore, it was not possible to establish the size distribution, and the Pd particle size was only estimated by counting a few visible Pd particles for $Pd/ZrO_{2\text{-col}}$.

Concerning the impregnated catalysts, the images show that the Pd particles are quite different in size. Among them, $Pd/Al_2O_{3\text{-imp}}$ and $Pd/HZSM5_{\text{-imp}}$ exhibited the largest

average particle size of Pd (24 nm), while $Pd/SiO_{2\text{-imp}}$ and $Pd/Nb_2O_{5\text{-imp}}$ showed the smallest one (7.2 and 6.8 nm, respectively) (Table 2.1). This result is in accordance with the crystallite size estimated by the Scherrer equation. Compared to the impregnated catalysts, the colloidal catalysts exhibited smaller Pd particle sizes, indicating that the preparation method strongly affected the metal particle size. For these catalysts, the Pd particles exhibited narrow size distribution and the images show that Pd particles are well dispersed over the support. For instance, the average Pd particle size for $Pd/Nb_2O_{5\text{-imp}}$ and $Pd/Nb_2O_{5\text{-col}}$ catalysts were 6.8 and 2.0 nm, respectively (Fig.4.4 a-d). Correlating the mean diameter of Pd particles for $Pd/Al_2O_{3\text{-imp}}$ with its X-ray diffraction pattern (Fig. 4.1 b), despite the large Pd particle observed by TEM for $Pd/Al_2O_{3\text{-imp}}$, the lines of metallic Pd were not detected probably because these lines are overlapping with the diffraction lines of the support.

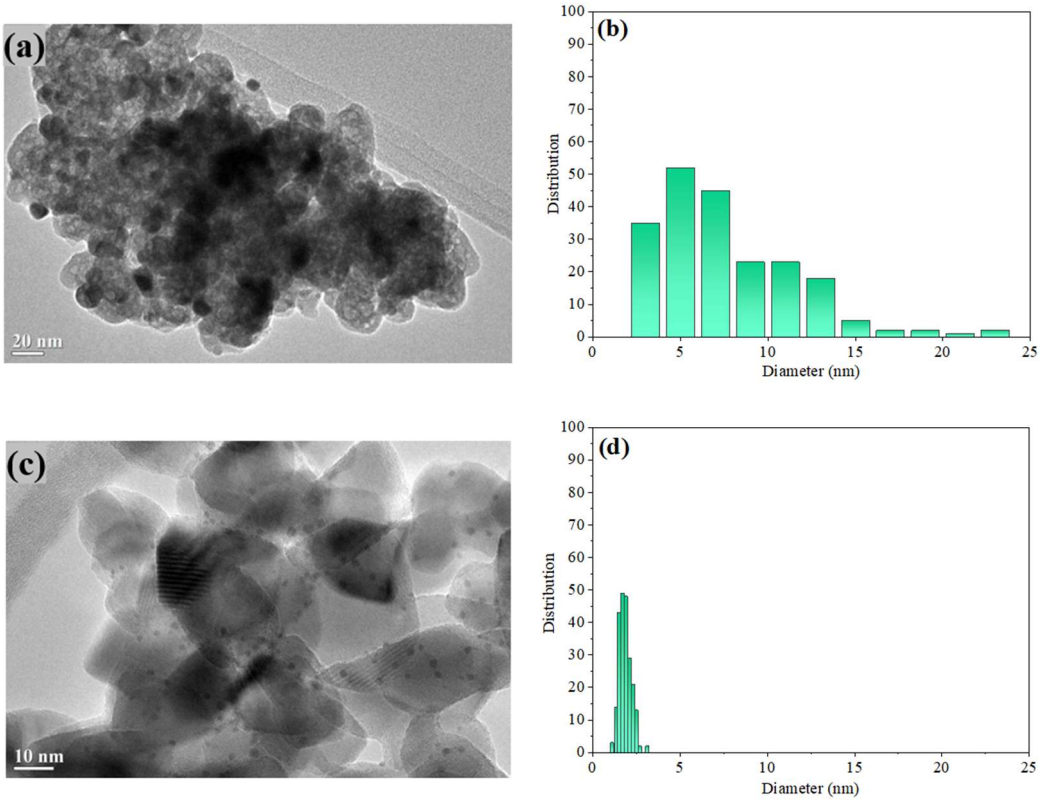

Figure 4.4: TEM image and particle size distribution for (a-b) $Pd/Nb_2O_{5\text{-imp}}$ and (c-d) $Pd/Nb_2O_{5\text{-col}}$.

From the STEM results, the metal dispersion was calculated considering $D = 1{,}1093/d_p$. The metal dispersion varied between 5 to 51% depending on the support and the preparation method (Table 4.1).

4.2 RUTHENIUM-BASED CATALYSTS

Table 4.3 reports the chemical composition, specific surface area, and pore volume of Ru-based catalysts supported over SiO_2 and HZSM5. The Ru content varied from 0.6 to 0.7 wt. %. The specific surface area of the supported catalysts did not show significant changes after the impregnation and calcination steps. Concerning the pore volumes, the values for catalyst and support are also quite similar, indicating that there is no pore blockage. The N_2 adsorption-desorption isotherms of Ru-supported catalysts are presented in Annex 2 (Fig. A2.7). $Ru/SiO_{2\text{-imp}}$ displays a type IV isotherm characteristic of mesoporous materials with a type H1 hysteresis loop. For Ru/HZSM5, a type I isotherm, typical of microporous materials, was observed.

The diffractograms of supports as well as of those of the Ru-based catalysts are presented in Fig. 4.5. The diffractograms of SiO_2 and $Ru/SiO_{2\text{-imp}}$ showed a broad peak at $2\theta = 22.7°$ corresponding to non-crystalline SiO_2, while the diffractograms of HZSM5 and $Ru/HZSM5_{\text{-imp}}$ exhibited the characteristic diffraction lines of MFI zeolites (PDF: 00-057-0145). The characteristic lines of metallic Ru at $2\theta = 43.96°$ (PDF: 04-001-1921) could be observed for both supported catalysts, and the estimated crystallite size is reported in Table 4.3. $Ru/SiO_{2\text{-imp}}$ and $Ru/HZSM5_{\text{-imp}}$ present a Ru° crystallite size of 12 and 15 nm, respectively.

Table 4.3: Ru content, specific surface area, pore volume, particle size, and dispersion of Ruthenium-supported catalysts.

Catalysts	wt% Ru [a]	BET (m^2g^{-1})	Pore volume ($cm^3 . g^{-1}$)	d_p (nm) [c]	D (%)
$Ru/SiO_{2\text{-imp}}$	0.6	190 (189) [b]	0.72 (0.63)	8.3 (10)	16.0
$Ru/HZSM5_{\text{-imp}}$	0.7	518 (485)	0.34 (0.33)	12.0 (15)	11.0

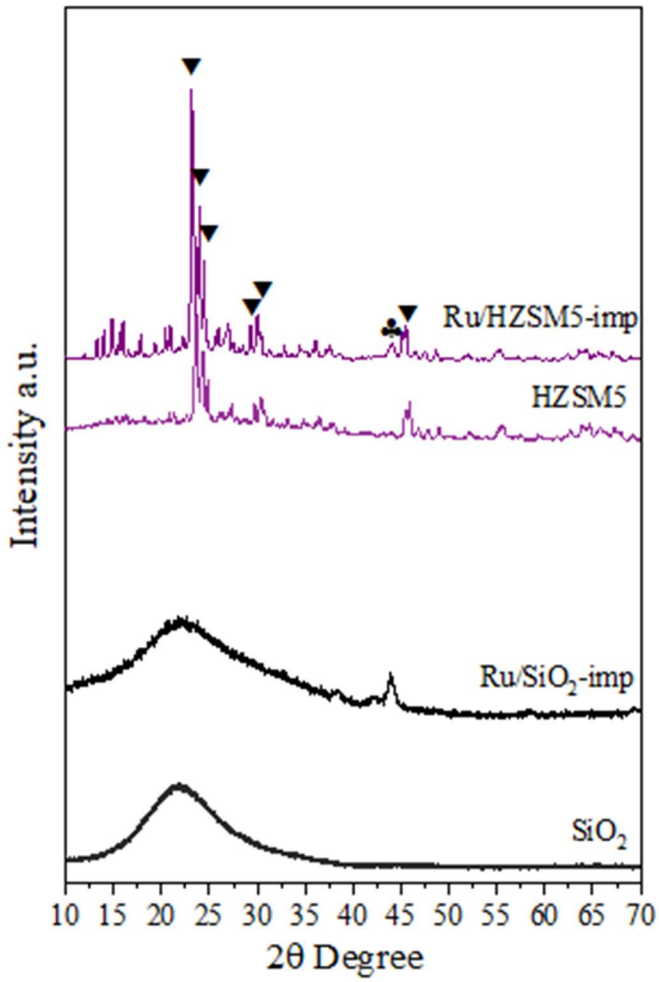

Figure 4.5: XRD patterns of supports and Ru-based catalysts. (▼) HZSM5, (♣) Ru.

The H_2-TPR of calcined Ru-based catalysts was performed in order to study the reduction of RuO_2. Temperature-programmed reduction profiles of Ru-supported catalysts are shown in Fig. 4.6. One intense peak at 164 °C was observed for the TPR profile of $Ru/SiO_{2\text{-imp}}$, while two peaks with T_{max} at 122 and 141 °C were detected to Ru-supported on HZSM5, but profiles are quite similar. All peaks are attributed to the

complete reduction of RuO_2 to metallic Ru[57–59]. As the reduction of Ru species takes place at low temperatures (< 150 °C), the reduction condition used (400 °C, 30 bar H_2) is enough to completely reduce Ru catalysts.

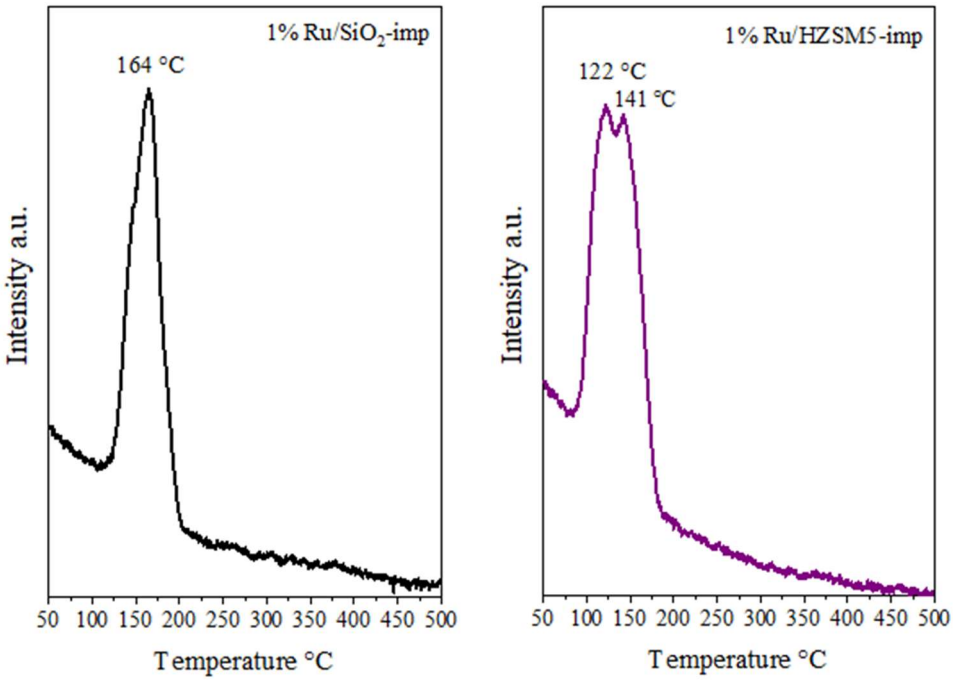

Figure 4.6: TPR profiles of Ruthenium-supported catalysts.

Regarding the acidic properties of Ru-based catalysts, as observed for $Pd/SiO_{2\text{-imp}}$, $Ru/SiO_{2\text{-imp}}$ did not retain NH_3. The NH_3-TPD profile of desorbed ammonia for Ru-supported on HZSM5 is shown in Fig. 4.7 a. Poorly resolved multiple peaks between 100 and 500 °C were observed, indicating the presence of acidic sites with different strengths. Table 4.4 reports the total density of acidic sites as well as the distribution of the acidic sites calculated from NH_3-TPD profiles. The total density of acidic sites for $Ru/HZSM5_{\text{-imp}}$ was 521 µmol/g of NH_3. Compared to Pd/HZSM5 (699 µmol/g of NH_3), Ru/HZSM5 exhibited a lower density of acidic sites, but the distribution of acidic sites did not change significantly.

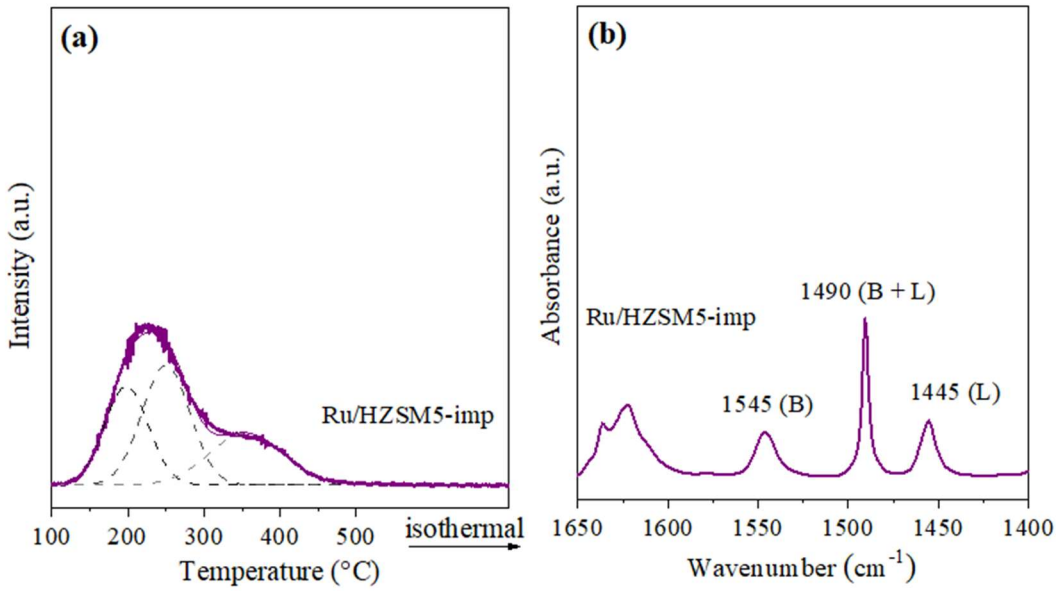

Figure 4.7: Acidic properties of Ru/HZSM5 (a) NH_3-TPD profiles (b) Infrared spectrum of adsorbed pyridine.

The concentration of Lewis and Brønsted acidic sites was measured by FTIR of adsorbed pyridine, and the spectra of pyridine adsorbed on Ru/HZSM5$_{-imp}$ at 150 °C is presented in Fig. 4.7 b. Brønsted (1545 cm^{-1}) and Lewis (1445 cm^{-1}) acidic sites were detected. The concentration of LAS and BAS for Ru/HZSM5 is 169 and 231 µmol g^{-1}, respectively. Compared to Pd/HZSM5, the Ru-supported catalysts exhibited a higher amount of LAS and BAS acidic sites.

Table 4.4: Total amount of ammonia desorbed, acidic sites strength distribution, and concentration of Lewis and Brønsted acid sites for ruthenium-based catalysts.

Catalysts	Ammonia desorbed (µmol/g) [a]	Acidic sites strength distribution (%) [a]			Lewis [b] (µmol g^{-1})	Brönsted [b] (µmol g^{-1})
		Weak	Medium	Strong		
Ru/HZSM5$_{-imp}$	521	31	42	27	169	231

STEM images of Ru/SiO_{2-imp} and Ru/HZSM5$_{-imp}$ and their respective particle size distribution are shown in Fig.4.8. For both catalysts, the ruthenium particles had a

spherical shape easily to distinguish due to the good contrast with the support. The Ru particle size for $Ru/SiO_{2\text{-imp}}$ and $Ru/HZSM5_{\text{-imp}}$ were 8.3 and 12 nm, respectively (Table 4.3). This result is in accordance with the crystallite size estimated by the Scherrer equation. In addition, the images show that Ru particles are uniform in size and well dispersed on the support.

The ruthenium dispersion was also calculated considering $D = 1.3521/d_p$ and the results showed that the dispersion for $Ru/SiO_{2\text{-imp}}$ and $Ru/HZSM5_{\text{-imp}}$ was 16 and 11%, respectively (Table 4.3).

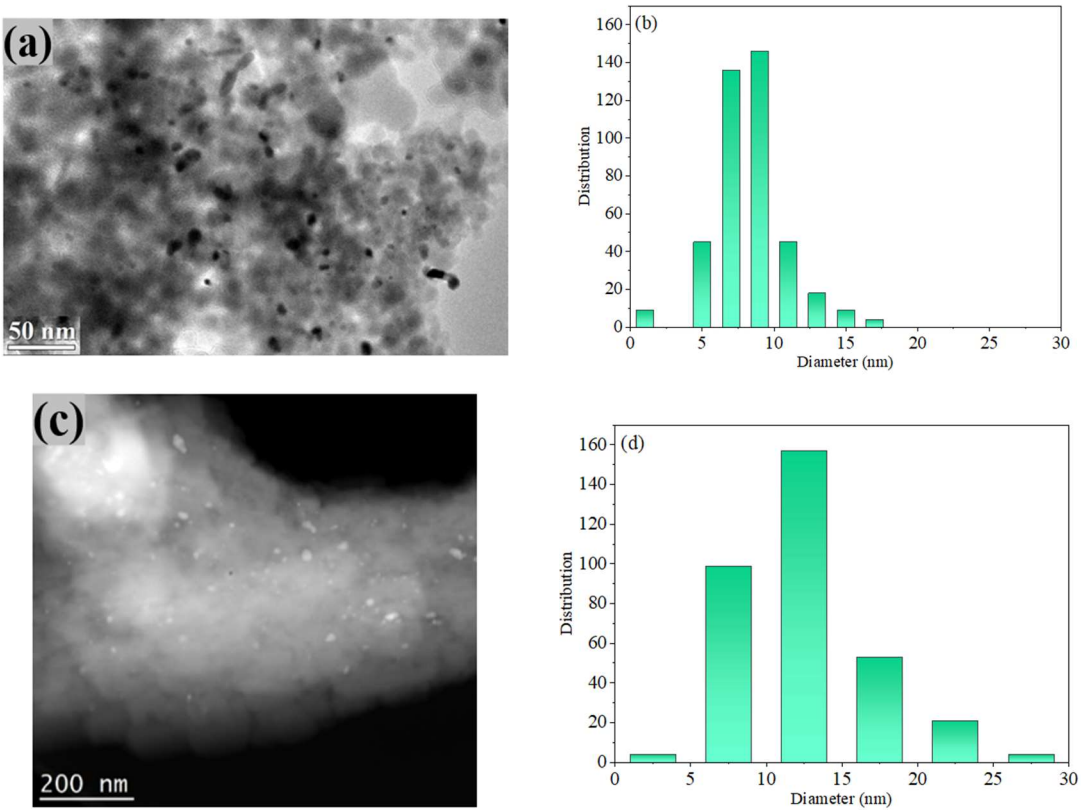

Figure 4.8: TEM images and particle size distribution for (a-b) $Ru/SiO_{2\text{-imp}}$ and (c-d) $Ru/HZSM5_{\text{-imp}}$.

Chapter 5

Conversion of dimeric aryl ethers over supported Ru and Pd-based catalysts

5.1 Introduction

The present chapter aims at screening the role of the nature of the metal, as well as the effect of the support acidity, in the cleavage of model molecules representative of the main ether linkages present in lignin, α-O-4, β-O-4, and 4-O-5. Recently, our group has studied the effect of the nature of the metal (Pt, Pd, Rh, Ru, Ni, and Co) in the HDO of phenol in the gas phase, [60] and we have demonstrated that the deoxygenation activity of the catalysts was strongly affected by the type of metal.

Therefore, Pd and Ru-based catalysts supported on SiO_2 and HZSM5 were synthesized by incipient wetness impregnation, as detailed in Chapter 3. SiO_2 was chosen as a material devoid of acidic catalytic sites, and HZSM5 was selected due to its high density of acidic sites. According to the STEM analysis, the average particle size obtained for Pd/SiO_2 and Ru/SiO_2 were quite similar, but it must be acknowledged that for the catalysts supported over HZSM5, the Pd particle size was significantly larger. Benzyl phenyl ether (BPE), phenethoxybenzene (PEB), and diphenyl ether (DPE) were used as feedstock and all reactions were carried out at 230 °C, 18 bar of H_2, in decalin for 3 h.

5.2 Hydrodeoxygenation of BPE over Ru and Pd-based catalysts

The product distribution for BPE conversion over Pd and Ru-supported over SiO_2 and HZSM5, as well as over the bare supports, are presented in Table 5.1. No conversion was detected in the absence of a catalyst.

Table 5.1: Conversion of BPE, mass balance, and product distribution for Ru and Pd-based catalysts

Entry	Catalysts	X_{BPE} (%)	MB (%)	Yield (%)		
				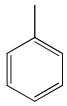	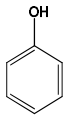	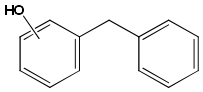
1	SiO_2	0	100	0.0	0.0	0.0
2	$Pd/SiO_{2\text{-imp}}$	41	90	18.2	13.0	0.0
3	$Ru/SiO_{2\text{-imp}}$	31	91	6.1	5.2	10.9
4	HZSM5	29	95	0.2	4.9	19.1
5	$Pd/HZSM5_{\text{-imp}}$	59	91	4.7	10.9	33.6
6	$Ru/HZSM5_{\text{-imp}}$	62	91	1.0	8.6	42.9

Reaction conditions: Reactant (62 mmol), decalin (15 mL), SiO_2 (250 mg), $Pd/SiO_{2\text{-imp}}$ (250 mg), $Ru/SiO_{2\text{-imp}}$ (300 mg), HZSM5 (60 mg), $Pd/HZSM5_{\text{-imp}}$ (60 mg), and $Ru/HZSM5_{\text{-imp}}$ (45 mg), 230 °C, 18 bar H_2, 3h.

SiO_2 did not exhibit any activity for BPE conversion even using a high amount of support (250 mg), due to the absence of acidic sites. However, when HZSM5 was used, 29 % of BPE was converted producing phenol and 2-benzylphenol (2-BPH) as the main products. In addition, toluene appeared as a minor product.

In the literature, the conversion of BPE using undecane at 250 °C and 40 bar of H_2 in the absence of catalysts was reported to produce high amounts of 2 and 4-benzylphenol (2 and 4-BPH) [31]. Theoretical calculations demonstrated that in a non-polar solvent, BPE was homolytically cleaved into phenoxy and benzyl radicals by free radical reactions, instead of being heterolytically cleaved to form benzyl and benzyloxy radicals, due to the lower bond dissociation energy for the homolytically cleavage (184.3 and 332.9 kJ mol^{-1}, respectively). The conversion of BPE via free radical reactions at high temperature (275 °C) was also proposed by Kidder et al.[61] for the pyrolysis of BPE confined in mesoporous silica. After cleavage, the phenoxy and benzyl radicals would follow two different reaction pathways: (i) hydrogenation to form phenol and toluene or (ii) recombination to form 2-BPH or 4-BPH.

For HZSM5 in undecane, He et al.[31] proposed that the Brønsted acidic sites of HZSM5 donate their proton to the oxygen of the BPE molecule possessing a lone pair of electrons, which weakens the C-O linkage, leading to BPE cleavage into phenoxy and benzyl radicals. These radicals are stabilized by H radicals, producing phenol and toluene. Finally, phenol can be attacked in the ortho or para position to form 2 and 4-BPH.

According to our results, the cleavage of BPE over HZSM5 proceeds via radical reactions as proposed by the literature. In the presence of acidic sites, BPE can be broken to form phenoxy and benzyl radicals. Then, these radicals can be hydrogenated into phenol and toluene, respectively, or benzyl radicals can attack phenol to form alkylated products, 2 and 4-BPH.

For the Pd-based catalysts, toluene and phenol were formed over Pd/SiO_2 and Pd/HZSM5 through the hydrogenolysis of BPE catalyzed by metal sites, which is in agreement with the literature [14,24,38]. Furthermore, due to the presence of acidic sites, 2 and 4-BPH were also observed for Pd/HZSM5. When Ru-supported catalysts were used, toluene and phenol were also produced. However, 2 and 4-BPH were produced even in the absence of acidity (Ru/SiO_2). In addition, a larger formation of 2 and 4-BPH was observed for Ru/HZSM5 compared to Pd/HZSM5.

The hydrogenolysis of BPE catalyzed by metallic sites has been investigated in the literature over noble metals using a polar and non-polar solvent.

Pd/C in the presence of HZSM5 was used for BPE conversion at 200 °C, 50 bar of H_2 in aqueous phase [37]. Cyclohexane and methylcyclohexane were the only products observed. The authors proposed that after hydrogenolysis, the Brønsted acidic sites of HZSM5 catalyzed the dehydration of cyclohexanol to produce cyclohexane. In these reaction conditions, the formation of alkylated products was only reported in the presence of bare HZSM5. When Pd/C was used, the formation of these products was suppressed.

Ru/Nb_2O_5-SiO_2 selectively converted BPE into benzene and toluene (water and isopropanol mixture at 230 °C, without an external source of hydrogen) [35]. The authors proposed that the deoxygenation of BPE proceeds through the direct cleavage of the C-O ether bonds to produce arenes. Phenol and toluene were formed by hydrogenolysis of the C_{aliph}-O bond of BPE, then benzene was produced by direct cleavage of the C_{arom}-O bond of phenol. Additionally, the authors suggested that the HDO of BPE was promoted by a synergistic effect between Ru and NbO_x species from the support.

Under reaction conditions similar to those used in our work (220 °C, 20 bar of H_2) with *n*-hexane as solvent, cyclohexane, methylcyclohexane, and *t*-butylcyclohexane were the only products detected for BPE conversion over 1 wt. % Ru/HZSM5 [11]. However, the formation of these products was not proposed by the authors. The smaller Ru particle size (2.3 nm) and the higher amount of strong acidic sites, compared to our catalysts, could be responsible for the complete deoxygenation of BPE after C-O bond cleavage.

Therefore, for supported catalysts, the formation of alkylated products has only been reported in the literature over acidic supports. According to our results of NH_3-TPD, no acidity was measured for Pd/SiO_2 and Ru/SiO_2. Furthermore, the H_2-TPR profiles of Ru-based catalysts showed that the Ru oxide was completely reduced at 400 °C, excluding the possibility of the creation of Lewis acidic sites associated with the presence of ruthenium oxide. Therefore, these results suggest that the oxophilicity of the metal, i. e., the ability of the metal to bind to the oxygen atom from the substrate, may be involved in the promotion of the alkylation reactions.

The metal oxophilicity is directly associated with the position of the d-band center relative to the Fermi level. As the d-band center is closer to the Fermi level, the anti-bonding orbital of the hybridization between metal and oxygen is further away from the

Fermi level and has low electron occupancy. Therefore, the M-O bond becomes stronger and the metal more oxophilic [62,63].

Duong et al [63] reported a correlation between the activation energy for the direct deoxygenation (DDO) of m-cresol to toluene and the adsorption energy of oxygen over different metals. They observed that the energy barrier for the DDO of m-cresol increased linearly from Fe to Pt, as the metal oxophilicity decreases. For the metals evaluated, the oxophilicity increased in the order Pt < Pd < Rh < Ru < Fe. As consequence, the DDO was favored over Rh, Ru, and Fe.

The effect of the nature of the metal was previously investigated by our group for the HDO of phenol in the gas phase at 300 °C [60]. It was observed that over Pt, Pd, and Rh, phenol was mainly tautomerized and hydrogenated to cyclohexanone/cyclohexanol, whereas the direct dehydroxylation of phenol to benzene was favored for oxophilic metals (Ru, Co, and Ni). Similar results were observed by Tan et al. [64] for the HDO of m-cresol over Pt and Ru-supported on SiO_2. DFT calculations showed that the direct dehydroxylation of m-cresol to toluene was favored over the oxophilic Ru (0001) surface due to the lower energy barrier (98 kJ mol^{-1}) compared to Pt (111) (242 kJ mol^{-1}). The authors proposed that over Ru sites, the dehydroxylation of m-cresol produces an unsaturated hydrocarbon radical C_7H_7*, which can be hydrogenated to form toluene. Over Pt (111), the same intermediate was not formed.

The activity of Ru, Pd, and Mo_2C supported on carbon was compared for the HDO of guaiacol at 330 °C, 34 bar of H_2 in decalin as solvent [65]. The authors reported that the hydrogenation of the guaiacol aromatic ring occurred before the C-O bond cleavage for the Pd and Ru catalysts. Pd exhibited a hydrogenation activity 6 times higher than Ru, but Ru was more efficient for oxygen removal. Mo_2C was less active than Ru and Pd and promoted mainly the direct demethoxylation of guaiacol to phenol.

Therefore, we propose that the cleavage of BPE into phenoxy and benzyl radicals occurs not only in the presence of the acidic sites of HZSM5 but also on the surface of Ru due to its high oxophilicity. According to the literature, due to the Ru lower hydrogenation ability compared with Pd, Ru does not easily promote the hydrogenation of phenoxy and benzyl radicals into phenol and toluene, respectively. Thus, the higher concentration of phenoxy and benzyl radicals may favor their recombination into 2 and 4-BPH (Scheme 5.1).

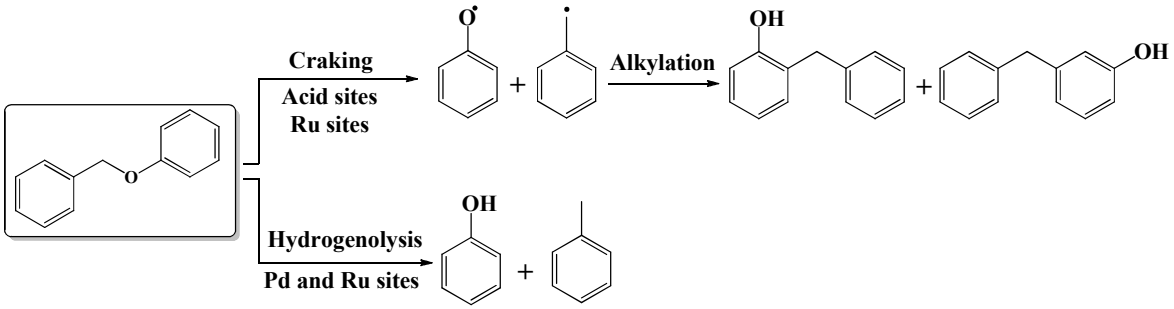

Scheme 5.1: Reaction route for BPE conversion over Pd and Ru-based catalysts.

5.3 Hydrodeoxygenation of PEB over Ru and Pd-based catalysts

The PEB conversion and product yield for Pd and Ru-based catalysts supported over SiO_2 and HZSM5 are shown in Table 5.2. As observed for BPE, no conversion of PEB was detected in the absence of catalysts, nor over SiO_2. In the presence of the Brønsted and Lewis acidic sites of HZSM5, 6 % of PEB was converted into phenol, ethylbenzene, and alkylated products, 2 and 4-phenethylphenol (2 and 4-PPE), indicating that acidic sites are required to break the β-O-4 ether linkage of PEB.

The PEB conversion over bare oxides has been reported in the literature in a non-polar solvent, under high hydrogen pressure and temperature. PEB was selectively converted into phenol and ethylbenzene over Nb_2O_5 at 260 °C and 10 bar of H_2 using *n*-

decane as solvent [26]. Over Hβ (220 °C, 40 bar H_2) [28] and USY (345 °C and 50 bar H_2) zeolites [44], phenol and alkylated products (2, 3, and 4-phenethylphenol) were the main products observed after PEB cleavage in *n*-hexane and dodecane, respectively. The authors proposed that the cleavage of PEB occurred by H^+ addition to produce phenol and 2-phenyleth-1-ylium as intermediates, which can attack phenol at the ortho, meta, or para positions to form 2, 3, and 4-phenethylphenol, respectively, via a transalkylation reaction catalyzed over acidic sites.

However, the literature also reports that in the presence of water at 240 °C and under 8 bar of H_2, PEB remained unreacted even in the presence of acidic supports such as sulfated zirconia, HZSM5, zeolite Hβ, and HY [25,27].

Table 5.2: Conversion of PEB, mass balance, and product distribution for Ru and Pd-based catalysts

Ent.	Catalysts	X_{PEB} (%)	MB (%)	Yield (%)		
				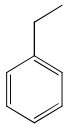	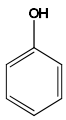	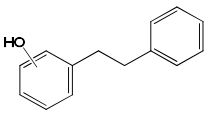
1	SiO_2	0	99	0.0	0.0	0.0
2	$Pd/SiO_{2\text{-imp}}$	0	98	0.0	0.0	0.0
3	$Ru/SiO_{2\text{-imp}}$	0	98	0.0	0.0	0.0
4	HZSM5	6	98	1.6	1.9	1.2
5	$Pd/HZSM5_{\text{-imp}}$	43	92	5.0	5.3	25.6
6	$Ru/HZSM5_{\text{-imp}}$	47	93	3.5	5.3	30.5

Reaction conditions: Reactant (62 mmol), decalin (15 mL), SiO_2 (250 mg), $Pd/SiO_{2\text{-imp}}$ (250 mg), $Ru/SiO_{2\text{-imp}}$ (250 mg), HZSM5 (65 mg), $Pd/HZSM5_{\text{-imp}}$ (65 mg), $Ru/HZSM5_{\text{-imp}}$ (65 mg), 230 °C, 18 bar H_2, 3h.

In our work, the product distribution observed for PEB conversion over HZSM5 suggests that the conversion of PEB proceeds by a similar radical route as reported in the literature. The Brønsted acidic sites of HZSM5 can donate their H^+ proton to the oxygen of PEB, weakening the C_{aliph}-O bond and resulting in its cleavage into phenoxy and 2-

phenyleth-1-ylium radicals. Then, the radicals formed can be hydrogenated to phenol ethylbenzene, or 2-phenyleth-1-ylium can attack phenol at ortho or para positions to form 2 and 4-PPE, respectively.

Unlike the former molecule, Pd/SiO_2 and Ru/SiO_2 did not exhibit any activity for the PEB conversion at 230 °C and 18 bar of H_2. These results suggest that in the absence of acidic sites, the metal oxophilicity does not appear as a relevant and sufficient parameter to explain the conversion of PEB, in contrast with BPE. This is likely due to the higher bond energy dissociation required for the cleavage of β-O-4 linkage compared to the α-O-4 bond.

When Pd/HZSM5 and Ru/HZSM5 were used, 43 and 47 % of PEB conversion were achieved. Compared to bare HZSM5, the presence of metal increased the conversion of PEB, indicating that metal and acidic sites are required for a better performance. Regarding the products yield, the metal type did not significantly affect the product distribution. Phenol, ethylbenzene, and alkylated products were observed for both catalysts with similar yields.

In the literature, palladium and Ruthenium-supported over sulfated zirconia were used for PEB conversion in aqueous phase at 240 °C and 8 bar of H_2 [25,27]. The authors observed that the hydrogenolysis of the C_{aliph}-O bond of PEB to produce ethylbenzene and phenol occurred for both metals. After cleavage, ethylbenzene remained unreacted while phenol was hydrogenated to cyclohexanone/cyclohexanol by the Pd and Ru metal sites. However, over Ru/SZ, the conversion of phenol to cyclohexanol, followed by its dehydration to cyclohexane, took place. Cyclohexane was then dehydrogenated to form benzene. The authors proposed that the rate of hydrogenation of phenol to cyclohexanol over Pd/SZ was slower than for Ru/SZ, producing less cyclohexanol and inhibiting the formation of benzene over Pd/SZ.

Salam et al.[44] proposed that the formation of alkylated products by transalkylation reaction occurred simultaneously with the hydrogenolysis of the C_{aliph}-O bond of PEB into phenol and ethylbenzene for NiMoS supported over USY zeolite (345 °C, 50 bar of H_2 in dodecane as solvent). Then, the hydrocracking of alkylated products to produce mono and alkyl phenols (m-cresol and 2 and 4-ethylphenol) took place. The formation of benzene, toluene, and ethylbenzene was attributed to the HDO of mono and alkyl phenols.

According to our results, the conversion of PEB over Pd and Ru-supported on HZSM5 occurs via two parallel reaction routes: (i) the cleavage of PEB into phenol and 2-phenyleth-1-ylium catalyzed by the acidic sites of HZSM5 and (ii) the hydrogenolysis of the C_{aliph}-O bond of PEB into phenol and ethylbenzene, catalyzed by the metallic sites. The presence of the acidic sites leads to the alkylation reaction between phenol and 2-phenyleth-1-ylium, to form 2 and 4-phenylethyl phenol (Scheme 5.2).

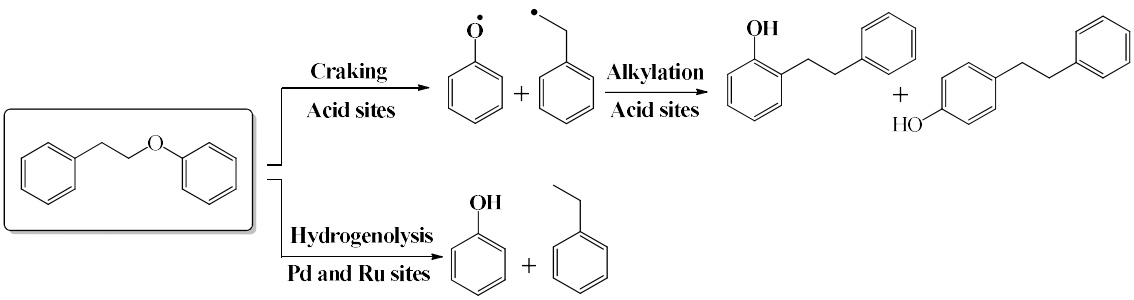

Scheme 5.2: Reaction route for PEB conversion over Pd and Ru-based catalysts.

5.4 Hydrodeoxygenation of DPE over Ru and Pd-based catalysts

The initial tests with DPE, at the same concentration and reaction conditions used for the conversion of BPE and PEB (62 mmol, 230 °C, and 18 bar H_2) over impregnated Pd-based catalysts, exhibited no conversion. Reactions were then carried out at the same temperature and pressure, but using half the substrate concentration (31 mmol). The

conversion and product distribution for the HDO of DPE over supported Pd and Ru catalysts are shown in Table 5.3. As observed for BPE and PEB, SiO_2 was not active for the DPE conversion, which was likely due to the absence of acidity. However, in contrast with the former molecules, bare HZSM5 was also unable to convert DPE under the reaction conditions used (230 °C, 18 bar H_2, decalin). These results are in good agreement with the literature, which reported that DPE remained unreacted in the presence of non-acidic[30] and acidic oxides [29,38].

Table 5.3: Conversion of DPE, mass balance, and product distribution for Ru and Pd-based catalysts

Ent.	Catalysts	X_{PEB} (%)	MB (%)	Yield (%)						
				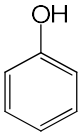		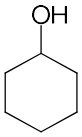		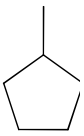	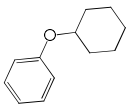	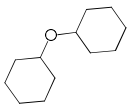
1	SiO_2	0	99	0.0	0.0	0.0	0.0	0.0	0.0	0.0
2	$Pd/SiO_{2\text{-imp}}$	0	99	0.0	0.0	0.0	0.0	0.0	0.0	0.0
3	$Ru/SiO_{2\text{-imp}}$	47	78	5.0	5.8	0.0	8.9	0.0	4.2	1.0
4	HZSM5	0	98	0.0	0.0	0.0	0.0	0.0	0.0	0.0
5	$Pd/HZSM5_{\text{-imp}}$	30	81	0.0	0.0	1.0	5.6	4.1	0.0	0.0
6	$Ru/HZSM5_{\text{-imp}}$	19	100	0.0	0.0	0.0	5.5	13.8	0.0	0.0

Reaction conditions: Reactant (31 mmol), decalin (15 mL), SiO_2 (250 mg), $Pd/SiO_{2\text{-imp}}$ (250 mg), $Ru/SiO_{2\text{-imp}}$ (300 mg), HZSM5 (250 mg), $Pd/HZSM5_{\text{-imp}}$ (250 mg), $Ru/HZSM5_{\text{-imp}}$ (25 mg), 230 °C, 18 bar H_2, 3h.

In the presence of metallic sites, no conversion of DPE was observed for Pd/SiO_2, whereas 47 % of DPE was converted over Ru/SiO_2. For Ru/SiO_2, cyclohexane (8.9 %) was the main product formed, followed by benzene (5.8 %), phenol (5.0 %), and cyclohexyl phenyl ether (4.2 %).

Wu et al. [45] studied the performance of Ru, Pt, and Pd-supported on carbon for the HDO of DPE at 120 °C in isopropanol as a solvent, without an external source of H_2. Ru completely converted DPE into cyclohexanol, benzene, and cyclohexane. For Pt/C, a

lower DPE conversion (77.6 %) was observed and the same products were detected. Finally, Pd/C exhibited the lowest activity, converting less than 5 % of DPE into phenol and benzene. The authors proposed that unlike Pd and Pt, Ru can coordinatively bind to the oxygen atom of DPE, promoting its cleavage into phenoxide and phenyl radicals. Then, the radicals formed over Ru can be further hydrogenated to form benzene and phenol by the active hydrogen from isopropanol on the surface of Ru.

Ru, Pd, and Pt supported on carbon were also tested for the HDO of DPE (methanol as solvent, at 120 °C, and 5 bar of H_2)[46]. Ru exhibited the highest activity for DPE conversion and the highest selectivity to hydrogenolysis products. Cyclohexane, cyclohexanol, and dicyclohexyl ether were formed as main products. For Pd/C and Pt/C, cyclohexyl phenyl ether was the main product detected, with a selectivity above 80 % for both catalysts. The better performance of the Ru-based catalyst was attributed to a smaller Ru particle size and higher metal dispersion.

Regarding the products obtained over Ru/C in our reaction conditions, DPE can be cleaved into phenoxide and benzyl radicals over the Ru surface and not over Pd sites. Then, the hydrogenation of the radicals formed after DPE cleavage can produce phenol and benzene, respectively. At the same time, the partial hydrogenation of the DPE aromatic rings occurs over Ru/C. Following the DPE cleavage, benzene can be also formed by hydrogenolysis of the C_{arom}-O bond of phenol, but because of the absence of acidic sites, cyclohexane could be formed via benzene hydrogenation. Therefore, the results suggest that the higher oxophilicity of Ru could favor the hydrogenolysis of the C_{arom}-O bond of DPE.

For Pd/HZSM, 30 % of DPE was converted into cyclohexane (5.6 %) and methyl cyclopentane (4.1 %). A DPE conversion of 19 % was achieved for Ru/HZSM5 and, although the same products were obtained, the yield of methyl cyclopentane increased

from 4.1 to 13.8 % over the Ru-based catalyst. In comparison to Ru/SiO_2, products from the partial hydrogenation of the DPE aromatic rings were not detected.

The conversion of DPE over catalysts containing acidic sites has been reported in the literature, in aqueous phase as well as using a non-polar solvent. Ru-supported on Al_2O_3 and different zeolites (HZSM5, H-beta, H-USY) were tested for the conversion of DPE at 120 °C, 40 bar of H_2 in water [35]. For the same DPE conversion, Ru/HZSM5 exhibited the highest selectivity to cyclohexane (73.2 %), while Ru/Al_2O_3 showed the lowest one (33.5 %). In addition, a considerable amount of cyclohexanol and products from partial and complete hydrogenation of the DPE aromatic rings was observed for all the catalysts. The authors proposed that the hydrogenolysis of DPE into phenol and benzene occurs as the main reaction pathway, while the hydrogenation of the DPE aromatic rings takes place to a minor extent. After the C-O bond cleavage, cyclohexane can be formed by two different pathways: (i) benzene hydrogenation or (ii) cyclohexanol dehydration into cyclohexene, followed by its hydrogenation. The higher selectivity to cyclohexane obtained over Ru/HZSM5 compared to the other catalysts was attributed to its stronger acidity.

Over 1 wt. % Ru/HZSM5 [39] and over Pd/C in the presence of HZSM5 [37] and using the same reaction conditions (200 °C, 50 bar of H_2, water), cyclohexane was the main product observed for DPE conversion. However, its formation was not proposed by the author in both works.

DPE was completely converted to cyclohexane over $Pd/Nb_2O_5/SiO_2$ at 170 °C, 25 bar of H_2 in dodecane as solvent [52]. The authors did not propose the reaction route for cyclohexane formation but suggested that NbO_x species could efficiently promote the C_{arom}-O cleavage of DPE and assist the hydrodeoxygenation process. Zhao et al [29] investigated the conversion of DPE over Pd/HZSM5 and Pd-Ni/HZSM5 catalysts (220

°C, 20 bar of H_2 in n-hexane as solvent). For Pd/HZSM5, 70 % of DPE was converted into cyclohexane, cyclohexyl phenyl ether, and dicyclohexyl ether, whereas it was completely converted to cyclohexane on the bimetallic catalyst. They proposed that cyclohexyl phenyl ether is an important intermediate in DPE conversion, with two main reaction pathways: (i) hydrogenation to form dicyclohexyl ether, or (ii) hydrogenolysis of its C_{aliph}-O bond into phenol and cyclohexane. Then, cyclohexanol, formed from phenol hydrogenation or via cyclohexyl phenyl ether cleavage, can be dehydrated to cyclohexene, upon catalysis by the acidic sites. Cyclohexane was finally produced by cyclohexene hydrogenation

According to our results, the products obtained over Pd and Ru-supported over HZSM5 suggest that DPE was mostly cleaved by hydrogenolysis into phenol and benzene in the presence of metallic and acidic sites. Cyclohexane can be formed by hydrogenation of phenol and subsequent dehydration, or by benzene hydrogenation. Finally, the isomerization of cyclohexane catalyzed by the acidic sites can lead to the formation of methyl cyclopentane [66] (Scheme 5.3).

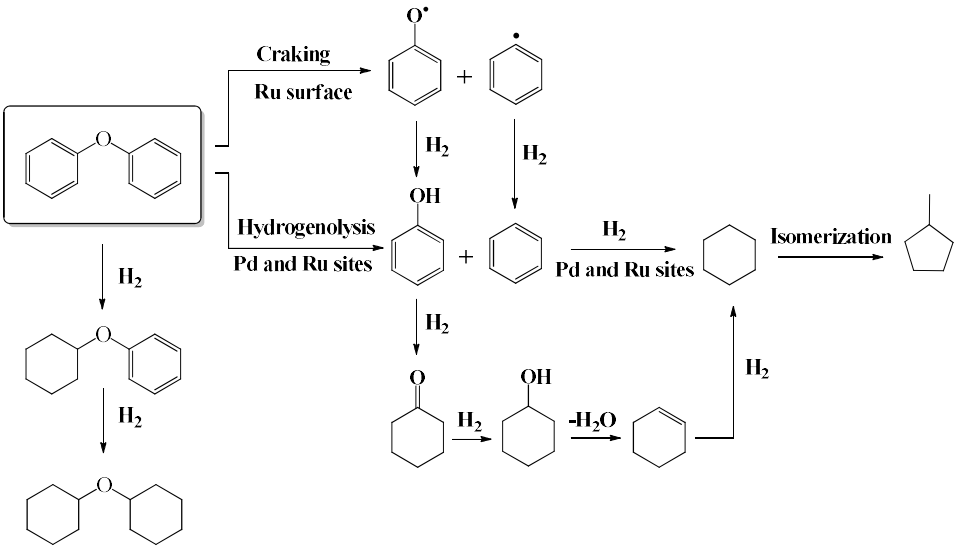

Scheme 5.3: Reaction route for DPE conversion over Pd and Ru-based catalysts.

5.5 Conclusion

The effect of the nature of the metal (Pd and Ru), as well as the effect of the type of the support (SiO_2 and HZSM5) was investigated for the hydrodeoxygenation of BPE, PEB, and DPE in the liquid phase. In the presence of SiO_2, no conversion was observed for any molecule due to the absence of acidic sites. However, for HZSM5, the selected model molecules were converted to a large or minor extent. As the C-O ether bond strength increases, the effect of the support acidity for C-O cleavage is less relevant. As a result, the conversion of dimeric aryl ethers over bare HZSM5 followed the order: BPE (29 %) >> PEB (6 %) > DPE (0 %). Furthermore, due to the presence of acidic sites, oxygenated alkylated products were mainly formed over HZSM5.

For the supported catalysts, the product distribution for BPE conversion was highly affected by the oxophilicity of Ru, and alkylated products were produced even in the absence of acidic sites (Ru/SiO_2). The conversion of DPE was also affected by Ru oxophilicity. Pd/SiO_2 did not exhibit any activity for DPE conversion, while 47 % of DPE was converted over Ru/SiO_2, producing cyclohexane as the main product. Despite the advantages of Ru in terms of activity, it is noted that oxygenated alkylated products were extensively produced over Ru catalysts for BPE and PEB conversion. Therefore, it was chosen to prefer Pd-supported catalysts for further studies.

Chapter 6

Effect of support and metal particle size for the hydrodeoxygenation of benzyl phenyl ether over Pd-based catalysts.

6.1 Introduction

The conversion of benzyl phenyl ether (BPE), a typical model molecule representative of the α-O-4 ether bond, has been widely studied in the literature, as shown in Chapter 2. Different catalysts and reaction conditions have been used for the HDO of BPE. From the existing literature, acidic sites are required to achieve the complete deoxygenation of dimeric aryl ethers. However, how the properties of the support affect the mechanism of the conversion of BPE is not clear yet.

Therefore, this chapter investigates the role of the support in the performance of Pd-based catalysts for the conversion of BPE. Pd-based catalysts supported on different oxides (SiO_2, TiO_2, Nb_2O_5, Al_2O_3, ZrO_2, and HZSM5) were synthesized by incipient wetness impregnation and their activity was evaluated in the HDO of BPE in a liquid phase.

The effect of the metal particle size on the cleavage of the α-O-4 bond, not yet studied in the literature, was also evaluated by preparing Pd-based catalysts supported on TiO_2, Nb_2O_5, Al_2O_3, and ZrO_2 using a sol-immobilization method. Finally, the effect of temperature and pressure conditions was studied.

6.2 Action of bare supports on BPE conversion

The product distribution for the conversion of BPE at 3 h over the bare supports at 230 °C, under 18 bar of H_2, in decalin, is presented in Table 6.1.

In the absence of a solid, no conversion of BPE was observed. When an oxide was introduced, BPE was converted to a minor or large extent, except for SiO2. This oxide did not exhibit any activity even using a four-fold larger mass compared to the other oxides. This is likely due to its total absence of acidity (Table 6.1, entry 1). Using the

same mass of solid (60 mg), Al_2O_3 and TiO_2 showed the lowest BPE conversion, while Nb_2O_5 and ZrO_2 presented the highest one (Table 6.1, entries 2-5). Regarding the product distribution, alkylated products 2-benzylphenol and 4-benzylphenol (2-BPH and 4-BPH), and to a lesser extent, phenol were the main products formed. Toluene always appeared as a minor product. In addition, a trimer (2,6-dibenzylphenol) was also detected in a significant amount over ZrO_2 and especially Nb_2O_5. The yield to dimers and trimers followed the order: Nb_2O_5 > ZrO_2 > HZSM5 >> TiO_2 ≈ Al_2O_3. This result reveals that in these experimental conditions, an oxide with Brønsted acidic sites, without metallic phase, exhibits a high activity and selectivity to alkylated products, compared with oxides with only Lewis acidic sites such as alumina. The cleavage of the ether linkage can thus take place in the absence of a metallic phase.

Table 6.1: Conversion of BPE, mass balance, and product distribution for supports and impregnated Pd catalysts

				Yield (%)			
Ent.	**Catalyst**	**X_{BPE} (%)**	**MB (%)**	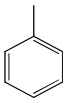	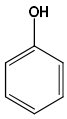	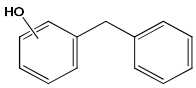	Trimer
1	SiO_2	0	100	0.0	0.0	0.0	0.0
2	Al_2O_3	7	98	0.1	2.7	1.6	0.0
3	TiO_2	9	98	1.4	2.1	3.5	0.0
4	Nb_2O_5	100	89	0.0	15.0	45.0	29.3
5	ZrO_2	100	71	1.0	16.0	48.0	9.4
6	HZSM5	29	95	0.2	4.9	19.1	0.0
7	$Pd/SiO_{2\text{-imp}}$	41	90	18.2	13.0	0.0	0.0
8	$Pd/Al_2O_{3\text{-imp}}$	60	94	23.3	22.1	8.3	0.0
9	$Pd/TiO_{2\text{-imp}}$	52	100	24.8	23.9	4.7	0.0
10	$Pd/Nb_2O_{5\text{-imp}}$	58	91	21.5	20.0	8.2	0.0
11	$Pd/ZrO_{2\text{-imp}}$	65	85	11.4	13.4	25.4	0.0
12	$Pd/HZSM5_{\text{-imp}}$	59	91	4.7	10.9	33.6	0.0
13*	$Pd/Nb_2O_{5\text{-imp}}$	100	95	13.6	22.2	38.7	20.8

Reaction conditions: Reactant (62 mmol), decalin (15 mL), SiO_2 (250 mg), Al_2O_3 (60 mg) TiO_2 (70 mg), Nb_2O_5 (60 mg) ZrO_2 (60 mg), HZSM5 (60 mg), $Pd/SiO_{2\text{-imp}}$ (250 mg), $Pd/Al_2O_{3\text{-imp}}$ (25 mg) $Pd/TiO_{2\text{-imp}}$ (130 mg), $Pd/Nb_2O_{5\text{-imp}}$ (30 mg), $Pd/ZrO_{2\text{-imp}}$ (65 mg), $Pd/HZSM5_{\text{-imp}}$ (45 mg), 230 °C, 18 bar H_2, 3h.
*Reaction performed with 60 mg of $Pd/Nb_2O_{5\text{-imp}}$ to achieve complete BPE conversion

The formation of alkylated products has been reported for the conversion of BPE in polar [31,32,35,41] or non-polar [31] solvents, in particular using a few acidic supports such as silica-alumina [34] and HZSM5 [31].

For the BPE conversion in a polar solvent (water), phenol and benzyl alcohol were detected in the experiments without catalyst. In this case, the hydrolysis of the C_{aliph}-O bond of BPE was catalyzed by the hydronium ions formed from water dissociation at high temperature (250 °C). The alkylated products were reported to be produced through the recombination of radical intermediates.

In a non-polar solvent, as has been chosen in our work, whether in the absence of a catalyst or in the presence of non-acidic support like silica, a high selectivity to alkylated products such as 4-BPH and 2-BPH (above 90%) was sometimes observed [31]. The authors proposed that the cleavage of the C_{aliph}-O bond of BPE proceeded through reactions between the resulting phenoxy and benzyl radicals. This is the same mechanism proposed for the cracking of BPE during pyrolysis at high temperature over silica or mesoporous silica [61,67]. According to Robert et al. [32], toluene and phenol would also be produced when these radicals could combine with hydrogen.

The formation of alkylated products at low temperatures (< 250 K) has also been reported when an acidic support like silica-alumina was used [34]. In this case, it was proposed that carbocation intermediates were formed on Brønsted acid sites, and the alkylated products were produced through a Claisen rearrangement. As observed here, a significant formation of phenol was observed but the production of toluene was negligible. According to the authors, the formation of alkylated products was promoted by the H_2-deficient environment, since silica-alumina does not adsorb and activate hydrogen. Trimers would be formed by the reaction between one phenol molecule with two toluene molecules, which explains the depletion of toluene with respect to phenol.

He et al.[68] rather suggested that the protons from Brønsted acid sites of zeolites are donated to the oxygen atom of BPE and merely activate the bond. The weakened C-O bond is broken, producing radicals leading to the formation of alkylated products, or of toluene and phenol if H radicals are also present. For the conversion of BPE in undecane over HZSM5, He et al.[31] also suggested that the alkylated products were formed through free-radical reactions via pyrolysis, instead of carbocation formation, due to the lower bond dissociation energy required to form phenoxy and benzyl radicals compared to benzyl cation and phenoxy anion (184.3 and 627.7 kJ mol -1, respectively).

Therefore, in our work, the BPE conversion into dimers (2-BPH and 4-BPH) and trimers probably proceed through the free-radical reactions described in the literature. This reaction appears to be catalyzed by the acidic sites of a wider range of oxides than reported so far, following the order: non-acidic supports < supports with Lewis acidic sites < supports with Brønsted acidic sites. Concerning the trimer formation, 2,6-dibenzylphenol was only formed over Nb_2O_5 and ZrO_2. Despite the high acidity of HZSM5, the trimer formation did not occur, which is likely due to steric hindrance caused by the small pore diameter of the zeolite channels. The HZSM5 structure consists of two types of pores (straight channels with a pore size of 0.53 nm x 0.56 nm and cross-linked sinusoidal channels of 0.51 nm x 0.55 nm) [69,70], while Nb_2O_5 and ZrO_2 exhibit mesopores of 4.5 and 4.3 nm, respectively. Then, only external acidic sites are involved, and a correlation with the number of sites detected by NH_3 desorption or pyridine adsorption is probably not relevant. The coupling between a large molecule (2-BPH) with a second benzyl radical is consequently suppressed.

6.3 The competition between Pd and acidic sites for BPE conversion

The product distribution for the conversion of BPE over impregnated Pd-based catalysts, at 230 °C, under 18 bar of H_2 in decalin, after 3 h, is presented in the lower part of Table 6.1. In contrast with bare supports, phenol and toluene were formed over all the catalysts. Metallic particles thus bring active sites for the hydrogenolysis of the C_{aliph}-O bond of BPE (which agrees very well with the literature [14,24,37–39]), but the hydrogenation of toluene and phenol is not performed in these reaction conditions.

Dimers (2-BPH and 4-BPH) were not produced over $Pd/SiO_{2\text{-imp}}$, and trimers were not detected at low conversion. For $Pd/Al_2O_{3\text{-imp}}$, $Pd/TiO_{2\text{-imp}}$, and $Pd/Nb_2O_{5\text{-imp}}$ catalysts, alkylated products were also formed, indicating a competition between the hydrogenolysis of BPE on the Pd particles, and the participation of the acidic sites of the support in the cleavage of the C_{aliph}-O bond of BPE. Indeed, for $Pd/ZrO_{2\text{-imp}}$ and $Pd/HZSM5_{\text{-imp}}$ catalysts, alkylated products were mainly formed, which is likely due to the presence of Brønsted sites on these catalysts. The formation of alkylated products has also been reported in the literature for the conversion of BPE over metal supported on acidic sites such as HZSM5 [31,39] and beta zeolites [40,41].

Increasing the BPE conversion confirms the prominence of the "acid sites" pathway leading to the production of alkylated products. Fig. 6.1 shows the product distribution as a function of BPE conversion over $Pd/HZSM5_{\text{-imp}}$ at 230 °C, under 18 bar of H_2 in decalin. The increase of conversion was obtained by increasing the amount of catalyst. When the conversion was increased from 39 to 82 %, the yield of alkylated products linearly increased while the yields to phenol and toluene only slightly increased. For instance, the yields of 2-BPH increased from 10 % (X_{BPE} = 39 %) to 38 % (X_{BPE} = 82%). In addition, 2-BPH was the main alkylated product formed, with a small formation of 4-BPH in the whole range of conversion. This result indicates that the attack of the benzyl radical onto the ortho position of phenol was preferential for all conversion. The

preferential formation of 2-BPH was also observed by Yoon et al [34] over silica-alumina. The same trend was observed for the $Pd/Nb_2O_{5\text{-imp}}$ catalyst (Table 6.1, entry 13). At higher conversion, the yield to toluene decreased and the yield to dimers increased. In addition, trimers were now formed.

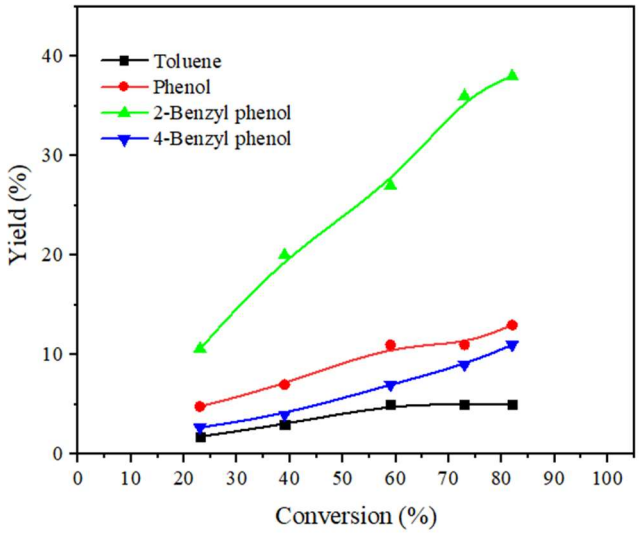

Figure 6.1: Yield to different products as a function of BPE conversion. Reaction condition: 62 mmol BPE, 15 mL decalin, Pd/HZSM5 (15 – 75 mg), 230 °C, 18 bar of H_2 in decalin, 3h.

Based on the literature, it has been supposed above that the mechanism for the cleavage of the C_{aliph}-O bond by the acid sites of the supports involves the formation of radicals, that may lead to phenol and toluene by reaction with H radicals. The formation of dimers on the supported Pd-based catalysts prepared by impregnation indicates that the metal sites are not able to transfer enough activated hydrogen to the support in order to terminate free-radical reactions and block the formation of dimers. This is likely due to the low metal-support interface at the periphery of the large Pd particles present on the impregnated catalysts (Table 4.1).

6.4 The influence of Pd particle size

In order to study the influence of the Pd particle size on the reaction pathways, a colloidal method was used to synthesize Pd-based catalysts with small metal particles (< 4 nm). In this procedure, the growth of the metal particles is controlled by the addition of a stabilizing agent, polyvinyl alcohol (PVA). Reduced metal nanoparticles are formed by the addition of a reducing agent, sodium borohydride, and then deposited onto the support [71–73].

The catalysts prepared by the colloidal method were more active than the impregnated ones. For $Pd/Al_2O_{3\text{-col}}$ and $Pd/TiO_{2\text{-col}}$, methylcyclohexane and cyclohexanol were the main products formed. Cyclohexane was also produced from cyclohexanol for $Pd/Nb_2O_{5\text{-col}}$ and $Pd/ZrO_{2\text{-col}}$, two catalysts that possess Brønsted acidic sites (Table 6.2, entries 1 - 4). Unlike impregnated catalysts, phenol and toluene were not observed, suggesting that both were rapidly hydrogenated to cyclohexanol and methylcyclohexane, respectively, whatever the support. Furthermore, the partial hydrogenation of BPE was also observed in some cases. This confirms that the small Pd particles are active in the hydrogenation of aromatic rings, which to some extent becomes a competing pathway with respect to the hydrogenolysis of BPE. Furthermore, alkylated products (2-BPH, 4-BPH, and 2,6-dibenzylphenol) were not detected despite the presence of Brønsted acidic sites on some of the catalysts. The product distribution for $Pd/Nb_2O_{5\text{-imp}}$ and $Pd/Nb_2O_{5\text{-col}}$ catalysts was compared at the same BPE conversion (Table 6.1, entry 13 and Table 6.2, entry 3, respectively). The yield to dimers was high (38.7%) and even trimers were formed (20.8%) for $Pd/Nb_2O_{5\text{-imp}}$. This reaction did not occur over the catalysts synthesized by the colloidal method.

Table 6.2: Conversion of BPE, mass balance, and product distribution using catalysts prepared by the colloidal method

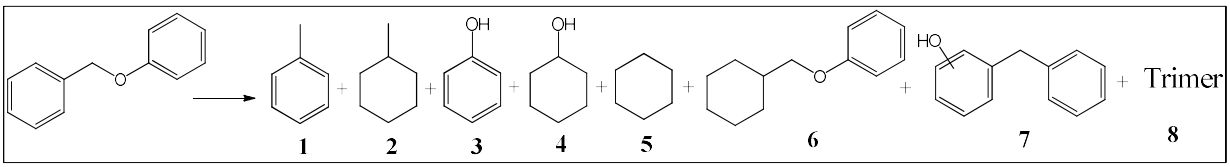

Ent.	Catalyst	X_{BPE} (%)	MB (%)	Yield (%)							
				1	2	3	4	5	6	7	8
1	$Pd/Al_2O_{3\text{-}col}$	100	97	0.0	50.5	0.0	45.5	1.0	0.0	0.0	0.0
2	$Pd/TiO_{2\text{-}col}$	100	98	0.0	50.5	0.0	47.0	1.0	2.0	0.0	0.0
3	$Pd/Nb_2O_{5\text{-}col}$	100	95	0.0	45.9	0.0	16.7	23.6	6.6	0.0	0.0
4	$Pd/ZrO_{2\text{-}col}$	100	86	0.0	48.0	0.0	1.0	37.0	0.0	0.0	0.0
5	$Pd/Nb_2O_{5\text{-}col}$*	88	93	5.8	0.0	17.0	0.0	0.0	0.0	39.7	19.3

Reaction conditions: Reactant (62 mmol), decalin (15 mL), $Pd/Al_2O_{3\text{-}col}$ (30 mg) $Pd/TiO_{2\text{-}col}$ (30 mg), $Pd/Nb_2O_{5\text{-}col}$ (30 mg), $Pd/ZrO_{2\text{-}col}$ (30 mg), 230 °C, 18 bar H_2, 3h.
*Reaction performed under 18 bar of N_2, $Pd/Nb_2O_{5\text{-}col}$ (30 mg).

For sol-immobilized Pd-based catalysts, the conversion of BPE thus starts with the hydrogenolysis of the C_{aliph}-O bond catalyzed by the metal sites and by the production of phenol and toluene. Due to the small Pd particle size, phenol and toluene were rapidly hydrogenated to cyclohexanol and methylcyclohexane, respectively. For $Pd/Nb_2O_{5\text{-}col}$ and $Pd/ZrO_{2\text{-}col}$ catalysts, the significant formation of cyclohexane comes from the dehydration of cyclohexanol to cyclohexene by the acid sites of the support, followed by cyclohexene hydrogenation on metal sites. These two catalysts appear especially active in the HDO process because of the presence of both small Pd particles and acidic sites. Finally, because of the high activity of these catalysts in hydrogenation, BPE can be also partially hydrogenated over Pd particles to form cyclohexyl benzyl ether over $Pd/Nb_2O_{5\text{-}col}$ and $Pd/ZrO_{2\text{-}col}$, but this reaction occurs in a limited extent.

An additional experiment was performed to confirm the activity in hydrogenation of $Pd/Nb_2O_{5\text{-col}}$ The conversion of phenol was carried out in the same reaction conditions over Pd/Nb_2O_5 catalysts prepared by impregnation and colloidal methods, using the same mass of catalyst. The $Pd/Nb_2O_{5\text{-col}}$ catalyst exhibited a higher phenol conversion than $Pd/Nb_2O_{5\text{-imp}}$ (100 and 15%, respectively). For $Pd/Nb_2O_{5\text{-col}}$, the main products formed were cyclohexane (83.5 %) and cyclohexanol (2.7 %), whereas cyclohexanone, an intermediate in the pathway from phenol to cyclohexanol, was produced over $Pd/Nb_2O_{5\text{-imp}}$. All in all, these results reveal the high hydrogenation ability of the catalysts prepared by the colloidal method compared to those prepared by impregnation, and a combination between small metal Pd particles and acidic sites is required for cyclohexane formation.

The lack of formation of alkylated products on the colloidal catalysts could be due to: (i) the high rate of hydrogenolysis on these small metal particles, compared with the rate of cleavage of the C-O bond on the acid sites of the support; and (ii) the availability of hydrogen both for the hydrogenation of phenoxy and benzyl radicals, cutting the way to 2 and 4-BPH. To evaluate this hypothesis formed on the acid sites, the conversion of BPE was performed over $Pd/Nb_2O_{5\text{-col}}$ at 230 °C, and under 18 bar of N_2 instead of H_2. The results are presented in Table 6.2, entry 5. In the absence of hydrogen, 88 % of BPE was converted to phenol, toluene, and alkylated products, which is the typical product distribution of the impregnated Pd/Nb_2O_5 catalyst.

The hydrogenation properties of the metallic phase thus indirectly affect the formation of alkylated products. Not only an appropriate balance between metal sites and acidic functions is required for the promotion of the last steps of the process leading to deoxygenation, but metals with a high hydrogenation ability and a large metal-support interface suppress the alkylation reaction by hydrogenating the radicals formed on the

acidic support. These important conclusions have not been reported before for this molecule.

These observations may explain the contradictory results obtained in the literature. The formation of alkylated products (2 and 4-BPH) was also observed for the conversion of BPE using a non-polar solvent (undecane) at 250 °C and 40 bar of H_2 over Ni/SiO_2 and Ni/HZSM5 catalysts[31]. The alkylated products were preferentially formed over the acidic support. However, alkylated products were not reported for Pd-Ni/HZSM5 (20 °C, 20 bar of H_2, *n*-hexane) [29], Ni/HZSM5 (250 °C, 50 bar of H_2, water) [38] or Ru/HZSM5 (200 °C, 50 bar of H_2, water) [39]. Therefore, the characteristics of the metal, nature, and particle size, significantly influence the formation or suppression of the alkylated products by modulating the hydrogenation pathway.

From the results obtained in our work, we propose the following network of reactions for the conversion of BPE over supported Pd-based catalysts in a non-polar solvent (decalin) (Scheme 6.1). The BPE molecule adsorbs either on the acidic sites of the support and on the metallic Pd particles. Then, the cleavage of the C_{aliph}-O bond may proceed by two different reaction pathways: (i) cleavage of the C_{aliph}-O bond over acid sites of support, with the production of radicals followed by alkylation reaction and formation of dimers and trimers (Scheme 6.1, red route); or (ii) hydrogenolysis of the C_{aliph}-O bond promoted by the metallic Pd particles, producing toluene and phenol (Scheme 6.1, blue and green routes). On the catalysts possessing small Pd particles (catalysts prepared by the colloidal method), toluene and phenol are further hydrogenated to methylcyclohexane and cyclohexanone/cyclohexanol, respectively. Then, cyclohexanol is dehydrated to cyclohexene when the support bears acidic sites, and this is followed by the hydrogenation of cyclohexene to cyclohexane on the metallic particles (Scheme 6.1, green routes). The formation of alkylated products is inhibited due to the

hydrogenation of the radicals. Such a reaction network that takes simultaneously into account the characteristics of the metal (particle size) and of the support (acidity) has never been proposed in the literature. Thus, the results revealed that the HDO reaction of BPE is strongly influenced by the metal-support interface, which is in agreement with recent work realized by our group for the HDO of monomers in gas phase [74].

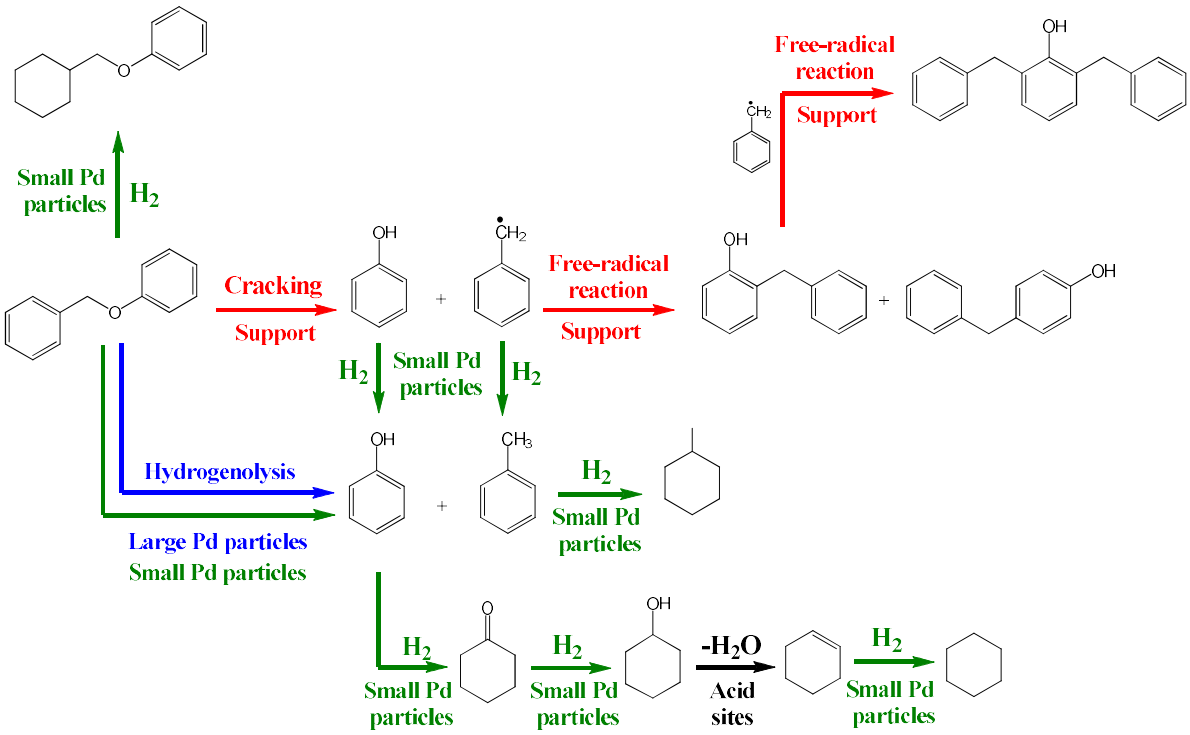

Scheme 6.1: Reaction pathways for the conversion of BPE over supported Pd catalysts.

6.5 Pressure and temperature effect for the conversion of BPE over $Pd/Nb_2O_{5\text{-col}}$

Due to its high selectivity to deoxygenated products, $Pd/Nb_2O_{5\text{-col}}$ was selected to study the effect of hydrogen pressure and reaction temperature on the conversion of BPE. First, the reaction was performed at different hydrogen pressures (5, 10, and 18 bar of H_2) at 230 °C, for 3 h, using decalin as solvent (Fig. 6.2).

Under 5 bar of H_2, toluene (23 %) and methylcyclohexane (21 %) on the one hand, and cyclohexanone (22 %) and cyclohexanol (14 %) on the other hand, were formed, indicating that phenol was completely hydrogenated to cyclohexanone/cyclohexanol after

the cleavage of the C_{aliph}-O bond of BPE, while toluene was only partially hydrogenated to methylcyclohexane. In addition, small amounts of cyclohexane (7 %) and bicyclohexylone (5 %), probably formed by the coupling between cyclohexanone and cyclohexene [75], were also produced. For this reaction time, 5 bar of hydrogen was thus not enough to perform the full hydrogenation of the hydrogenolysis products.

Upon increasing the H_2 pressure to 10 bar, toluene was completely transformed into methylcyclohexane, while cyclohexanone was totally hydrogenated into cyclohexanol. In addition, the yield to cyclohexane increased from 7 % to 29 % with the pressure increase.

At 18 bar of H_2, the yield of methylcyclohexane and cyclohexane slightly decreased compared to 10 bar H_2, while the yield of cyclohexanol increased. Furthermore, BPE was also partially hydrogenated. A high hydrogen pressure may thus be detrimental to the HDO process because the hydrogenation of the BPE aromatic ring competes with the hydrogenolysis reaction, which leads to a lesser formation of deoxygenated products.

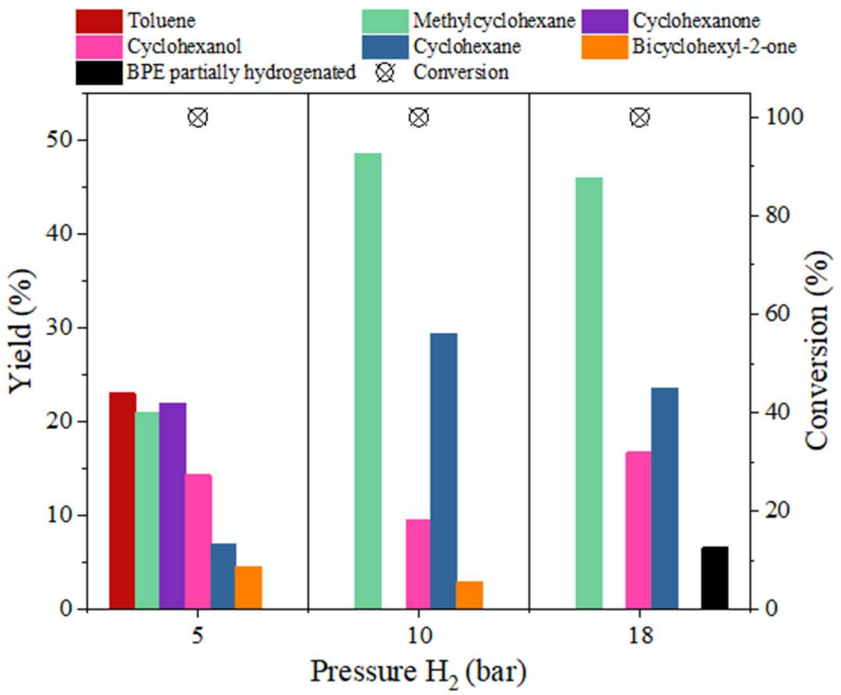

Figure 6.2: Conversion of BPE and product distribution at different H_2 pressures over $Pd/Nb_2O_{5\text{-col}}$ catalyst. Reaction conditions: reactant (62 mmol), decalin (15 mL), $Pd/Nb_2O_{5\text{-col}}$ (30 mg), 230 °C, 3h.

Fig. 6.3 shows the conversion of BPE and product distribution for $Pd/Nb_2O_{5\text{-col}}$, at different temperatures (100, 150, and 230 °C) under 18 bar of H_2, for 3 h, in decalin. At 100 °C, 64 % of BPE was converted to form toluene and phenol. Upon increasing the temperature to 150 °C, complete conversion of BPE was achieved. Toluene was partially hydrogenated to methylcyclohexane, whereas phenol was completely hydrogenated to cyclohexanone and cyclohexanol, confirming that the reaction rate for the hydrogenation of phenol was higher than that for the hydrogenation of toluene. A further increase of the temperature to 230 °C led to the complete hydrogenation of toluene to methylcyclohexane, while cyclohexanol was partially dehydrated to cyclohexene and converted to cyclohexane. Therefore, the hydrogenolysis reaction occurs at low temperatures, but increasing the temperature to 150 °C and above promotes the hydrogenation reactions. A further increase to 230 °C favors the deoxygenation reaction.

In addition, the partial hydrogenation of BPE was observed at all temperatures and the production of partially hydrogenated ethers remained roughly constant.

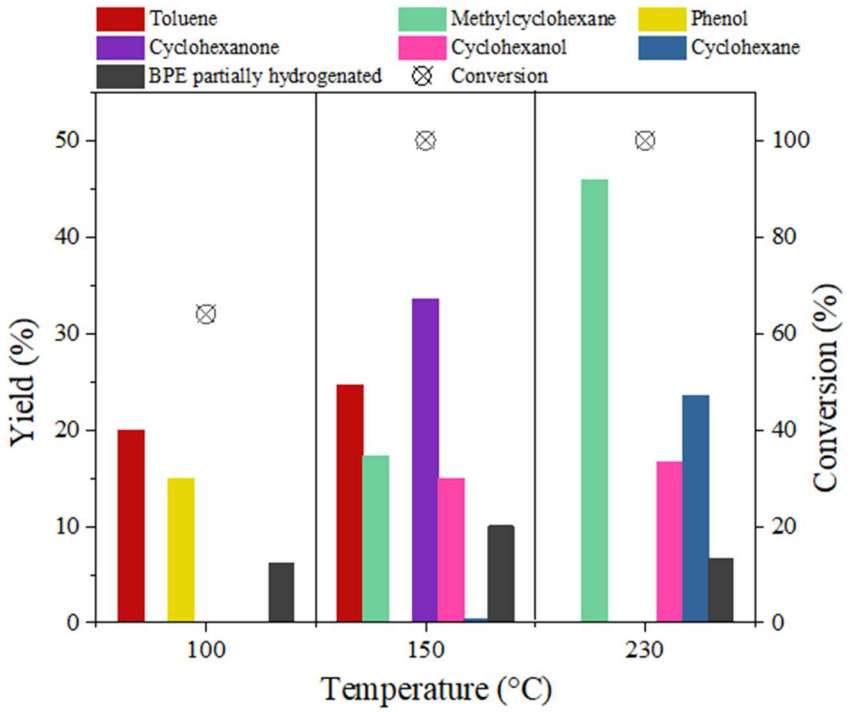

Figure 6.3: Conversion of BPE and product distribution at different reaction temperatures over $Pd/Nb_2O_{5\text{-col}}$ catalyst. Reaction conditions: Reactant (62 mmol), decalin (15 ml), $Pd/Nb_2O_{5\text{-col}}$ (30 mg), 18 bar H_2, 3h.

The highest yield to deoxygenated products was thus obtained at 230 °C under 10 bar of H_2 pressure.

6.6 Conclusion

The conversion and the product distribution for the HDO of BPE are significantly affected by the Pd particle size as well as by the type the support. The large Pd particles, observed for impregnated catalysts, favored the hydrogenolysis of BPE into phenol and toluene, however, their subsequent hydrogenation did not occur. In this case, after BPE cleavage, alkylated products were produced in a larger or lesser extent according to the

total density of acidic sites. $Pd/ZrO_{2\text{-imp}}$ and $Pd/HZSM5_{\text{-imp}}$, which exhibited the highest amount of acidic sites, presented the largest formation of 2 and 4-BPH. Over colloidal catalysts, the smaller Pd particle size promoted the hydrogenation of phenol and toluene after C-O cleavage, to form cyclohexanone/cyclohexanol and methylcyclohexane, respectively. Due to the high hydrogenation capacity of the small Pd particles, the radicals formed in the presence of acidic sites were quickly hydrogenated, and the formation of alkylated products was suppressed. Furthermore, the deoxygenated product formed from the dehydration of cyclohexanol, cyclohexane, was only produced in the presence of Brønsted acidic sites ($Pd/Nb_2O_{5\text{-col}}$ and $Pd/ZrO_{2\text{-col}}$). Thus, the results revealed that the HDO reaction of BPE is strongly influenced by the metal-support interface, which has been proposed for the HDO of other molecules. The experimental conditions of pressure and temperature also affect the product distribution. A low temperature (< 230 °C) did not favor the formation of cyclohexane, and a high hydrogen pressure (> 10 bar of H_2) promoted the hydrogenation of BPE aromatic rings, competing with the hydrogenolysis of BPE and consequently with the formation of cyclohexane.

Chapter 7

Hydrodeoxygenation of phenethoxybenzene over Pd-based catalysts.

7.1 Introduction

The conversion of phenethoxybenzene (PEB), a typical model molecule representative of the β-O-4 ether bond, has been well studied in the literature, since β-O-4 is the most predominant ether linkage present in the lignin structure. As mentioned in Chapter 2, compared to the α-O-4 bond, a higher energy is required to break the β-O-4 linkage.

The results obtained in Chapter 6 showed that the type of support as well as the size of palladium particles play a key role in the conversion of BPE. Besides, the effect of the Ni particle size on the hydrogenolysis of PEB over Ni/SiO_2 in the aqueous phase was reported in the literature [24]. It was observed that the increase of Ni particle size from 4.5 to 5.9 nm favored the hydrogenolysis of PEB into phenol and ethylbenzene. However, the relationship between a small metal particle size and the deoxygenation activity was not explored. Do the properties of the support and the metal affect the conversion of PEB in the same way as observed for BPE?

Thus, the present chapter investigates the effect of the type of support as well as the Pd particle size for the conversion of PEB. Pd-based catalysts supported on different oxides (SiO_2, TiO_2, Nb_2O_5, Al_2O_3, ZrO_2, and HZSM5), synthesized by incipient wetness impregnation and colloidal sol-immobilization methods, were used.

7.2 HDO of PEB over impregnated Pd catalysts

Table 7.1 shows the product distribution for the conversion of PEB at 230 °C, under 18 bar of H_2, using decalin as a solvent over the bare supports as well as over supported catalysts prepared by incipient wetness impregnation. No reaction was

observed in the blank test without a catalyst, which is in agreement with the literature [27]. As PEB presents a higher activation energy compared to the α-O-4 linkage, the solvent did not affect its C-O cleavage. Over bare supports, PEB was converted only in the presence of Nb_2O_5, ZrO_2, and HZSM5. Using the same mass of material (250 mg), ZrO_2 presented the highest PEB conversion (93 %), (Table 7.1, entry 5), converting PEB into phenol, ethylbenzene, and alkylated products (2 and 4-phenethylphenol). This result reveals that only catalysts with Brønsted acidic sites were active for PEB conversion. Supports without any acidity (SiO_2) or that exhibited only Lewis acidic sites (Al_2O_3 and TiO_2) did not show activity in the conversion of PEB. The similar conclusion reached in the former chapter is thus confirmed.

Table 7.1: Conversion of PEB, mass balance, and product distribution for supports and impregnated catalysts

				Yield (%)						
Ent.	**Catalyst**	**X_{PEB} (%)**	**MB (%)**	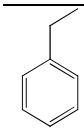	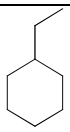	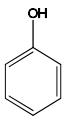	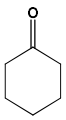		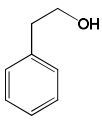	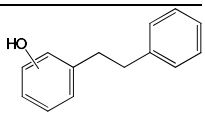
1	SiO_2	0	99	0.0	0.0	0.0	0.0	0.0	0.0	0.0
2	Al_2O_3	0	98	0.0	0.0	0.0	0.0	0.0	0.0	0.0
3	TiO_2	0	99	0.0	0.0	0.0	0.0	0.0	0.0	0.0
4	Nb_2O_5	16	90	1.0	0.0	3.0	0.0	0.0	2.2	1.0
5	ZrO_2	93	56	6.0	0.0	26.2	0.0	0.0	0.0	14.8
6	HZSM5	6	98	1.6	0.0	1.9	0.0	0.0	0.0	1.2
7	$Pd/SiO_{2\text{-imp}}$	0	97	0.0	0.0	0.0	0.0	0.0	0.0	0.0
8	$Pd/Al_2O_{3\text{-imp}}$	38	89	13.0	1.4	5.3	0.0	7.0	0.0	1.2
9	$Pd/TiO_{2\text{-imp}}$	36	91	14.1	1.7	3.1	0.0	5.0	0.0	1.9
10	$Pd/Nb_2O_{5\text{-imp}}$	32	93	13.0	0.0	8.5	0.0	1.4	0.0	1.9
11	$Pd/ZrO_{2\text{-imp}}$	40	83	8.0	0.5	1.8	0.8	2.6	0.0	9.0
12	$Pd/HZSM5_{\text{-imp}}$	43	92	5.0	0.0	5.3	0.0	0.0	0.0	25.6

Reaction conditions: Reactant (62 mmol), decalin (15 mL), SiO_2 (250 mg), Al_2O_3 (250 mg) TiO_2 (250 mg), Nb_2O_5 (250 mg), ZrO_2 (250 mg), HZSM5 (65 mg), $Pd/SiO_{2\text{-imp}}$ (250 mg), $Pd/Al_2O_{3\text{-imp}}$ (70 mg), $Pd/TiO_{2\text{-imp}}$ (250 mg), $Pd/Nb_2O_{5\text{-imp}}$ (250 mg), $Pd/ZrO_{2\text{-imp}}$ (250 mg), $Pd/HZSM5_{\text{-imp}}$ (65 mg), 230 °C, 18 bar H_2, 3h.

The PEB conversion over bare supports has been reported in the literature in the presence of a non-polar solvent, under high pressure and temperature conditions. When *n*-decane was used, PEB was selectively converted into phenol and ethylbenzene at 260 °C and 10 bar of H_2 over bare Nb_2O_5 [26]. In the presence of zeolite Hβ (220 °C, 40 bar H_2) [28] and USY zeolite (345 °C, 50 bar H_2) [44] phenol and alkylated products (2, 3, and 4-phenethyl phenol) were the main products observed. However, in the aqueous phase at 240 °C and under 8 bar H_2, PEB remained unreacted even in the presence of acidic supports sulfated zirconia, HZSM5, zeolite Hβ, and HY) [25,27].

The literature has reported that the formation of alkylated products occurs through transalkylation reactions catalyzed over acidic sites. The cleavage of PEB takes place when H^+ is present, to produce phenol and 2-phenyleth-1-ylium as intermediates. Then, phenol can be attacked by 2-phenyleth-1-ylium in ortho, meta, or para position to form 2, 3, and 4-phenethylphenol [28,44].

In the presence of a metal, ethylbenzene and phenol were produced over all catalysts, except over $Pd/SiO_{2\text{-imp}}$ which was not active, likely due to the absence of acidic sites. These results show that the Pd particles are also active for cleavage of β-O-4 linkage via hydrogenolysis, but the assistance of acidic sites is required to C-O breaking. After PEB cleavage, ethylbenzene was hydrogenated to ethylcyclohexane over $Pd/Al_2O_{3\text{-imp}}$ and $Pd/TiO_{2\text{-imp}}$, whereas phenol was hydrogenated to cyclohexanone/cyclohexanol. Cyclohexanol was then dehydrated into cyclohexane over $Pd/Al_2O_{3\text{-imp}}$, $Pd/TiO_{2\text{-imp}}$, $Pd/Nb_2O_{5\text{-imp}}$, and $Pd/ZrO_{2\text{-imp}}$. As cyclohexanone/ cyclohexanol were not detected, it can be assumed that the dehydration rate of cyclohexanol was higher than the phenol hydrogenation rate over these catalysts.

One can compare these results to the BPE conversion in the same reaction conditions (Chapter 6, table 6.1). After C-O cleavage, the hydrogenolysis products

(phenol and toluene) were not hydrogenated over impregnated catalysts, probably due to the less quantity of catalysts used in the reaction with BPE (30 mg). Similar results were also reported by He et al [24], for the conversion of BPE and PEB over Ni/SiO_2 in water. The authors suggested that the lower amount of Ni/SiO_2 (30 mg) used for the conversion of BPE was sufficient to catalyze the BPE hydrogenolysis but not enough to hydrogenate phenol after C-O cleavage. On the other hand, for PEB conversion, phenol was completely hydrogenated to cyclohexanol when 300 mg of catalyst was used.

In addition, alkylated products, 2 and 4-phenethylphenol, were also detected over all catalysts to a minor or large extent. It is also possible to observe that the formation of alkylated products increases with the increase of acidity. $Pd/HZSM5_{-imp}$ exhibits the highest total density of acidic sites (699 μmol/g) and the largest formation of 2 and 4-phenethylphenol (25.6 %). Pd/Al_2O_{3-imp}, Pd/TiO_{2-imp}, and Pd/Nb_2O_{5-imp}, which exhibited similar and lower acidity (160, 167, and 251 μmol/g, respectively), showed the lowest formation of alkylated products (1.2, 1.9, and 1.9, respectively) at similar conversion. The same behavior was observed for the conversion of BPE. Pd/HZSM5 formed the highest amount of alkylated products and, as for toluene, the ortho position of phenol was preferentially attacked by ethylbenzene to produce 2-phenethylphenol.

The PEB conversion and products yield as a function of time over Pd/Nb_2O_{5-imp} at 230 °C, 18 bar of H_2, using decalin as a solvent, are shown in Fig. 7.1. At the beginning of the reaction, PEB was converted into phenol and ethylbenzene via the hydrogenolysis of its C_{aliph}-O bond, catalyzed by the metal sites. It is also possible to observe that phenol was transformed into cyclohexane by a sequential hydrogenation and dehydration steps due to the presence of the acidic sites of Nb_2O_5. As the reaction progressed, the yield of cyclohexane slightly increased from 2 to 3 %. Furthermore, after 1 h, 2-phenethylphenol was formed by the reaction between phenol and ethylbenzene.

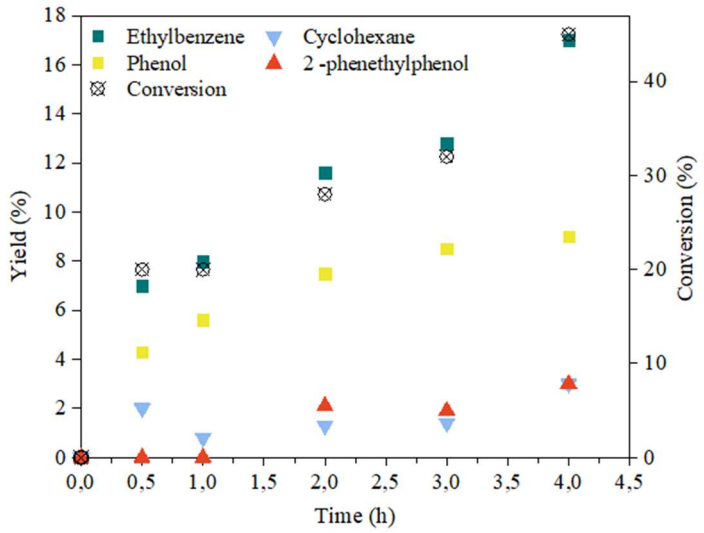

Figure 7.1: Product distribution as a function of time for the conversion of PEB over $Pd/Nb_2O_{5\text{-imp}}$

7.3 HDO of PEB over colloidal Pd catalysts

The product distribution for PEB conversion over Pd-based catalysts prepared by the colloidal method at 230 °C, 18 bar of H_2, using decalin as a solvent, are presented in Table 7.2. After 3 h, ten products were identified in the final reaction mixture, suggesting that the conversion of PEB proceeds through different reaction pathways.

For all the catalysts evaluated, the main products formed were (2-(cyclohexyloxy) ethyl) benzene (2COEB) and (2-(cyclohexylethoxy) benzene (2CEB) produced by the partial hydrogenation of the PEB aromatic rings. Ethylbenzene, ethylcyclohexane, cyclohexanone, cyclohexanol, cyclohexane, phenylethanol, cyclohexyl ethanol, and (2-(cyclohexylethoxy) cyclohexane (2CEC), were also observed. Phenol was not detected for any of the catalysts, indicating that after cleavage, phenol was rapidly hydrogenated to cyclohexanone and cyclohexanol, due to the high hydrogenation ability of colloidal

catalysts. Additionally, unlike what was seen for the impregnated catalysts, the formation of 2 and 4-phenethylphenol was not observed.

Table.7.2: Conversion of PEB, mass balance, and product distribution for colloidal catalysts

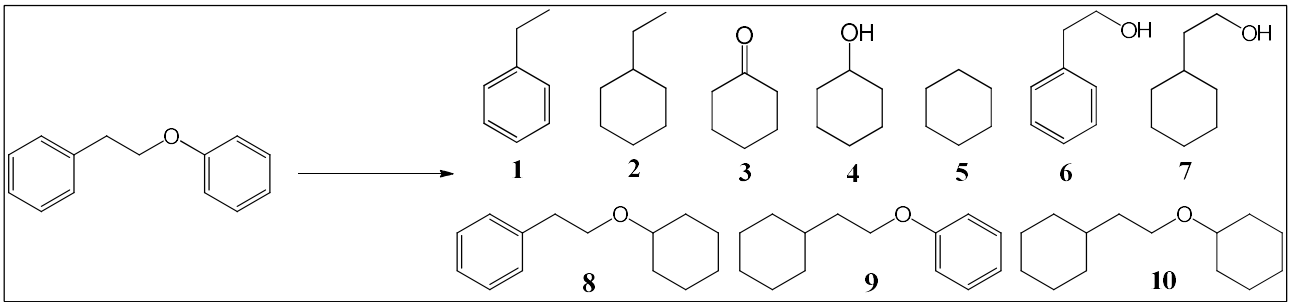

Ent.	Catalyst	X_{PEB} (%)	MB (%)	Yield (%)									
				1	2	3	4	5	6	7	8	9	10
1	$Pd/Al_2O_{3\text{-col}}$	22	96	1.0	0.0	2.0	1.0	0.0	2.4	0.0	5.9	5.5	0.0
2	$Pd/TiO_{2\text{-col}}$	26	97	1.7	0.0	1.9	0.0	0.0	0.0	0.0	10.6	8.5	1.0
3	$Pd/Nb_2O_{5\text{-col}}$	33	96	3.9	0.5	4.4	0.0	0.8	0.0	1.6	7.3	10.5	1.1
4	$Pd/ZrO_{2\text{-col}}$	31	100	3.0	1.0	0.0	5.8	2.0	3.6	2.1	4.0	8.8	0.0

Reaction conditions: Reactant (62 mmol), decalin (15 ml), $Pd/Al_2O_{3\text{-col}}$ (20 mg) $Pd/TiO_{2\text{-col}}$ (20 mg), $Pd/Nb_2O_{5\text{-col}}$ (20 mg), $Pd/ZrO_{2\text{-col}}$ (60 mg), 230 °C, 18 bar H_2, 3h.

Over $Pd/Al_2O_{3\text{-col}}$ and $Pd/TiO_{2\text{-col}}$, catalysts that only exhibited Lewis acidic sites, the amount of products from direct PEB hydrogenation (11.4 and 19.1 %, respectively), was higher than the products resulting from the C-O bond cleavage. For $Pd/Nb_2O_{5\text{-col}}$ and $Pd/ZrO_{2\text{-col}}$, which presented Lewis and Brønsted acidic sites, similar amounts of 2COEB, 2CEB, and 2CEC were also observed (18.9 and 12.8 %, respectively). However, the selectivity to products issued from the PEB cleavage increased, suggesting that in the presence of Brønsted acidic sites, the hydrogenolysis pathway was facilitated. The catalyst selectivity to C-O cleavage by hydrogenolysis followed the trend: $Pd/TiO_{2\text{-col}}$ (3.6 %) < $Pd/Al_2O_{3\text{-col}}$ (6.4 %) < $Pd/Nb_2O_{5\text{-col}}$ (10.4 %) < $Pd/ZrO_{2\text{-col}}$ (15.5 %).

The presence of phenyl ethanol and of its hydrogenated derivative, cyclohexyl ethanol, suggests that the hydrogenolysis of the C_{arom}-O bond of PEB into benzene and phenyl ethanol can also occur over all the colloidal Pd-based catalysts, except Pd/TiO_{2-col}. In addition, Pd/Nb_2O_{5-col} and Pd/ZrO_{2-col} promoted the formation of cyclohexane, likely due to the presence of Brønsted acidic sites.

In order to explore the differences in activity between catalysts that possess only Lewis acidic sites, and those that possess both Lewis and Brønsted acidic sites, Pd/TiO_{2-col} and Pd/Nb_2O_{5-col} were evaluated at different conversions of PEB in the same reaction conditions (230 °C, 18 bar H_2, in decalin).

At low PEB conversion (26 %), the partially hydrogenated products from PEB (2COEB and 2CEB) were the main products formed over Pd/TiO_{2-col}, with yields of 10.6 and 8.5 %, respectively (Fig. 7.2). Ethylbenzene (1.6 %), cyclohexanone (1.9 %), and 2CEC (1 %), the product formed by the full hydrogenation of PEB aromatic rings, were also detected in small quantities. Probably, the hydrogenolysis of the C_{aliph}-O bond of PEB into ethylbenzene and phenol took place to a minor extent, and cyclohexanone was formed by phenol hydrogenation. Upon increasing the conversion of PEB from 26 to 57 %, the yield of 2COEB, 2CEB, and 2CEC continued to increase progressively (22, 15, and 6.3 %, respectively), while the yield of ethylbenzene and cyclohexanone only slightly increased (4 and 2.7 %, respectively). Ethylcyclohexane (1 %) and cyclohexanol (1.8 %) formed by hydrogenation of ethylbenzene and cyclohexanone were also observed. The further increase in PEB conversion kept increasing the yield of fully and partially hydrogenated products. When the complete PEB conversion was achieved, 2CEC (69.4 %) became by far the major product formed over Pd/TiO_{2-col}. In addition, small amounts of 2-cyclohexyl ethanol (3.9 %) and only 1 % of cyclohexane were detected. It is thus obvious that on this catalyst, the major pathway is the direct hydrogenation of PEB.

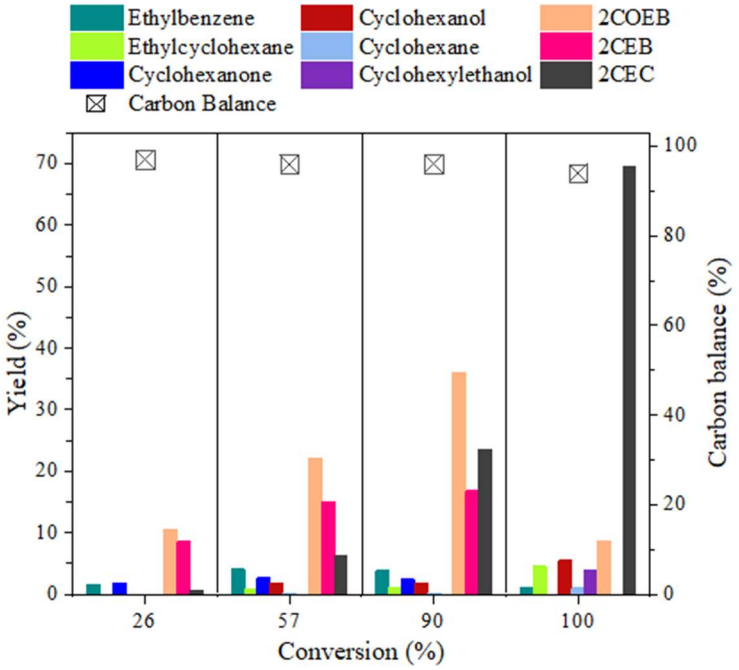

Figure 7.2: Product distribution as a function of PEB conversion over $Pd/TiO_{2\text{-col}}$. Reaction conditions: 62 mmol PEB, 15 mL of decalin, 230 °C, 18 bar H_2, 3 h. Mass of catalysts: X_{PEB}=26 % (20 mg), X_{PEB}=57 % (30 mg), X_{PEB}=90 % (40 mg), and X_{PEB} = 100 % (100 mg).

Regarding the product distribution as function of PEB conversion over $Pd/Nb_2O_{5\text{-col}}$ (Fig. 7.3) in the same reaction conditions (230 °C, 18 bar H_2 in decalin), ethylbenzene (3.9 %), cyclohexanone (4.4 %), 2COEB (7.3 %), and 2CEB (10.5 %) were the main products formed at low PEB conversion (33 %). This result suggests that the hydrogenolysis of the C_{aliph}-O bond of PEB and the hydrogenation of PEB aromatic rings occur at the same time, in a more balanced way compared to $Pd/TiO_{2\text{-col}}$. The formation of the partially hydrogenated products of PEB was still favored probably because of the low Pd particle size. But compared to $Pd/TiO_{2\text{-col}}$, ethylcyclohexane, cyclohexane, 2-phenyl ethanol, and 2CEC can be also observed over $Pd/Nb_2O_{5\text{-col}}$ at a minor extent, even at low conversion. As the conversion of PEB increased from 33 to 46 %, the yield of

ethylbenzene and cyclohexanone increased along with the yield of PEB hydrogenated products.

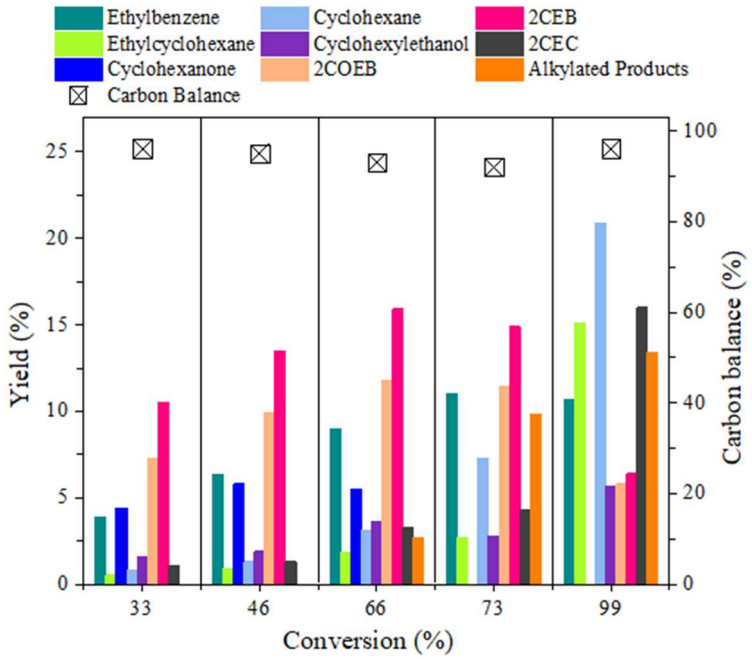

Figure 7.3: Product distribution as a function of PEB conversion over $Pd/Nb_2O_{5\text{-col}}$ Reaction conditions: 62 mmol PEB, 15 mL of decalin, 230 °C, 18 bar H_2, 3 h. Mass of catalysts: X_{PEB}=33 % (20 mg), X_{PEB}=46 % (30 mg), X_{PEB}=66 % (60 mg), X_{PEB}=73 % (80 mg) and X_{PEB}=99 % (100 mg).

When 66 % of PEB conversion was achieved, bicyclohexyl-2-one (2.7 %) was formed as an alkylated product. At 73 % of conversion, cyclohexanone was fully converted to cyclohexane, whereas the yield of ethylcyclohexane slowly increased to 2.8 %, indicating that the hydrogenation of phenol was faster than ethylbenzene hydrogenation. He et al [24] reported that in the presence of a non-polar solvent (hexadecane), the rate of phenol hydrogenation (87 $mol.mol_{Ni}(surf)^{-1}.h^{-1}$) was indeed higher than that of ethylbenzene hydrogenation (13 $mol.mol_{Ni}(surf)^{-1}.h^{-1}$) at 120 °C.

Compared to $Pd/TiO_{2\text{-col}}$, cyclohexanone was quickly hydrogenated to cyclohexanol over $Pd/Nb_2O_{5\text{-col}}$ and cyclohexanol was not detected even at low PEB conversion (33 %), which indicates that the dehydration rate was higher than the hydrogenation rate over this catalyst. Considering the average Pd particle size for

$Pd/TiO_{2\text{-col}}$ and $Pd/Nb_2O_{5\text{-col}}$ (3.4 and 2.0 nm, respectively), the small particle size of Pd on $Pd/Nb_2O_{5\text{-col}}$ favored cyclohexanone hydrogenation. In addition, regarding BPE conversion (Chapter 6), phenol and toluene were completely converted into cyclohexanone/ cyclohexanol and methylcyclohexane over $Pd/Nb_2O_{5\text{-col}}$ and $Pd/TiO_{2\text{-col}}$. However, the same trend was not observed for the hydrogenation of ethylbenzene and phenol over the same catalysts in the case of PEB conversion.

Besides bicyclohexyl-2-one (5.4 %), dicyclohexyl ethane was also formed (4.4 %) as alkylated product when the conversion reached 73 %. Furthermore, the yield of 2COEB and 2CEB started to decrease while the yield of 2CEC smoothly increased: the partially hydrogenated products from PEB started to be fully hydrogenated. Finally, when PEB was almost completely converted (99 %), cyclohexane (20.9 %), 2CEC (16 %), ethylcyclohexane (15.1 %), and alkylated products (13.4 %), including bicyclohexyl-2-one, dicyclohexyl ethane and bicyclohexyl, became the main products formed.

The formation of bicyclohexyl-2-one was reported by Zhao et al.[76] in the conversion of phenol over Pd/C and zeolite H-BEA at 200 °C, under 60 bar H_2 in aqueous phase, by condensation between phenol and cyclohexene in the presence of acidic sites. After coupling, 2-cyclohexyl phenol was formed as an intermediate, and its further hydrogenation, catalyzed over metallic sites, led to the formation of bicyclohexyl-2-one. In addition, bicyclohexyl-2-one can be hydrogenated and dehydrated to form bicyclohexyl.

The dehydration followed by hydrogenation of 2 and 4-phenethylphenol was proposed by Zhou et al.[28] as the reaction pathway for the formation of dicyclohexyl ethane over Ni/Hβ at 220 °C, 40 bar H_2 in *n*-hexane as a solvent. However, considering the absence of alkylated products from phenol and ethylbenzene during the whole PEB conversion, and the lack of benzene produced by hydrogenolysis of the C_{arom}-O bond of

PEB, the formation of dicyclohexyl ethane was suggested to take place by alkylation between ethylbenzene and benzene.

Therefore, regarding the results for the conversion of PEB over Pd/$TiO_{2\text{-col}}$ and Pd/$Nb_2O_{5\text{-col}}$, it was observed that the presence of Brønsted acidic sites strongly affects the PEB conversion as well as the formation of cyclohexane.

According to the results obtained in our work, the probable reaction pathways for the conversion of PEB over Pd-based catalysts are summarized in Scheme 7.1. The cleavage of the C_{aliph}-O bond of PEB can be catalyzed over Brønsted acidic sites followed by the formation of phenethyl phenols (Scheme 7.1, red route), or by metallic sites, through hydrogenolysis and formation of ethylbenzene and phenol (Scheme 7.1, blue and green routes). Over colloidal catalysts, due to the small Pd particle size, the hydrogenation of the PEB aromatic rings occurs in parallel to PEB hydrogenolysis. After C-O cleavage, ethylbenzene and phenol are hydrogenated to ethylcyclohexane and cyclohexanone/ cyclohexanol, respectively, and the production of phenethyl phenols is suppressed. In the presence of Brønsted acidic sites, cyclohexanol can be dehydrated to cyclohexene which is hydrogenated to form cyclohexane (Scheme 7.1, green route). Bicyclohexyl-2-one can be formed from the alkylation reaction between cyclohexene and phenol, over Brønsted acidic sites. Then bicyclohexyl-2-one is hydrogenated to form bicyclohexyl-2-ol, which is dehydrated and hydrogenated to produce 1,1-bicyclohexyl. Dicyclohexyl ethane is supposed to be formed by alkylation reaction between benzene and ethylbenzene.

7.4 Conclusions

As reported for BPE, the product distribution for PEB conversion is strongly affected by the Pd particle size as well as by the type of the support. Unlike BPE, the conversion of PEB was only observed in the presence of bare supports with Brønsted

acidic sites (Nb_2O_5, ZrO_2, and HZSM5). For PEB as well as for BPE, the large Pd particle size favored the hydrogenolysis of PEB to form phenol and ethylbenzene. However, probably due to the higher bond dissociation energy of the β-O-4 linkage, the assistance of acidic sites was fundamental to the C-O cleavage of PEB, since no conversion was observed over $Pd/SiO_{2\text{-imp}}$. The formation of oxygenated alkylated products (2 and 4-phenethylphenol) was observed to a large extent over the impregnated materials, while over colloidal catalysts their formation was suppressed, as observed for the conversion of BPE.

If one compares the conversion of BPE and PEB over $Pd/TiO_{2\text{-col}}$ and $Pd/Nb_2O_{5\text{-col}}$, the effect of Lewis and Brønsted acidic sites was more pronounced for the conversion of PEB. When only Lewis acidic sites are present ($Pd/TiO_{2\text{-col}}$), the hydrogenation of PEB aromatic rings is by far the major reaction pathway observed for PEB conversion. The presence of small Pd particles did not favor the hydrogenolysis of PEB over this catalyst. However, in the presence of Brønsted acidic sites ($Pd/Nb_2O_{5\text{-col}}$), the hydrogenolysis route becomes much more competitive, and cyclohexane is formed to a larger extent via cyclohexanol dehydration, due to the assistance of Brønsted acidic sites

Therefore, a balance between small metal particles and Brønsted acidic sites was required to achieve the hydrodeoxygenation of PEB.

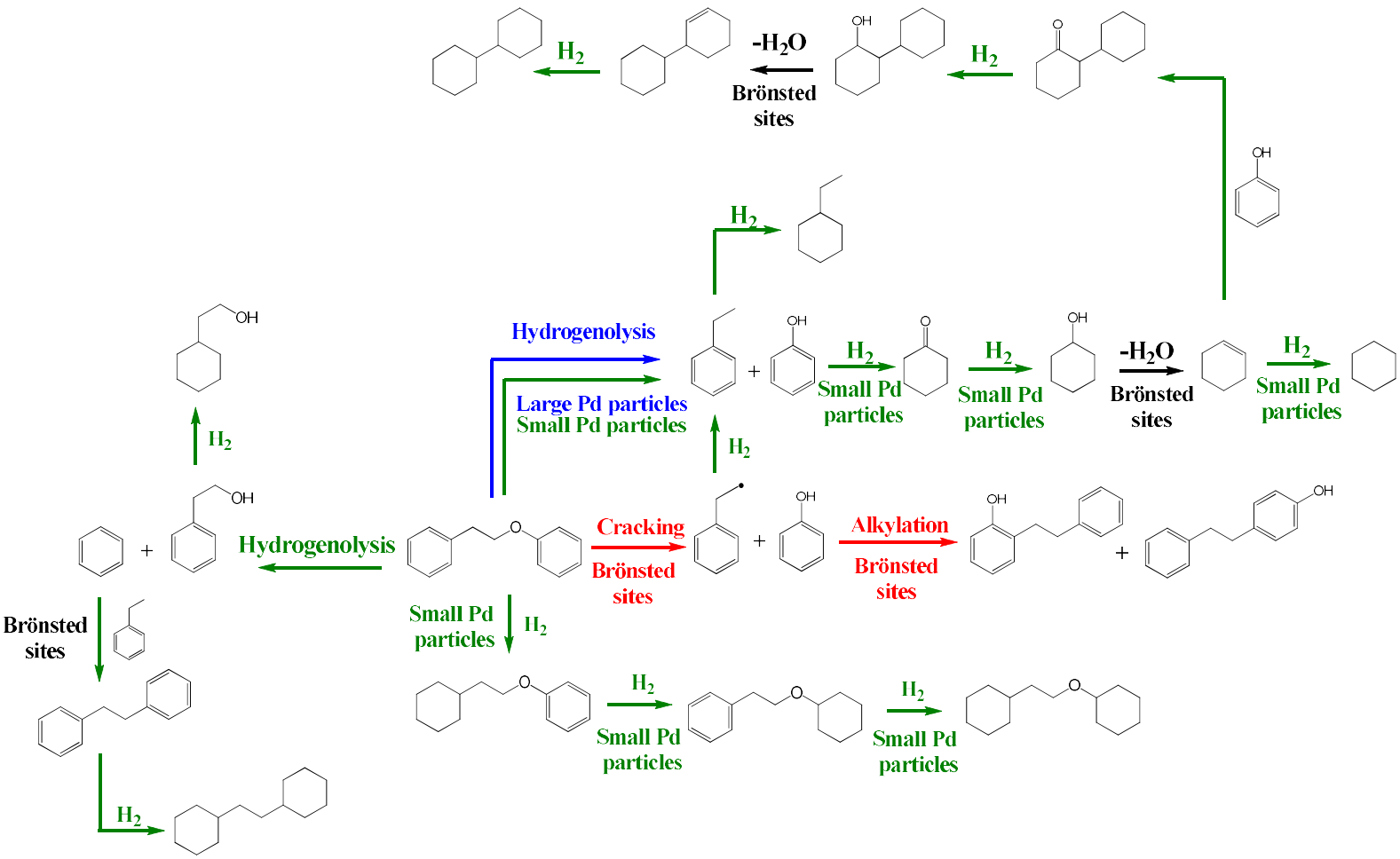

Scheme 7.1: Reaction pathways for the conversion of PEB over supported Pd catalysts.

Chapter 8

Hydrodeoxygenation of diphenyl ether (DPE) and typical model molecules of lignin over Pd-based catalysts.

8.1 Introduction

As previously commented, the study of the conversion of diphenyl ether (DPE) is very attractive, since among the main ether linkages present in the lignin fraction, the 4-O-5 is the strongest and the most stable one. As a consequence, the literature has reported DPE remains unreacted in the absence of catalyst [24,30,45] or in the presence of acidic HZSM5 [29,38].

The preceding chapters revealed that the co-existence of small Pd particles and Brønsted acidic sites is fundamental to improve the conversion of BPE and PEB, as well as to increase the yield of deoxygenated products. However, the relationship between small metal particle size, acidic sites, and DPE conversion has not been studied yet.

Therefore, this chapter evaluates the effect of the type of support as well as the particle size for the conversion of DPE, using Pd-based catalysts supported on different oxides (SiO_2, TiO_2, Nb_2O_5, Al_2O_3, ZrO_2, and HZSM5), synthesized by incipient wetness impregnation and colloidal sol-immobilization methods. In addition, in order to explore the activity of colloidal catalysts for the HDO of bio-oil, the performance of $Pd/Nb_2O_{5\text{-col}}$ for the conversion of a series of monomers (phenol, anisole, guaiacol, and 4-propylphenol) as well as a typical molecule representative of a C-C linkage (2,3-dihydrobenzofuran) will be evaluated.

8.2 DPE conversion over large Pd particles

As mentioned in Chapter 5, unlike BPE and PEB, no DPE conversion was observed over Pd-impregnated catalysts for the same amount (62 mmol) and in the same reaction conditions (230 °C and 18 bar of H_2) used for the former molecules. Then, in order to study the conversion of DPE, a lower amount of DPE (31 mmol) was used. The

product distribution for the conversion of DPE over impregnated Pd-based catalysts is presented in Table 8.1.

Table 8.1: Conversion of DPE, mass balance, and product distribution for impregnated catalysts.

Ent.	Catalysts	X_{DPE} (%)	MB (%)	Yield (%)				
				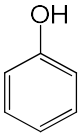	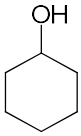		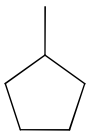	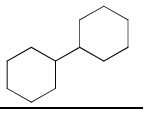
1	$Pd/SiO_{2\text{-imp}}$	0	99	0.0	0.0	0.0	0.0	0.0
2	$Pd/Al_2O_{3\text{-imp}}$*	6	98	0.3	0.6	1.0	0.0	0.0
3	$Pd/TiO_{2\text{-imp}}$**	3	100	0.0	0.0	1.0	0.0	0.0
4	$Pd/Nb_2O_{5\text{-imp}}$	35	90	0.0	1.0	23.3	0.0	1.4
5	$Pd/ZrO_{2\text{-imp}}$	3	100	0.0	0.0	3.0	0.0	0.0
6	$Pd/HZSM5_{\text{-imp}}$	30	81	0.0	1.0	5.6	4.1	0.0

*2% of cyclohexyl phenol and dicyclohexyl ether. **2% of cyclohexyl phenol. Reaction conditions: Reactant (31 mmol), decalin (15 mL), mass of catalysts: 250 mg, 230 °C, 18 bar H_2, 3h.

As observed for the previous molecules, no conversion of DPE was observed in the absence of catalysts as well as over $Pd/SiO_{2\text{-imp}}$, probably due to the absence of acidic sites. Using the same mass of material (250 mg), a low DPE conversion was achieved over $Pd/Al_2O_{3\text{-imp}}$, $Pd/TiO_{2\text{-imp}}$, and $Pd/ZrO_{2\text{-col}}$ (5, 3, and 3 %, respectively), whereas 35 and 30 % of DPE was converted by $Pd/Nb_2O_{5\text{-imp}}$ and $Pd/HZSM5_{\text{-imp}}$ after 3 h. These results suggest that the assistance of Brønsted acidic sites is also important for DPE conversion. Regarding the product distribution, cyclohexane was the main product formed over all catalysts, but only $Pd/Nb_2O_{5\text{-imp}}$ and $Pd/HZSM5_{\text{-imp}}$ produced it in significant amounts. Traces of phenol and cyclohexanol could be also observed. In addition, cyclohexyl phenol, dicyclohexyl ether, bicyclohexyl, and methylcyclopentane

were also detected. This result is in agreement with the former chapters and reveals that over impregnated catalysts, the hydrogenolysis of DPE into phenol and benzene occurred as main reaction pathway, due to the low hydrogenation capacity of Pd-based catalysts prepared by impregnation. After C-O cleavage, phenol was hydrogenated into cyclohexanone/cyclohexanol and then, dehydrated into cyclohexene. Finally, cyclohexane can be formed from cyclohexene and benzene hydrogenation (Scheme 8.1).

The formation of bicyclohexyl was reported in the literature for DPE conversion using a non-polar solvent over Ru/TiO_2 (260 °C, 10 bar H_2) and Ni/Al-SBA15 (200 °C, 50 bar H_2) [76]. However, the mechanism of its formation was not elucidated by the authors. As mentioned in the former chapter, in the presence of acidic sites, bicyclohexyl can be formed via phenol through a process of hydrogenation and dehydration of bicyclohexyl-2-one. Unlike bicyclohexyl, the formation of methylcyclopentane was not reported in the literature in the conversion of DPE, but its formation can occur by cyclohexane isomerization in the presence of acidic sites[77].

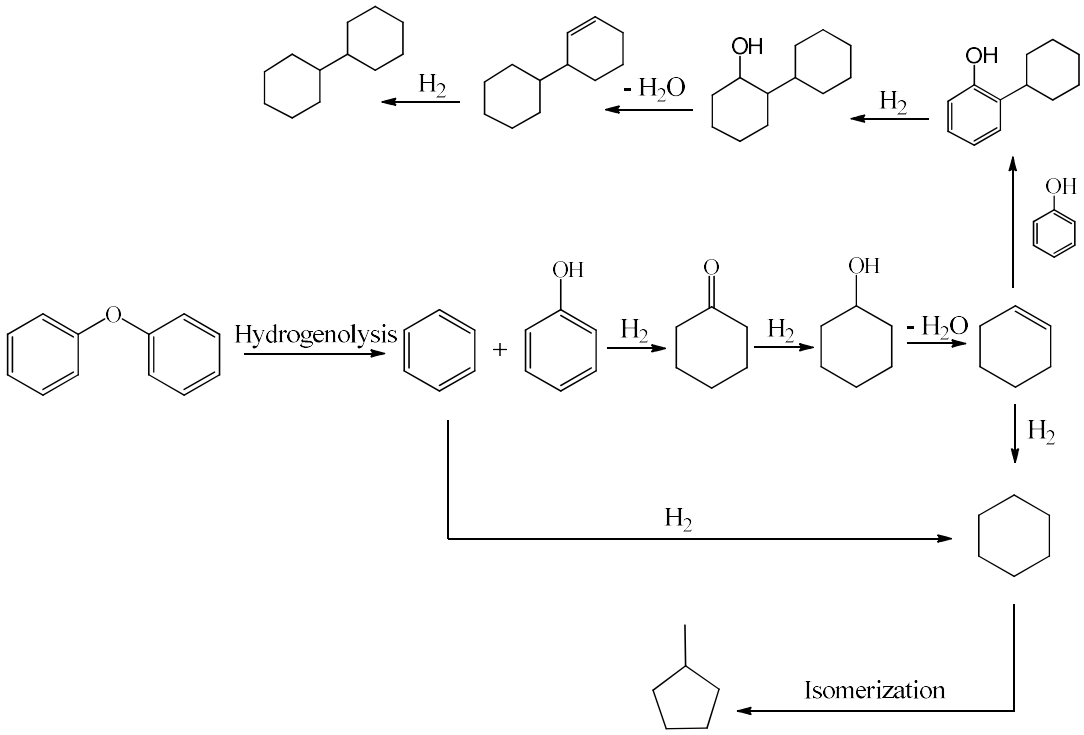

Scheme 8.1: Reaction pathways for the conversion of DPE over impregnated catalysts.

8.3 Effect of support and metal particle size for DPE conversion

Table 8.2 shows the product distribution for DPE conversion over Pd-based catalysts prepared by the colloidal method at 230 °C, 18 bar H_2 in decalin. Due to the higher activity of colloidal catalysts compared to the impregnated ones, for a low DPE amount (31 mmol), $Pd/Nb_2O_{5\text{-col}}$ completely converted DPE to cyclohexane. So, in order to compare the activity of colloidal catalysts, the conversion of DPE over colloidal catalysts was carried out using the same amount as for the BPE and PEB molecules (62 mmol).

Table 8.2: Conversion of DPE, mass balance, and product distribution for colloidal catalysts

Ent.	Catalysts	X_{DPE} (%)	MB (%)	Yield (%)				
				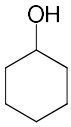	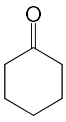		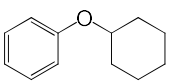	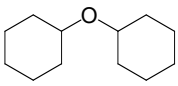
1	$Pd/Al_2O_{3\text{-col}}$	84	99	26.5	15.6	4.4	34.0	12.5
2	$Pd/TiO_{2\text{-col}}$	100	100	16.0	0.0	3.0	0.0	81.0
3	$Pd/Nb_2O_{5\text{-col}}$	100	99	12.7	0.0	8.1	0.0	78.3
4	$Pd/ZrO_{2\text{-col}}$	100	86	23.0	0.0	57.0	1.0	6.0

Reaction conditions: Reactant (62 mmol), decalin (15 mL), mass of catalysts 10 mg, 230 °C, 18 bar H_2, 3h.

Using the same mass of material (10 mg), all catalysts were active for DPE conversion. For $Pd/Al_2O_{3\text{-col}}$, 84 % of DPE was converted into dicyclohexyl ether, cyclohexyl phenyl ether, cyclohexanol, cyclohexanone, and cyclohexane. On the other hand, complete DPE conversion was achieved over $Pd/TiO_{2\text{-col}}$, $Pd/Nb_2O_{5\text{-col}}$, and $Pd/ZrO_{2\text{-col}}$. Dicyclohexyl ether and cyclohexanol were the main products formed over $Pd/TiO_{2\text{-col}}$ and $Pd/Nb_2O_{5\text{-col}}$, while cyclohexane was mainly formed over $Pd/ZrO_{2\text{-col}}$.

As observed for PEB, the hydrogenation of the DPE aromatic ring occurred to a large extent over colloidal catalysts. However, unlike PEB, the effect of the Brønsted acidic sites of $Pd/Nb_2O_{5\text{-col}}$ was less evident. Although $Pd/Nb_2O_{5\text{-col}}$ produced more cyclohexane (8.0 %) than $Pd/Al_2O_{3\text{-col}}$ (4.4 %) and $Pd/TiO_{2\text{-col}}$ (3.0 %), the DPE hydrogenation was still favored over $Pd/Nb_2O_{5\text{-col}}$. When $Pd/ZrO_{2\text{-col}}$ was used, 57 % of cyclohexane was formed, indicating that over this catalyst the hydrogenolysis pathway was favored.

Regarding the product distribution, the reaction pathway for DPE conversion is proposed in Scheme 8.2. As well as for PEB, the hydrogenation of DPE aromatic rings occurs in parallel to its hydrogenolysis into phenol and benzene. $Pd/Al_2O_{3\text{-col}}$, $Pd/TiO_{2\text{-col}}$, and $Pd/Nb_2O_{5\text{-col}}$ favor the DPE hydrogenation while the hydrogenolysis is favored over $Pd/ZrO_{2\text{-col}}$.

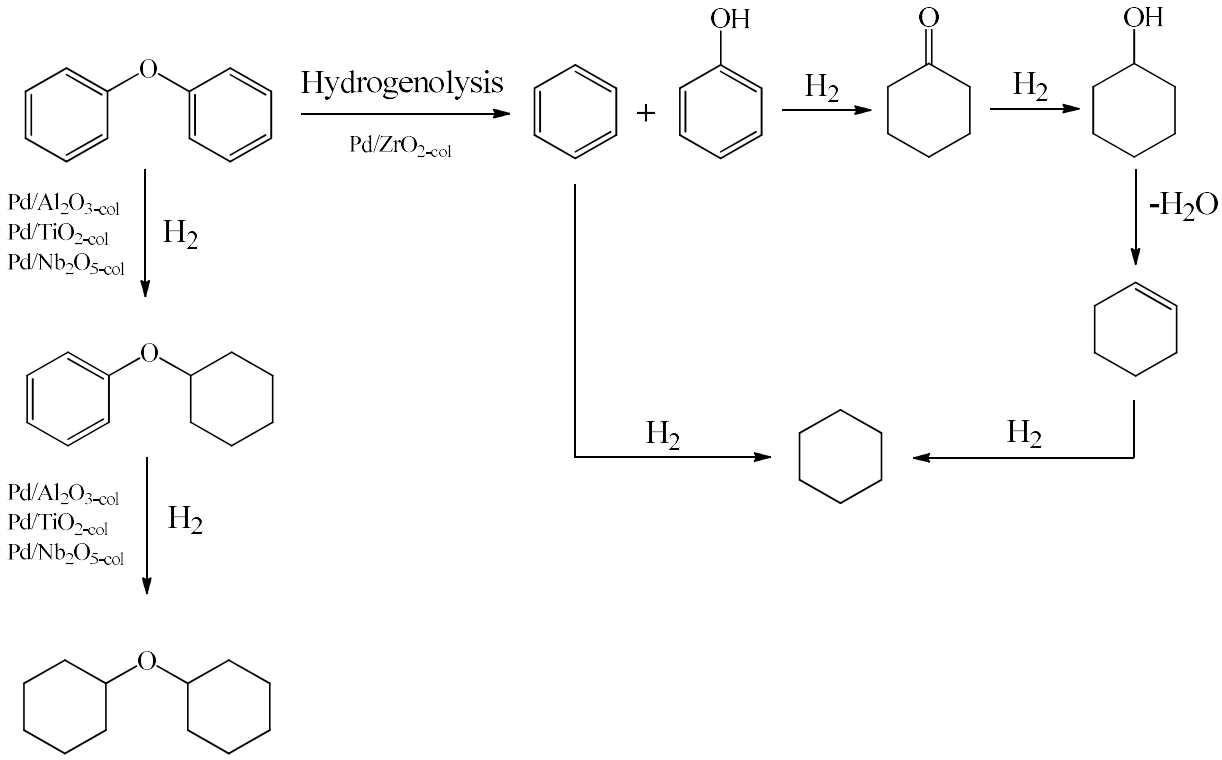

Scheme 8.2: Reaction pathways for the conversion of DPE over colloidal catalysts.

Fig 8.1 shows a correlation between the activity of colloidal catalysts ($Pd/TiO_{2\text{-col}}$ and $Pd/Nb_2O_{5\text{-col}}$) with the bond dissociation energy required to break the ether linkages. The products obtained for each molecule were divided into three groups: (i) hydrogenation, represented by the products formed from the hydrogenation of the ether aromatic ring, (ii) hydrogenolysis, which consists of the products obtained from the direct ether hydrogenolysis and their hydrogenated products (phenol, cyclohexanol, cyclohexanone, methyl/ethylbenzene, and methyl/ethylcyclohexane), and (iii) the deoxygenation of the phenol derivatives, represented by cyclohexane. The yield of products used in this comparison were taken from tables 6.2 and 8.2 and Figs. 7.2 and 7.3. The reactions considered here are the same reaction condition (230 °C, 18 bar H_2, and 3h), substrate amount (62 mmol), and conversion (100%). Regarding $Pd/TiO_{2\text{-col}}$ which exhibited only Lewis acidic sites and $Pd/Nb_2O_{5\text{-col}}$ possesses Lewis and Brønsted acidic sites, it is possible to observe that regardless of the type of support, the increase in the bond dissociation energy decreases the weight of the hydrogenolysis and deoxygenation groups, whereas the weight of the hydrogenation group increases. However, in the presence of Lewis acidic sites, the difference between the hydrogenation and hydrogenolysis groups are much more pronounced than for the catalyst which has Brønsted acidic sites. In addition, the presence of Brønsted acidic sites clearly favored the deoxygenation group.

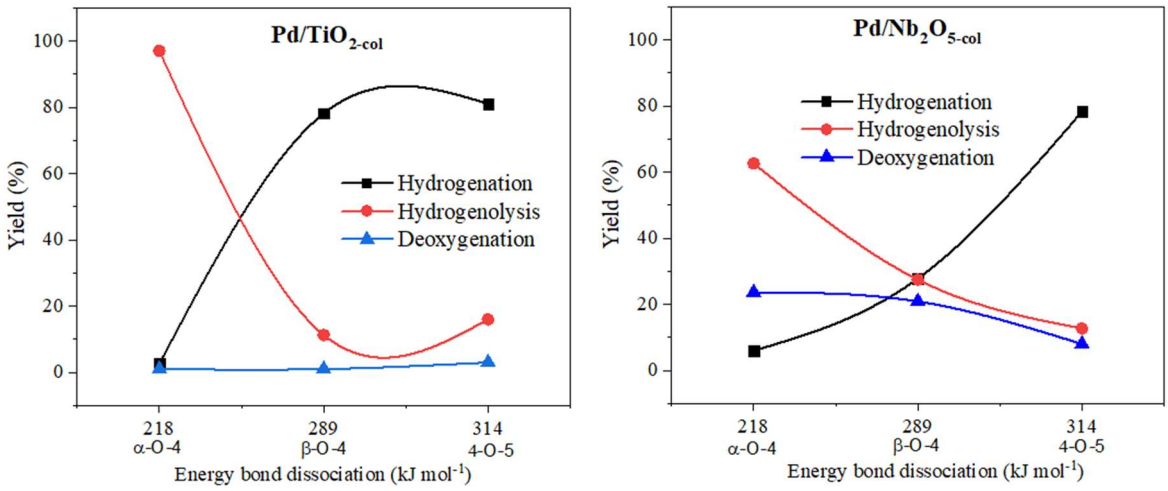

Figure 8.1: Comparison between the assistance of Lewis vs. Lewis + Brønsted acidic sites of the support in the conversion of the three ethers

8.3 Conversion of typical monomers and dimers representative of lignin over $Pd/Nb_2O_{5\text{-col}}$

In order to explore the activity of $Pd/Nb_2O_{5\text{-col}}$, the HDO of other model molecules representative of lignin was performed at 230 °C, 18 bar of H_2 using decalin as solvent. Monomers such as phenol, anisole, guaiacol, 4-propylphenol, and the dimer 2,3-dihydrobenzofuran, typical molecule representative of a β-5 linkage, were selected as feedstock because they are widely studied in the literature. All reactions were done in the same mass of catalysts (30 mg). The detailed product distribution for each molecule is shown in Table 8.3.

Table 8.3: HDO of model molecules representative of lignin over Pd/Nb_2O_5-col

Ent.	Substrate	Conv. (%)	Yield (%)			
1	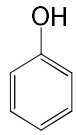	X: 100 CB: 86	 (83.5)	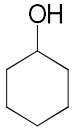 (2.7)		
2	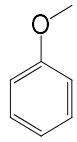	X: 100 CB: 78	 (46.0)	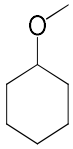 (32.4)		
3	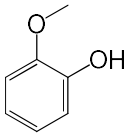	X: 76 CB: 66	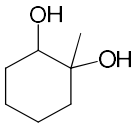 (24.4)	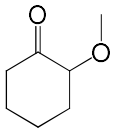 (11.0)	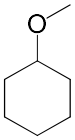 (2.0)	 (2.3)
5	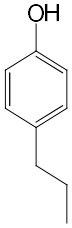	X: 100 CB: 85	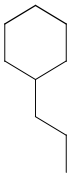 (69.4)	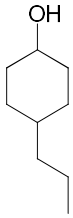 (16.2)		
6	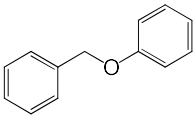	X: 100 CB: 93	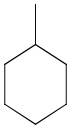 (45.9)	 (23.6)	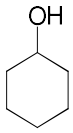 (16.7)	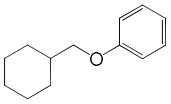 (6.6).
7	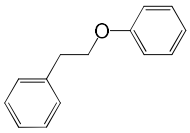	X: 46 CB: 95	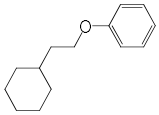 (13.5)	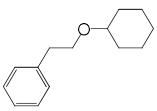 (9.9)	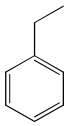 (6.3)	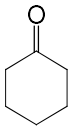 (5.8)
8	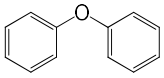	X: 100 CB: 84	 (84.3)			
9	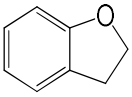	X: 100 CB: 82	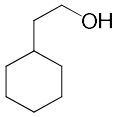 (48.0)	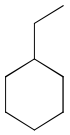 (30.0)	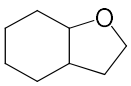 (2.0)	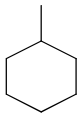 (2.0)

Reaction conditions: substrate (62 mmol), $Pd/Nb_2O_{5\text{-col}}$ (30 mg), 15 mL of decalin, 230 °C, and 18 bar of H_2.

Over $Pd/Nb_2O_{5\text{-col}}$, phenol was completely converted into cyclohexane (83.5 %) and cyclohexanol (2.7 %). First, phenol was hydrogenated into cyclohexanone and cyclohexanol over Pd metallic sites. Then, the Brønsted acidic sites of Nb_2O_5 catalyzed the dehydration of cyclohexanol to form cyclohexene, which was not detected. Finally, cyclohexane was produced via cyclohexene hydrogenation, scheme 8.3.

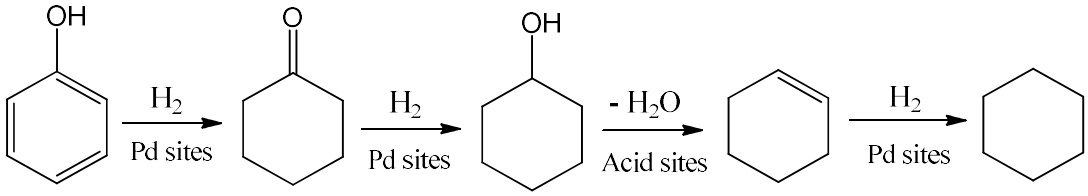

Scheme 8.3: Hydrodeoxygenation of phenol over $Pd/Nb_2O_{5\text{-col}}$

The conversion of phenol has been investigated in the literature at high hydrogen pressure and temperature conditions in aqueous phase and non-polar solvent. At 200 °C, under 50 bar of H_2 and using water as a solvent, Zhao et al.[78], reported that cyclohexanol and cyclohexanone were the only products formed for phenol conversion over Pd/C, Pd/SiO_2, Pd/Al_2O_3 and Pd-supported over amorphous silica-alumina (ASA). The authors proposed that Lewis acidic sites can stabilize the cyclohexanone intermediate, which consequently inhibits the dehydration of cyclohexanol. In contrast, when, acetic acid (Brønsted acid) was added to the reaction solution, the selectivity to cyclohexane increased up to 75 % over Pd/C. Similar results were observed by Hong et al.[79] at 200 °C, under 40 bar of H_2 in water. Over Pt/SiO_2 and Pt/Al_2O_3, cyclohexanol was the main product observed (> 93 %), whereas cyclohexane was mainly produced over Pt supported on zeolites HZSM5, HY, and Hβ. In the presence of a non-polar solvent (tetralin), cyclohexane and cyclohexanol were the only products formed with a selectivity of 95 and 5 %, respectively, over Pt-Ir/HZSM5 (200 °C and 30 bar of H_2) [80].

Recently, our group investigated the hydrodeoxygenation of phenol over Pd-based catalysts supported on SiO_2 and Nb_2O_5 in vapor phase at 300 °C [81,82]. The results showed that over Pd/SiO_2, the formation of cyclohexanone was favored, whereas for Pd/Nb_2O_5, benzene was the main product. The higher performance for phenol deoxygenation over Pd/Nb_2O_5 was attributed to the oxophilic sites of Nb_2O_5 (Nb^{4+}/ Nb^{5+}) which promote the interaction with the oxygen atom in the phenol molecule. In this case, phenol was first tautomerized into cyclohexadienone, followed by its hydrogenation to 2,4-cyclohexadienol, which was dehydrated to benzene in the interface metal-support.

Anisole was also completely converted into cyclohexane (45 %) and methoxycyclohexane (28.3 %) over Pd/$Nb_2O_{5\text{-col}}$ (Table 8.3, entry 2). The literature reported that the conversion of anisole in the liquid phase can proceed via different parallel and sequential reaction routes (scheme 8.4) [83–85]. Three main reaction pathways may occur: (i) anisole can be demethylated to phenol, which can produce cyclohexane by a hydrogenation and dehydration sequential reaction; (ii) benzene can be yielded by hydrogenolysis of the C_{arom}-O bond of anisole and then, cyclohexane can be formed by benzene hydrogenation; or (ii) anisole can be hydrogenated to methoxycyclohexane and the hydrogenolysis of its C_{aliph}-O bond can take place to form cyclohexane.

Compared to Pd/SiO_2 and Pd/$NbOPO_4$, Pd/Nb_2O_5 was the most active catalyst for the anisole hydrodeoxygenation in gas phase at 300 °C [82]. Benzene, phenol, methane, and methanol were observed as main products for all catalysts evaluated. However, over Pd/Nb_2O_5, the formation of benzene and methanol was favored, suggesting that the demethoxylation of anisole occurred as main reaction pathway.

Considering the products obtained in our work and the hydrogenation ability of colloidal catalysts, the conversion of anisole is probably initiated by the hydrogenation of

the anisole aromatic ring into methoxycyclohexane. Then, cyclohexane is produced by hydrogenolysis of methoxycyclohexane or cyclohexanol dehydration.

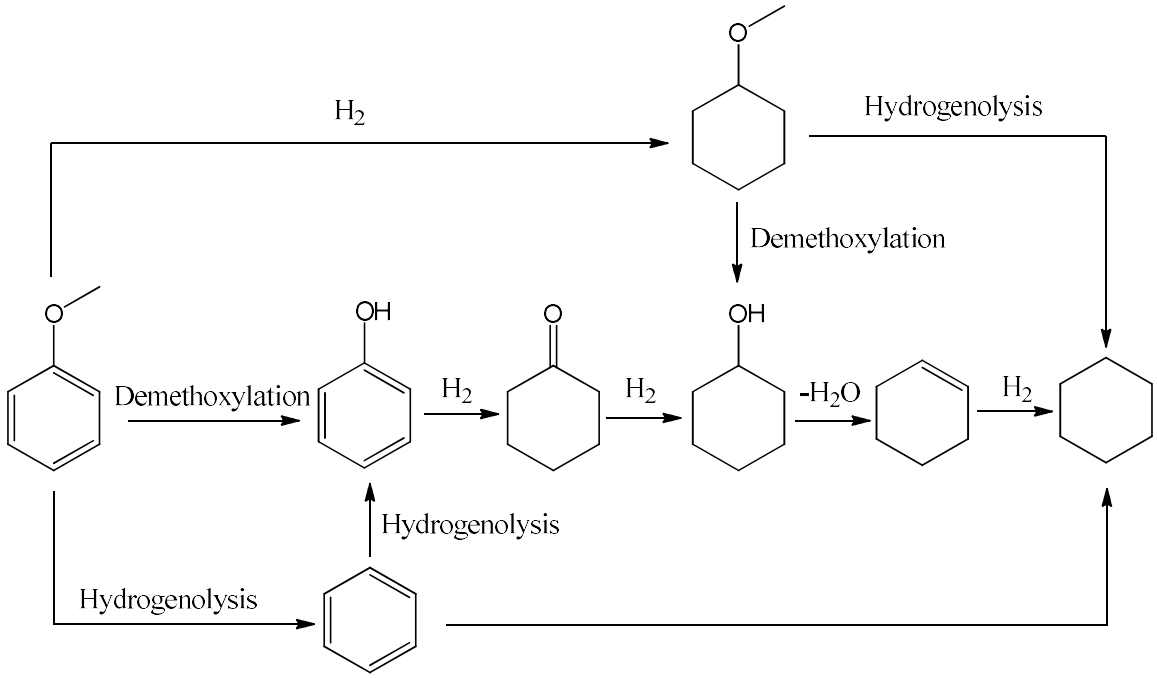

Scheme 8.4: Hydrodeoxygenation of anisole proposed by the literature [83–85].

Unlike phenol and anisole, guaiacol was not completely converted over $Pd/Nb_2O_{5\text{-}col}$ (table 8.3, entry 3). In the same reaction conditions, 76 % of guaiacol was converted to form 1-methyl-1,2-cyclohexanediol, 2-methoxycyclohexone, 1-methoxycyclohexane, and cyclohexane.

The conversion of guaiacol was studied by Song et al[86] over Ni/Nb_2O_5 at 200 °C and 25 bar of H_2, using water and decalin as solvent. The authors reported that in the aqueous phase, the conversion rate of guaiacol was 18 times higher than that in decalin (1.07 and 0.06 h^{-1}, respectively) and due to it, a low guaiacol conversion was achieved when decalin was used (25.5 %). According to the products, cyclohexanol was mainly formed in the presence of water, while 1-methyl-1,2-cyclohexanediol was favored in the non-polar solvent. Phenol, cyclohexene and 1,2-cyclohexanediol were also detected in the reaction mixture. The authors proposed three possible reaction routes for guaiacol

conversion: (i) hydrolysis to obtain catechol, followed by hydrogenation into 1,2-cyclohexanediol, (ii) hydrogenation to yield 2-methoxycyclohexanone and 2-methoxycyclohexanol, followed by hydrogenolysis and demethanolation to obtain cyclohexanol, and (iii) direct hydrodeoxygenation of guaiacol to produce phenol, followed by phenol hydrogenation into cyclohexanol.

The results obtained in our work suggest that the conversion of guaiacol proceeds through two different reaction pathways (Scheme 8.5). In the first one, guaiacol was first hydrogenated to 2-methoxycyclohexone and 2-methoxycyclohexol, which was then transalkylated into 1-methyl-1,2-cyclohexanediol. To a minor extent, guaiacol was dehydroxylated to anisole, which was hydrogenated to form 1-methoxycyclohexane. Then, cyclohexane was produced by demethoxylation of 1-methoxycyclohexane.

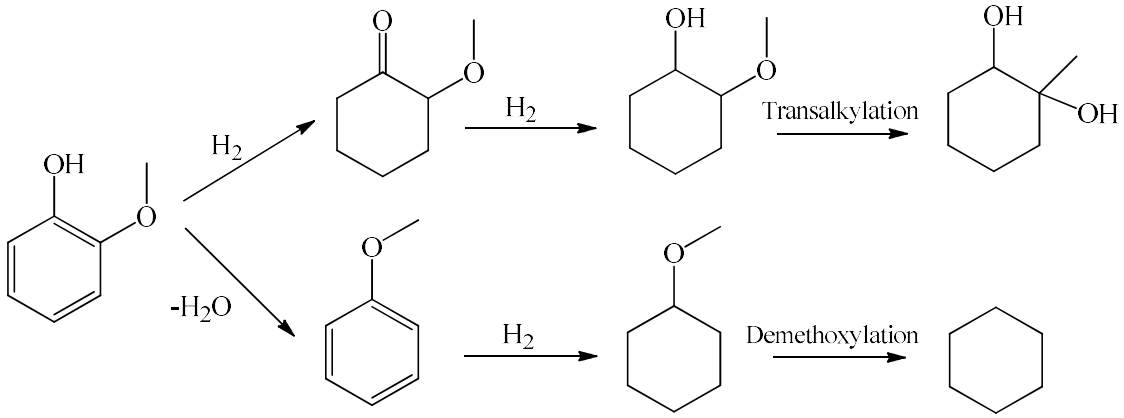

Scheme 8.5: Hydrodeoxygenation of guaiacol over $Pd/Nb_2O_{5\text{-col}}$

4-propyl phenol was completely converted over $Pd/Nb_2O_{5\text{-col}}$ (table 8.3, entry 4). The only products observed were propyl cyclohexane (69.4%) and 4-propyl cyclohexanol (16.2 %), suggesting that the conversion of 4 propyl phenol started by its hydrogenation to 4-propyl cyclohexanol over metallic sites. Then, 4-propyl cyclohexanol was dehydrated to propyl cyclohexane by the Brønsted acidic sites of Nb_2O_5 (Scheme 8.6).

Zhao and Lercher[37] evaluated the conversion of 4-propyl phenol over Pd/C in the presence of a series of acidic supports at 200 °C, 50 bar of H_2 in water as a solvent. Propyl cyclohexane was mainly produced over Brønsted solid acids such as sulfated zirconia, Amberlyst 15, HZSM5, and Nafion/SiO_2, whereas Lewis solid acids (alumina and amorphous silica-alumina) were ineffective for alcohol dehydration and produced propyl cyclohexanol and propyl cyclohexanone.

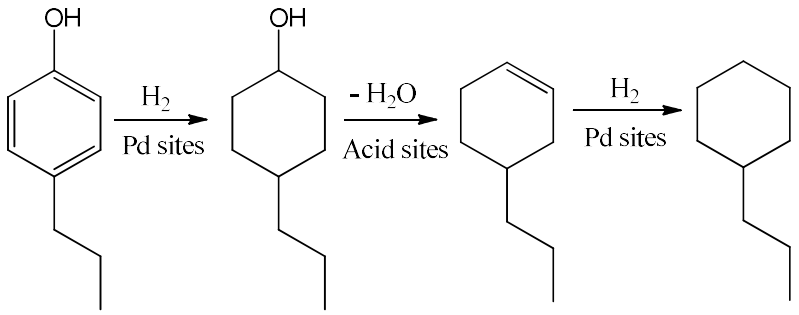

Scheme 8.6: Hydrodeoxygenation of 4-propylphenol over Pd/$Nb_2O_{5\text{-col}}$

Concerning the phenolic dimers BPE, PEB, and DPE, complete conversion was achieved only for BPE and DPE, model molecules representative of the α-O-4 and 4-O-5 ether linkages, respectively. BPE was converted into methylcyclohexane, cyclohexane, cyclohexanol and (cyclohexylmethoxy)benzene, indicating that the hydrogenolysis of its C_{aliph}-O bond and partial hydrogenation of its aromatics rings occur in parallel. In contrast, DPE was selectively converted into cyclohexane. For PEB, a conversion of 46 % was observed over Pd/$Nb_2O_{5\text{-col}}$. The main products observed were (2-(cyclohexyloxy) ethyl) benzene and (2-(cyclohexylethoxy) benzene, produced by the partial hydrogenation of its aromatic rings (table 8.3, entry 7). Ethylbenzene and cyclohexanone were also detected, suggesting that the hydrogenolysis of the C_{aliph}-O bond of PEB also occurred.

Finally, as well as for BPE and DPE, 2,3-dihydrobenzofuran (2,3-DHBF) was also completely converted over Pd/$Nb_2O_{5\text{-col}}$, producing cyclohexane ethanol (48 %),

ethylcyclohexane (30 %), octahydro-1-benzofuran (2 %), and methylcyclohexane (2 %) as products (table 8.3, entry 9).

Ru/HZSM5 was used by Zhang et al [39] for the HDO of 2,3-DHBF in water, at 200 °C and 50 bar of H_2. Ethylcyclohexane (70.4 %), methylcyclohexane (22.6 %), and cyclohexane (3.8 %) were observed as products. The authors suggested that the formation of ethylcyclohexane occurs by hydrogenation of the aromatic ring, followed by dehydration and hydrogenation reactions. However, the reaction route for the other products was not elucidated.

The performance of a bimetallic Pd-Pt catalyst supported over silica-alumina was evaluated for the conversion of benzofuran at 280 °C and 30 bar of hydrogen in decalin as solvent[87]. Ethylcyclohexane was formed as main product, but methylcyclohexane and octahydrobenzofuran were also observed to a minor extent. The authors proposed that benzofuran was first hydrogenated to 2,3-DHBF, and octahydrobenzofuran was formed by further hydrogenation of 2,3-DHBF. The complete deoxygenation occurred by dehydration of octahydrobenzofuran to form 2-ethylcyclohexanol, followed by its dehydration/hydrogenation into ethylcyclohexane. Methylcyclohexane was finally produced by ethylcyclohexane cleavage.

According to the products obtained in our work, the conversion of 2,3-DHBF indeed starts by the hydrogenation of its aromatic ring into octahydrobenzofuran. However, unlike what has been reported in the literature, the hydrogenolysis of the C_{aliph}-O bond of octahydrobenzofuran occurs, producing cyclohexyl ethanol instead of 2-ethylcyclohexanol. Ethylcyclohexane can be formed by cyclohexyl ethanol cleavage, while methylcyclohexane is produced through the cleavage of ethylcyclohexane (Scheme 8.7).

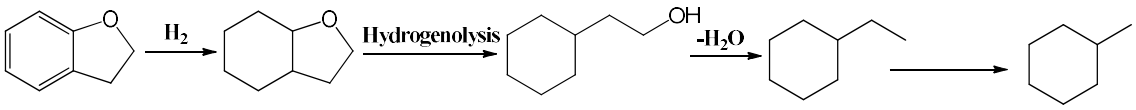

Scheme 8.7: Hydrodeoxygenation of 2,3-dihydrobenzofuran over $Pd/Nb_2O_{5\text{-col}}$

8.4 Conclusions

As observed for the previous molecule representative of β-O-4 bond, the impregnated materials favored the hydrogenolysis of DPE into phenol and benzene, while the colloidal catalysts exhibited high activity in the hydrogenation of its aromatic rings.

By comparing the activity of Lewis and Brønsted acidic sites of supported colloidal catalysts for the conversion of BPE, PEB, and DPE, it was possible to observe that regardless of the type of support, when the bond dissociation energy increases, the proportion of hydrogenolysis and deoxygenation products decreases, while the proportion of the products of direct hydrogenation of the ether aromatic rings increases. In addition, the presence of Lewis acidic sites did not exhibit a significant influence for the deoxygenation step in any case, and Brønsted acidic sites were necessary.

Regarding the conversion of other typical molecules representative of lignin, $Pd/Nb_2O_{5\text{-col}}$ was active to convert all the selected substrates and to cleave different C-O and C-C linkages.

Chapter 9

General conclusions and perspectives

9.1 Conclusions

Bio-oil produced by fast pyrolysis of the lignocellulosic biomass has been considered as a potential alternative source for petroleum-based fuel and the chemical industry. However, due to its intrinsic characteristics, bio-oil must be upgraded to be used as fuel. In particular, the oxygen content of the molecules composing bio-oil must be decreased. The catalytic hydrodeoxygenation reaction (HDO) appears as the most effective process to reach this goal. But bio-oil is a complex mixture, and model molecules representative of the linkages found in lignocellulosic biomass are rather used in a first approach to better understand the mechanism of the HDO reactions, as well as to comprehend how the characteristics of a catalyst can affect them.

In this respect, the HDO of benzyl phenyl ether (BPE), phenethoxybenzene (PEB) and diphenyl ether (DPE), three dimeric aryl ethers representative of the α-O-4, β-O-4, and 4-O-5 linkages, respectively, has been studied in the literature. Different metals, mainly Ni, Pd, Pt, and Ru, supported on non-acidic materials (SiO_2, C) or acidic materials (such as a large range of zeolites) have been tested for the HDO of dimeric aryl ethers. The literature has suggested that the conversion of dimeric aryl ethers involves metal sites responsible for the ether hydrogenolysis and hydrogenation of the intermediates formed after cleavage, and acidic sites that promote the dehydration step necessary to produce deoxygenated compounds. Side-reactions include coupling reactions between the aromatics resulting from hydrogenolysis (alkylation products), and the partial hydrogenation of the initial substrate can also occur. However, the effects of the nature of the metal and of the acidity of the support on these parallel and successive steps of the HDO process cannot be clearly delineated so far.

In this context, the main focus of this thesis was to investigate the role of the support, as well as the type of metal, in the cleavage of the dimeric aryl ethers mentioned

above, and to explore the balance with the competitive and subsequent reactions: direct hydrogenation of the substrate; coupling between the aromatics resulting from hydrogenolysis (alkylation products); and the final stages of oxygen removal from the aromatics produced by hydrogenolysis.

The following Ru and Pd-based catalysts were prepared and tested:

- Pd and Ru-supported on SiO_2 and HZSM5 prepared by incipient wetness impregnation.
- Pd-based catalysts supported on SiO_2, TiO_2, Nb_2O_5, Al_2O_3, ZrO_2, and HZSM5 prepared by incipient wetness impregnation.
- Pd-based catalysts supported on TiO_2, Nb_2O_5, Al_2O_3, and ZrO_2 prepared by a method of immobilization of a Pd sol prepared via a colloidal route ("colloidal catalysts").

The colloidal catalysts exhibited a higher density of acidic sites as well as the smallest average Pd particle size (< 4 nm), compared to the respective impregnated catalysts. As a consequence, the dispersion of the metal was larger on the surface of the colloidal catalysts, conferring a higher activity.

In the first chapter of experimental results, the influence of the type of metal and acidic sites was initially be studied, using Pd and Ru-supported on SiO_2 and HZSM5. It was found that the mere metal oxophilicity can affect the product distribution: for BPE, alkylated products were formed even in the absence of acidic sites over Ru/SiO_2. This effect was attributed to the higher oxophilicity of Ru compared to Pd. Benzyl and phenyl radicals are formed even in the absence of acidic sites, and, due to its lower hydrogenation ability, Ru does not promote the fast hydrogenation of these radicals, which can recombine into alkylated products. The formation of deoxygenated products (cyclohexane and methylcyclopentane) was nevertheless favored over Ru-based

catalysts. However, for the conversion of PEB and DPE, this effect was less pronounced. Despite the advantages of Ru in terms of activity, it was noted that oxygenated alkylated products were extensively produced over Ru catalysts for BPE and PEB conversion. Therefore, it was chosen to prefer Pd-supported catalysts for further studies.

Over Pd-based catalysts, the conversion and the product distribution for the HDO of BPE, PEB, and DPE were significantly affected by the Pd particle size, as well as by the type of support. For BPE, the large size of Pd particles observed for the impregnated catalysts (7.2 – 24.6 nm) favored the hydrogenolysis of BPE into phenol and toluene. However, the hydrogenation of these hydrogenolysis products did not occur. In this case, after BPE cleavage, alkylated products were produced in a larger or lesser extent depending on the total density of acidic sites; $Pd/ZrO_{2\text{-imp}}$ and $Pd/HZSM5_{\text{-imp}}$ exhibited the highest amount of acidic sites and the largest formation of oxygenated alkylated products. Over colloidal catalysts, the smaller Pd particle size (2.0 – 3.8 nm) promoted the hydrogenation of phenol and toluene after C-O cleavage and, due to a more important hydrogenation ability, the formation of alkylated products was suppressed. Furthermore, cyclohexane, formed from the dehydration of cyclohexanol, was only formed in the presence of Brønsted acidic sites ($Pd/Nb_2O_{5\text{-col}}$ and $Pd/ZrO_{2\text{-col}}$). The reaction conditions of pressure and temperature also affected the product distribution. A low temperature (< 230 °C) did not favor the formation of cyclohexane and a high hydrogen pressure (> 10 bar of H_2) promoted the hydrogenation of BPE aromatic rings, competing with the hydrogenolysis of BPE, and consequently with the HDO route.

Regarding PEB conversion, large particles of Pd also favored the hydrogenolysis of PEB into phenol and ethylbenzene. After cleavage, ethylbenzene remained almost unreacted, whereas phenol was transformed into cyclohexane. Additionally, the formation of alkylated products, 2 and 4-phenethylphenol, was observed. On the other

hand, over small Pd particles, products from the hydrogenation of PEB aromatic rings were mainly formed, and oxygen-free cyclohexane was only formed in the presence of Brønsted acidic sites. Like for the former molecules, the hydrogenolysis of DPE was also favored over large Pd particles, and after cleavage cyclohexane and methylcyclopentane were the main products. When catalysts prepared with particles formed by a colloidal route were used, the hydrogenolysis and the hydrogenation of DPE aromatic rings occurred in parallel. For $Pd/Al_2O_{3\text{-col}}$, $Pd/TiO_{2\text{-col}}$, and $Pd/Nb_2O_{5\text{-col}}$, the DPE hydrogenation was favored, while for $Pd/ZrO_{2\text{-col}}$ hydrogenolysis occurred as the main reaction pathway and a high yield of cyclohexane was measured.

It was observed that depending on the ether linkage, some parameters are more relevant than others, which makes it difficult to define a general rule to achieve the full HDO of the different ether linkages. For instance, the assistance of the support acidic sites becomes less pronounced when the energy bond dissociation increases. In addition, regarding the colloidal catalysts, regardless of the type of support, when the bond dissociation energy of the C-O ether linkage increases, the proportion of the hydrogenolysis and deoxygenation products decreases, whereas the proportion of direct hydrogenation products increases.

Therefore, regarding the results obtained in this work, $Pd/Nb_2O_{5\text{-col}}$ and $Pd/ZrO_{2\text{-col}}$ were globally found to be the best catalysts for the HDO of the selected dimeric aryl ethers. A main conclusion is that the hydrogenolysis of the C-O ether bonds occurs in the presence of Pd metal particles as well as of the Brønsted acidic sites of the support. A large Pd particle size favors the hydrogenolysis, but the subsequent deoxygenation requires small Pd particles. In the presence of large Pd particles supported over an oxide possessing Lewis acidic sites, the deoxygenation route was inhibited. On the other hand,

for catalysts with small Pd particles, the assistance of Brønsted acidic sites was required to promote both the hydrogenolysis and the deoxygenation reactions.

9.2 Perspectives

The present work investigated the effect of metal particle size as well the type of support for the hydrodeoxygenation of dimeric aryl ethers in a non-polar solvent. From the results discussed above, we concluded that a small particle size of Pd is required in order to favor the formation of deoxygenated products. In addition, Brønsted acidic sites were fundamental to improve the hydrodeoxygenation of phenolic dimers. In this direction, we suggest for future work:

- The investigation of the effect of Ru and Ni supported over Nb_2O_5 and ZrO_2 prepared by the colloidal method for the HDO of dimeric aryl ethers representative of the main C-C and C-O ether linkages.
- The use of sol-immobilized catalysts for the hydrodeoxygenation of real biomass feedstock.
- A systematic study on the re-use and on deactivation of the colloidal catalysts during the HDO reaction of dimeric aryl ethers has not been performed, and therefore it is also recommended.
- Finally, to study the performance of $Pd/Nb_2O_{5\text{-col}}$ and $Pd/ZrO_{2\text{-col}}$ with other solvents (water and isopropanol) for the HDO of a mixture of dimeric aryl.

References

1. S. De, B. Saha, and R. Luque. Hydrodeoxygenation processes: Advances on catalytic transformations of biomass-derived platform chemicals into hydrocarbon fuels. *Bioresour. Technol.* **2015**, 178, 108–118.

2. C. Li, X. Zhao, A. Wang, G.W. Huber, and T. Zhang. Catalytic Transformation of Lignin for the Production of Chemicals and Fuels. *Chem. Rev.* **2015**, 115 (21), 11559–11624.

3. M. Araque-Marin, F. Bellot Noronha, M. Capron, F. Dumeignil, M. Friend, E. Heuson, I. Itabaiana, L. Jalowiecki-Duhamel, B. Katryniok, A. Löfberg, S. Paul, and R. Wojcieszak. Strengthening the Connection between Science, Society and Environment to Develop Future French and European Bioeconomies: Cutting-Edge Research of VAALBIO Team at UCCS. *Molecules* **2022**, 27 (12), 3889.

4. K. Tomishige, M. Yabushita, J. Cao, and Y. Nakagawa. Hydrodeoxygenation of potential platform chemicals derived from biomass to fuels and chemicals. *Green Chem.* **2022**, 24 (15), 5652–5690.

5. R. Shu, R. Li, B. Lin, C. Wang, Z. Cheng, and Y. Chen. A review on the catalytic hydrodeoxygenation of lignin-derived phenolic compounds and the conversion of raw lignin to hydrocarbon liquid fuels. *Biomass Bioenergy.* **2020**, 132, 105432.

6. M. Zaheer and R. Kempe. Catalytic Hydrogenolysis of Aryl Ethers: A Key Step in Lignin Valorization to Valuable Chemicals. *ACS Catal.* **2015**, 5 (3), 1675–1684.

7. A.N. Kay Lup, F. Abnisa, W.M.A.W. Daud, and M.K. Aroua. A review on reaction mechanisms of metal-catalyzed deoxygenation process in bio-oil model compounds. *Appl. Catal. A.* **2017**, 541, 87–106.

8. M. Patel and A. Kumar. Production of renewable diesel through the hydroprocessing of lignocellulosic biomass-derived bio-oil: A review. *Renew. Sust. Energ. Rev.* **2016**, 58, 1293–1307.

9. J.-S. Kim. Production, separation and applications of phenolic-rich bio-oil – A review. *Bioresour. Technol.* **2015**, 178, 90–98.

10. Md.M. Rahman, R. Liu, and J. Cai. Catalytic fast pyrolysis of biomass over zeolites for high quality bio-oil – A review. *Fuel Process. Technol.* **2018**, 180, 32–46.

11. L. Qu, X. Jiang, Z. Zhang, X.-G. Zhang, G.-Y. Song, H.-L. Wang, Y.-P. Yuan and Y.-L. Chang. A review of hydrodeoxygenation of bio-oil: model compounds, catalysts, and equipment. *Green Chem.* **2021**, 23 (23), 9348–9376.

12. X. Li, G. Chen, C. Liu, W. Ma, B. Yan, and J. Zhang. Hydrodeoxygenation of lignin-derived bio-oil using molecular sieves supported metal catalysts: A critical review. *Renew. Sust. Energ. Rev.* **2017**, 71, 296–308.

13. J. Zakzeski, P.C.A. Bruijnincx, A.L. Jongerius, and B.M. Weckhuysen. The Catalytic Valorization of Lignin for the Production of Renewable Chemicals. *Chem. Rev.* **2010**, 110 (6), 3552–3599.

14. W. Song, W. Lai, Y. Lian, X. Jiang, and W. Yang. Sulfated ZrO_2 supported CoMo sulfide catalyst by surface exsolution for enhanced hydrodeoxygenation of lignin-derived ethers to aromatics. *Fuel* **2020**, 263, 116705.

15. B. Gómez-Monedero, M.P. Ruiz, F. Bimbela, and J. Faria. Selective hydrogenolysis of α-O-4, β-O-4, 4-O-5 C-O bonds of lignin-model compounds and lignin-containing stillage derived from cellulosic bioethanol processing. *Appl. Catal. A.* **2017**, 541, 60–76.

16. X. Chen, W. Guan, C.-W. Tsang, H. Hu, and C. Liang. Lignin Valorizations with Ni Catalysts for Renewable Chemicals and Fuels Productions. *Catalysts* **2019**, 9 (6), 488.

17. T. Dickerson and J. Soria. Catalytic Fast Pyrolysis: A Review. *Energies* **2013**, 6 (1), 514–538.

18. A.S. Ouedraogo and P.R. Bhoi. Recent progress of metals supported catalysts for hydrodeoxygenation of biomass derived pyrolysis oil. *J. Clean. Prod.* **2020**, 253, 119957.

19. A.N. Kay Lup, F. Abnisa, W.M.A.W. Daud, and M.K. Aroua. A review on reaction mechanisms of metal-catalyzed deoxygenation process in bio-oil model compounds. *Appl. Catal. A.* **2017**, 541, 87–106.

20. Z. Lin, R. Chen, Z. Qu, and J.G. Chen. Hydrodeoxygenation of biomass-derived oxygenates over metal carbides: from model surfaces to powder catalysts. *Green Chem.* **2018**, 20 (12), 2679–2696.

21. X. Han, Y. Guo, X. Liu, Q. Xia, and Y. Wang. Catalytic conversion of lignocellulosic biomass into hydrocarbons: A mini review. *Catal. Today* **2019**, 319, 2–13.

22. T. Cordero-Lanzac, J. Rodríguez-Mirasol, T. Cordero, and J. Bilbao. Advances and Challenges in the Valorization of Bio-Oil: Hydrodeoxygenation Using Carbon-Supported Catalysts. *Energy Fuels* **2021**, 35 (21), 17008–17031.

23. S. Kim, E.E. Kwon, Y.T. Kim, S. Jung, H. J. Kim, G. W. Huber, and J. Lee. Recent advances in hydrodeoxygenation of biomass-derived oxygenates over heterogeneous catalysts. *Green Chem.* **2019**, 21 (14), 3715–3743.

24. J. He, C. Zhao and J.A. Lercher. Ni-Catalyzed Cleavage of Aryl Ethers in the Aqueous Phase. *J. Am. Chem. Soc.* **2012**, 134 (51), 20768–20775.

25. Z. Luo and C. Zhao. Mechanistic insights into selective hydrodeoxygenation of lignin-derived β-O-4 linkage to aromatic hydrocarbons in water. *Catal. Sci. Technol.* **2016**, 6 (10), 3476–3484.

26. W. Guan, X. Chen, H. Hu, C.-W Tsang, J. Zhang, C. S. K. Lin, and C. Liang. Catalytic hydrogenolysis of lignin β-O-4 aryl ether compound and lignin to aromatics over Rh/Nb2O5 under low H_2 pressure. *Fuel Process. Technol.* **2020**, 203, 106392.

27. Z. Luo, Y. Wang, M. He, and C. Zhao. Precise oxygen scission of lignin derived aryl ethers to quantitatively produce aromatic hydrocarbons in water. *Green Chem.* **2016**, 18 (2), 433–441.

28. X. Zhou, X.-Y. Wei, Y.-M. Ma, and Z.-M. Zong. Effects of reaction conditions on catalytic hydroconversion of phenethoxybenzene over bifunctional Ni/Hβ. *Asia-Pac J Chem Eng.* **2018**, 13 (5), e2228.

29. Y.-P. Zhao, F.-P. Wu, Q.-L. Song, X. Fan, L.-J. Jin, R.-Y. Wang, J.-P. Cao and X.-Y. Wei. Hydrodeoxygenation of lignin model compounds to alkanes over Pd–Ni/HZSM-5 catalysts. *J.Energy Inst.* **2020**, 93 (3), 899–910.

30. J. He, C. Zhao, D. Mei, and J.A. Lercher. Mechanisms of selective cleavage of C–O bonds in di-aryl ethers in aqueous phase. *J.Catal.* **2014**, 309, 280–290.

31. J. He, L. Lu, C. Zhao, D. Mei, and J.A. Lercher. Mechanisms of catalytic cleavage of benzyl phenyl ether in aqueous and apolar phases. *J. Catal.* **2014**, 311, 41–51.

32. V. Roberts, S. Fendt, A.A. Lemonidou, X. Li, and J.A. Lercher. Influence of alkali carbonates on benzyl phenyl ether cleavage pathways in superheated water. *Appl. Catal. B* **2010**, 95 (1–2), 71–77.

33. X. Wang and R. Rinaldi. Solvent Effects on the Hydrogenolysis of Diphenyl Ether with Raney Nickel and their Implications for the Conversion of Lignin. *ChemSusChem* **2012**, 5 (8), 1455–1466.

34. J.S. Yoon, Y. Lee, J. Ryu, Y.-A. Kim, E. D. Park, J.-W. Choi, J.-M. Ha, D. J. Suh, and H. Lee. Production of high carbon number hydrocarbon fuels from a lignin-derived α-O-4 phenolic dimer, benzyl phenyl ether, via isomerization of ether to alcohols on high-surface-area silica-alumina aerogel catalysts. *Appl. Catal. B.* **2013**, 142–143, 668–676.

35. T. Guo, Q. Xia, Y. Shao, X. Liu, and Y. Wang. Direct deoxygenation of lignin model compounds into aromatic hydrocarbons through hydrogen transfer reaction. *Appl. Catal. A.* **2017**, 547, 30–36.

36. L. Jiang, H. Guo, C. Li, P. Zhou, and Z. Zhang. Selective cleavage of lignin and lignin model compounds without external hydrogen, catalyzed by heterogeneous nickel catalysts. *Chem. Sci.* **2019**, 10 (16), 4458–4468.

37. C. Zhao and J.A. Lercher. Selective Hydrodeoxygenation of Lignin-Derived Phenolic Monomers and Dimers to Cycloalkanes on Pd/C and HZSM-5 Catalysts. *ChemCatChem.* **2012**, 4 (1), 64–68.

38. C. Zhao and J.A. Lercher. Upgrading Pyrolysis Oil over Ni/HZSM-5 by Cascade Reactions. *Angew. Chem. Int. Ed.* **2012**, 51 (24), 5935–5940.

39. W. Zhang, J. Chen, R. Liu, S. Wang, L. Chen, and K. Li. Hydrodeoxygenation of Lignin-Derived Phenolic Monomers and Dimers to Alkane Fuels over Bifunctional Zeolite-Supported Metal Catalysts. *ACS Sustain. Chem. Eng.* **2014**, 2 (4), 683–691.

40. G. Yao, G. Wu, W. Dai, N. Guan, and L. Li. Hydrodeoxygenation of lignin-derived phenolic compounds over bi-functional Ru/H-Beta under mild conditions. *Fuel* **2015**, 150, 175–183.

41. X. Dou, W. Li, C. Zhu, X. Jiang, H.-M. Chang and H. Jameel. Cleavage of aryl–ether bonds in lignin model compounds using a Co–Zn-beta catalyst. *RSC Adv.* **2020**, 10 (71), 43599–43606.

42. Q. Song, J. Cai, J. Zhang, W. Yu, F. Wang, and J. Xu. Hydrogenation and cleavage of the C-O bonds in the lignin model compound phenethyl phenyl ether over a nickel-based catalyst. *Chinese J. Catal.* **2013**, 34 (4), 651–658.

43. J. Kong, B. Li, and C. Zhao. Tuning Ni nanoparticles and the acid sites of silica-alumina for liquefaction and hydrodeoxygenation of lignin to cyclic alkanes. *RSC Adv.* **2016**, 6 (76), 71940–71951.

44. M.A. Salam, Y.W. Cheah, P.H. Ho, L. Olsson, and D. Creaser. Hydrotreatment of lignin dimers over NiMoS-USY: effect of silica/alumina ratio. *Sustain. Energy Fuels* **2021**, 5 (13), 3445–3457.

45. H. Wu, J. Song, C. Xie, C. Wu, C. Chen, and B. Han. Efficient and Mild Transfer Hydrogenolytic Cleavage of Aromatic Ether Bonds in Lignin-Derived Compounds over Ru/C. *ACS Sustain. Chem. Eng.* **2018**, 6 (3), 2872–2877.

46. D. Wu, Q. Wang, O.V. Safonova, D. P. Peron, W. Zhou, Z. Yan, M. Marinova, A. Y. Khodakov, and V. V. Ordomsky. Lignin Compounds to Monoaromatics: Selective Cleavage of C−O Bonds over a Brominated Ruthenium Catalyst. *Angew. Chem. Int. Ed.* **2021**, 60 (22), 12513–12523.

47. B. Güvenatam, O. Kurşun, E.H.J. Heeres, E.A. Pidko, and E.J.M. Hensen. Hydrodeoxygenation of mono- and dimeric lignin model compounds on noble metal catalysts. *Catal. Today* **2014**, 233, 83–91.

48. M. Wang, H. Shi, D.M. Camaioni, and J.A. Lercher. Palladium-Catalyzed Hydrolytic Cleavage of Aromatic C−O Bonds. *Angew. Chem. Int. Ed.* **2017**, 56 (8), 2110–2114.

49. L. Zhang, Y. Wang, L. Zhang, Z. Chi, Y. Yang, Z. Zhang, B. Zhang, J. Lin, and S. Wan. Hydrogenolysis of Aryl Ether Bond over Heterogeneous Cobalt-Based Catalyst. *Ind. Eng. Chem. Res.* **2020**, 59 (39), 17357–17364.

50. R. Shu, B. Lin, J. Zhang, C. Wang, Z. Yang, and Y. Chen. Efficient catalytic hydrodeoxygenation of phenolic compounds and bio-oil over highly dispersed Ru/TiO_2. *Fuel Process. Technol.* **2019**, 184, 12–18.

51. X. Wang and R. Rinaldi. Bifunctional Ni catalysts for the one-pot conversion of Organosolv lignin into cycloalkanes. *Catal. Today* **2016**, 269, 48–55.

52. Y. Shao, Q. Xia, X. Liu, G. Lu, and Y. Wang. Pd/Nb_2O_5/SiO_2 Catalyst for the Direct Hydrodeoxygenation of Biomass-Related Compounds to Liquid Alkanes under Mild Conditions. *ChemSusChem* **2015**, 8 (10), 1761–1767.

53. W. Jiang, J.-P. Cao, C. Zhu, T. Xie, X.-Y. Zhao, M. Zhao, Y.-P. Zhao and H.-C. Bai. Selective cleavage of lignin-derived diphenyl ether C-O bond over weakly acidic Ni/Nb_2O_5 catalyst. *Fuel* **2021**, 295, 120635.

54. S. Jin, X. Chen, C. Li, C.-W. Tsang, G. Lafaye, and C. Liang. Hydrodeoxygenation of Lignin-derived Diaryl Ethers to Aromatics and Alkanes Using Nickel on Zr-doped Niobium Phosphate. *ChemistrySelect* **2016**, 1 (15), 4949–4956.

55. M. Thommes, K. Kaneko, A.V. Neimark, J. P. Olivier, F. Rodriguez-Reinoso, J. Rouquerol, and K.S.W. Sing. Physisorption of gases, with special reference to the evaluation of surface area and pore size distribution (IUPAC Technical Report). *Pure Appl. Chem.* **2015**, 87 (9–10), 1051–1069.

56. G. Pereira Costa, R.A. Rafael, J.C.S. Soares, and A.B. Gaspar. Synthesis and characterization of ZnO-Nb_2O_5 catalysts for photodegradation of bromophenol blue. *Catal. Today.* **2020**, 344, 240–246.

57. P. Betancourt, A. Rives, R. Hubaut, C.E. Scott, and J. Goldwasser. A study of ruthenium alumina system. *Appl. Catal.* C. **1998**, 170, 307-314.

58. K.V.R. Chary and C.S. Srikanth. Selective Hydrogenation of Nitrobenzene to Aniline over Ru/SBA-15 Catalysts. *Catal Lett.* **2009**, 128 (1–2), 164–170.

59. W. Tolek, N. Nanthasanti, B. Pongthawornsakun, P. Praserthdam, and J. Panpranot. Effects of TiO_2 structure and Co addition as a second metal on Ru-based catalysts supported on TiO_2 for selective hydrogenation of furfural to FA. *Sci Rep* **2021**, 11 (1), 9786.

60. C.A. Teles, R.C. Rabelo-Neto, J.R. de Lima, L.V. Mattos, D.E. Resasco, and F.B. Noronha. The Effect of Metal Type on Hydrodeoxygenation of Phenol Over Silica Supported Catalysts. *Catal Lett* **2016**, 146 (10), 1848–1857.

61. M.K. Kidder, P.F. Britt, and A.C. Buchanan. Pyrolysis of Benzyl Phenyl Ether Confined in Mesoporous Silica. *Energy Fuels* **2006**, 20 (1), 54–60.

62. J. Greeley and J.K. Nørskov. A general scheme for the estimation of oxygen binding energies on binary transition metal surface alloys. *Surf. Sci.* **2005**, 592 (1–3), 104–111.

63. N. Duong, Q. Tan, and D.E. Resasco. Controlling phenolic hydrodeoxygenation by tailoring metal–O bond strength via specific catalyst metal type and particle size selection. *C. R. Chim.* **2018**, 21 (3–4), 155–163.

64. Q. Tan, G. Wang, L. Nie, A. Dinse, C. Buda, J. Shabaker, and D. E. Resasco. Different Product Distributions and Mechanistic Aspects of the Hydrodeoxygenation of m-Cresol over Platinum and Ruthenium Catalysts. *ACS Catal.* **2015**, 5 (11), 6271–6283.

65. S. Liu, H. Wang, K.J. Smith, and C.S. Kim. Hydrodeoxygenation of 2-Methoxyphenol over Ru, Pd, and Mo_2C Catalysts Supported on Carbon. *Energy Fuels* **2017**, 31 (6), 6378–6388.

66. C. Zhao, J. He, A.A. Lemonidou, X. Li, and J.A. Lercher. Aqueous-phase hydrodeoxygenation of bio-derived phenols to cycloalkanes. *J. Catal.* **2011**, 280 (1), 8–16.

67. N. Zheng, J.C. McWilliams, F.J. Fleitz, J.D. Armstrong, and R.P. Volante. Palladium-Catalyzed Synthesis of Aryl Sulfides from Aryl Triflates. *J. Org. Chem.* **1998**, 63 (26), 9606–9607.

68. Y. He, L. Yan, Y. Liu, Y. Liu, Y. Bai, J. Wang, and F. Li. Effect of SiO_2/Al_2O_3 ratios of HZSM-5 zeolites on the formation of light aromatics during lignite pyrolysis. *Fuel Process. Technol.* **2019**, 188, 70–78.

69. P.M. de Souza, L.A. de Sousa, F.B. Noronha, and R. Wojcieszak. Dehydration of levoglucosan to levoglucosenone over solid acid catalysts. Tuning the product distribution by changing the acid properties of the catalysts. *Mol. Catal.* **2022**, 9.

70. M.A. den Hollander, M. Wissink, M. Makkee, and J.A. Moulijn. Gasoline conversion: reactivity towards cracking with equilibrated FCC and ZSM-5 catalysts. *Appl. Catal. A.* **2002**, 223 (1–2), 85–102.

71. A. Villa, D. Wang, G.M. Veith, F. Vindigni, and L. Prati. Sol immobilization technique: a delicate balance between activity, selectivity and stability of gold catalysts. *Catal. Sci. Technol.* **2013**, 3 (11), 3036.

72. C.P. Ferraz, M. Zieliński, M. Pietrowski, S. Heyte, F. Dumeignil, L. M. Rossi, and R. Wojcieszak. Influence of Support Basic Sites in Green Oxidation of Biobased Substrates Using Au-Promoted Catalysts. *ACS Sustain. Chem. Eng.* **2018**, 6 (12), 16332–16340.

73. E. Monti, A. Ventimiglia, C.A. Garcia Soto, F. Martelli, E. Rodriguez-Aguado, J. A. Cecilia, A. Sadier, F. Ospitali, T. Tabanelli, S. Albonetti, F. Cavani, R. Wojcieszak, and N. Dimitratos. Effect of the Colloidal Preparation Method for Supported Preformed Colloidal Au Nanoparticles for the Liquid Phase Oxidation of 1,6-Hexanediol to Adipic Acid. *Catalyst.s* **2022**, 12 (2), 196.

74. C.A. Teles, R.C. Rabelo-Neto, N, Duong, J. Quiroz, P.H.C. Camargo, G. Jacobs, D. E. Resasco, and F.B. Noronha. Role of the metal-support interface in the hydrodeoxygenation reaction of phenol. *Appl. Catal. B.* **2020**, 270, 119238.

75. T. Nimmanwudipong, R.C. Runnebaum, K. Tay, D.E. Block, and B.C. Gates. Cyclohexanone Conversion Catalyzed by $Pt/\gamma\text{-}Al_2O_3$: Evidence of Oxygen Removal and Coupling Reactions. *Catal Lett.* **2011**, 141 (8), 1072–1078.

76. C. Zhao, W. Song, and J.A. Lercher. Aqueous Phase Hydroalkylation and Hydrodeoxygenation of Phenol by Dual Functional Catalysts Comprised of Pd/C and H/La-BEA. *ACS Catal.* **2012**, 2 (12), 2714–2723.

77. X. Zhang, T. Wang, L. Ma, Q. Zhang, X. Huang, and Y. Yu. Production of cyclohexane from lignin degradation compounds over Ni/ZrO_2–SiO_2 catalysts. *Appl. Energy* **2013**, 112, 533–538.

78. C. Zhao, J. He, A.A. Lemonidou, X. Li, and J.A. Lercher. Aqueous-phase hydrodeoxygenation of bio-derived phenols to cycloalkanes. *J. Catal.* **2011**, 280 (1), 8–16.

79. D.-Y. Hong, S.J. Miller, P.K. Agrawal, and C.W. Jones. Hydrodeoxygenation and coupling of aqueous phenolics over bifunctional zeolite-supported metal catalysts. *Chem. Commun.* **2010**, 46 (7), 1038–1040.

80. B. Pawelec, C.V. Loricera, C. Geantet, N. Mota, J.L.G. Fierro, and R.M. Navarro. Factors influencing selectivity in the liquid-phase phenol hydrodeoxygenation over ZSM-5 supported Pt/Ir and Pt+Ir catalysts. *Mol. Catal.* **2020**, 482, 110669.

81. A.M. Barrios, C.A. Teles, P.M. de Souza, R.C. Rabelo-Neto, M.B. Griffin, C. Mukarakate, K.A. Orton, D.E. Resasco, and F.B. Noronha. Hydrodeoxygenation of phenol over niobia supported Pd catalyst. *Catal. Today* **2018**, 302, 115–124.

82. C.A. Teles, P.M. de Souza, R.C. Rabelo-Neto, M.B. Griffin, C. Mukarakate, K.A. Orton, D.E. Resasco, and F.B. Noronha. Catalytic upgrading of biomass pyrolysis vapors and model compounds using niobia supported Pd catalyst. *Appl. Catal. B.* **2018**, 238, 38–50.

83. T.M. Sankaranarayanan, A. Berenguer, C. Ochoa-Hernández, I. Moreno, P. Jana, J.M. Coronado, D.P. Serrano, and P. Pizarro. Hydrodeoxygenation of anisole as bio-oil model compound over supported Ni and Co catalysts: Effect of metal and support properties. *Catal. Today* **2015**, 243, 163–172.

84. T.N. Phan, Y.-K. Park, I.-G. Lee, and C.H. Ko. Enhancement of C-O bond cleavage to afford aromatics in the hydrodeoxygenation of anisole over ruthenium-supporting mesoporous metal oxides. *Appl. Catal. A.* **2017**, 544, 84–93.

85. N.S. Nesterov, A.A. Smirnov, V.P. Pakharukova, V.A. Yakovlev, and O.N. Martyanov. Advanced green approaches for the synthesis of NiCu-containing catalysts for the hydrodeoxygenation of anisole. *Catal. Today* **2021**, 379, 262–271.

86. W. Song, Y. He, S. Lai, X. Yi, W. Yang, and X. Jiang. Selective hydrodeoxygenation of lignin phenols to alcohols in the aqueous phase over a hierarchical Nb_2O_5-supported Ni catalyst. *Green Chem.* **2020**, 22 (5), 1662–1670.

87. C. Liu, Z. Shao, Z. Xiao, C.T. Williams, and C. Liang. Hydrodeoxygenation of Benzofuran over Silica−Alumina-Supported Pt, Pd, and Pt-Pd catalysts. *Energy Fuels*. **2012**, 26, 4205-4211.

Annexes

Annex 1 TYPICAL CHROMATOGRAMS AND MASS SPECTRA

Reagents and products were identified and quantified by the chromatographic method described in Chapter 3. The fragmentation standards were obtained from the NIST Mass Spectrometry Data Center.

Figs. A1.1 and A1.2 show a typical chromatogram of the reaction charge containing 62 mmol of benzyl phenyl ether in decalin; and the reaction products over $Pd/Nb_2O_{5\text{-col}}$, respectively.

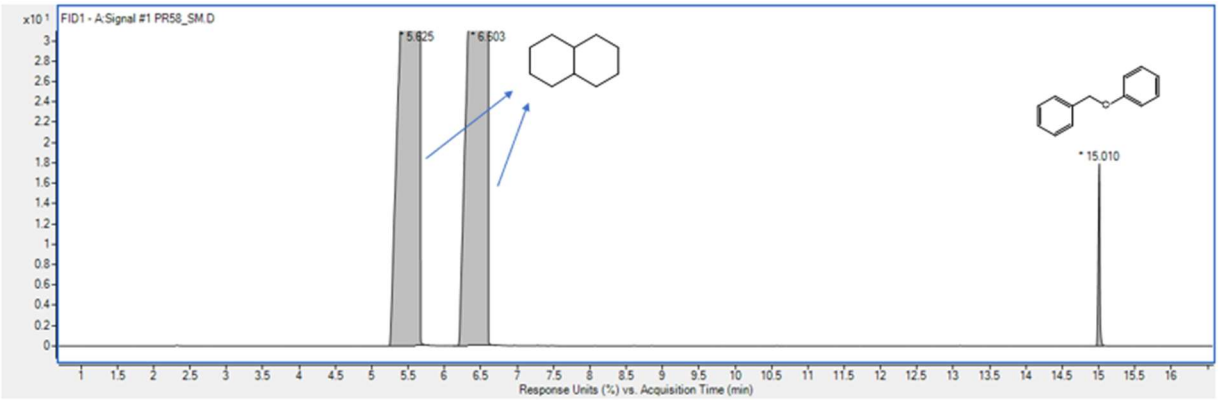

Figure A1.1: Chromatogram of the reaction charge containing 62 mmol of benzyl phenyl ether in decalin.

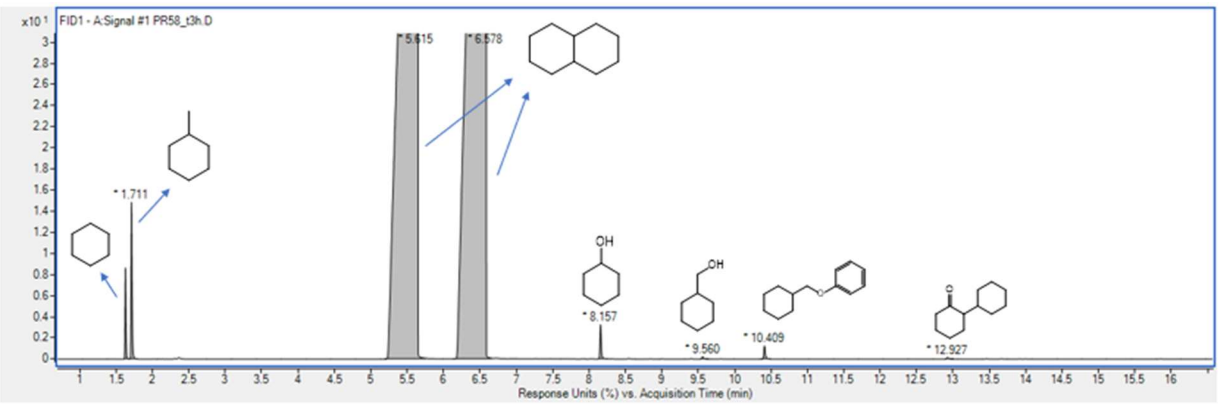

Figure A1.2: Chromatogram of reaction products for the hydrodeoxygenation of benzyl phenyl ether over Pd/Nb_2O_5-col.

The chromatograms and mass spectra of each feedstock and of the main products for the hydrodeoxygenation reaction are presented in figs. A1.3-A1.40.

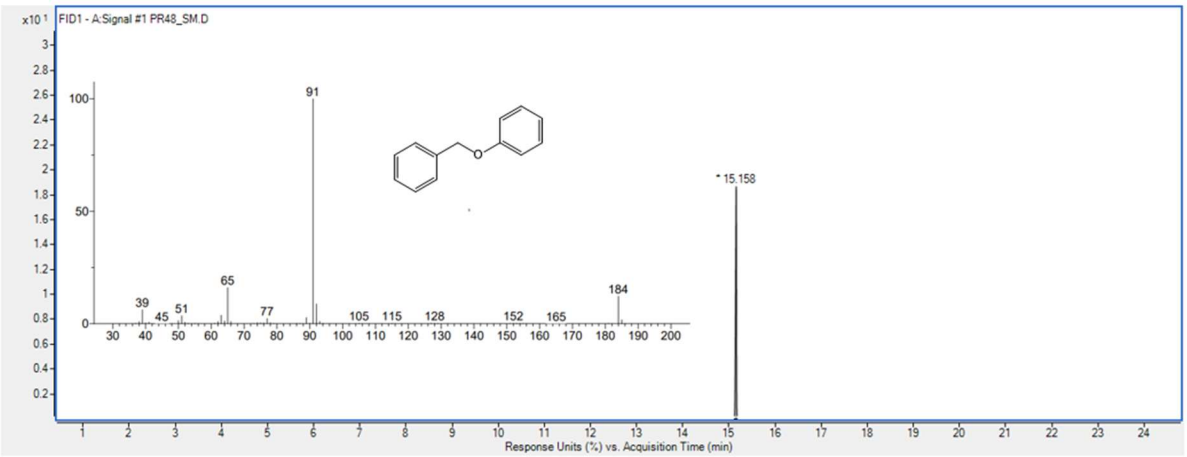

Figure A1.3: Typical chromatogram and mass spectrum of benzyl phenyl ether

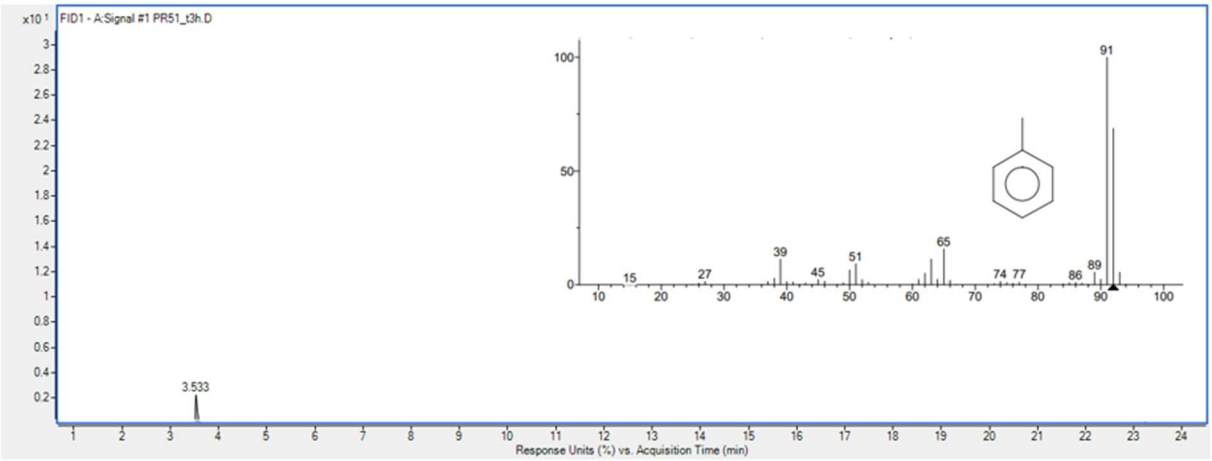

Figure A1.4: Typical chromatogram and mass spectrum of toluene

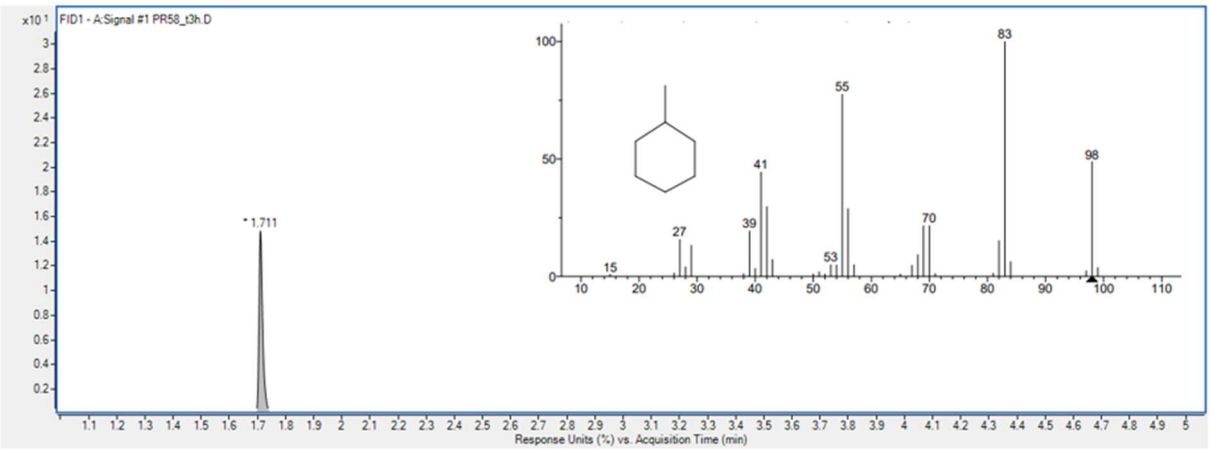

Figure A1.5: Typical chromatogram and mass spectrum of methylcyclohexane.

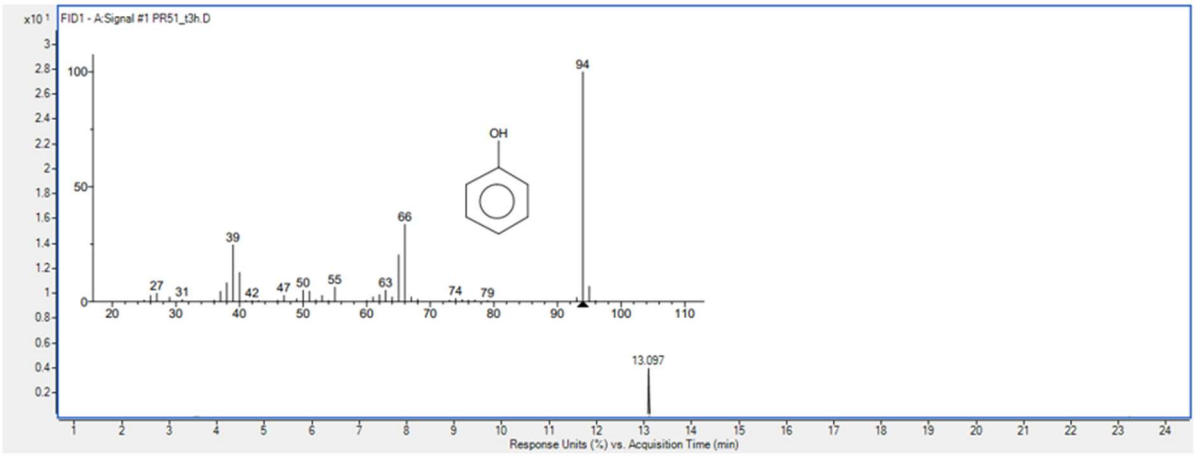

Figure A1.6: Typical chromatogram and mass spectrum of phenol.

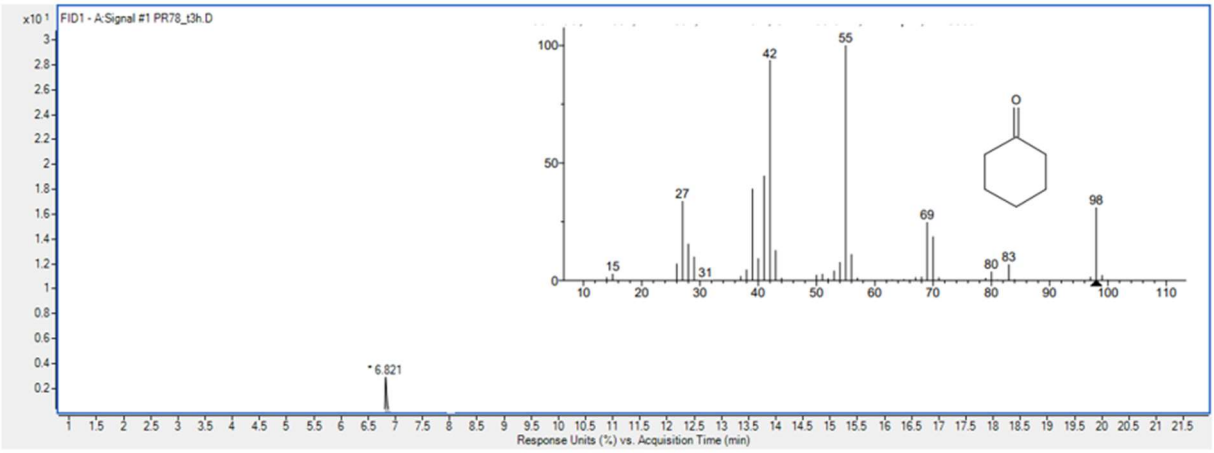

Figure A1.7: Typical chromatogram and mass spectrum of cyclohexanone.

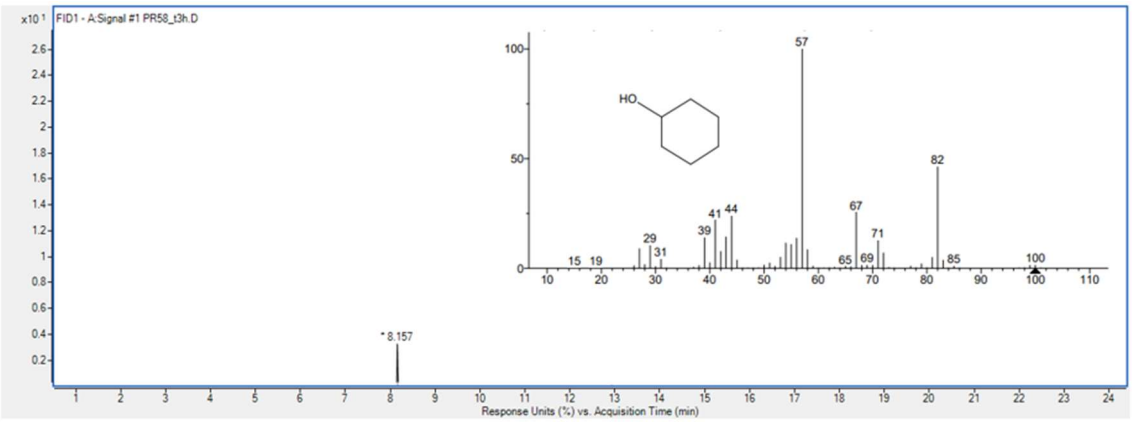

Figure A1.8: Typical chromatogram and mass spectrum of cyclohexanol.

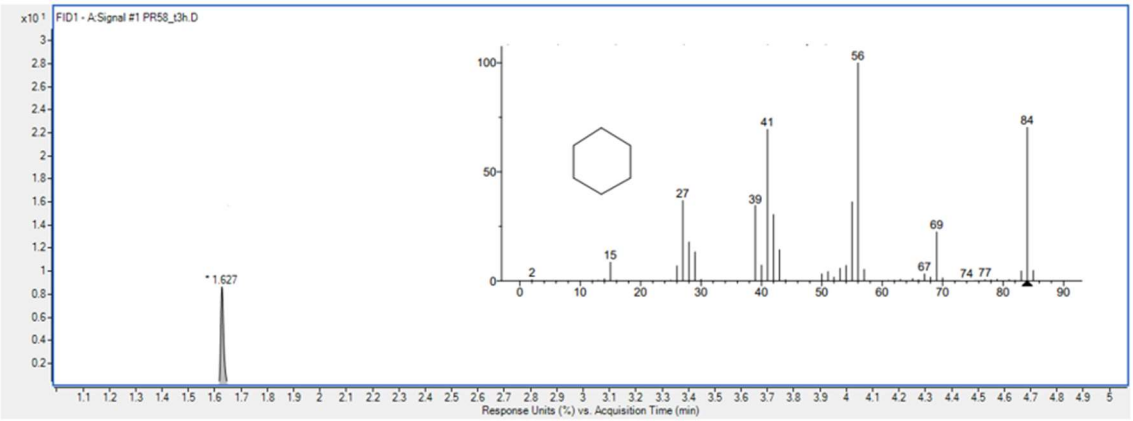

Figure A1.9: Typical chromatogram and mass spectrum of cyclohexane.

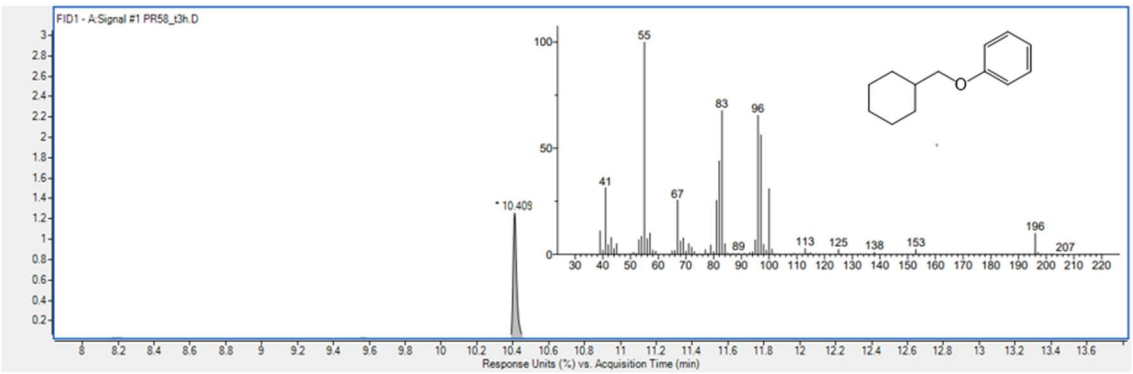

Figure A1.10: Typical chromatogram and mass spectrum of (cyclohexylmethoxy)benzene.

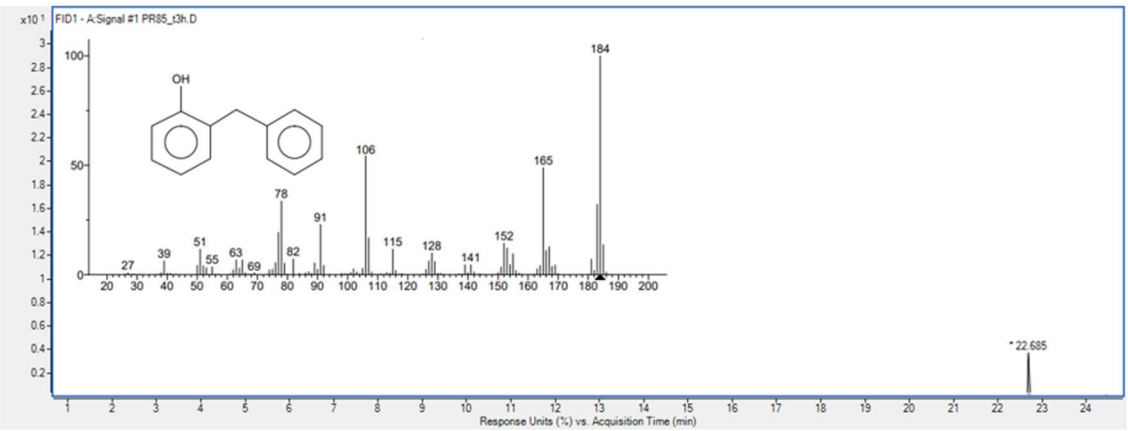

Figure A1.11: Typical chromatogram and mass spectrum of 2-benzylphenol.

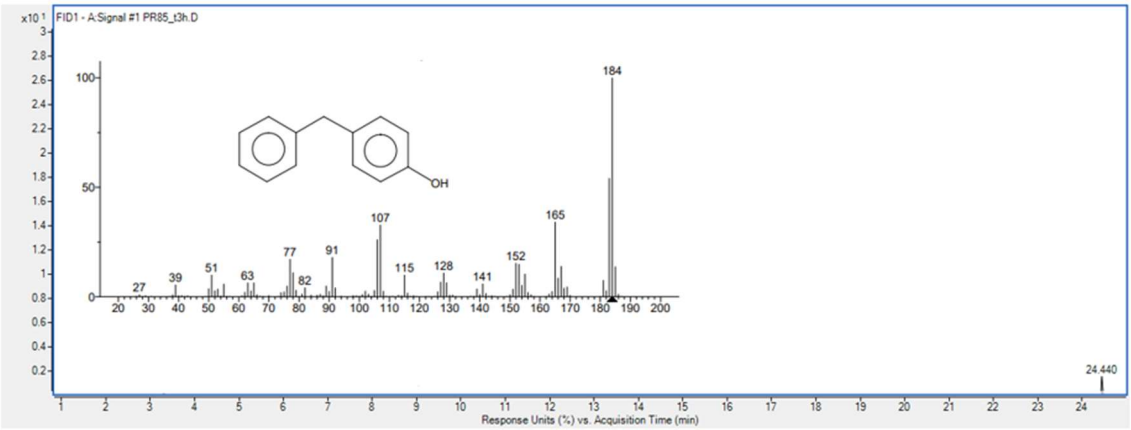

Figure A1.12: Typical chromatogram and mass spectrum of 4-benzylphenol.

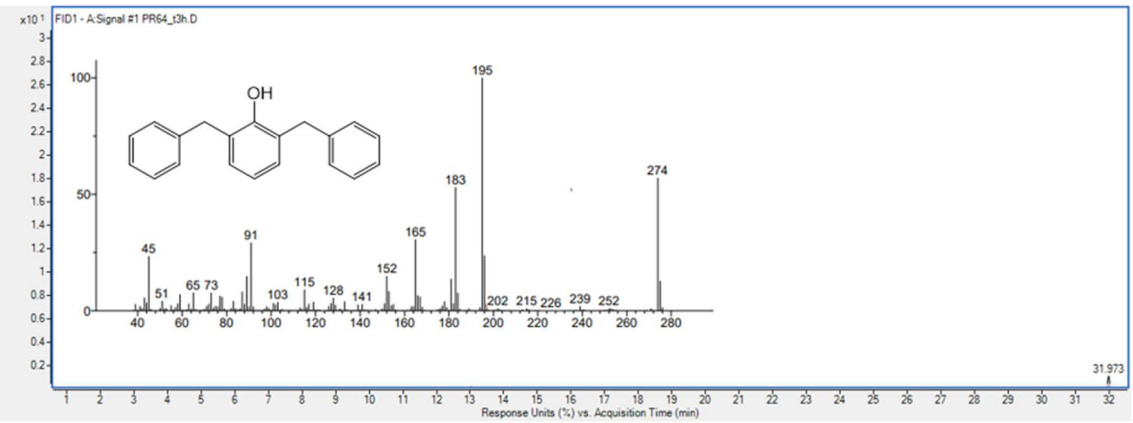

Figure A1.13: Typical chromatogram and mass spectrum of 2,6-dibenzylphenol.

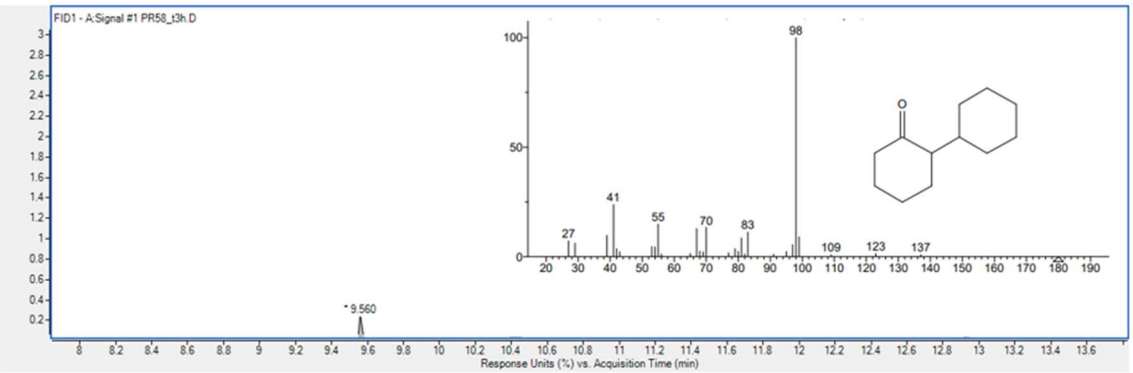

Figure A1.14: Typical chromatogram and mass spectrum of 1,1-bicyclohexyl-2-one.

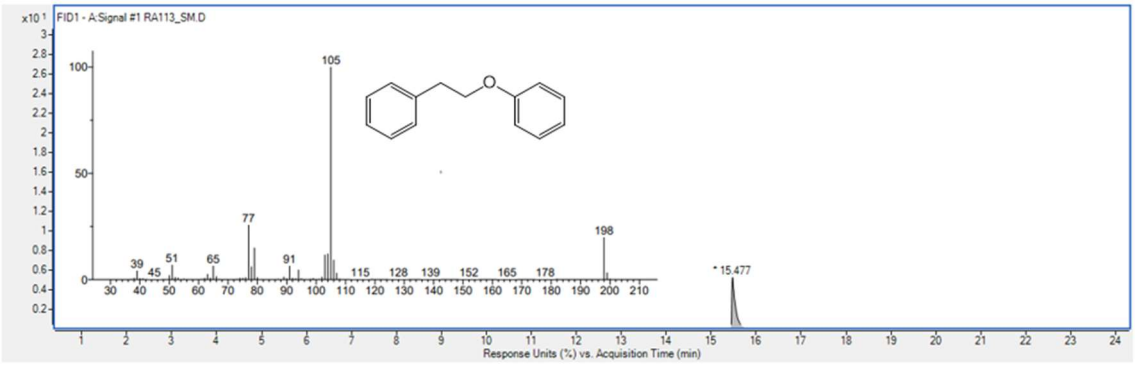

Figure A1.15: Typical chromatogram and mass spectrum of phenethoxybenzene.

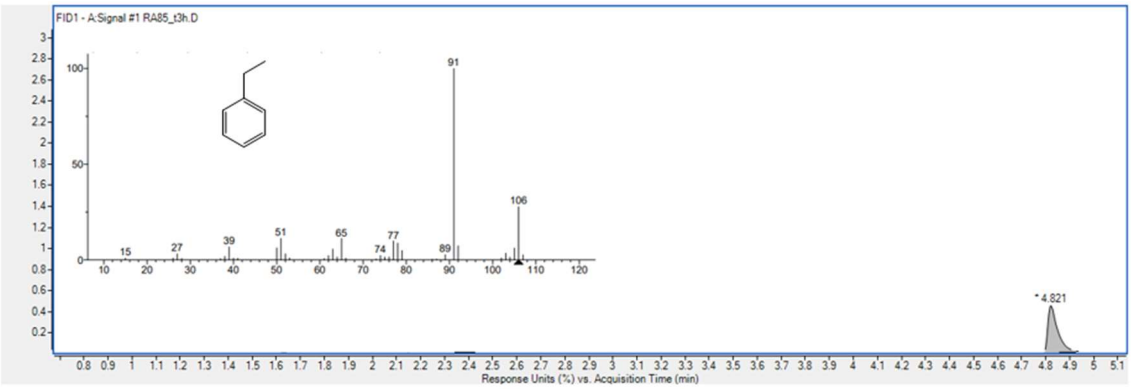

Figure A1.16: Typical chromatogram and mass spectrum of ethylbenzene.

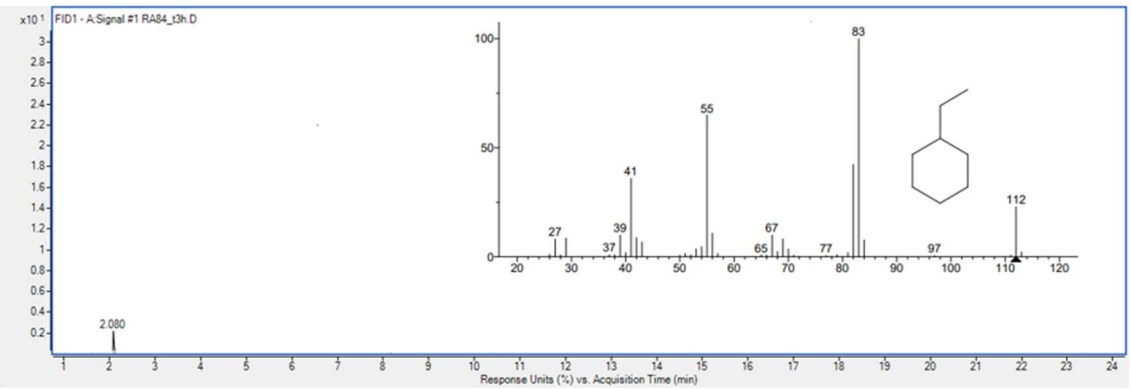

Figure A1.17: Typical chromatogram and mass spectrum of ethylcyclohexane.

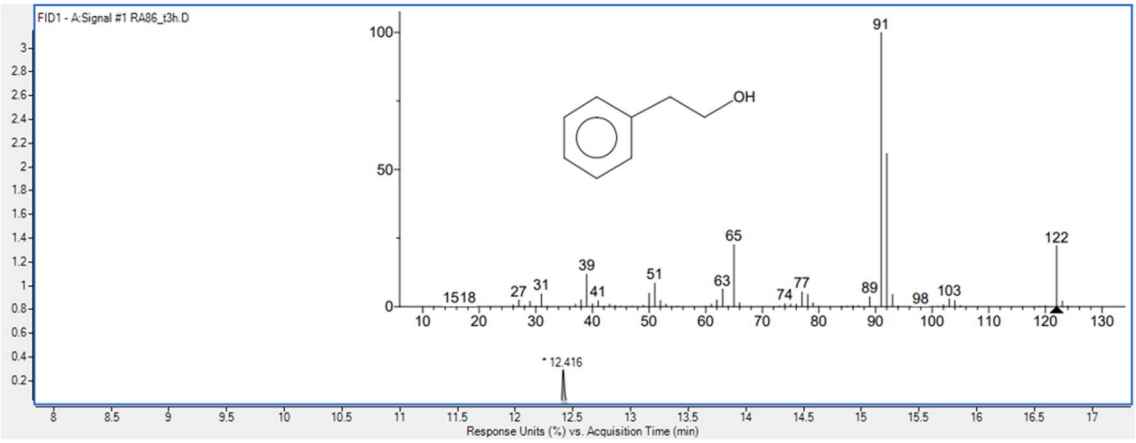

Figure A1.18: Typical chromatogram and mass spectrum of phenylethanol.

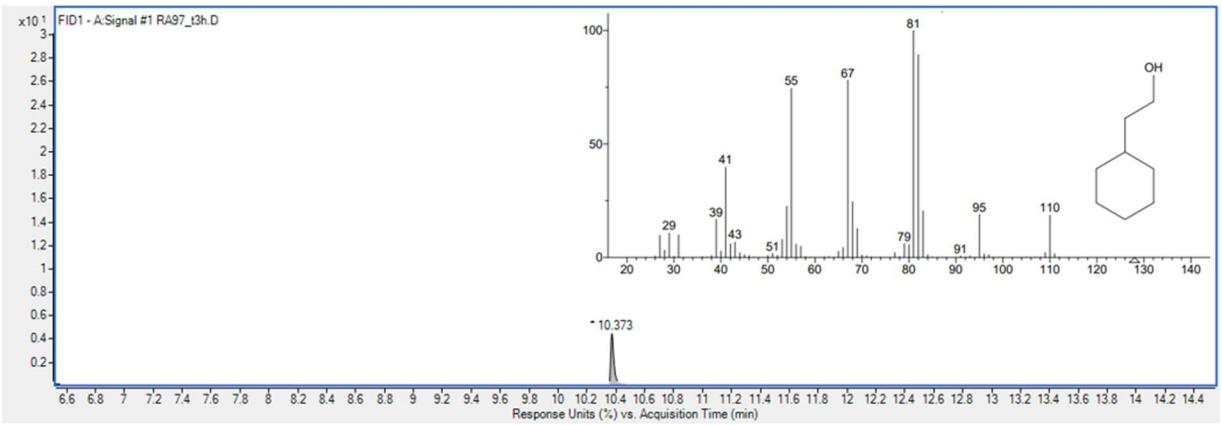

Figure A1.19: Typical chromatogram and mass spectrum of cyclohexylethanol.

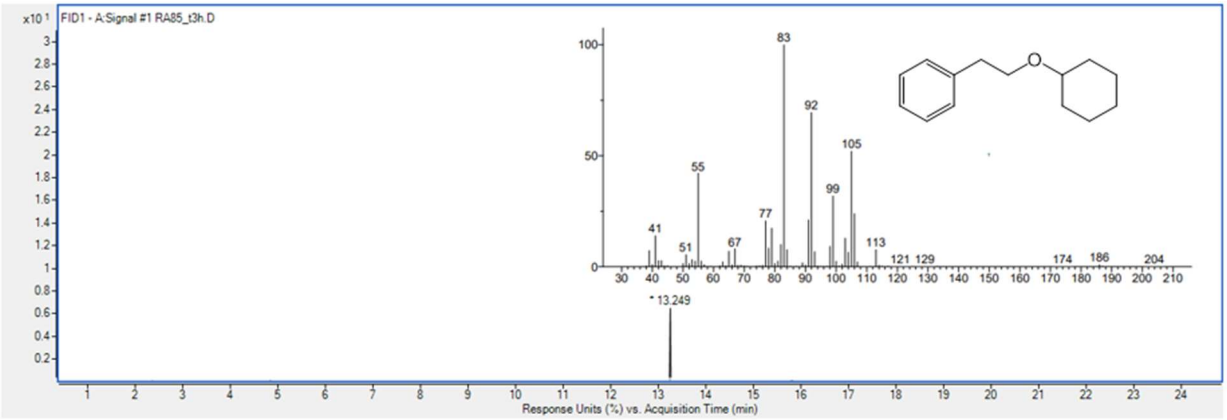

Figure A1.20: Typical chromatogram and mass spectrum of (2-(cyclohexyloxy) ethyl) benzene.

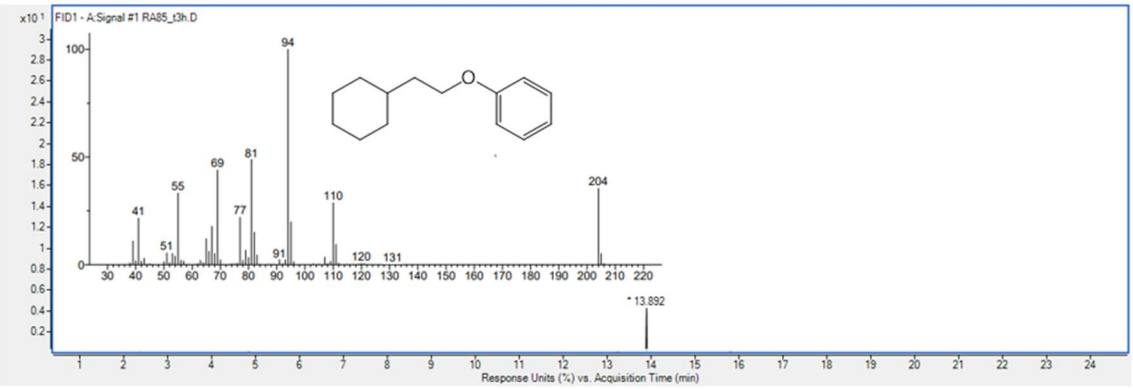

Figure A1.21: Typical chromatogram and mass spectrum of (2-(cyclohexylethoxy) benzene.

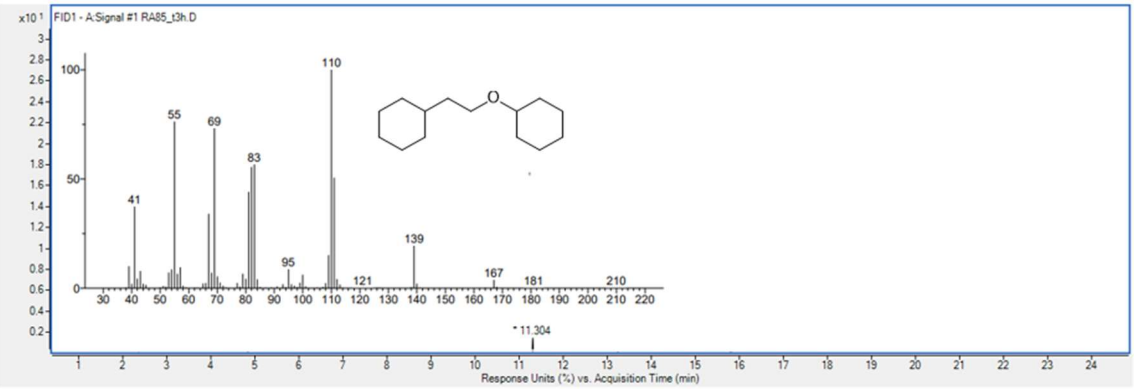

Figure A1.22: Typical chromatogram and mass spectrum of (2-cyclohexylethoxy) cyclohexane.

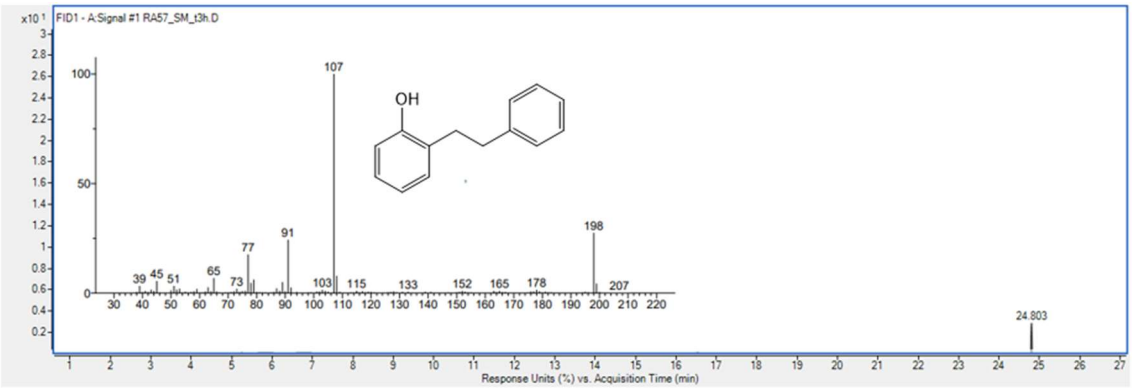

Figure A1.23: Typical chromatogram and mass spectrum of 2-phenethylphenol.

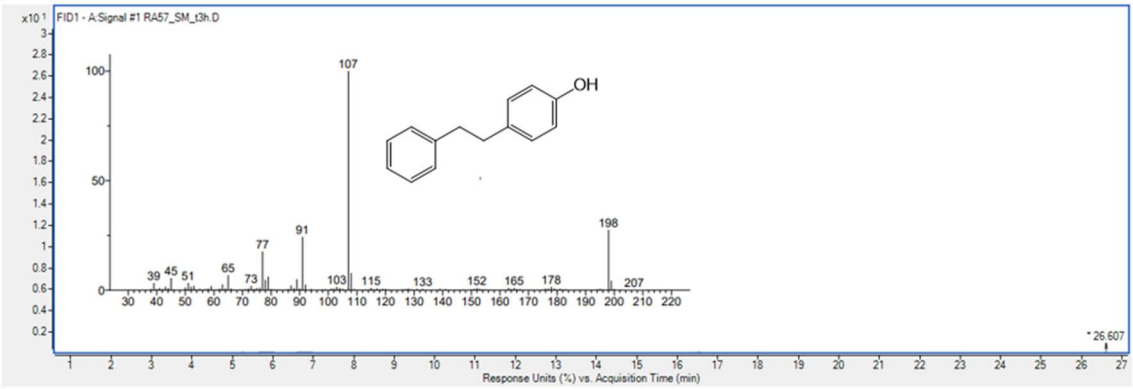

Figure A1.24: Typical chromatogram and mass spectrum of 4-phenethylphenol.

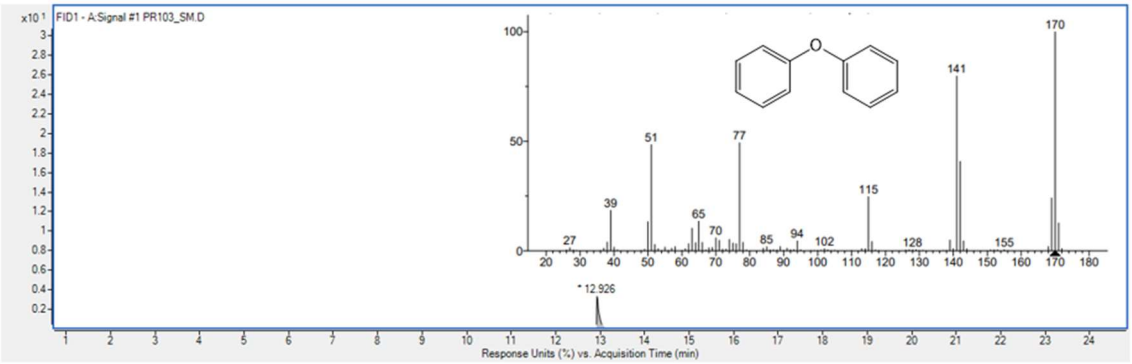

Figure A1.25: Typical chromatogram and mass spectrum of diphenyl ether.

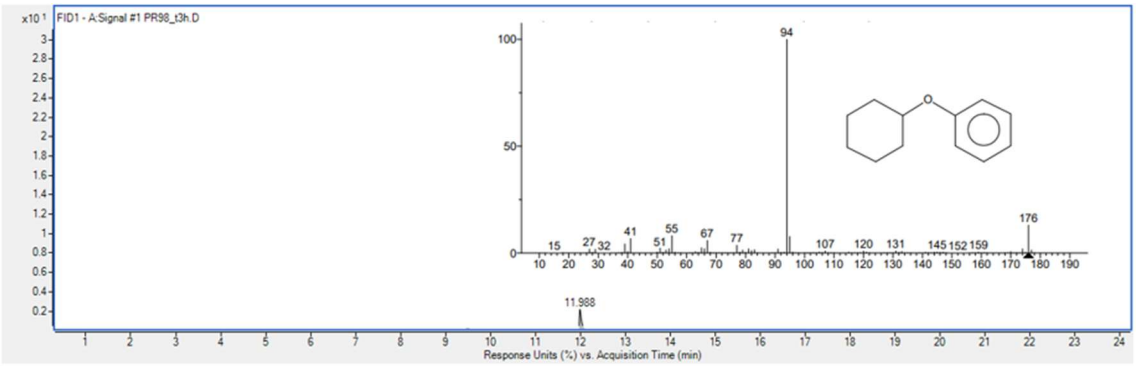

Figure A1.26: Typical chromatogram and mass spectrum of cyclohexyl phenyl ether.

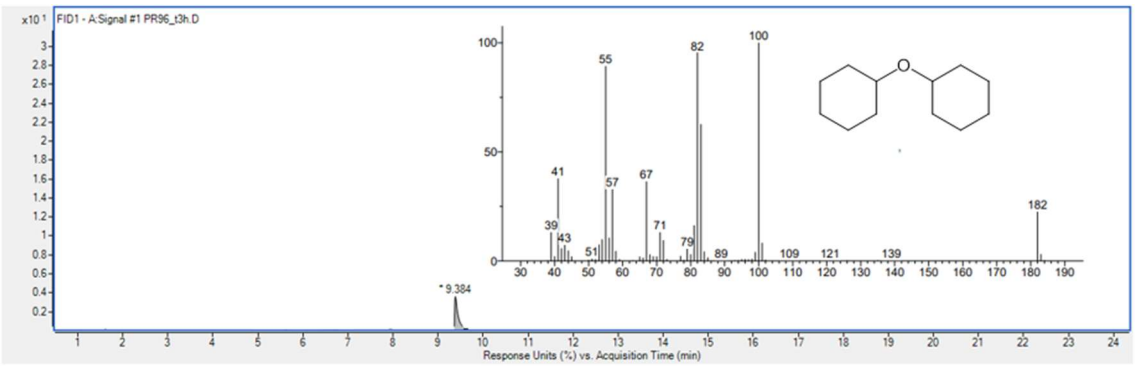

Figure A1.27: Typical chromatogram and mass spectrum of dicyclohexyl ether.

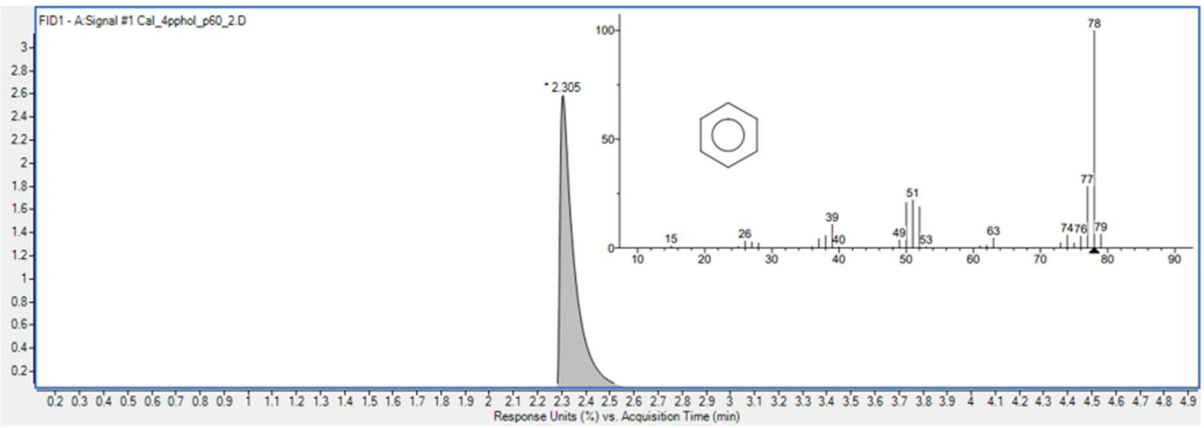

Figure A1.28: Typical chromatogram and mass espectrum of benzene.

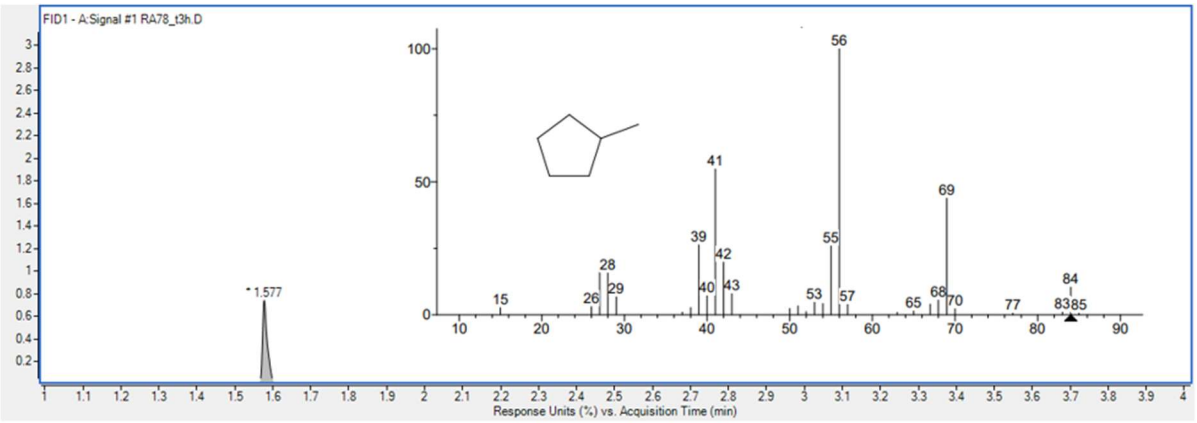

Figure A1.29: Typical chromatogram and mass espectrum of methyl cyclopentane.

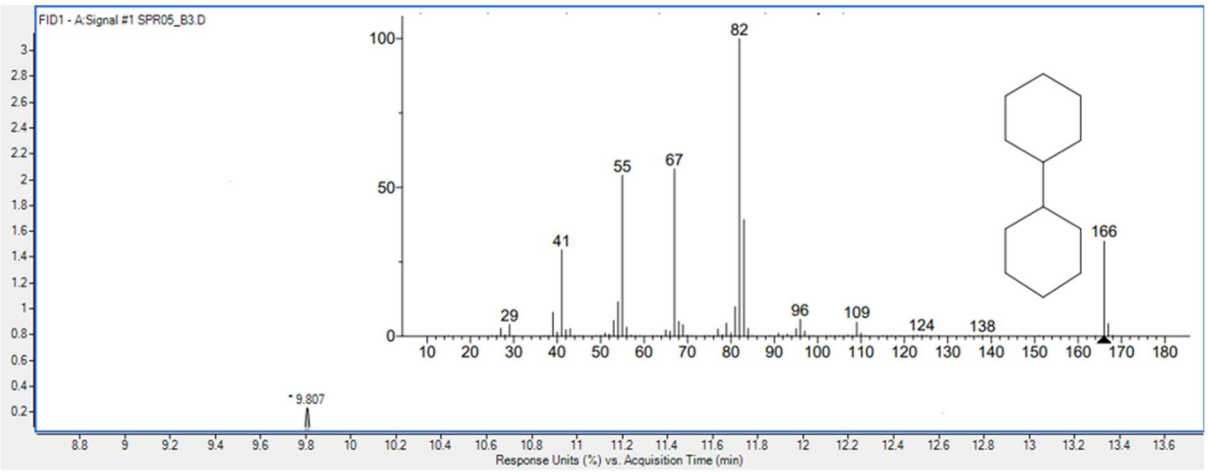

Figure A1.30: Typical chromatogram and mass spectrum of bicyclohexyl.

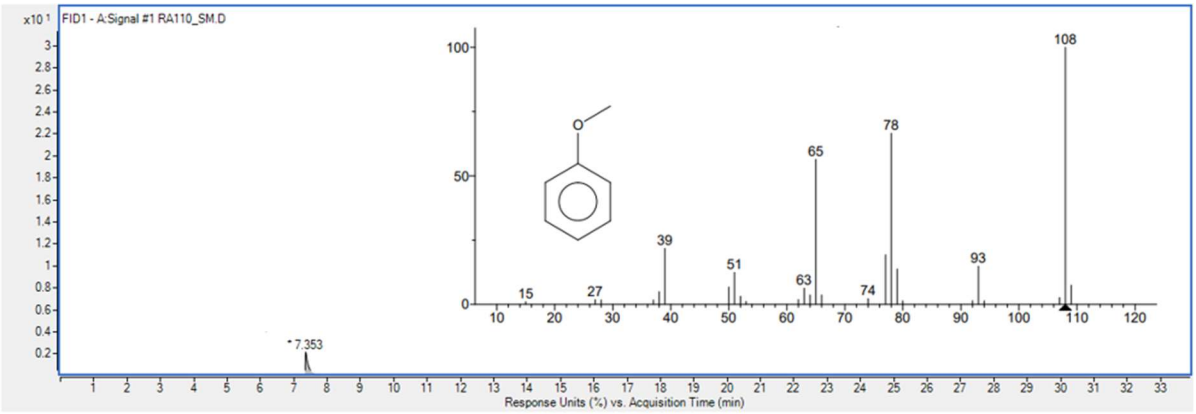

Figure A1.31: Typical chromatogram and mass spectrum of anisole.

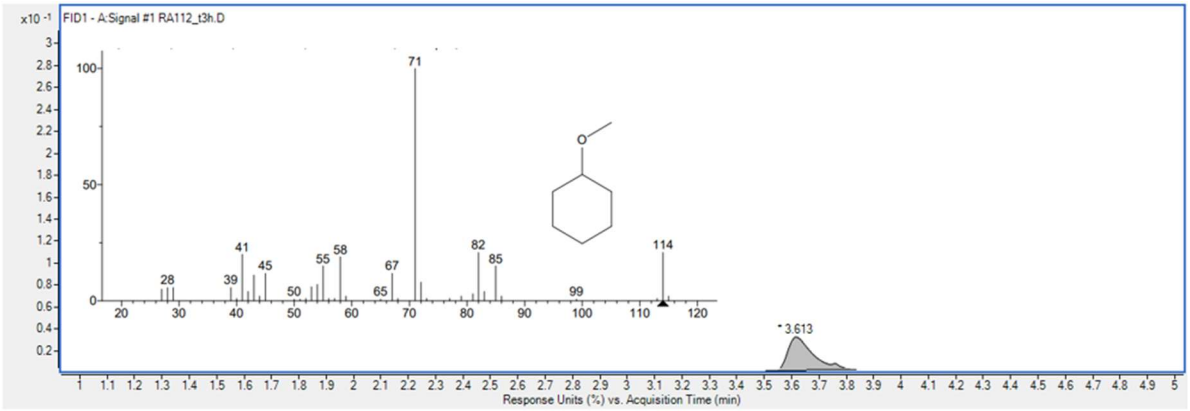

Figure A1.32: Typical chromatogram and mass spectrum of methoxycylohexane.

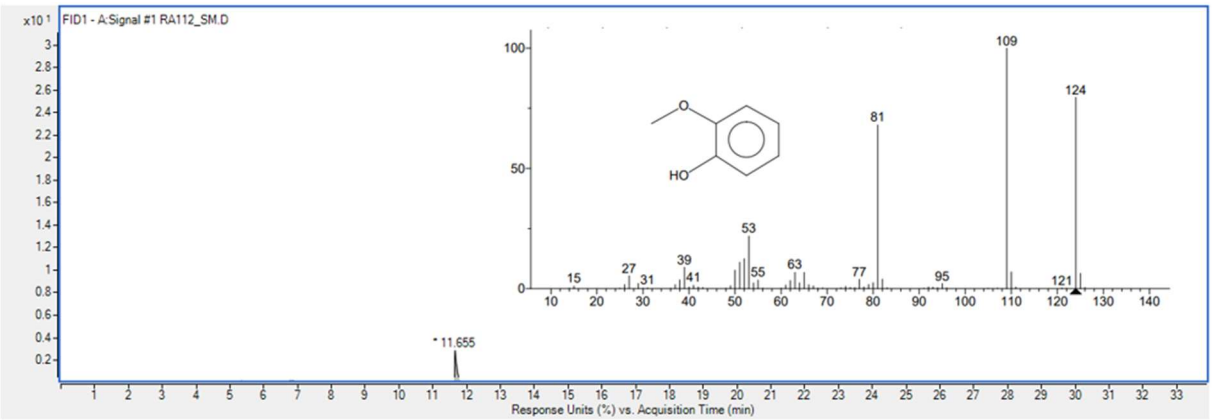

Figure A1.33: Typical chromatogram and mass spectrum of guaiacol.

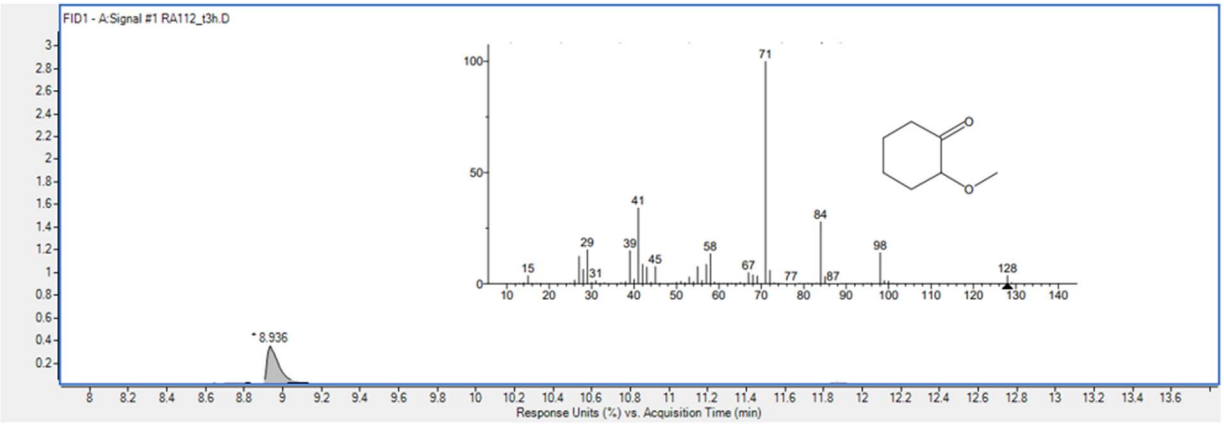

Figure A1.34: Typical chromatogram and mass spectrum of 2-methoxycyclohexanone.

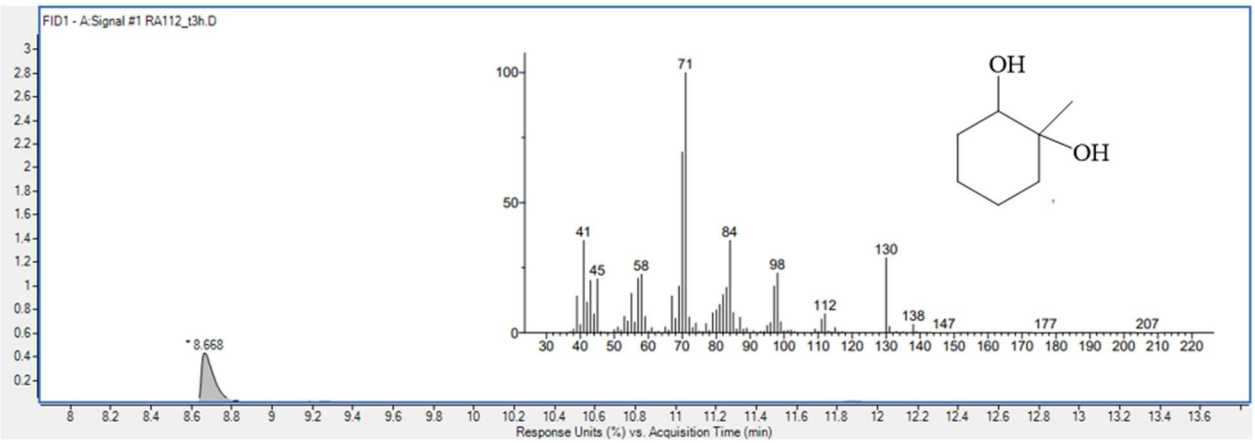

Figure A1.35: Typical chromatogram and mass spectrum of 1-methyl-1,2-cyclohexanediol.

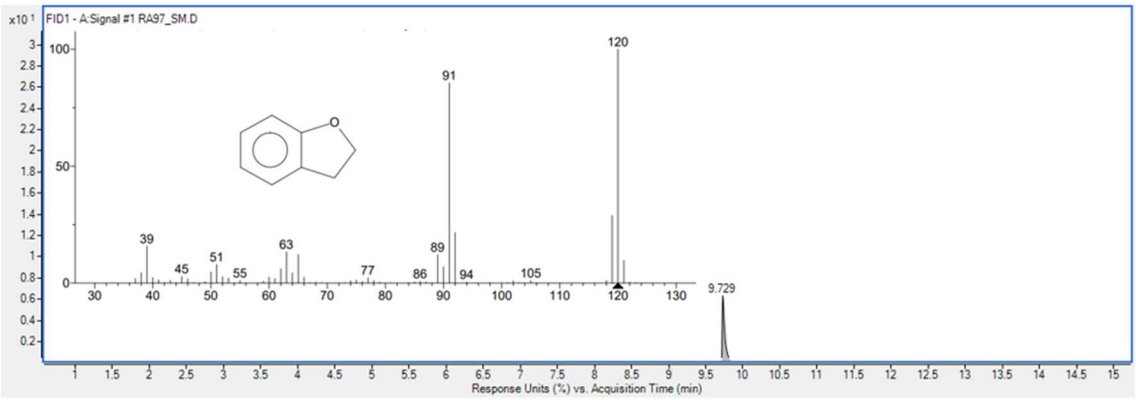

Figure A1.36: Typical chromatogram and mass spectrum of 2,3-Dihydrobenzofuran.

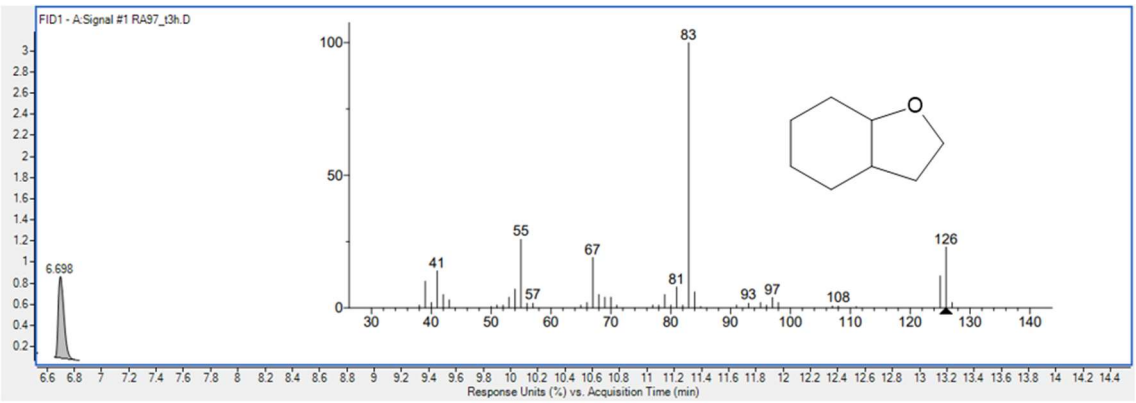

Figure A1.37: Typical chromatogram and mass spectrum of octahydro-1-benzofuran.

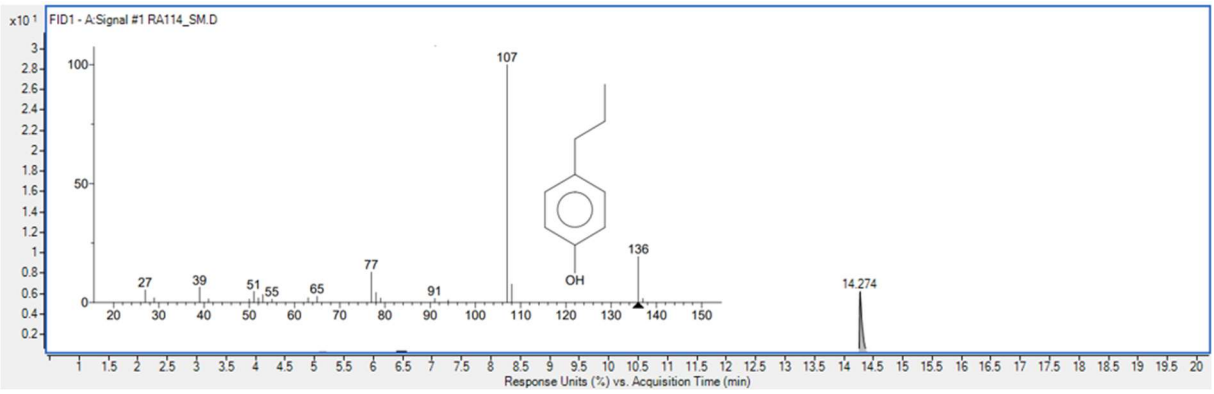

Figure A1.38: Typical chromatogram and mass spectrum of 4-propylphenol.

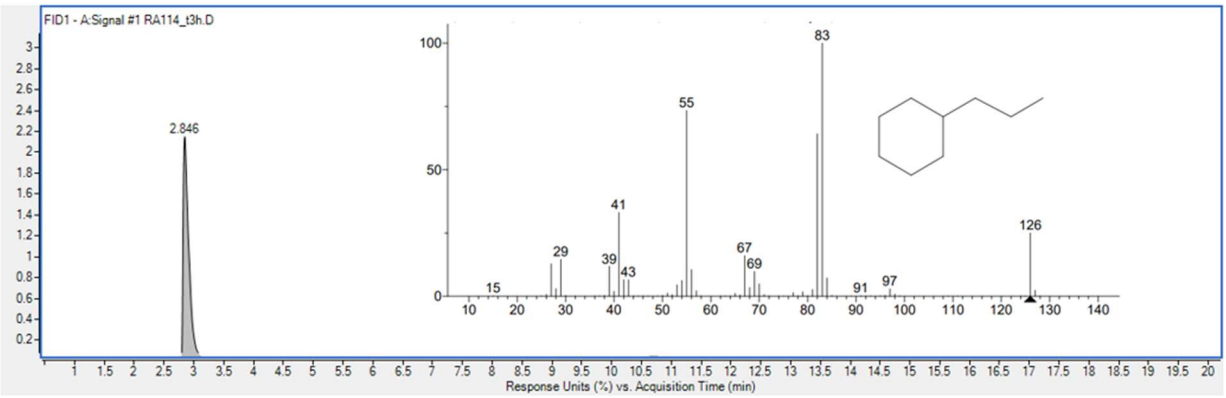

Figure A1.39: Typical chromatogram and mass espectrum of propylcyclohexane.

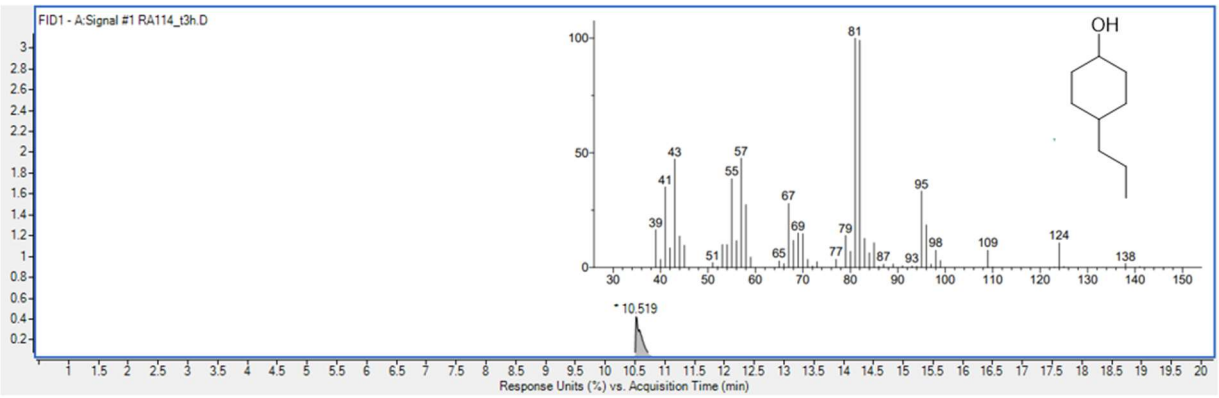

Figure A1.40: Typical chromatogram and mass espectrum of 4-propyl cyclohexanol.

Annex 2 NITROGEN ADSORPTION-DESORPTION ISOTHERMS

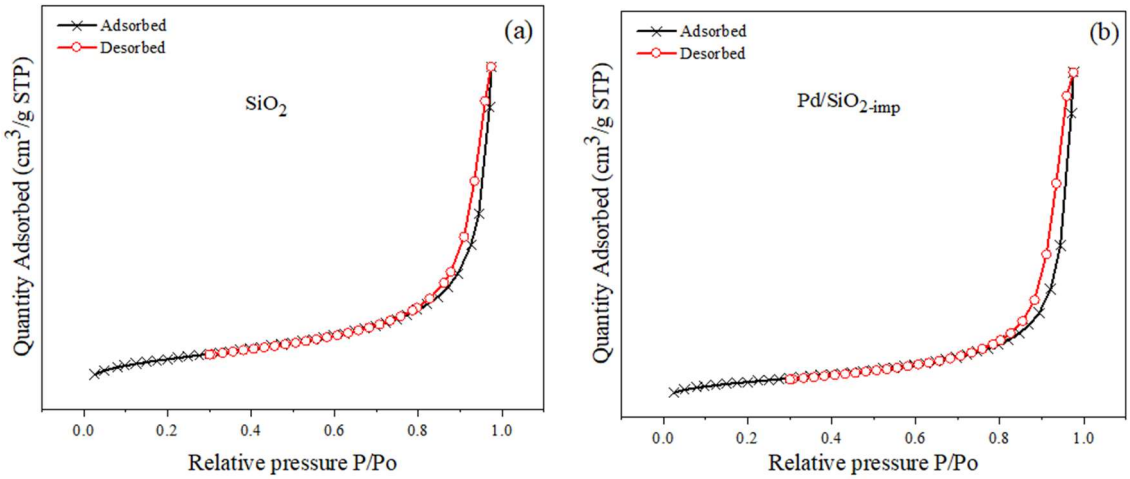

Figure A2.1: Isotherm N_2 adsorption-desorption of (a) SiO_2 and (b) $Pd/SiO_{2\text{-imp}}$.

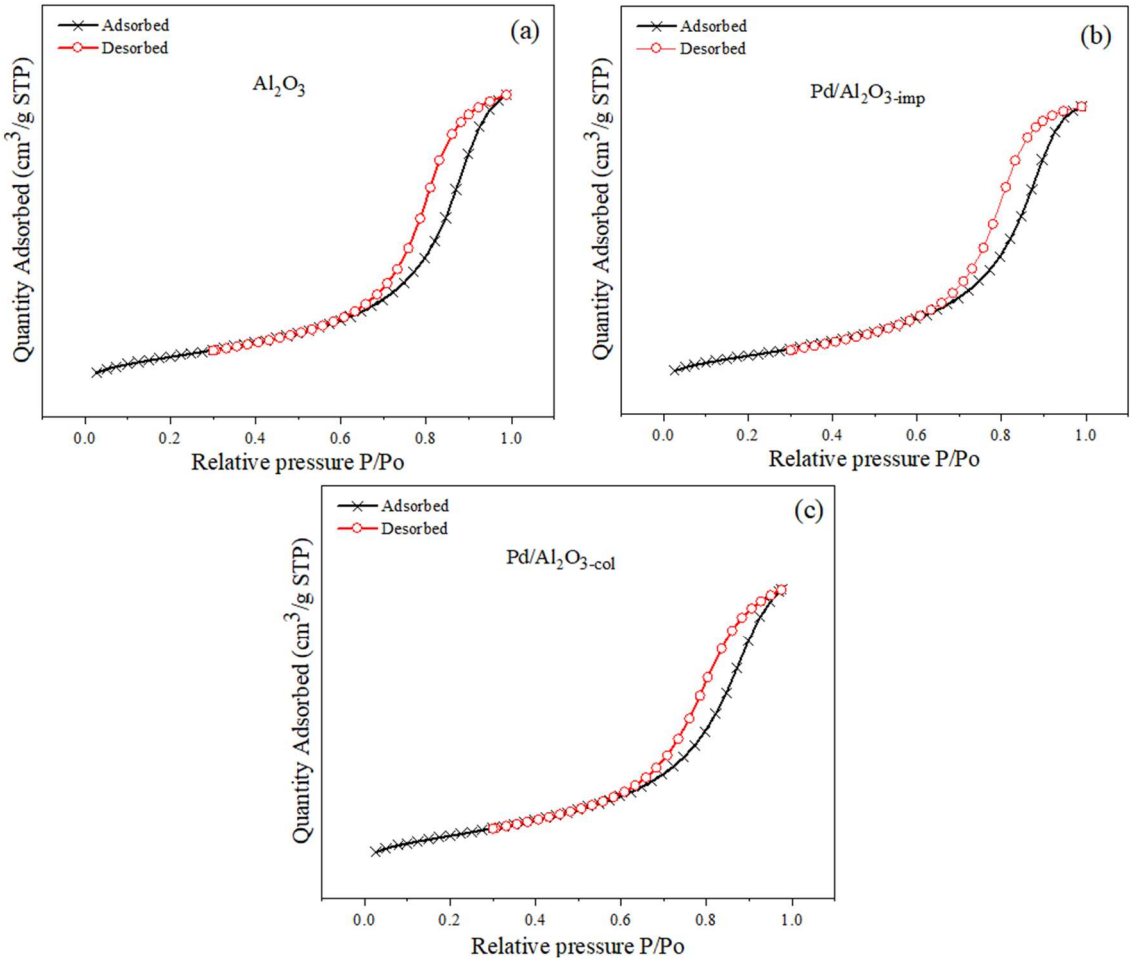

Figure A2.2: Isotherm N_2 adsorption-desorption of (a) Al_2O_3, (b) $Pd/Al_2O_{3\text{-imp}}$, and (c) $Pd/Al_2O_{3\text{-col}}$.

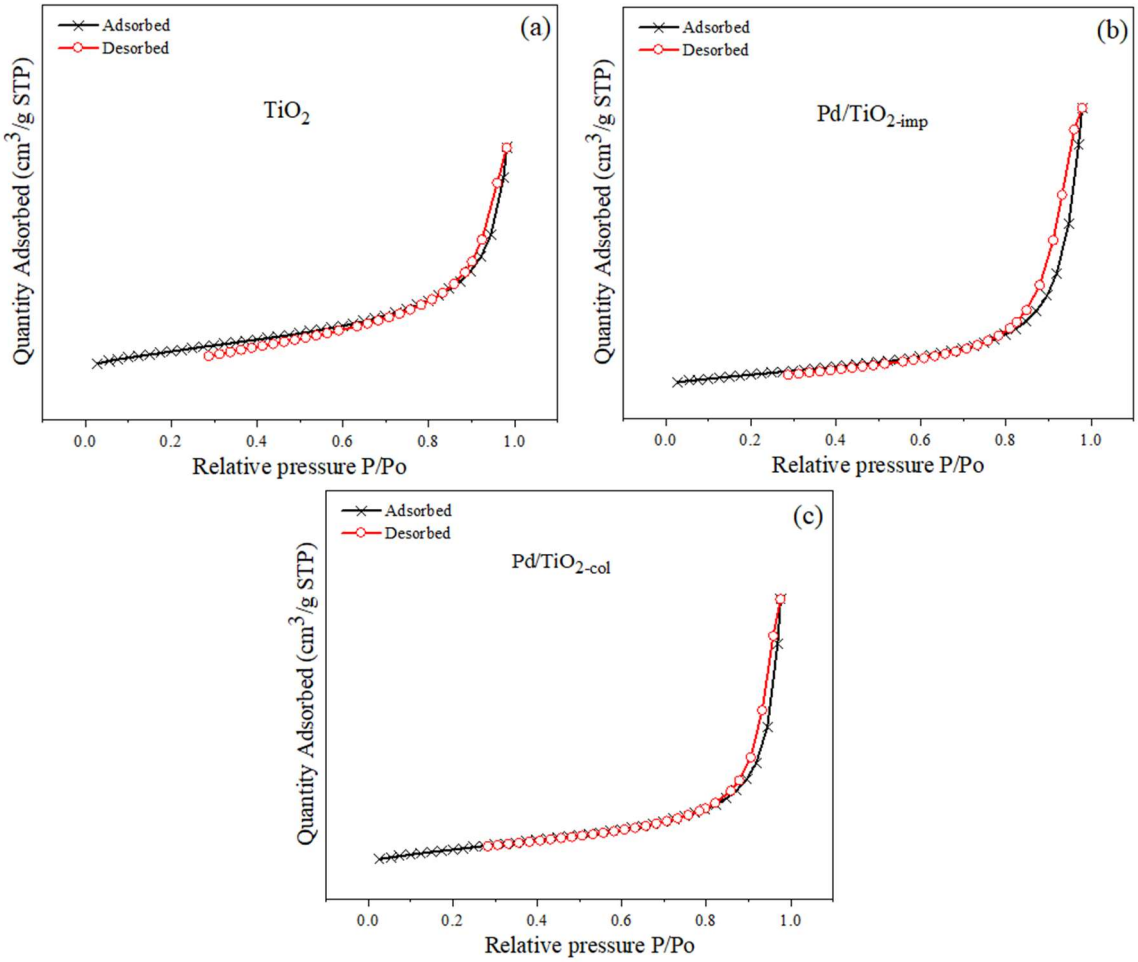

Figure A2.3: Isotherm N_2 adsorption-desorption of (a) TiO_2, (b) $Pd/TiO_{2\text{-imp}}$, and (c) $Pd/TiO_{2\text{-col}}$.

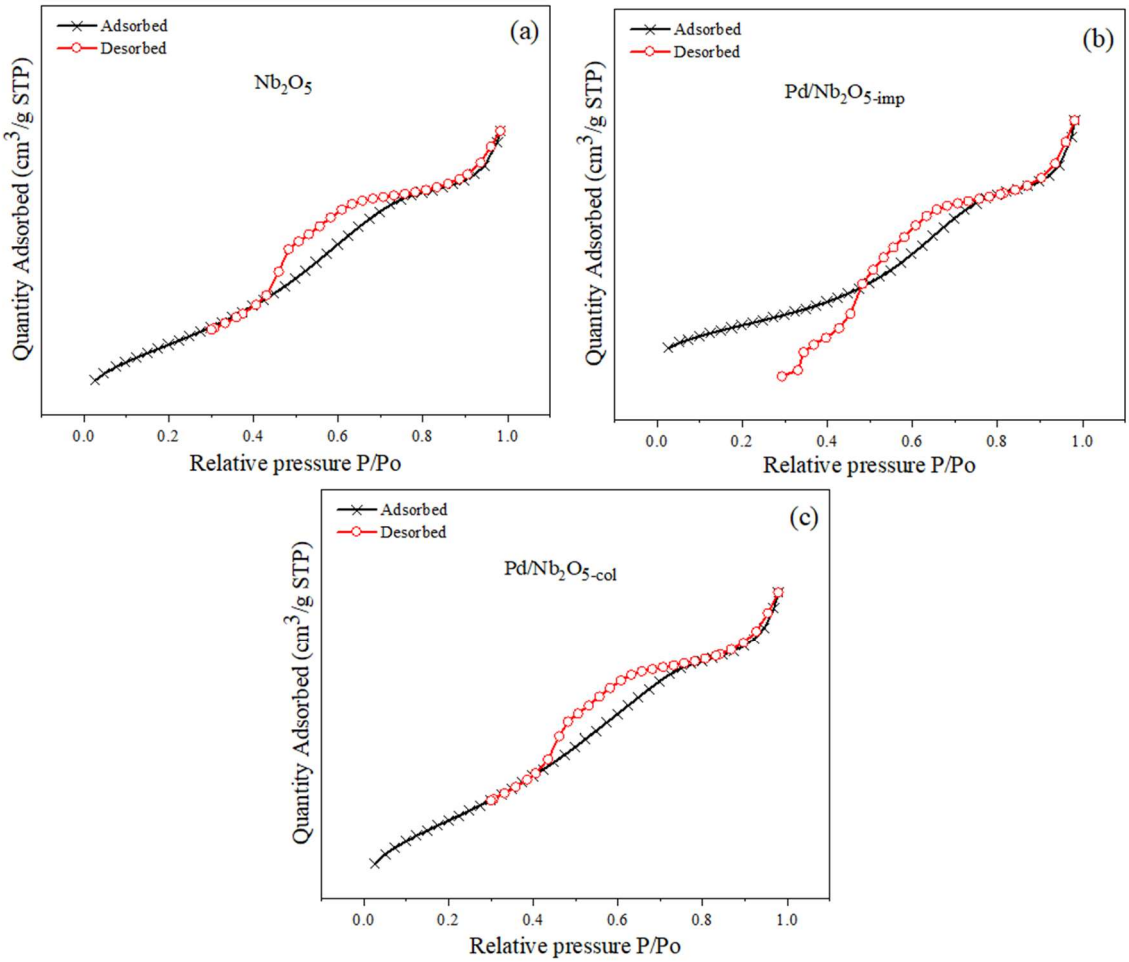

Figure A2.4: Isotherm N_2 adsorption-desorption of (a) Nb_2O_5, (b) $Pd/Nb_2O_{5\text{-imp}}$, and $Pd/Nb_2O_{5\text{-col}}$ (c).

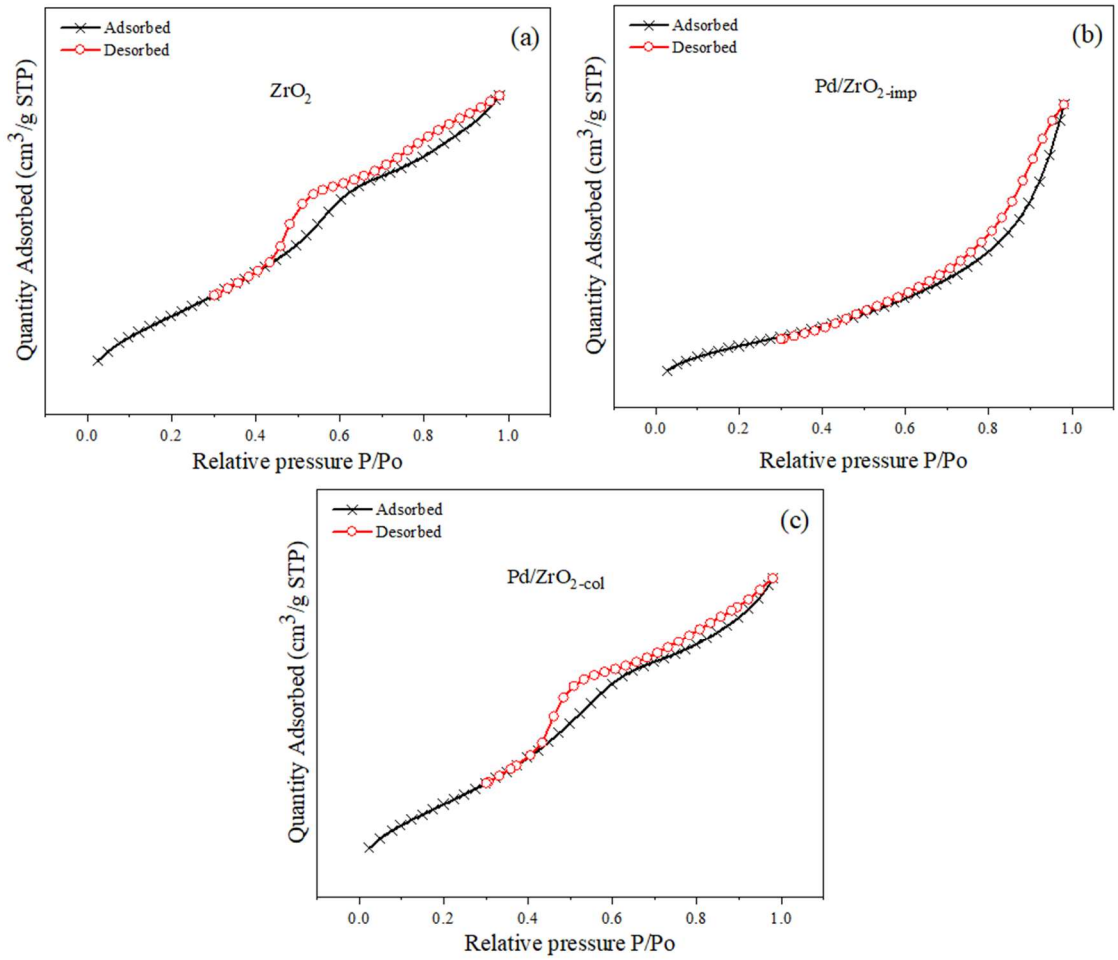

Figure A2.5: Isotherm N_2 adsorption-desorption of (a) ZrO_2, (b) $Pd/ZrO_{2\text{-imp}}$, and (c) $Pd/ZrO_{2\text{-col}}$.

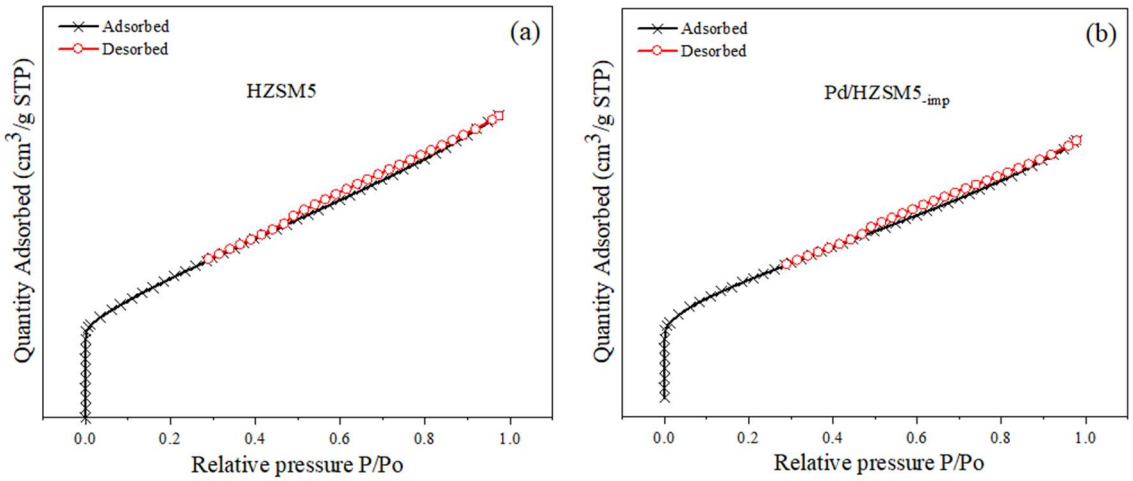

Figure A2.6: Isotherm N_2 adsorption-desorption of (a) HZSM5 and (b) $Pd/HZSM5_{\text{-imp}}$.

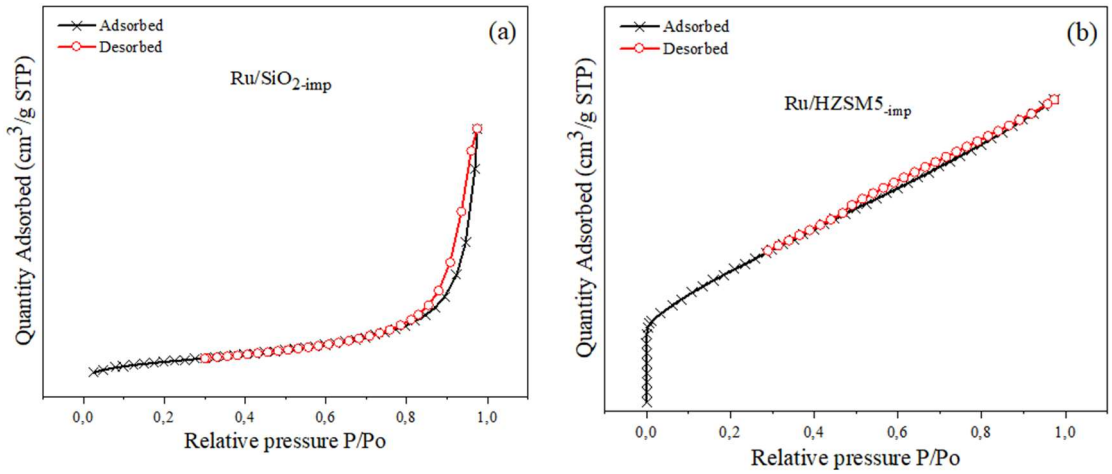

Figure A2.7: Isotherm N_2 adsorption-desorption of (a) $Ru/SiO_{2\text{-imp}}$ and (b) Ru/HZSM5-imp.

Annex 3 PDF DATA CARDS

PDF# 01-087-0638

Palladium **Pd**

Radiation: CuKα1 (1.5406 Å) d-Spacing: Calculated Intensity: Calculated – Peak

Chemical Formula: Pd Empirical Formula: Pd Weight %: Pd100.00 Atomic %:

Pd100.00 Crystal System: Cubic SPGR: Fm-3m (225)

Author's Unit Cell [a: 3.95 Å Volume: 61.63 Å³ Z: 4.00 MolVol: 15.41

Calculated Density: 11.469 g/cm³

2q (°)	d (Å)	I	h	k	L	2q (°)	d (Å)	I	H	K	L
40.235	2.239540	1000	1	1	1	86.927	1.119770	60	2	2	2
46.801	1.939500	450	2	0	0	105.180	0.969750	27	4	0	0
68.342	1.371430	216	2	2	0	119.897	0.889904	89	3	3	1
82.387	1.169560	217	3	1	1	125.262	0.867371	84	4	2	0

PDF# 04-001-1921

Ruthenium **Ru**

Radiation: CuKα1 (1.5406 Å) d-Spacing: Calculated Intensity: Calculated – Peak

Chemical Formula: Ru Empirical Formula: Ru Weight %: Ru100.00 Atomic %:

Ru100.00 Compound Name: Ruthenium Mineral Name: Ruthenium, syn

Crystal System: Hexagonal SPGR: P63/mmc (194)

Author's Unit Cell a: 2.704 Å c: 4.278 Å Volume: 27.09 Å³ Z: 2.00 MolVol:

13.54 c/a: 1.582] Calculated Density: 12.391 g/cm³ Structural Density:

12.39 g/cm³ SS/FOM: F(18) = 999.9(0.0001, 18) I/Ic: 13.88 I/Ic - CW ND: 0.49

2q (°)	d (Å)	I	h	k	L	2q (°)	d (Å)	I	H	K	L
38.408	2.341.730	261	1	0	0	84.753	1.142.850	120	1	1	2
42.214	2.139.000	254	0	0	2	86.011	1.129.330	85	2	0	1
44.048	2.054.120	1000	1	0	1	92.146	1.069.500	15	0	0	4
58.383	1.579.320	120	1	0	2	97.178	1.027.060	20	2	0	2
69.463	1.352.000	123	1	1	0	104.705	0.972841	17	1	0	4
78.461	1.217.950	118	1	0	3	116.689	0.904912	42	2	0	3
82.275	1.170.870	17	2	0	0	120.983	0.885092	14	2	1	0
125.424	0.866736	78	2	1	1	140.728	0.817841	24	2	1	2
133.365	0.838789	50	1	1	4	146.867	0.803639	36	1	0	5

PDF# 00-029-1486

Aluminum Oxide **Al_2O_3**

Radiation: CuKα1 (1.5406 Å) d-Spacing: Calculated Intensity: Calculated – Peak

Phase: γ Chemical Formula: Al2.66 O4 Empirical Formula: Al2.66 O4 Refined Formula: Al2.669 O4

Weight %: Al52.86 O47.14 Atomic %: Al39.94 O60.06 Compound Name: Aluminum Oxide

Crystal System: Cubic SPGR: Fd-3m (227)

Author's Unit Cell [a: 7.906 Å Volume: 494.16 Å³ Z: 8.00 MolVol: 61.77 Calculated Density: 3.65 g/cm³ Structural Density: 3.656 g/cm³ SS/FOM: F(24) = 999.9(0.0001, 30) R-factor: 0.06 I/Ic: 0.64

2q (°)	d (Å)	I	h	k	L	2q (°)	d (Å)	I	H	K	L
19.431	4.564530	85	1	1	1	50.262	1.813760	4	3	3	1
31.992	2.795190	104	2	2	0	57.019	1.613810	22	4	2	2
37.706	2.383750	471	3	1	1	60.830	1.521510	71	5	1	1
39.450	2.282270	131	2	2	2	66.891	1.397600	966	4	4	0
45.874	1.976500	1000	4	0	0	70.396	1.336360	3	5	3	1
76.078	1.250050	5	6	2	0	105.783	0.965872	1	7	3	3
79.418	1.205650	19	5	3	3	111.526	0.931731	2	8	2	2
84.911	1.141130	54	4	4	4	115.080	0.912906	8	7	5	1
88.180	1.107060	3	7	1	1	121.252	0.883918	34	8	4	0
93.622	1.056480	5	6	4	2	125.153	0.867796	1	9	1	1
96.900	1.029270	28	7	3	1	136.689	0.828774	2	9	3	1
102.418	0.988250	57	8	0	0	145.343	0.806903	78	8	4	4

PDF# 01-073-1764

Titanium oxide **TiO_2**, Anatase, sny

Radiation: CuKα1 (1.5406 Å) d-Spacing: Calculated Intensity: Calculated - Peak

Chemical Formula: Ti O2 Empirical Formula: O2 Ti Weight %: O40.06 Ti59.94 Atomic %: O66.67 Ti33.33

Compound Name: Titanium Oxide Mineral Name: Anatase, syn

Crystal System: Tetragonal SPGR: I41/amd (141)

Author's Unit Cell [a: 3.776(2) Å c: 9.486(6) Å Volume: 135.25 Å³ Z: 4.00 MolVol: [33.81c/a: 2.512] Calculated Density: 3.922 g/cm³ Structural Density: 3.923 g/cm³

2q (°)	d (Å)	I	h	k	L	2q (°)	d (Å)	I	H	K	L
25.367	3.508270	1000	1	0	1	95.459	1.040950	17	3	2	1
37.052	2.424270	61	1	0	3	98.709	1.015190	11	1	0	9
37.908	2.371500	191	0	0	4	100.189	1.004140	7	2	0	8
38.666	2.326700	71	1	1	2	101.574	0.994164	5	3	2	3
48.157	1.888000	249	2	0	0	107.879	0.952847	20	3	1	6
54.050	1.695250	153	1	0	5	109.368	0.944000	11	4	0	0
55.202	1.662540	147	2	1	1	113.280	0.922234	1	3	0	7
62.278	1.489560	24	2	1	3	114.308	0.916859	19	3	2	5
62.865	1.477070	108	2	0	4	115.343	0.911576	11	4	1	1
68.974	1.360400	45	1	1	6	119.025	0.893864	28	1	1	10
70.477	1.335020	49	2	2	0	119.025	0.893864	28	2	1	9
74.301	1.275490	4	1	0	7	120.651	0.886548	5	2	2	8
75.275	1.261380	73	2	1	5	122.245	0.879662	4	4	1	3
76.245	1.247730	19	3	0	1	122.863	0.877067	12	4	0	4
81.025	1.185750	3	0	0	8	123.424	0.874744	3	3	3	2
82.399	1.169420	5	3	0	3	131.647	0.844339	16	4	2	0
82.924	1.163350	35	2	2	4	132.759	0.840717	3	1	0	11
83.398	1.157940	13	3	1	2	136.730	0.828657	2	3	2	7
93.572	1.056910	4	2	1	7	138.120	0.824751	16	4	1	5
94.515	1.048840	15	3	0	5	144.808	0.808089	6	3	0	9

PDF# 01-073-1764

Titanium oxide **TiO_2**, Rutile, sny

Radiation: CuKα1 (1.5406 Å) d-Spacing: Calculated Intensity: Calculated - Peak

Chemical Formula: Ti O2 Empirical Formula: O2 Ti Weight %: O40.06 Ti59.94 Atomic %: O66.67 Ti33.33

Compound Name: Titanium Oxide Mineral Name: Rutile, syn

Crystal System: Tetragonal SPGR: I41/amd (141)

Author's Unit Cell [a: 3.776(2) Å c: 9.486(6) Å Volume: 135.25 Å³ Z: 4.00 MolVol: [33.81c/a: 2.512] Calculated Density: 3.922 g/cm³ Structural Density: 3.923 g/cm³

2q (°)	d (Å)	I	h	k	l	2q (°)	d (Å)	I	H	K	L
27.446	3.247	100	1	1	0	89.555	1.093	8	2	2	2
36.085	2.487	50	1	0	1	90.705	1.082	4	3	3	0
39.187	2.297	8	2	0	0	95.272	1.042	6	4	1	1
41.225	2.188	25	1	1	1	96.014	1.036	6	3	1	2
44.05	2.054	10	2	1	0	97.173	1.027	4	4	2	0
54.322	1.687	60	2	1	1	98.511	1.016	1	3	3	1
56.64	1.623	20	2	2	0	105.095	0.97	2	4	2	1
62.74	1.479	10	0	0	2	106.015	0.964	2	1	0	3
64.038	1.452	10	3	1	0	109.402	0.943	2	1	1	3
65.478	1.424	2	2	2	1	116.222	0.907	4	4	0	2
69.008	1.359	20	3	0	1	117.522	0.9	4	5	1	0
69.788	1.346	12	1	1	2	120.054	0.889	8	2	1	3
72.408	1.304	2	3	1	1	122.783	0.877	8	4	3	1
74.409	1.273	1	3	2	0	123.655	0.873	8	3	3	2
76.508	1.244	4	2	0	2	131.841	0.843	6	4	2	2
79.819	1.2	2	2	1	2	136.541	0.829	8	3	0	3
82.333	1.17	6	3	2	1	140.044	0.819	12	5	2	1
84.258	1.148	4	4	0	0	143.107	0.812	2	4	4	0
87.461	1.114	2	4	1	0	155.856	0.787	2	5	3	0

PDF# 00-050-1089

Zirconium oxide, **ZrO_2**, tetragonal

Radiation: CuKα1 (1.5406 Å) d-Spacing: Calculated Intensity: Calculated - Peak

Chemical Formula: Zr O2 Empirical Formula: O2 Zr Weight %: O25.97 Zr74.03

Atomic %: O66.67 Zr33.33 Compound Name: Zirconium Oxide

Crystal System: Tetragonal SPGR: P42/nmc (137)

Author's Unit Cell [a: 3.5984(5) Å c: 5.152(1)Å Volume: 66.71 Å Z: 2.00

MolVol: 33.35 c/a: 1.432] Calculated Density: 6.134 g/cm³ SS/FOM: F(18) =

55.2(0.0136, 24) Space Group: P42/nmc (137) Molecular Wt: 123.22 g/mol

2q (°)	d (Å)	I	h	k	l	2q (°)	d (Å)	I	H	K	L
30.270	295.020	100	0	1	1	73.464	128.793	3	0	0	4
34.811	257.504	8	0	0	2	74.538	127.202	5	2	2	0
35.255	254.361	12	1	1	0	81.971	117.444	11	1	2	3
43.138	209.529	1	0	1	2	82.475	116.854	6	0	3	1
50.377	180.989	43	1	1	2	84.195	114.899	4	1	1	4
50.711	179.875	22	0	2	0	84.917	114.106	3	2	2	2
59.610	154.970	14	0	1	3	85.223	113.774	3	1	3	0
60.205	153.580	24	1	2	1	94.715	104.715	3	0	2	4
62.967	147.491	7	2	0	2	95.477	104.080	9	1	3	2

PDF# 04-002-8305

Zirconium oxide, **ZrO_2**, monoclinic

Radiation: CuKα1 (1.5406 Å) d-Spacing: Calculated Intensity: Calculated - Peak

Chemical Formula: Zr O2 Empirical Formula: O2 Zr Weight %: O25.97 Zr74.03

Atomic %: O66.67 Zr33.33 Compound Name: Zirconium Oxide

Crystal System: Monoclinic SPGR: P42/nmc (137)

Author's Unit Cell [a: 3.5984(5) Å c: 5.152(1)Å Volume: 66.71 Å Z: 2.00

MolVol: 33.35 c/a: 1.432] Calculated Density: 6.134 g/cm³ SS/FOM: F(18) =

55.2(0.0136, 24) Space Group: P42/nmc (137) Molecular Wt: 123.22 g/mol

2q (°)	d (Å)	I	h	k	l	2q (°)	d (Å)	I	H	K	L
8,709	5,087	3	0	0	1	28,93	1,592	4	-1	3	1
12,024	3,697	14	1	1	0	29,133	1,582	3	-2	2	2
12,22	3,639	10	0	1	1	29,887	1,545	8	1	3	1
14,087	3,164	100	-1	1	1	30,027	1,539	7	-2	0	3
15,734	2,84	68	1	1	1	30,683	1,509	5	3	1	1
17,08	2,622	21	2	0	0	30,991	1,496	5	-3	1	2
17,191	2,606	11	0	2	0	31,418	1,477	8	1	1	3
17,654	2,539	13	0	0	2	32,039	1,452	1	3	2	0
17,95	2,499	2	-2	0	1	32,124	1,448	2	2	3	0
19,198	2,342	1	-2	1	0	32,482	1,434	1	0	3	2
19,27	2,334	4	1	2	0	32,691	1,426	2	-2	3	1
19,705	2,284	1	0	1	2	32,849	1,42	6	0	2	3
19,995	2,252	1	-2	1	1	32,941	1,416	4	-1	3	2
20,362	2,213	12	-1	1	2	34,455	1,361	1	2	3	1
20,574	2,191	5	2	0	1	34,809	1,349	1	3	2	1
20,686	2,18	5	-1	2	1	35,094	1,339	1	-3	2	2
22,412	2,02	7	2	1	1	35,535	1,325	2	-2	2	3
22,76	1,991	6	-2	0	2	35,649	1,321	4	-4	0	1
24,474	1,859	2	-2	1	2	35,974	1,311	1	4	0	0
24,632	1,848	18	2	2	0	36,051	1,308	1	-2	3	2
25,057	1,818	22	0	2	2	36,224	1,303	1	0	4	0
25,279	1,803	13	-2	2	1	36,32	1,3	1	3	1	2
25,596	1,783	5	-1	2	2	36,789	1,286	1	-3	1	3
27,051	1,693	11	0	0	3	37,34	1,27	2	0	0	4
27,339	1,677	1	2	2	1	37,522	1,264	4	1	4	0
27,634	1,66	11	1	2	2	38,204	1,245	1	-1	1	4
27,699	1,657	11	3	1	0	38,695	1,232	1	3	3	0
27,784	1,652	9	-3	1	1	39,038	1,223	1	4	0	1
27,941	1,643	6	0	3	1	39,432	1,212	1	0	3	3
28,583	1,61	7	-1	1	3						

PDF# 00-057-0145

MFI HZSM5

Radiation: CuKα1 (1.5406 Å) d-Spacing: Calculated Intensity: Calculated - Peak

Chemical Formula: Al2 O3 - Si O2 Empirical Formula: Al2 O5 Si

Weight %: Al33.30 O49.37 Si17.33 Atomic %: Al25.00 O62.50 Si12.50

Compound Name: Aluminum Silicate Zeolite Name: HZSM5

Molecular Wt: 162.05 g/mol Subfiles: Inorganic, Micro & Mesoporous (Zeolite) Zeolite

Classification: MFI (HZSM5)

2q (°)	d (Å)	I	h	k	l	2q (°)	d (Å)	I	H	K	L
7.824	11.290	52				23.058	3.854	100			
8.757	10.090	34				23.765	3.741	39			
11.790	7.500	7				24.312	3.658	24			
13.080	6.763	5				25.779	3.453	9			
13.832	6.397	10				26.538	3.356	11			
14.649	6.042	12				29.159	3.060	8			
15.408	5.746	6				29.827	2.993	14			
15.829	5.594	7				32.630	2.742	6			
17.653	5.020	5				33.317	2.687	6			
19.141	4.633	7				36.010	2.492	9			
20.751	4.277	10				37.312	2.408	6			
22.083	4.022	7									

Annex 4 STEM IMAGES AND PARTICLE SIZE DISTRIBUTIONS

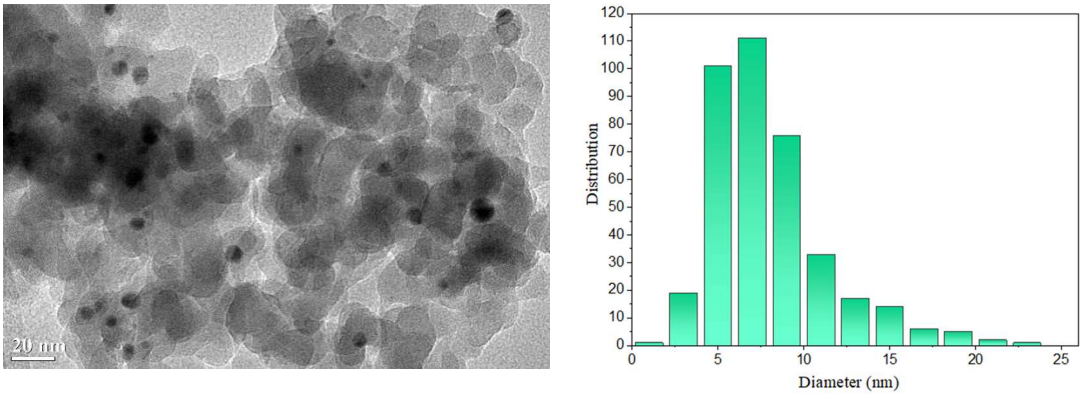

Figure A4.1: TEM images and particle size distribution for $Pd/SiO_{2\text{-imp}}$.

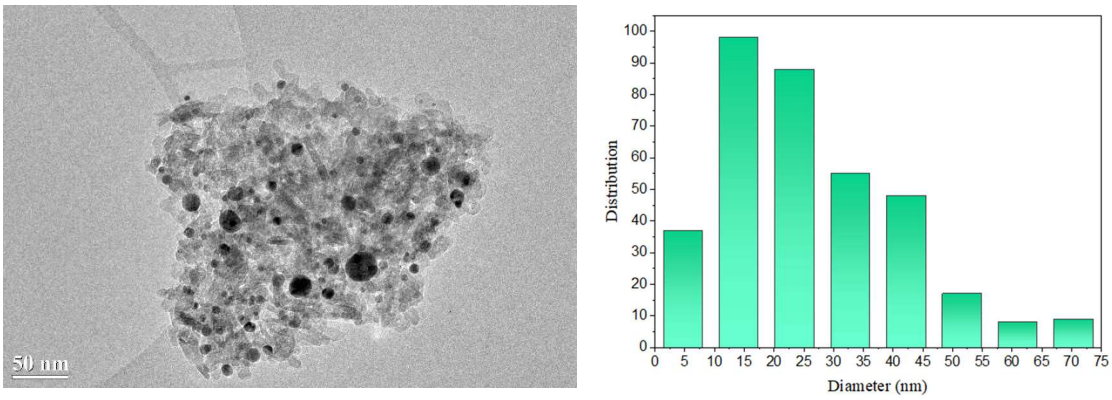

Figure A4.2: TEM images and particle size distribution for $Pd/Al_2O_{3\text{-imp}}$.

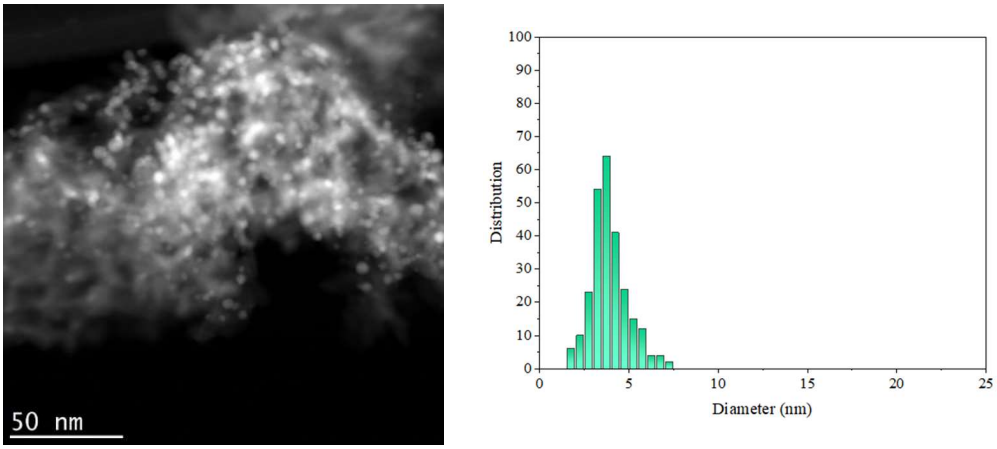

Figure A4.3: TEM images and particle size distribution for $Pd/Al_2O_{3\text{-col}}$.

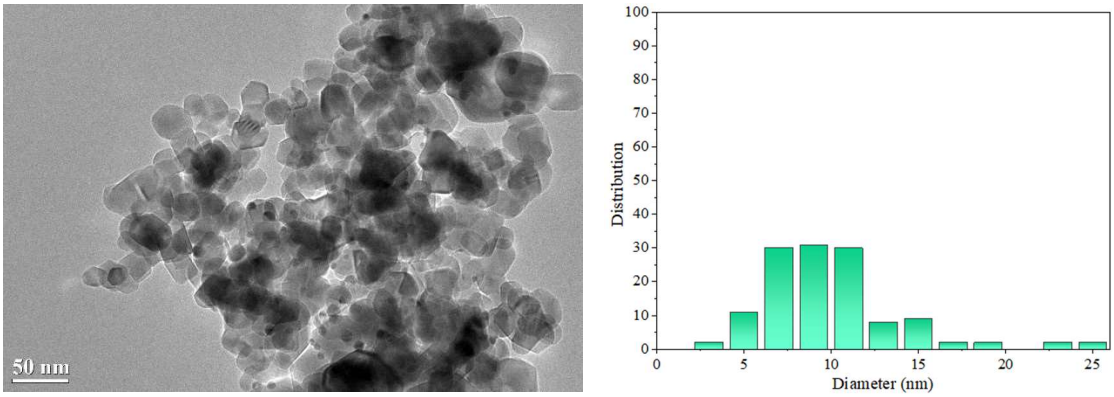

Figure A4.4: TEM images and particle size distribution for Pd/$TiO_{2\text{-imp}}$

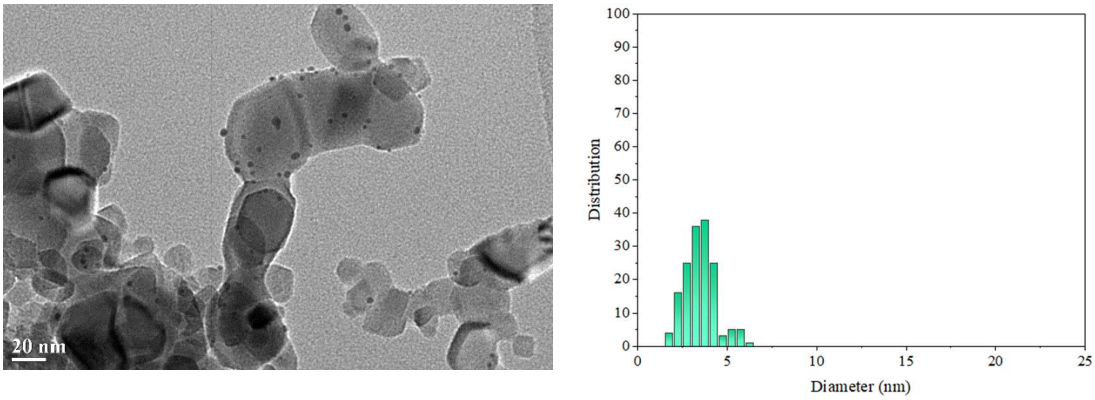

Figure A4.5: TEM images and particle size distribution for Pd/$TiO_{2\text{-col}}$.

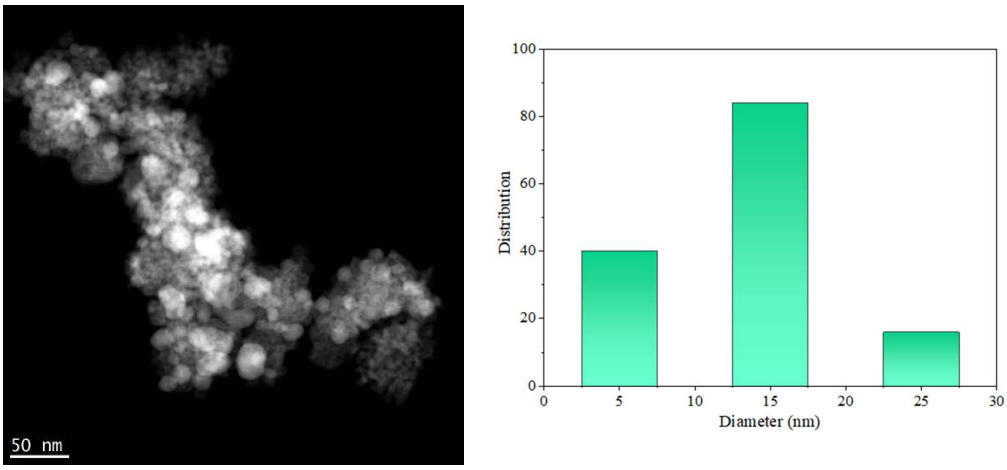

Figure A4.6: TEM images and particle size distribution for Pd/$ZrO_{2\text{-imp}}$.

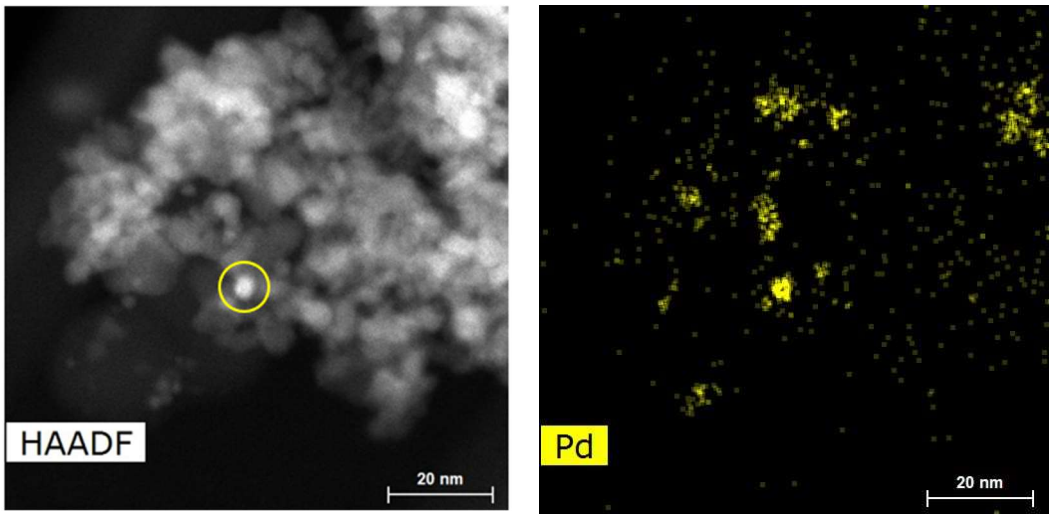

Figure A4.7: Chemical mapping for $Pd/ZrO_{2\text{-col}}$

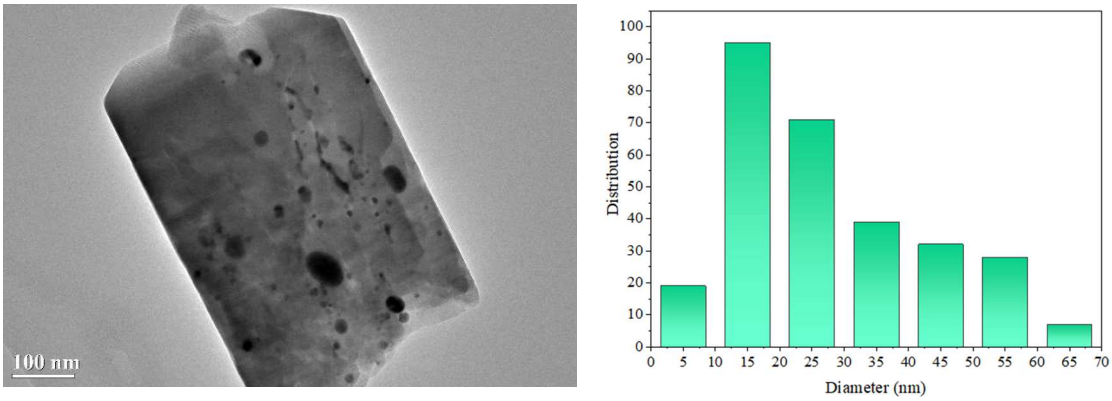

Figure A4.8: TEM images and particle size distribution for $Pd/HZSM5_{\text{-imp}}$

Annex 5 PORE VOLUME FOR THE CATALYSTS PREPARED BY INCIPIENT WETNESS IMPREGNATION

To determine the pore volume for each support, first, approximately 0.5000 g of support was dried at 100°C for 1 hour. Then, the dried material was moistened with water drop by drop until it reached the saturation, which indicates the complete filling of the pore volume. The

(1) SiO_2 – 0.5 mL

(2) Al_2O_3 – 0.3 mL

(3) TiO_2 – 0.3 mL

(4) Nb_2O_5 – 0.2 mL

(5) ZrO_2 – 0.1 mL

(6) HZSM5 – 0.4 mL

ANNEX 6: CORRESPONDING FACTOR

Anisole – 9.32926×10^{-09}

Bicyclohexyl – 4.39781×10^{-09}

Benzene – 9.3442×10^{-09}

Benzyl phenyl ether – 3.7335×10^{-09}

Cyclohexane – 7.84175×10^{-09}

Cyclohexene – 9.29046×10^{-09}

Cyclohexanol – 8.44299×10^{-09}

Cyclohexanone – 1.0942×10^{-08}

Cyclohexyl ethanol – 5.81888×10^{-09}

Dihydrobenzofuran – 6.42815×10^{-09}

Diphenyl ether – 3.95056×10^{-09}

Ethylbenzene – 5.53098×10^{-09}

Ethylcyclohexane – 5.53853×10^{-09}

Guaiacol – 7.82962×10^{-09}

Methylcyclohexane – 6.71621×10^{-09}

Toluene – 6.83122×10^{-09}

Phenethoxybenzene – 3.31621×10^{-09}

Phenol – 8.42569×10^{-09}

Propylphenol – 5.33156×10^{-09}

Development of catalysts for the valorization of lignin: Hydrodeoxygenation of dimeric aryl ethers

The present thesis aims at studying the role of the support and metal particle size on the hydrodeoxygenation reactions (HDO) of benzyl phenyl ether (BPE), phenethoxybenzene (PEB), and diphenyl ether (DPE) chosen as model molecules representative of the main ether linkages present in the lignocellulosic biomass. The reactions were carried out in the liquid phase at 230 °C and 18 bar of H_2. Pd-supported on different oxides (SiO_2, TiO_2, Nb_2O_5, Al_2O_3, ZrO_2, and HZSM5) were synthesized by incipient wetness impregnation and deposition of metal particles prepared by the colloidal method. The acidic sites of the support promote the cracking of the C-O ether bond of BPE, but for PEB and DPE, this effect is less pronounced due to the higher energy required to break these linkages. The hydrogenolysis of the C-O ether bond takes place on the metallic Pd particles, producing the respective arenes. However, the Pd particle size can directly affect the product distribution after C-O cleavage. Due to the larger Pd particle size, impregnated catalysts favor the hydrogenolysis and exhibit a higher selectivity to alkylated products, whereas a smaller Pd particle size, obtained for catalysts prepared by the colloidal route, increases the selectivity to deoxygenated products. Over these catalysts, the formation of alkylated products is suppressed, but the hydrogenation of BPE, PEB, and DPE aromatic rings occurs in parallel to hydrogenolysis also promoted by Pd particles. The performance of Ru-based catalysts was also evaluated in the same reaction conditions. In the presence of Ru, alkylated products are produced even in the absence of acidic sites.

Keywords: Hydrodeoxygenation; Hydrogenolysis; Alkylation; Ether linkage

Développement de catalyseurs pour la valorisation de la lignine, hydrodésoxygénation d'aryl éthers dimériques

Cette thèse a pour but d'étudier le rôle du support et de la taille des particules métalliques sur les réactions d'hydrodésoxygénation (HDO) du benzyl phényl éther (BPE), du phenethoxybenzène (PEB) et du diphényl éther (DPE) choisis comme molécules modèles représentatives des principales liaisons éther présentes dans la biomasse lignocellulosique. Les réactions ont été réalisées en phase liquide à 230 °C et sous 18 bar de H_2. Les catalyseurs au Pd supporté sur différents oxydes (SiO_2, TiO_2, Nb_2O_5, Al_2O_3, ZrO_2 et HZSM5) ont été synthétisés par imprégnation par voie humide et par dépôt de particules métalliques préparées par voie colloïdale. Les sites acides du support favorisent le craquage de la liaison éther C-O du BPE mais pour le PEB et le DPE, cet effet est moins prononcé en raison de l'énergie plus élevée requise pour rompre ces liaisons. L'hydrogénolyse de la liaison éther C-O a lieu sur les particules de Pd métallique, produisant les arènes respectifs. Cependant, la taille des particules de Pd peut directement affecter la distribution des produits après le clivage de la liaison C-O. En raison de la taille plus importante des particules de Pd, les catalyseurs imprégnés favorisent l'hydrogénolyse et présentent une sélectivité plus élevée pour les produits alkylés, tandis que la taille plus petite des particules de Pd, obtenue pour les catalyseurs préparés par voie colloïdale, augmente la sélectivité pour les produits désoxygénés. Sur ces catalyseurs, la formation de produits alkylés est supprimée, mais l'hydrogénation du cycle aromatique des BPE, PEB et DPE se produit parallèlement à l'hydrogénolyse, également favorisée par les particules de Pd. La performance des catalyseurs à base de Ru a également été évaluée dans les mêmes conditions de réaction. En présence de Ru, des produits alkylés ont été produits même en l'absence de sites acides.

Mots clés : Hydrodésoxygénation ; Hydrogénolyse ; Alkylation ; Liaison éther